NAVAL POSTGRADUATE SCHOOL
Monterey, California

THESIS

The Influence of Cumulus Parameterization on Model Forecasts of Rapid Oceanic Cyclogenesis

by

James W. Allen

December, 1993

Thesis Advisor: Patricia M. Pauley

Approved for public release; distribution is unlimited.

REPORT DOCUMENTATION PAGE

Form Approved OMB No. 0704

1. AGENCY USE ONLY *(Leave blank)*	2. REPORT DATE December 1993.	3. REPORT TYPE AND DATES COVERED Master's Thesis

4. TITLE AND SUBTITLE The Influence of Cumulus Parameterization on Model Forecasts of Rapid Oceanic Cyclogenesis	5. FUNDING NUMBERS
6. AUTHOR(S) James W. Allen	
7. PERFORMING ORGANIZATION NAME(S) AND ADDRESS(ES) Naval Postgraduate School Monterey CA 93943-5000	8. PERFORMING ORGANIZATION REPORT NUMBER
9. SPONSORING/MONITORING AGENCY NAME(S) AND ADDRESS(ES)	10. SPONSORING/MONITORING AGENCY REPORT NUMBER

11. SUPPLEMENTARY NOTES The views expressed in this thesis are those of the author and do not reflect the official policy or position of the Department of Defense or the U.S. Government.

12a. DISTRIBUTION/AVAILABILITY STATEMENT Approved for public release; distribution is unlimited.	12b. DISTRIBUTION CODE A

13. ABSTRACT *(maximum 200 words)*

Numerous studies have left little doubt that latent heat release (LHR) can significantly influence many features of extratropical cyclone systems. Recent experiments with the NCAR/PSU mesoscale model indicated that not only did different moisture parameterizations significantly affect model forecasts, but that forecasts for different cyclonic systems responded very differently to the parameterizations. Model output from the NCAR/PSU model is examined for two cyclonic systems, with four different parameterization experiments used to produce four forecasts for each system. The output was then examined in three and four dimensions to qualitatively and quantitatively determine the direct and indirect effects of latent heat release on model output. The results clearly showed the difference in the general dynamics of the two cyclones. One demonstrated a very strong reliance on diabatic processes for its early development, becoming more adiabatic late in its history, while the other initially developed very adiabatically and became more diabatic after about the mid-point of the forecast period. The cyclonic system that started out diabatically was more sensitive to moisture parameterization. The models clearly showed the differences between precipitation fields generated by the different parameterizations. In particular, allowing evaporation of precipitation in non-saturated layers greatly decreased the areal extent of light precipitation, while having minimal effect in areas of heavy precipitation.

14. SUBJECT TERMS latent heat release, cumulus parameterization, oceanic cyclogenesis,			15. 235 16. PRICE CODE
17. SECURITY CLASSIFICATION OF REPORT Unclassified	18. SECURITY CLASSIFICATION OF THIS PAGE Unclassified	19. SECURITY CLASSIFICATION OF ABSTRACT Unclassified	20. LIMITATION OF ABSTRACT UL

NSN 7540-01-280-5500

Standard Form 298 (Rev. 2-89)

Prescribed by ANSI Std. 239-18

Approved for public release; distribution is unlimited.

The Influence of Cumulus Parameterization on Model Forecasts
of Rapid Oceanic Cyclogenesis

by

James W. Allen
Lieutenant Commander, United States Navy
B.S., State University of New York, College at Oswego, 1980

Submitted in partial fulfillment
of the requirements for the degree of

MASTER OF SCIENCE IN METEOROLOGY AND PHYSICAL OCEANOGRAPHY

from the

NAVAL POSTGRADUATE SCHOOL
DECEMBER 1993

Author: James W. Allen

James W. Allen

Approved by: Patricia M. Pauley

Patricia M. Pauley, Thesis Advisor

Carlyle H. Wash, Second Reader

Robert L. Haney, Chairman,
Department of Meteorology

ABSTRACT

Numerous studies have left little doubt that latent heat release (LHR) can significantly influence many features of extratropical cyclone systems. Recent experiments with the NCAR/PSU mesoscale model indicated that not only did different moisture parameterizations significantly affect model forecasts, but that forecasts for different cyclonic systems responded very differently to the parameterizations. Model output from the NCAR/PSU model is examined for two cyclonic systems, with four different parameterization experiments used to produce four forecasts for each system. The output was then examined in three and four dimensions to qualitatively and quantitatively determine the direct and indirect effects of latent heat release on model output. The results clearly showed the difference in the general dynamics of the two cyclones. One demonstrated a very strong reliance on diabatic processes for its early development, becoming more adiabatic late in its history, while the other initially developed very adiabatically and became more diabatic after about the mid-point of the forecast period. The cyclonic system that started out diabatically was more sensitive to mositure parameterization. The models clearly showed the differences between precipitation fields generated by the different parameterizations. In particular, allowing evaporation of precipitation in non-saturated layers greatly decreased the areal extent of light precipitation, while having minimal effect in areas of heavy precipitation.

TABLE OF CONTENTS

ACKNOWLEDGEMENTS

The author wishes to thank Dr. Patricia M. Pauley, thesis advisor par excellance, who got me interested enough in this project that for brief moments, in between massive frustration, I actually had fun doing it, and the NPS Visualization Lab Staff, particularly Mathew Koebbe, who spent many hours trying to convince the various pieces of hardware and software needed to produce the visualizations to work together. Thanks to Lt. Chip Weddle, who politely suffered through, and answered, more dumb VMS and UNIX questions than anyone should ever have to.

Special thanks to my wife, Linda, who despite working, and going to school herself, patiently put up with me, and is still married to me.

I. INTRODUCTION

Kuo and Low-Nam (1990) did a series of 14 numerical experiments using the National Center for Atmospheric Research/Penn State University mesoscale model on nine cases of explosive marine cyclogenesis. Four of the experiments involved only a change in the precipitation parameterization for each of the storms. Specifically the parameterizations included Kuo (based on Kuo (1974) and Anthes (1977)), Arakawa-Schubert (1974) as modified by Grell et al. (1988), explicit (Hsie et al. 1984), and a fourth experiment which excluded latent heating.

One of Kuo and Low-Nam's (1990) main results was that the structure of the simulated cyclones was sensitive to the details of precipitation parameterization. Averaged over the nine cases, precipitation parameterization was the third most important model component, only ranking behind initial conditions and horizontal grid resolution. However, the effects of changes in precipitation parameterization varied greatly from storm to storm. Two of their cyclones, case 6 and case 7, demonstrated the most and least sensitivity, respectively, to precipitation parameterization; those are the storms that are the subject of this thesis.

The overall objective of this thesis was to examine the case 6 and 7 storms in detail to determine why cumulus parameterization effects varied so much between these two storms. A calculation of the diabatic component of vertical motion was performed to examine this important link between thermodynamic and dynamical processes and its variation associated with precipitation parameterization. A second objective was to use 4-D visualization to dynamically investigate the differences in the model output the parameterizations produced.

This thesis will continue with a background section followed by a discussion of the methodology used to prepare the data. A comparison of the actual synoptic systems and

model output will constitute the forth chapter. Results of the model forecasts will be presented in Chapter V followed by conclusions and references.

II. BACKGROUND

Our understanding of the atmosphere and the ability to numerically model it with some degree of accuracy have advanced considerably over the past 30 years. Along with and partly as a result of numerical modeling advances have come better understanding of the physics of the atmosphere. Numerous studies have left little doubt that latent heat release (LHR) can significantly influence many features of extratropical cyclone systems. As summarized in Pauley and Smith (1988), LHR has a wide variety of effects including increased upper-level temperatures, increased upper-level and decreased lower-level isobaric heights, and lowered sea level pressure. These changes can cause an alteration in the dynamics of the atmospheric system as well. It has been shown that LHR increases upper- and lower-level circulations (Anthes et al. 1982; Chang et al. 1982; Chen et al. 1983) and enhances upward vertical motions (Aubert 1957; Danard 1964; Krishnamurti 1968; Dimego and Bosart 1982; Pagnotti and Bosart 1984; Smith et al. 1984). In addition enhanced vorticity fields (Tracton 1973; Chang et al. 1982; Chen et al. 1983) and more vigorous energy cycles (Danard 1964, 1966, Chang et al. 1984.; Kenney and Smith 1983; Robertson and Smith 1983; Smith and Dare 1986) have been noted.

However, much of the LHR in extratropical cyclone systems is associated with cumulus convection, which has horizontal space and time scales that are two or more orders of magnitude smaller than those of the synoptic weather systems themselves. While an individual cloud will not have much impact on a large-scale system, cumulus clouds frequently organize on a scale comparable to that of synoptic systems. The cumulative effect of a large number of these clouds may have a significant impact on the large-scale system (Haltiner and Williams 1980, pp. 319-320). Current mesoscale models generally have a mesh length in the 40 to 80 km range and therefore cannot simulate subgrid-scale cumulus activity directly. Thus schemes for determining the statistical effects of many

cumuli on large-scale systems, a procedure known as cumulus parameterization is used. Cumulus parameterizations combined with a method of handling larger scale non-convective precipitation makes up the precipitation parameterization of a modeled system.

As demonstrated in Kuo and Low-Nam (1990) the results produced by models can depend greatly on the precipitation parameterization. While this is not unexpected given the differences in the way various parameterizations handle moisture, the extreme variation in the model response to different storms using the same parameterizations is. As stated in Kuo and Low-Nam (1990) the removal of moisture and latent heating results in a much weaker (39% of actual final MSLP value) storm in their case 6, but had little influence (90% of actual final MSLP value) in their case 7. This clearly demonstrates that some storms are more dynamically forced and some are more diabatically driven. In fact model results from their case 7 storm were minimally different no matter what precipitation parameterization was used, while model results from their case 6 storm varied greatly as will be discussed in Chapter IV.

Smith et al. (1984) proposed that the various influences of LHR could be categorized as either "direct" or "indirect". A direct influence is one that immediately alters some property of an atmospheric system, while an indirect influence is one that changes some other variable which in turn forces a change in that property. In the case of numerical model studies, one can examine this through equations that explicitly contain LHR. The direct effect is given by terms in the equations that explicitly contain diabatic heating. Indirect influences are represented by the extent to which LHR affects the other terms in the equations. Determining these "indirect" influences requires that they be computed when LHR is active, and the results compared with computations made in the absence of LHR -- i.e., a model simulation with no LHR. Therefore a numerical comparison of model experiments where the LHR fields are changed can provide insight into both direct and

indirect effects. Four-dimensional visualization of the model results is a particularly effective tool in examining such model differences.

The generalized omega and diabatic omega equations used here are as presented by Pauley and Nieman (1992). Their scale analysis of the generalized omega equation revealed that it would simplify to the quasigeostrophic omega equation if higher-order terms in Rossby number are neglected. However, a typical, rapidly intensifying extratropical cyclone has large latent heating rates and a characteristic Rossby number approaching 0.5, leading to significant non-quasigeostrophic vertical motions. Pauley and Nieman's (1992) results show that substantial differences exist between the generalized and QG vertical motions as computed for a model simulation of the QE II storm. Part of these differences are due to additional terms in ω placed on the left-hand side of the generalized omega equation. They also state that the nonquasigeostrophic forcing provided by diabatic processes yields the greatest departure from QG theory in regions of ascent, with upward motions as great as -40 $\mu b\ s^{-1}$. Their computations confirmed the results of their scale analysis and yielded generalized vertical motions that compare well with both the model's own predicted vertical motions as well as satellite imagery. The Pauley and Nieman (1992) comparison is the basis for the further investigations in this thesis.

III. METHODOLOGY

A. Model Description

The data used in this thesis are model output from the National Center for Atmospheric Research/ Pennsylvania State University (NCAR/PSU) model (Anthes et al. 1987) that were originally described in Kuo and Low-Nam (1990). This model is a hydrostatic primitive-equation mesoscale model. The vertical coordinate is $\sigma=(p-p_t)/(p_s-p_t)$ where p is pressure, p_s is surface pressure, and p_t is the constant pressure at the top of the model (100 mb). For the experiments used in this research, there are 16 σ levels (0.00, 0.10, 0.20, 0.30, 0.40, 0.50, 0.60, 0.70, 0.78, 0.84, 0.89, 0.93, 0.96, 0.98, 0.99, 1.00), which give 15 layers of unequal thickness in which temperature, moisture, and wind components are defined. This provides for the highest resolution near the surface (σ=1.00). The computational domain (Fig. 3.1) contains a staggered array of 46x61 grid points on a Lambert conformal projection, spaced approximately 80 km apart.

The parameterization of the surface layer and planetary boundary layer (PBL) was originally developed by Blackadar (1979). In this scheme, vertical fluxes of heat, moisture, and momentum are calculated explicitly between layers. Under stable conditions, the turbulent fluxes are parameterized by a local Richardson number. In unstable regimes, vertical fluxes are modeled by mixing convective eddies originating at the surface with the environmental air in the PBL. The surface sensible and latent heat fluxes are formulated as functions of surface wind speed and stability parameters. Radiation is the driving force of the diabatic PBL and is made up of net short and long wave irradiances at the surface.

Experiments using three different precipitation parameterizations were run for each of the cases, along with an experiment which excluded latent heat release (LHR). In the first experiment (KUO), the cumulus parameterization and treatment of nonconvective

precipitation follow methods developed by Kuo (1974) and Anthes (1977). If a stability check indicates the possibility of convection, latent heat is released based on the vertically integrated moisture convergence in a column and an assumed vertical distribution of convective heating. The heating function takes a parabolic shape with the maximum located at the middle of the cloud layer. For the nonconvective precipitation, the excess water vapor over saturation (relative humidity $\geq$ 100%) is removed as rain and the corresponding latent heat is added in the thermodynamic equation. Evaporation in unsaturated layers is not allowed.

The second experiment (EXP) uses the so-called explicit scheme by Hsie et al. (1984). In this scheme, prognostic equations are included for water vapor, cloud water, and rain water. Simple microphysical parameterizations are included for condensation of water vapor, evaporation of cloud droplets, accretion of cloud droplets by raindrops, and autoconversion of cloud droplets to raindrops. The mass-weighted mean terminal velocity of raindrops is also parameterized. Therefore, evaporation of rainwater in unsaturated layers is explicitly considered. This scheme produces precipitation only when a grid point is saturated, and so the convective parameterization is bypassed when this option is activated.

In the third experiment, the Arakawa-Schubert (1974) scheme (AS) as modified by Grell et al. (1988) to include convective-scale downdrafts, is used to handle the convective precipitation. This scheme partitions the cumulus into cloud types, each characterized by a fractional entrainment rate. The vertical structure of the environment determines the cloud vertical mass flux, the cloud thermodynamic properties, and the height of zero buoyancy for each cloud type. The distribution of the vertical mass flux at the cloud base into cloud types is determined by large-scale dynamical and physical processes. The nonconvective precipitation parameterization remains the same as that of the KUO experiment.

In the fourth experiment (DRY), the latent heat of condensation is set to zero with water vapor treated as a passive variable. Consequently, the latent heat release associated with precipitation has no thermodynamic feedback to the model atmosphere.

B. Post Processing of Model Output

Since the NCAR/PSU model does not output the diabatic heating rates ($\dot{q}$) required for the diabatic omega calculation, a heat budget approach (Kuo and Anthes 1984) was used to estimate these heating rates. Terms in the σ-coordinate flux divergence form of the thermodynamic equation used in the model itself were computed from model output, with the temperature tendency estimated using a two-hour centered finite difference. A Shapiro (1975) filter was applied after the calculation of each term. The diabatic heating rate was then computed as a residual and therefore includes the effects of shortwave and longwave radiation, sensible heat flux, diffusion, and latent heat release, as well as errors in the heat budget calculation. Comparison of vertically integrated estimates of the diabatic heating with precipitation fields showed excellent agreement in placement and magnitude of maxima. However an anomalous heating/cooling couplet was found along the Appalachians in all four experiments for both cases. The source of this feature is not known; it does not correspond to precipitation and is the most prominant feature in the DRY experiments. Even so, the calculation was judged to be satisfactory as will be descussed in the results section.

The model isobaric vertical motion, ω, was computed from

$$\omega \equiv \frac{dp}{dt} = p^* \dot{\sigma} + \sigma \left[\frac{\partial p^*}{\partial t} + m \left(u \frac{\partial p^*}{\partial x} + v \frac{\partial p^*}{\partial y} \right) \right] \tag{3.1}$$

using σ-level model output, where m is the Lambert-conformal map factor, $\dot{\sigma}$ is the vertical motion in σ coordinates, and $p^* = (p_s - p_t)$. In this calculation, the surface pressure tendancy was computed kinematically as the vertical integral of divergence from the topmost to the bottommost σ levels. The vertical motion $\dot{\sigma}$ was also computed by vertically integrating divergence, but this time from the top model level where $\dot{\sigma}$ is defined as zero to the σ level of interest. All quantities were computed using the model's numerics.

Post-processing of the model output as well as the computed heating rate estimates and ω was performed to transform the data to a nonstaggered grid in isobaric coordinates. Values of the u and v wind components from the four momentum grid points surrounding a mass grid point were averaged to yield values coincident with all other quantities at mass grid points. Specific humidity was converted to relative humidity before the vertical interpolation, in order to avoid the supersaturation that can occur when specific humidity itself is interpolated. The quantities u, v, T, H, $\dot{q}$, RH, and ω on σ levels were then interpolated to pressure surfaces spaced 50 mb apart from 1050 to 100 mb using a linear in ln p approach. Where necessary, values were interpolated below the earth's surface using the standard atmospheric lapse rate (6.5°C/km) for temperature, and maintaining a constant specific humidity at the surface value, and setting all other quantities to zero. Finally, heights of the 20 pressure surfaces were computed from the hysometric equation using virtual temperature.

C. Diabatic Omega Calculation

In order to examine the influence of diabatic processes on the dynamics of these two storms, the component of the isobaric vertical motion resulting from diabatic processes was computed. The derivation and calculation of the resulting diabatic omega is described in the following section.

As shown by Pauley and Nieman (1992) a generalized omega equation can be written as

$$\nabla^2\sigma\omega + (\zeta+f)\frac{\partial^2\omega}{\partial p^2} - \left(\frac{\partial v}{\partial p}\frac{\partial^2\omega}{\partial x\partial p} - \frac{\partial u}{\partial p}\frac{\partial^2\omega}{\partial y\partial p}\right) - \left(\frac{\partial^2 v}{\partial p^2}\frac{\partial\omega}{\partial x} - \frac{\partial^2 u}{\partial p^2}\frac{\partial\omega}{\partial y}\right)$$

(LHS1) (LHS2) (T1) (T2)

$$-\omega\frac{\partial^2\zeta}{\partial p^2} - \frac{\beta}{f}\frac{\partial\sigma\omega}{\partial y} = \nabla^2\left(V\bullet\nabla\alpha\right) + \frac{\partial}{\partial p}\left[V\bullet\nabla\left(\zeta+f\right)\right] - \frac{R}{c_p p}\nabla^2\dot{q} \qquad (3.2)$$

(VA) (BE) (LTAD) (DVAD) (LDHT)

$$+\frac{\partial}{\partial p}\frac{\partial\zeta_{ag}}{\partial t} - \frac{\partial}{\partial p}\left(k\bullet\nabla\times F\right) - \frac{\beta}{f}\frac{\partial}{\partial y}\left(V\bullet\nabla\alpha - \frac{R}{c_p p}\dot{q}\right)$$

(AVTN) (FRIC) (BETA)

where the static stability parameter is defined as

$$\sigma \equiv \frac{-RT}{p\theta}\frac{\partial\theta}{\partial p}, \qquad (3.3)$$

and where F is the frictional force, ζ_{ag} is the ageostrophic relative vorticity, and other variables take their usual meanings. This form assumes only hydrostatic balance, which is required for the use of isobaric coordinates. The vertical motion computed from this equation can be thought of as the actual flow through pressure surfaces in a hydrostatic atmosphere.

The instantaneous contribution to the vertical motion by diabatic processes can be computed by using the diabatic term alone as forcing. Neglecting small left-hand-side terms, the diabatic omega equation can therefore be written in Lambert conformal coordinates as

$$m^2\nabla^2\sigma\omega+(\zeta+f)\frac{\partial^2\omega}{\partial p^2}=-m^2\frac{R}{C_p p}\nabla^2\dot{q} \qquad (3.4)$$

(LHS1) (LHS2) (LDHT)

Values of diabatic omega were calculated from (3.4) using centered second-order finite differencing in a relaxation procedure similar to that used by Pauley and Nieman (1992). A single pass of a Shapiro (1975) filter was applied to the diabatic heating field to remove noise prior to the calculation. Elliptical relaxation techniques will not handle negative values of the left-hand-side coefficients so both absolute vorticity and sigma were set to small positive values in these regions. These positive values were chosen to be in the

range of the smallest neighboring positive values so artificial gradients were minimized. Underrelaxation was then performed using a relaxation coefficient of .8 for all experiments.

Difficulty with convergence of the relaxation solution was encountered for the case 7 KUO and AS experiments. Close examination of the problem forecast times revealed that the difficulty was very strong vorticity gradients. To alleviate this problem progressive amounts of low-pass filtering were applied to the vorticity field prior to its introduction into the relaxation. Filtering was only applied at the times that caused the relaxation to fail; and filtering was added incrementally until the relaxation ran successfully. The case 7 AS experiment ran with three passes of a Shapiro (1975) filter on the vorticity field at forecast hour 8. The case 7 KUO experiment required two passes of the filter at forecast hour 22, 5 at forecast hour 18, 6 at forecast hour 19, and 7 at forecast hour 20. This low-pass filtering will affect the maximum and minimum diabatic omega values, thus making absolute comparisons between diabatic and model omegas more difficult. The filtering will also introduce some error into the comparisons between the case 7 AS and KUO experiments, as well as comparisons between these two experiments and the other experiments.

IV. SYNOPTIC DISCUSSION AND MODEL COMPARISON

This section will begin with an overview of the results from the two storms that Kuo and Low-Nam (1990) labeled cases 6 and 7. Then, a complete history of the two cases will be presented using the NMC North American surface analyses and NMC upper-air charts at 850, 500 and 300 mb compared with the NCAR/PSU model forecasts. The surface analyses will also be compared with surface marine data compiled by the ERICA data office. The systems will be examined together so that their development can be compared directly. For the purposes of this review, the upper-air discussion will commence 24 h prior to forecast initialization and the surface discussion will begin six hours prior. Surface conditions will be described every three hours, and upper-air conditions every twelve. Note that the locations of features discussed here are very subjective in nature. The model generated positions are based on grid point number which were subjectively converted to the nearest .1 latitude longitude point. Locations derived from the analyzed fields was even more subjective, since locating the center of the feature was sometimes very difficult in itself, then subjectively trying to determine the latitude and longitude of the point that was chosen.

A. Forecast Overview

The Kuo and Low-Nam (1990) cases 6 and 7 showed a dramatically different response to the four precipitation parameterizations used in the model experiments, as will be discussed below (Fig. 4.1). In general, the case 6 experiments varied widely with two weaker than the analysis and two more intense at most forecast times. The case 7 experiments produced results that were much more consistent. All experiments produced central pressures weaker than analyzed until the last hour of the model forecast.

Predicted positions of the system centers (not shown) were generally good with the exception of the DRY experiment in case 6. It is obvious from these results that the case 6 storm was much more sensitive to precipitation parameterization than case 7.

1. Case 6

Case 6 model output for the four parameterizations differed greatly when compared to the NMC final analysis (Fig. 4.1). As might be expected, the DRY experiment showed the least deepening, a total of only 13 mb compared to the analyzed deepening of 42 mb. The DRY case contrasted sharply with the other experiments, which generally did a much better job in forecasting intensity. All three of the other experiments showed too much deepening in the first 6 hours, with the EXP and AS schemes very similar to each other and remaining too deep until hour 20. The KUO parameterization showed too little deepening from hour six through the end of the period. At the end of the period all four of the experiments forecast the storm as leveling off in intensity when the actual case 6 storm was deepening rapidly. However, surface analyses after the period of the model forecasts showed that the case 6 system did temporarily stop intensifying, agreeing with the model trend, but then intensified again.

The case 6 positions (not shown) showed good agreement with each other for the various cases with the exception of the DRY experiment. The DRY positions consistently lagged behind the others. Comparisons between the model forecasts and the analyzed storm positions shows reasonable agreement, though the subjective nature of the analyses and subsequent plotting make the analyzed positions no more accurate than a grid point in any direction, and in some of the early positions even that accuracy is not obtained.

2. Case 7

The case 7 experiments are in marked contrast to those for case 6 (Fig 4.1). To be specific, the experiments have quite uniform results. The KUO and DRY central pressures differ from each other by no more than 2 mb, while the AS and EXP differ by less than 1 mb through the first 20 h of the forecast, with a maximum difference of just over 2 mb. There is less than 3 mb difference between all four experiments at the 12 h forecast. Before the final forecast hours the model intensities are all weaker than analyzed; during the final hours the AS scheme is the only one more intense. The data clearly show that all of the experiments are intensifying the storm more rapidly at the end of the model forecast than the analyses which show that the system starts to rapidly fill after the model period.

Model forecasts and analyses of storm positions (not shown) showed good agreement, both among the experiments and with the analyses. The DRY experiment again showed the only unusual movement, in this case a westward movement in the first forecast hour. By the second forecast hour however, it was located within a grid point of the other experiments. The forecasts showed slightly better agreement with the analyses than in the case 6 results, but the same positioning caveat applies.

B. Conditions Prior to Model Initialization

1. Structure aloft 24 hours prior to model initialization

At 1200 UTC 5 Jan 1983 and 0000 UTC 4 Jan 1985 the case 6 and case 7 systems, respectively, showed considerable differences aloft. To the west of where the case 6 surface cyclone developed, a broad trough was evident at all levels (roughly oriented from the Upper Midwest through Texas), as shown in Figs. 4.2 a, b and c. This trough provided the upper-air support for the surface low in question which deepened rapidly as the upper-level trough crossed the East Coast. The surface cyclone will be associated with

the 850 mb trough off the Florida-Georgia coast at this time. Two jet streams were present. The northern branch extended along the U.S.-Canada border and dipped into western Nebraska with a break at the trough axis and continuing from Indiana northeast into Canada and Maine (Fig. 4.2c). The southern jet was centered just south of Texas, extending through central Florida and continuing east-northeast. The right-rear quadrant of the northern jet streak and the left-front quadrant of the Texas jet streak both will be seen to play a role in the development of the case 6 surface cyclone. The 850 mb temperature field (Fig. 4.2a) indicated warm air advection over the eastern U.S. and over the Plains States, which would aide ridging in these locations.

At this time case 7 had a cut-off low at all levels of the atmosphere, located over northern Alabama/Mississippi at 850 mb (Fig. 4.3a). The low center tilted sharply westward with height to a position over southeastern Oklahoma at 500 mb (Fig. 4.3b), where it was also located at 300 mb (Fig. 4.3c). There was an upstream shortwave at all three levels moving southeast out of Manitoba, though it was very weak at 300 mb. In this case, the upper-air support for the surface cyclone is provided by the phasing of the shortwave with the cut-off low and the transformation of the cutoff into an open wave. The 850 mb temperature field at this time mirrored the 500 mb height field. Immediately to the west of the 850 mb low there was a pocket of cold air located under the upper-level low, while further upstream centered over the Montana-North Dakota border there was a pocket of warm air. This created warm air advection northwest of the low, and cold air advection south of the low, which would help propagate the upper-level trough eastward. There was little temperature advection east of the low.

The jet stream pattern was similar to case 6 in that there were two jet streams over the central U.S. In case 7, however, the northern branch was much further north than in case 6, not dropping south of the U.S.-Canada border until the eastern Great Lakes (Fig.

4.3c.). The southern jet maximized along the Gulf Coast and turned northeastward up the coast, where it joined the northern jet to yield winds greater than 70 m s^{-1} extending eastward. In summary the major differences between the two cases were the open trough versus closed low center aloft, and the positioning of the jet and its resultant divergence aloft.

2. Structure aloft 12 hours prior to model initialization

At 0000 UTC 6 Jan 1983, the case 6 system showed large changes over the preceding 12 hours,while the case 7 system showed only minor changes over the 12 hour preceding 1200 UTC 4 Jan 1985. In case 6, the 850 mb trough over the Upper Midwest had flattened out, but there was evidence of a low center forming off the North Carolina coast associated with the northward propagating trough seen earlier (Fig. 4.4a). At 500 mb there was little amplification of the primary trough, but it slid eastward to a position where its axis was from the western Great Lakes south through Alabama/Mississippi (Fig. 4.4b). The trough is still too far upstream to have much influence on the incipient cyclogenesis, however. At 300 mb the trough and jet stream pattern had moved east with the 300 mb trough located almost directly above the 500 mb trough (Fig. 4.4c). Thus the upper part of the system was almost vertically stacked, with the newly developing low at 850 mb further east than the rest of the system. In addition, the exit region of the southern jet streak had propagated around the base of the trough to a position just south of the entrance to the eastern branch of the northern jet steak, providing a likely area of strong divergence aloft over the area where the 850 mb low was developing. The temperature advection at 850 mb remained about the same. The position of the troughs and location and orientation of the jet streaks indicate that there is strong support for the development of a surface low off the North Carolina coast, as the whole system was moving east toward the ocean.

In case 7, the 850 mb center had moved slightly north and deepened by 50 meters during this 12-h period (Fig. 4.5a), while the upstream short wave moved eastward until it was nearly in phase with the cut-off low at all levels. The temperature field remained about the same, with warm air advection northwest of the low center and cold air advection to its south. The 500 mb center moved east to a position almost directly over the 850 mb center and deepened 40 meters as it became more elongated (Fig. 4.5b). The jet streak south of the cutoff 12 h earlier increased in maximum velocity to 75 m s^{-1} and started to wrap around the cut-off low at this time (Fig. 4.5c) merging with the northern jet over the New England States. The 300 mb center had no change in height, and had moved east until just west of the 500 mb center. Like the 500 mb low center, the 300 mb center is becoming elongated, rather that circular. At this time the system was almost vertically stacked, with only a slight westward tilt.

At this time the case 6 system, and its jet streak exit/entrance configuration appears to be much more conducive to cyclogenesis than the case 7 system. However, elongation of the cutoff in system 7 is apparent at 500 and 300 mb, an indication that change is on the way.

3. Surface features 6 hours prior to model initialization

At 0600 UTC 6 Jan 1983, the case 6 surface cyclone was a 1009 mb closed low just off the North Carolina coast near 35°N 73°W (Fig. 4.6a). The surface analysis showed a well developed frontal cyclone with a warm front extending eastward and a cold front extending south and then southwest towards western Cuba. A trough extended north from the low along the New England coast, likely indicating a coastal front. The marine data (not shown) indicated that the system had surface winds in the 10-13 m s^{-1} range, both

near the center and along the cold front. Surface temperatures were about 14°C ahead of the warm front, about 20°C in the warm sector, and 13°-17°C behind the cold front.

On the other hand, the case 7 surface cyclone was a 1002 mb closed low at 1800 UTC 4 Jan 1985 located off the South Carolina coast near 33°N 76°W (Fig. 4.6b). A second weaker low of 1006 mb is located further northeast near 37°N and 70°W. However, little surface reflection of the upper-level cut-off low is apparent. The surface analysis at that time showed a stationary front extending northeast to the weaker low with a warm front continuing northeast from there. A cold front extends south from the stronger low. The marine data show that the system had surface winds of approximately 10 m s^{-1} near the center of the system and winds to 15 m s^{-1} on either side of the cold front. Surface temperatures were about 12°C ahead of the warm front, about 21-23°C in the warm sector, and 18-20°C immediately behind the cold front, decreasing toward the coast.

At this time the case 6 surface cyclone is 7 mb weaker than the case 7 surface cyclone; however, the case 6 cyclone is much more compact and has higher surface winds. Though this time is between the upper-air analyses, a quick extrapolation shows that both surface systems are developing downstream of 500 mb troughs. Both are also in the general area of jet streak exit regions, though their exact orientation with respect to those streaks is unknown. The case 6 system does appear to be in the more favorable left quadrant of the exit region, while the case 7 system appears to be more toward the right quadrant of the exit region.

4. Surface features 3 hours prior to model initialization

The case 6 surface analysis for 0900 UTC 6 Jan 1983 shows that the low had deepened to 1006 mb and had moved approximately 250 km northeast, to a position off the

central Virginia coast (Fig. 4.7a). The general features of the low remained the same. Useful marine data were not available for this time period.

The case 7 surface low was analyzed at 2100 UTC 4 Jan 1985 as an elongated closed low with two 1001 mb centers at 35°N 75°W and 37.5°N 70°W and a third 1001 mb center over West Virginia (Fig. 4.7b). The southern low center moved north while the northern center remained stationary, such that the lows were about 470 km apart. Again, useful marine data were not available.

C. Observed and Predicted Conditions During the Model Forecast Period

1. Model initialization

a. Case 6 synoptic situation

At 1200 UTC 6 Jan 1983 the case 6 surface low was analyzed with little change in strength or structure during the previous 3 h, remaining at 1006 mb with the same trough and frontal features. It had continued moving northeastward at approximately 12 m s^{-1} to a position near 38.5°N 70°W (Fig. 4.8a). The frontal boundaries were clearly defined in the surface marine data (not shown) with winds reported at 15 m s^{-1} in the vicinity of the center and along both the cold and warm fronts. The surface data also clearly defined the trailing trough, with winds of approximately 8 m s^{-1}. Temperatures were 12-15°C ahead of the warm front, 20°C in the warm sector, and 15-18°C immediately behind the cold front dropping to 11-12°C behind the trailing trough.

At 850 mb a low had formed in the northward propagating trough and was located off the southern New Jersey coast. This low was bringing cold air southward from the Great Lakes and warm air northward off the Atlantic coast (Fig. 4.8b), creating a southwest/northeast orientation of the isotherms across the East Coast and providing for deepening of the 500 mb trough to the west. At 500 mb the trough sharpened and continued to move eastward, with the axis located from the eastern Great

Lakes through South Carolina (Fig. 4.8c). The jet streaks at 300 mb maintained their relationship with the trough yielding upper-level divergence that was also well positioned to support surface cyclone development. The whole 300 mb system had moved east and was just slightly west of the 500 mb trough (Fig. 4.8d). The exit/entrance region overlap of the two jet streaks was very evident over the surface cyclone.

b. Case 6 model results

The case 6 model initial fields were very similar to the analyses in the area of the Atlantic cyclone (Fig. 4.10a-d). The surface low was centered near 38.6°N and 69.9°W, with a central pressure of 1004.7 mb, roughly 1 mb deeper than analyzed. Though not well defined, there are indications of the surface warm and cold front in the proper locations. At 850 and 500 mb the analysis and model initial fields also agree well. It is interesting to note that little PVA at 500 mb exists in the vicinity of the surface low center; the strongest PVA is still well west. However, at 300 mb there are some differences in the speed fields. Both the analysis and model fields show a weakening in the jet off the Mid-Atlantic states, though the model has much smaller wind speeds in that area. Model winds decrease below 30 m s^{-1} (60 kts) while the analysis maintains the winds at above 35 m s^{-1} (70 kts). The wind speed gradient difference in this location is significant since it is over the surface low, and the stronger model gradient indicates a potential for greater deepening via enhanced forcing in the exit/entrance regions of the jet streak. In addition, the maximum wind speeds associated with the downstream jet streak also appear to be underestimated in the model initial fields. Observations plotted on the NMC analysis depict 50 m s^{-1} (100 kts) winds as far south as Portland, Maine and extending across Newfoundland and the North Atlantic to at least 35°W.

c. Case 7 synoptic situation

The case 7 surface analysis at 0000 UTC 05 Jan 1985 showed that the three-low system became almost stationary. The southern low continued to deepen 3 mb to 998 mb, while the northern low remained weak and only deepened one mb to 1000 mb (4.10a). The western low filled 3 mb to 1004 mb. The frontal features also remained about the same. The surface marine data (not shown) clearly showed the warm and cold fronts. Ahead of the warm front there were northeasterly 5-10 m s^{-1} winds, there was a broad area of southwesterly 10-15 m s^{-1} winds in the warm sector, and behind the cold front the winds were west to northwest at 10-15 m s^{-1}. A second surface low center located almost due north of the case 7 system near 50°N 70°W (north of Maine) has moved close enough that the 1008 mb isobar now closes off both systems. This system has an associated cold front arcing down through the Great Lakes and back north into Canada.

The closed low center that existed at 850 mb 12 h earlier, weakened as the upper-level cut-off low began to lift out and now appears as the southern extent of a deep trough approaching the eastern seaboard (Fig. 4.10b). The short wave trough evident earlier moved into phase with the former cut-off low in the process. The trough at this time extended south from an 850 mb low center just east of Hudson Bay, dominating the eastern third of the U.S. A residual pocket of cold air remained over Alabama just west of the base of the trough. The changes in the 850 mb trough greatly increased cold air advection at the base of the trough. The result was a tightened temperature gradient over the southeastern seaboard and strong 500 mb height falls over the Carolinas. At 500 mb the low center deepened 20 meters and moved east at about 5 m s^{-1} (Fig. 4.10c) to a position just north of the 850 mb cold pocket. The center itself is no longer cut off as the trough to the north has built southward, and there is no longer a closed contour around the low.

During this same time, the 300 mb low center has moved slowly northeast and deepened by 20 meters (Fig. 4.10d). Though still a cut-off system, the trough to the north has also dug southward, and a 300 mb trough now extends from the Canadian Archipelago south through the eastern U.S. and southwestward through southern Texas. The northern section of the jet stream has a break at the trough axis, while the southern section has elongated downstream along the U.S. East Coast. The deeper of the two surface cyclones is located downstream of the almost vertically stacked trough axis and is on the equatorward edge of the main jet streak.

d. Case 7 model results

The case 7 model initial fields were overall very close to the analyses though some differences were present (Fig. 4.11a-d). The initialized surface low was centered near 35.3°N and 74.0°W, with a central pressure of 999.3 mb, 1 mb higher than observed. No evidence was seen of the weak low center just north of the primary low, but a hint of the center over West Virginia was present. The low center north of Maine was analyzed at 1000 mb, 2 mb weaker than observed. Troughing to the east and south of the low center suggested frontal positions similar to observed.

The fields aloft were also in good agreement. At 850 the model and NMC analyses were very close in their depiction of the position and structure of the trough and cold pocket. The 500 mb low center position was close to the observed, although the minimum height was 20 m higher than observed. The col north of the cut-off low was analyzed at a higher height than in the NMC analysis, but the Dayton and Pittsburgh rawinsonde observations of 547 dm support the higher values. As in case 6, little PVA is depicted over the surface low. At 300 mb the height fields and main jet off the East Coast are very similar, but the model intensity of the jet along the west coast of Hudson Bay is

much weaker, with a 30 m s^{-1} maximum positioned where the observed winds range between 50 and 60 m s^{-1}. The source of this gross underestimation in the model initial field is not known.

The main differences between the two cases noted at this time is the lower heights and much stronger curvature of the case 7 upper-level trough. This is associated with colder air over the Southeastern U. S. and a much stronger temperature gradient ahead of the trough in case 7. Although the two 500 mb trough axes are located at approximately the same longitude over Ontario, the neutral tilt in case 6 and positive tilt in case 7 leads to the case 7 trough being considerably inland from the case 6 trough over the southeastern U.S. Both surface systems are ahead of the area of strong positive vorticity advection aloft, but the case 6 cyclone is in a more favorable position for jet streak forcing at this time. The model initializations generally agree well with their respective cases, but the initial fields have different errors in each case. The case 6 low is overestimating the alongstream jet streak gradient (underestimating the speed over the surface low), and the case 7 initialization is missing the second surface low and grossly underestimating the jet streak near the Hudson Bay.

2. 3 hour forecast

a. Case 6 synoptic situation

The case 6 surface low had deepened 1 mb over the previous 3 hours and at 1500 UTC 6 Jan 1983 was moving northeast at 18 m s^{-1}. At this time it had a central pressure of 1005 mb and was located just southeast of Cape Cod. The orientation of the frontal features remained the same (Fig. 4.12).

b. Case 6 model results

The AS, EXP, and KUO experiments were all quite similar to each other in their sea-level pressure fields (Fig. 4.13a-d). Central pressures were all between 998 and 999 mb, and the low centers were located in the same position. In contrast the DRY experiment, although in the same location, was 4 mb weaker than the other experiments. At this time all of the experiments have deepened the storm more than observed and placed the center 500 km too far east. However the NMC surface analysis has few ship observations plotted, casting some doubt on its accuracy. All of the experiments except the EXP show a broad area of precipitation near the center of the main low, as well as in the trough to the north. In contrast the EXP experiment showed smaller amounts of rainfall only in the immediate vicinity of the low.

c. Case 7 synoptic situation

The case 7 surface low started to deepen rapidly and coalesced into a single low (Fig. 4.14) by 0300 UTC 5 Jan 1985. It reached a central pressure of 990 mb, an analyzed deepening rate of 8 mb in 3 hours. The combined low was located about 145 km off the central Virginia coast, roughly 180 km north of where the southern low was, and 180 km west of where the eastern low was. The second low, north of New England, has not changed in intensity and has moved east slowly. The cold front associated with this low is pushing south into upstate New York. Significant maritime data were not available for this time period.

The case 7 system has now commenced "explosive" deepening despite appearing to have much less upper-level support than case 6 only 3 hours earlier.

d. Case 7 model results

The output from the various experiments was quite similar with respect to the SLP fields and minimum pressures, however the location of the surface low in the DRY experiment departs from the other three (Fig. 4.15a-d). The DRY low was located very near the analyzed low, while the positions generated by the other experiments were well to the east. None of the experiments deepened the system enough; the four forecast cyclones were 6-7 mb too weak. The precipitation fields varied widely between the experiments. The KUO and DRY experiments had very similar broad precipitation fields with a central maximum. The AS experiment is similar though with less precipitation. The EXP case shows a very small area of precipitation and a smaller maximum value as in case 6. The shift in location of the model lows from the DRY position closer to the coast to the EXP, KUO, and AS positions coincident with their precipitation maxima further east provides considerable evidence of the effect LHR has on this system.

3. 6 hour forecast

a. Case 6 synoptic situation

By 1800 UTC 6 Jan 1983, the case 6 surface low had also started to deepen explosively. At this time the central pressure was 998 mb, an intensification of 7 mb in 3 hours (Fig. 4.16). The low had changed direction and was moving east, slowing slightly to about 16 m s^{-1}. The warm front extended southeast from the low, with the cold front maintaining its southward orientation. A new trough was analyzed running northeast from the surface center, while the previous trough (coastal front) dissipated as the required cross-coastal flow became along-coast under the influence of the strengthening low. Surface maritime data (not shown) was sparse in the area of the system center and warm

front, but showed 15 m s^{-1} winds across the cold front to the south and generally the same speeds across the trough. Temperature contrasts were 6°C across the trough, and about 4°C across the cold front. The maritime data also suggested that either the cold front was analyzed almost 5° too far east, or that a strong secondary trough existed behind the main front. A strong pressure gradient was developing between the cyclone center and a 1042 mb high located to its east near 39°N 42°W.

b. Case 6 model results

At the 6-h forecast, the model sea-level pressure fields were diverging from each other and from the analysis. The AS and EXP results were similar and had overdeveloped the surface low by 10 mb with a central pressure of 988 mb (Fig. 4.17a, b). Their low center locations were in good agreement with the analysis, and both showed a distinct cold front with little evidence of a warm front. Also of note was the difference in the precipitation pattern between the AS and EXP experiments. The AS experiment showed very broad areas of precipitation around not only the main low, but within nearly the entire region affected by the storm's cyclonic circulation. The EXP experiment had considerably less precipitation associated with it, both in amount and areal coverage. In contrast, the KUO experiment had a central pressure of 992 mb, closer to the analysis but still 6 mb too deep, and again the location is good (Fig. 4.17c) The precipitation associated with the KUO experiment was more like the AS experiment than the EXP. At this time the DRY experiment was the closest to the analysis with its central pressure of 1001 mb, but the model result was 3 mb too weak, and the location was slightly to the south and west of the analysis and the other model locations (Fig. 4.17d). The DRY experiment was 13 mb weaker than the AS and EXP cases, however it had a

precipitation field similar to the AS and KUO experiments but with less precipitation in the center of the cyclone system.

A comparison of the model upper-air results showed results similar to the surface results. At 850 mb the AS and EXP (Fig. 4.18a, b) experiments had very similar height fields, with a 6 m difference in the central height of the main low. The temperature fields were almost identical. Again the KUO field depicted a weaker cyclone (Fig. 4.18c), with the central height 47 m higher than the AS, though the temperature field compared well with the others. The DRY case had the weakest cyclone, with a central height just over 100 m higher than the AS (Fig. 4.18d). The DRY temperature field was similar to the others except immediately southeast of the 850 mb low, where the DRY temperatures were cooler. The 500 mb height fields were similar in all four cases (Fig. 4.19a-d). The main difference was over the surface low, where small-scale perturbations in the height field existed in the AS, EXP, and KUO experiments. The perturbations were strongest in the EXP case and were absent in the DRY case. The perturbations were also associated with differences in the vorticity fields. The EXP experiment showed the strongest vorticity in the vicinity of the surface low with a value of >20 (10^{-5} sec^{-1}). The AS vorticity perturbations were somewhat weaker with several areas at greater than 16 units, the KUO experiment showed slightly less vorticity (one area >16 units), and the DRY case portrayed only a broad area of >12 units.

At 300 mb the height fields were quite similar with the exception of perturbations over the area of the surface low (Fig. 4.20a-d). Again the perturbation was the greatest in the EXP experiment, smaller in the AS and KUO experiments, and absent in the DRY experiment. On the other hand, the speed fields are quite similar; all showed the low under the left-front quadrant of the upstream jet streak and the right-rear quadrant of the downstream jet streak.

c. Case 7 synoptic situation

The case 7 surface low only deepened 1 mb to 989 in this three-hour period ending at 0600 UTC 5 Jan 1985, according to both the standard NMC surface analysis (Fig. 4.21), and the NMC "final" analysis. Analysis problems at the intermediate time with this rapidly intensifying cyclone are suspected, since a sum of the deepening rates over the past two 3-hour periods would be 9 mb/6 h, a very rapid deepening rate. System motion was generally east-northeast at 22 m s^{-1}, and the system center appeared to be moving along the warm front which now extended northeast from the low. The cold front still extended to the south. The low north of Maine moved east and deepened 1 mb. Its associated cold front moved rapidly east across the Mid-Atlantic States and is located from eastern Maine south through Massachusetts and east through Pennsylvania. This put the front about 320 km northwest of the case 7 system. The surface maritime data reflected the increasing strength of the case 7 system. Winds north of the warm front were on the order of 8 m s^{-1} but had increased in the warm sector to 18 to 20 m s^{-1}. Winds behind the cold front had also increased, with reports to 20 m s^{-1}. Temperatures across the warm front showed values from about 20°C south of the front to 7-8°C north of the front over the open ocean. Across the cold front, the temperatures ranged from 21°C ahead of the front to 16-18°C immediately behind the front, decreasing to 7°C just off the coast.

d. Case 7 model results

At this forecast time the experiments showed some variety, but within the same overall pressure pattern (Fig. 4.22a-d). Central pressures ranged from 991 mb in the AS experiment to 993 mb in the DRY experiment, only a few millibars weaker than the analyzed 989 mb. The positions in the EXP and KUO experiments were virtually

identical to the observed, with the DRY position roughly 150 km to the northeast and the AS nearly 800 km to the east. The latter position was collocated with the precipitation maximum and seemed to result from the strong LHR in that region. Both a warm and a cold front were implied in the sea level pressure field in all of the experiments, though the features were less distinct in the DRY experiment. The warm and cold frontal pattern generally agreed with the analyses, though the analyzed warm front initially ran northeast out of the surface low, then curved to the southeast, while the model experiments all have the warm front extending directly eastward. All of the experiments also showed a trough extending westward out of the low center across the Maryland coast, though again this feature was weaker in the DRY case. The experiments also showed an area of strong precipitation to the east of the observed surface low. As in case 6, the AS, KUO, and DRY precipitation fields are similar in areal coverage, though the DRY field does not have as strong a maximum. The EXP experiment has a much smaller precipitation field in extent, though almost as large in magnitude as the others in areas of significant rainfall.

At 850 mb, the height fields were generally similar, though the DRY experiment lacks the small-scale perturbations evident in the other fields (Fig. 4.23a-d). The other three experiments all have perturbations in the height fields in the area of the previously mentioned precipitation maximum. As for case 6, the perturbation is the sharpest in the EXP experiment and weakest in the KUO experiment. Perturbations also exist along the main trough, particularly along the 1290 m contour which extends farther south in the experiments which incorporate LHR. The temperature fields were very similar, though the DRY field was smoother than the others.

At 500 mb, the closed low evident at initialization had become a very sharp trough extending along the eastern seaboard (Fig. 4.24a-d). This trough was very similar in all four experiments, as is the vorticity maximum associated with it. Differences

in the height field at this time were again collocated with the area of heavy precipitation located to the east of the surface low. There was considerable vorticity associated with this feature in the EXP experiment with a maximum of more than 16 units. As before the vorticity anomaly was smaller in the AS and KUO experiments, and absent in the DRY.

At 300 mb both height and speed fields were virtually identical in the four experiments with the exception near the area of the precipitation maximum (Fig. 4.25a-d). Major perturbations in both the height and speed fields were evident in the EXP experiment as a small-scale ridge and a windspeed minimum. Slightly smaller perturbations were evident in the AS experiment, with only minor changes in the KUO experiment. The DRY fields were essentially smooth.

During this period both systems were undergoing explosive deepening. At this stage the case 7 storm is 8 mb deeper and is about 335 km southwest of the case 6 storm with a position off the coast of Virginia for case 7 versus southeast of Cape Cod for case 6. Case 7 also had a cold front rapidly approaching the center of the system from the northwest, while case 6 was likely only being influenced by the 1042 mb high to its east. A comparison of the forecasts is beginning to show some substantial differences; specifically the case 7 surface low position forecasts show the effects of strong LHR that are not seen in case 6. The LHR effects also show up as perturbations in all of the fields aloft with the exception of the DRY forecasts. However, these forecast perturbations caused by the various parameterizations are not strongly affecting the intensity of the surface cyclone. This is in marked contrast with the case 6 system where the parameterization makes a great difference in the surface cyclone intensity but there are fewer LHR-induced perturbations. The precipitation fields forecast by the two cases show a striking similarity in the reduced precipitation extent in the EXP case.

4. 9 hour forecast

a. Case 6 synoptic situation

The case 6 low had deepened 10 mb in the 3 hours prior to 2100 UTC 6 Jan 1983, to an analyzed central pressure of 988 mb (Fig. 4.26). The center of the low was now moving almost northeast at an estimated 18 m s^{-1}, very different from the slower easterly movement of the preceding 3 hours, although this could be an artifact of the analysis in this data sparse region. Overall motion appeared to be along the existing trough that extended to the northeast. The current movement was possibly due to the effect of the high to the east forcing the system northeast to its position well offshore due east of Cape Cod. The system had occluded during this 3 h period, with the point of occlusion located approximately 500 km south-southeast of the system center. Useful maritime data were not available for this time period.

b. Case 6 model results

The pressure fields and central pressures in the AS and EXP experiments were quite similar and continued to diverge from the KUO and DRY experiments (Fig. 4.27a-d). The AS and EXP experiments have central pressures of 980 mb, 8 mb deeper than the analyzed system, but the isobars and the location of the low centers compared well with the analysis. The AS and EXP experiments handled the cold front well and also showed the presence of the trough that was noted behind the front in the maritime data three hours earlier. This trough is not noted in the present analysis. There is some indication of a warm front extending southeast from the low in both experiments, though it is more evident in the AS case, particularly in the precipitation maximum southeast of the surface low. Both experiments also show troughing extending northeast from the low, and this compares well with the analysis.

The KUO experiment was similar to the AS and EXP cases in the overall pressure field, although its central pressure of 989 mb was only 1 mb higher than the analysis. It depicted the warm and cold fronts and the trough to the northeast, but not the secondary trough behind the cold front. The DRY experiment underintensified the system by 10 mb with a central pressure of 998 mb; this was also reflected in a very smooth pressure field. There was only the slightest hint of the cold front and no evidence of the warm front. The only obvious feature was the trough extending to the northeast.

As before, the AS, KUO, and DRY experiments had the same very extensive precipitation field, though the amounts in the center of the DRY cyclone were less than the others. The EXP experiment had a much smaller precipitation field in extent, which is concentrated around the low and along the cold front and the trough extending to the northeast. However, the maximum precipitation is comparable to the other experiments.

c. Case 7 synoptic situation

The case 7 system deepened very rapidly over the 3 h prior to 0900 UTC 5 Jan 1985-- 7 mb compared to 1 mb during the previous 3 h and 8 mb in the 3 h before that (Fig. 4.28). This gave an analyzed deepening of 16 mb in 9 hours, with the rapid fluctuations likely due to the analysis difficulties. The low moved northeast at about 26 m s^{-1} along the warm front which is also oriented northeast from the low center. The current location of the center of the system was about 40.5°N 68°W. The cold front still extended south and the system had not yet occluded. The second low center and cold front approaching from the northwest continued to close on the center of the case 7 system, with the cold front about 175 km to the northwest. Significant maritime data were not available for this time period.

d. Case 7 model results

The 9 h forecasts for the four experiments show considerable diversity in the location of the surface low, though their central pressures were within 1 mb at 989-990 mb (Fig. 4.29a-d). However, that central pressure is 7 mb weaker than analyzed. The EXP, KUO and DRY experiments had the low near the location of the analyzed low, but all are slightly too far south. In contrast, the AS low was about 7° too far east and was again collocated with the precipitation maximum. All four experiments indicated a strong warm frontal trough roughly eastward from the low center, with the DRY case having the weakest trough. There was little to indicate the exact location of the cold front in any of the experiments, though there was a very distinct trough running southwestward from the low over the southeastern U. S. in all of the forecasts and in the analysis as well. None of the experiments was depicting the 998 low that was analyzed north of Maine, although all four portrayed a trough in this region. As before the overall precipitation fields were similar,with the exception of the EXP field which has a much smaller area of precipitation, though the area of maximum precipitation is about the same. The only difference in the precipitation maximum is in the DRY case where there is a reduced maximum.

At this point , the case 7 storm was still deeper than case 6 by 6 mb; however this was a reduction in the difference between the two from 8 mb 3 hours earlier. The case 6 system was occluded with the warm front well south of the low center and a very strong pressure gradient to the east of the low. The case 7 system lacked an analyzed occlusion at this stage despite being a deeper system. In addition, a very strong pressure gradient to the east does not exist. The spatial separation of the two surface lows at this development stage is 415 km with the case 7 system moving much slower than the case 6

system. The major external influences are the high pressure to the east of the case 6 system and the cold front approaching the case 7 system from the northeast. The model comparison remains about the same as 3 h previous. The diabatic heating in case 7 continues to drive the perturbations noted at all levels. It is also obvious that there is some dynamic forcing at work deepening the main case 7 cyclone. While the case 7 low is deepening dynamically, which none of the models is sufficiently reproducing, the more strongly diabatic deepening in case 6 is causing forecasts that are either too intense or too weak.

5. 12 hour forecast

a. Case 6 synoptic situation

The case 6 low continued to deepen with a central pressure of 980 mb at 0000 UTC 7 Jan 1983, an 8 mb decrease in 3 hours. During this period the system was moving northeast at 22 m s^{-1}, much slower than in the preceding 3 hours, and was located off the southeast coast of Nova Scotia near 43°N 59°W. The occluded front extended south from the low with the warm front extending southeast and the cold front continuing to the southwest (Fig. 4.30a). The trough that extended to the northeast had rotated cyclonically around the storm and now extended north-northeast from the center. The high pressure to the east remained stationary, yielding a considerable increase in the pressure gradient between the two systems as they move closer and the low deepens. Surface winds have increased to greater than 25 m s^{-1} west of the storm with no reports to the east in the area of the very tight gradient. A very strong wind shift is evident across the trough extending to the northeast.

The 850 mb analysis showed that the low center that formed at 850 mb off the New Jersey coast had moved up the coast and deepened to a minimum height of

1250 m (Fig. 4.30.b). At this time, the 850 mb low was nearly above the surface low southeast of Nova Scotia . There was extensive cold air advection west of the low and warm air advection to its east. The isotherms were now running southwest/northeast parallel to the U.S. East Coast, in the classic "S"-shaped pattern. The 500 mb analysis showed that the trough axis had moved east and was located off the East Coast (Fig. 4.30c). The main trough had flattened out, and two distinct shortwaves were easily identified. The easternmost edge of the trough was located just west of the surface low. The jet streaks at 300 mb maintained their orientation with respect to the surface cyclone and moved east with the system (Fig. 4.30d). The jet streaks upstream and downstream of the surface low had both increased in magnitude. The surface low was located mid-way between the entrance region of the upstream jet and exit region of the downstream jet which provided strong divergence aloft.

b. Case 6 model results

The sea level pressure fields continued the pattern from before. The AS and EXP experiments had similar results; they had forecast the surface low at almost the same position and central pressure (Fig. 4.31a-d). Their central pressure of 974 mb was 7 mb deeper than the analysis. The forecasts clearly defined the cold front, and a trough extending to the northeast from the low, in good agreement with the analysis. However, the forecasts did not show a surface warm front. The EXP experiment also clearly delineates a trough behind the cold front. The KUO and DRY experiments were much weaker than the other forecasts -- the KUO forecast was 8 mb weaker than the analysis and the DRY case was 17 mb too weak. Both the KUO and DRY experiments depicted the cold front, but the DRY experiment did not show the northeast trough. Neither of these experiments show the warm front either. The KUO low center was

located to the east of the AS and EXP positions and was slightly closer to the analyzed position than the AS and EXP. The DRY center was well to the southwest of the other centers. The precipitation fields also had the same pattern as before. The EXP experiment had a much smaller areal extent than the others, and the DRY case, while having a large extent had reduced intensities as compared to the other experiments.

The 850 mb height patterns were a reflection of the sea level pressure patterns (Fig. 4.32a-d). The AS and EXP cases had the lowest heights, which were about 100 m deeper than the analyzed height. In these two experiments, the general location of the height minimum as well as the contour pattern agreed very well with the analysis; however the EXP experiment showed some perturbations in the height field to the south of the low over the surface cold front. The KUO forecast also provided a good location of the height minimum, with a value that was only 6 m too low. The DRY experiment forecast put the height minimum to the west of the other forecast lows and the analyzed low, with a minimum value almost 100 m too shallow. The AS, EXP, and KUO experiments showed similar temperature fields, with the exception of some perturbations south of the low in the EXP experiment. These three forecasts agreed well with the analysis. The DRY case had a similar overall temperature field except immediately southeast of the low, where it is much smoother and colder.

The 500 mb height fields were quite similar in all four experiments, with the exception of the shortwave trough in the area of the surface low (Fig. 4.33a-d). In the AS and EXP experiments, this trough had a closed circulation which was associated with a 44 unit vorticity maximum located just north of the surface low. In the KUO case, a prominent trough was also present, but without a closed circulation and with a weaker vorticity maximum (32 units). In the DRY case, there was neither an enhanced trough nor a vorticity maximum. The KUO trough was closest to the analyzed, though the 40 kts

wind, 542 dm height, and 140 m height fall at Sable Island suggest a deeper trough than analyzed. The vorticity field also showed a prominent small-scale minimum southeast of the maximum in the AS and EXP experiments and other small-scale perturbations further to the south in the EXP experiment.

The AS, EXP, and KUO 300 mb height fields were very similar and differed from the DRY primarily in enhanced ridging over New Brunswick (Fig. 4.34a-d). All four forecasts had very similar speed forecasts with respect to jet location, however the northern jet streak in the AS, EXP, and KUO experiments was much stronger than the DRY case, and this northern section of the jet had significantly increased in intensity in the past 6 h. The AS, EXP and KUO forecasts also portrayed a weakening of the windspeeds in the vicinity of the enhanced ridging and in the exit region of the upstream jet streak, compared to the DRY forecast. All four forecasts underestimated the windspeeds in the northern tier of states, where the analysis showed a broad band of winds greater than 40 m s^{-1}. The analysis also extended the upstream jet streak further downstream than forecast, although few observations were present in this region to verify the actual extent of the feature. There was also disagreement between the analyses and the forecast on the location of the downstream jet streak . Based on an observation of > 150 kts the analyzed jet is about 2° latitude further north than in the forecasts. However, with the exception of the weaker DRY forecast, the speed forecasts for this jet streak were greater than 70 m s^{-1} (140 kts) which places the maximum within the proper contour. The surface low was located under the left-front quadrant of the weaker upstream jet, and under the right-rear quadrant of the of the strong downstream jet. The forecasts show a much weaker jet over the surface low, and thus a much stronger gradient between the exit of the upstream jet and the entrance to the downstream jet.

c. Case 7 synoptic situation

The case 7 surface system continued to deepen rapidly; at 1200 UTC 5 Jan 1985 its central pressure reached 978 mb, a decrease of 4 mb in 3 hours. The system had decreased its forward speed to 15 m s^{-1} and continued to move northeast along the warm front to a position about 175 km east of Cape Cod (Fig. 4.35a). During this 3 h period, the system had occluded with the triple point just northeast of the low. The whole frontal system was slowly rotating cyclonically about the low center with the warm front extending northeast from the center and the cold front southeast from the triple point. A trough extended southwest from the system between the cold front and the eastern seaboard. Surface maritime data were fairly extensive in the area of the system. Maximum winds were 25 m s^{-1} just ahead of the trough southwest of the surface low. Winds in general were 15 to 20 m s^{-1} in the warm sector and behind the cold front, while winds north of the warm front were about 15 m s^{-1}. Temperature differences were about 10 °C across the warm front, very small across the cold front, and about 10°C across the trough. The cold front approaching the low from the northwest was now about 130 km to the northwest.

At 850 mb the trough had moved east (Fig. 4.35b), and a closed low center had again formed. The minimum height was 1215 m, located just west of the surface low. Heights in the trough had fallen on the order of 100 m just west of the surface center. Cold air advection west of the trough and warm air advection east of the trough forced the isotherms into an southeast/northwest orientation along the U.S. East Coast. At 500 mb the trough had moved east to run north/south along the eastern seaboard, just west of the 850 mb trough (Fig. 4.35c). All evidence of the cut-off low was gone by this time, and the trough had become a very sharp feature which would provide very strong PVA

downstream. The 300 mb analysis showed that a very sharp trough extended from a low near 60° N south through the Pennsylvania/Virginia area, with a break at the trough axis between the jet streaks east and west of the trough (Fig. 4.35d). The northern and southern jet streams merged off the U.S. East Coast into one system with a jet steak directly over the surface low.

d. Case 7 model results

At the surface, the AS and EXP forecasts continued to be very similar (Fig. 4.36a, b). The forecast central pressures were within 1/2 mb of each other at 984 mb -- 6 mb weaker than analyzed. Both show a very distinct warm front but very little indication of the cold front. However, both experiments showed the trough evident just off the East Coast in the surface analysis. These two experiments were also depicting the front that was analyzed to the west of the low.

In comparison, the central pressure in the KUO experiment was 8 mb too weak at 986 mb, while that in the DRY experiment was 9 mb too weak at 987 mb (Fig. 4.36c, d). These two experiments also showed a strong warm front, but not as strong as the AS and EXP. Indications of the front approaching from the west were also evident and almost as distinct as in the AS and EXP cases. However, the post cold front trough was barely evident in the KUO experiment and non-existent in the DRY experiment.

At 850 mb, the forecast height fields were essentially identical except in the area of the surface low and along the warm front (Fig. 4.37a-d). In the AS, EXP, and KUO cases there was considerable troughing above the surface warm front, while there was none evident in the DRY case. The 850 mb analysis does not show this troughing either, but the 850 mb observations are too sparse over the ocean to depict such a small-scale feature. The AS and EXP had a minimum height of 1222 mb, which was close to the

analyzed height, with the KUO forecast 12 m higher, and the DRY forecast 17 m higher than AS and EXP. The 850 mb temperature fields were similar in all the experiments, although the DRY case had smoother isotherms and colder temperatures southeast of the surface low than the other experiments. In all three experiments with LHR there was an area of warming evident above the precipitation near 37°N, 49°W though it was weaker in the KUO experiment.

The 500 mb height and vorticity fields were almost identical for all four forecasts except over the surface warm front (Fig. 4.38a-d). The forecast height fields showed what appeared to be a short wave and an associated vorticity maximum just upstream of the long wave trough and its vorticity maximum in all four forecasts. This short wave was not obvious in the 500 mb height analysis. The primary difference in the forecast vorticity fields was a small-scale maximum above the area of precipitation located near 39°N and 57°W. This was also the area of greatest troughing in the sea level pressure and 850 height fields, which was sharpest in the AS and EXP experiments. Of note is that the KUO case shows at least as much precipitation at the surface as the AS and EXP, but has a much reduced vorticity maximum in this area. The DRY case has evidence of only the slightest increase in vorticity here.

The 300 mb forecast height fields were also nearly identical (Fig. 4.39a-d). The DRY speed field was much smoother than the other three. It had an elongated area of greater than 60 m s^{-1} winds over the area of the surface low, while the other three forecasts show a 60 m s^{-1} jet maximum upstream of the surface low, a decrease to less than 60 m s^{-1} over the low, and an increase to a jet maximum of greater than 70 m s^{-1} downstream of the surface low. This indicates some support from an jet exit/entrance regime in the AS, EXP, and KUO cases, though this support is much weaker than in the

case 6 forecasts. A windspeed minimum was also apparent over the precipitation maximum near 39°N 57°W in the AS, EXP, and KUO forecasts.

The jet streak forcing of the two systems was quite different at this time. Case 6 was under the influence of a jet streak exit/entrance pattern and deepened 18 mb in the previous 6 hours. The case 7 analysis had the surface low under the jet streak at this time, actually just downstream of a local jet max, and the surface low still deepened 11 mb in 6 hours. Though the deepening of case 7 was less than that for case 6 it was still very rapid, and may be accounted for by the larger PVA caused by very sharp troughing evident at 500 mb, which is in contrast to the broader tough in case 6. Both systems had well developed temperature advection patterns conducive to strong cyclone development.

The model continued to have a varied ability to forecast the two cases. The model was successful in case 6 in forecasting the cold front, in case 7 it was successful in warm front forecasts. The success among the experiments continued as before, with the AS and EXP too intense in case 6, and the DRY much too weak. In case 7 all four experiments produced central pressures that were too weak and within 2 mb of each other. The case 6 forecast positions differed significantly, while the case 7 positions were close to each other. Again both EXP forecasts had a reduced areal precipitation pattern.

6. 15 hour forecast

a. Case 6 synoptic situation

At 0300 UTC 7 Jan 1983 the case 6 surface low had reached 976 mb, a further decrease of 4 mb in 3 h. There had been a decrease in the rate of deepening over the past nine hours, from 10 mb/3 h and 8 mb/3 h during the previous two periods. The low center continued moving northeast at 20 m s^{-1}, about the same speed as in the previous three hours, to a position east of Nova Scotia at almost 45°N and 58°W (Fig.

4.40). The occluded front was starting to move cyclonically around the low and was now extended initially eastward before curving around toward the south. The warm front extended southeast from the occlusion well south of the low center, and the cold front continued southwestward toward Cuba. The surface analysis shows a weak secondary low developing at the triple point with a central pressure of 1002 mb. The trough to the north of the center also continued to move cyclonically around the system and extended northward before curving towards the northeast. A new trough was analyzed extending southwest from the low; it was located about halfway between the front and the coast. The only surface maritime winds in the area of the storm showed speeds of between 25 and 35 m s^{-1} southwest of the low center, on the upstream side of the trough. The gradient to the east of the system remained very strong.

b. Case 6 model results

The central pressures in the AS and EXP cases were 970 mb and 971 mb, respectively, about 6 mb too low compared to the analysis. The KUO experiment was now about 5 mb too weak at 981 mb, and the DRY experiment was about 19 mb too weak at 995 mb. The positions of the low center in the AS, EXP, and KUO forecasts were very close to the analyzed position (Fig. 4.41a-d). However the DRY forecast position lagged approximately 200 km to the southwest. The AS, EXP, and KUO forecasts also clearly showed the cold frontal trough while the DRY case had only weak evidence of it. The EXP experiment had some evidence of the warm front as well. The location of these features agreed with the analysis. The AS, EXP, and KUO forecasts also showed the post-frontal trough. However, none of the forecasts portray the 1002 mb low that was analyzed. The areal extent of the precipitation was about the same in the AS, KUO, and

DRY cases with the usual in the EXP case. The precipitation amounts associated with the DRY case were less than the others, as before.

c. Case 7 synoptic situation

The case 7 low at 1500 UTC 5 Jan 1985 had also deepened to 976 mb, a central pressure decrease of 2 mb in 3 hours, and was located well east of New Hampshire near 41°N and 66°W (Fig. 4.42). Movement of the center was southeast at only about 12 m s^{-1} and a general slowing of forward movement had occurred over the past 6 hours. Like in case 6, this system had also undergone a decrease in the intensification rate over the past 9 hours, down from 7 mb/3 h, and 4 mb/3 h. The low had developed all the features of a bent-back occlusion by this time. The occluded front extended almost straight to the east along the north side of the low, with the cold front extending south and then southwest from the occlusion. The trough extending southwest parallel to the eastern seaboard held its relative position. Limited surface maritime data showed winds near the triple point in the warm sector were about 20 m s^{-1}, with winds of 20 - 25 m s^{-1} north of the warm front. The cold front approaching from the northwest is within about 115 km, and a sharp bend in that front has developed at its closest approach to the case 7 low. A small surface ridge that extended north/south near 45°W was starting to increase the pressure gradient to the east of the surface low.

d. Case 7 model results

The AS, EXP, and KUO experiments all showed an elongated central low as in the analysis, but the location of the central pressure minimum within the innermost isobar differed between the experiments (Fig. 4.43a-d) The EXP and AS forecast central pressures were 978 mb, about 2 mb weaker than the analysis, and the KUO

forecast was about 6 mb weaker at 982 mb. The DRY experiment showed a more circular pressure pattern around the low, and the minimum pressure was about 7 mb weaker at 983 mb. All of the forecasts portrayed a strong warm front, with the DRY experiment the weakest. The cold front and trailing trough shown in the analysis were also now evident in the AS, EXP, and KUO cases. The frontal system approaching the low from the west in the analysis was not distinguishable in the forecasts. The precipitation patterns showed an increase near the low center in all of the cases, with precipitation weakening along the warm front.

The two systems continued to show differences although they had reached the same central pressure. Though both systems underwent a slowing in intensification rate, the case 6 low was moving relatively rapidly to the northeast likely in response to the high to its east, while the case 7 low moved slowly and erratically under little apparent outside influence. The case 7 system did not have a cold front to the northwest of the surface low.

Overall the forecasts were showing the same general patterns of deepening, with case 6 experiments very different, and case 7 reasonably close. However, the case 7 forecasts were now starting to break into the same pattern as the case 6, with the AS and EXP experiments very similar and different from the other two. There is a difference, however, since the case 7 KUO and DRY forecasts are very similar to each other, which is not true in case 6. The case 7 model output shows increasing diabatic influence near the low, and this is likely what is causing the divergence of the experiments.

7. 18 hour forecast

a. Case 6 synoptic situation

By 0600 UTC 7 Jan 1983 the case 6 low had filled to 978 mb according to the analysis (Fig 4.44). However, the NMC "final" analysis (not shown) had the pressure at 976 mb, the same as 3 h earlier. Though the actual central pressure was difficult to determine, it is clear that the system changed relatively little in intensity over the previous 6 hours (about 4 mb/6 hours). The system also maintained its northeastward movement at about 20 m s^{-1} to a position south of Newfoundland near 46°N and 55°W. The occluded front extended eastward from the low before curving southward to a triple point located south of the low. A secondary low was again analyzed at the triple point with a central pressure of 1008 mb, an increase in pressure of 6 mb. From this point, the cold front extended southeast and the warm front southwest. The trough to the north and the trough to the southwest were still analyzed, and remained stationary relative to the system center. The pressure gradient to the east remained strong; however the orientation of the strongest gradient was more northwest/southeast as the low moves north around the high. Maritime data were sparse, but due north of the occlusion on the Newfoundland coast there was a report of 45 m s^{-1}. There were reports up to 28 m s^{-1} directly to the west of the surface low.

b. Case 6 model results

As was seen 3 h earlier, the minimum central pressures in the AS and EXP cases were within 2 mb of each other at 969 and 971 mb, respectively, and were about 10 mb too low compared to the analysis (Fig. 4.45a-d). The KUO experiment, with a central pressure of 977 mb, was about 1 mb deeper than the analysis, while the DRY experiment, with a central pressure of 994 mb, was about 18 mb too weak. All four

forecasts did show the cold front, but only the EXP experiment had some evidence of the warm front. The location of these features was in agreement with the analysis. The EXP forecast also shows several post-frontal troughs, while the AS and KUO forecasts gave some evidence of the single trough in the analysis. None of the forecasts depicted the 1008 low that is analyzed. The extent of the precipitation was about the same in the AS, KUO, and DRY cases with the usual reduced areal extent in the EXP case. The precipitation amounts associated with the DRY case were now approaching that of the other forecasts.

At 850 mb, the height forecasts were starting to diverge between the AS and EXP experiments. The AS case was now 15 m lower than the EXP (Fig. 4.46a, b). As at the surface, the KUO and DRY experiments depicted much weaker storms, with minimum heights 100 m and 234 m higher than the AS, respectively (Fig. 4.46c, d). The AS and EXP minimum heights were collocated, with the KUO height minimum to the northeast and the DRY height minimum well to the southwest. The AS and EXP experiments have similar contours, however the EXP experiment showed some perturbations in the height field to the south of the low over the surface cold front. The AS, EXP, and KUO experiments also showed similar temperature fields, again with the exception of perturbations south of the low in the EXP experiment. The DRY case had a similar overall temperature field, except it was colder east and south of the low.

The 500 mb height fields had considerable differences in the short wave trough near the area of the surface low (Fig. 4.47a-d). The AS and EXP forecasts depicted a closed circulation with minimum heights of 5240 m and 5252 m, respectively. The KUO forecast did not depict a closed circulation, but did portray a prominant trough; the DRY height field was smooth over the surface low. In the AS and EXP experiments the closed lows were associated with a very strong vorticity maximum in excess of 40 units that was located above the surface low. In the KUO case the vorticity maximum was

smaller at about 32 units; in the DRY case there was no vorticity maximum. In addition a band of enhanced vorticity existed in the AS, EXP, and KUO experiments extending along the cold front.

All four 300 mb height fields were very similar (Fig. 4.48a-d), except for some pertubations in the height field in the AS and EXP experiments above the surface low. The KUO and DRY height fields were essentially smooth in the area of the surface low. All four forecasts had very similar speed forecasts with respect to jet location, however the northern jet in the AS, EXP and KUO experiments was much stronger than the DRY case and increased in intensity in the past 6. The surface low was located under the left-font quadrant of the weak upstream jet. However, the downstream jet was moving away from the surface cyclone and was located far enough away that its effect on the surface low would be much reduced.

c. Case 7 synoptic situation

Over the previous three hours, the case 7 system had again deepened rapidly. By 1800 UTC 5 Jan 1985 the central pressure in the NMC analysis (Fig. 4.49) was 966 mb (963 mb in the "final" analyses, not shown), a drop of 10 mb/3 h. This was a dramatic change from the decreasing deepening rate recorded earlier, casting suspicion on the central pressure for 1500 UTC. However unless the 1500 UTC value was off by 5 mb or more, there was a trend of slowing intensification with a subsequent increase. The decreasing intensification rate occurred at night, with the rapid intensification commencing about local sunrise. The system also increased forward motion and had moved at an average of 22 m s^{-1} over the previous 3 hours. This is a dramatic difference over the somewhat erratic movement recorded over the previous 9 h; again difficulty in locating the exact center of the system was a likely factor. The system was again analyzed with a bent-

back occlusion, with the occluded front running east-northeast from the center to the triple point, where the warm front continued east and then southeast, and the cold front extended south and then southwest. The trailing trough to the southwest had also moved closer to the cold front. Due east of the surface cyclone a 1010 mb high had developed in the ridge extending north south along 45°W. This continued to increase the surface pressure gradient ahead of the surface low. Maritime data clearly delineated the surface features of case 7. Winds to the north of the occlusion along the Nova Scotia coast were 20 m s^{-1}, reaching 28 m s^{-1} north of the warm front over the open ocean. There was a 13°C temperature drop in 215 km across the warm front to the Nova Scotia coast. The warm sector winds were about 20 m s^{-1} and temperatures were in the 20-22°C range. Temperatures drop sharply across the cold front to about 8°C off the coast in the north and 17°C in the south. The air being advected off the continent directly into the low from northern New England is in the 0°C range.

d. Case 7 model results

The forecasts are now split into pairs by their characteristics, with the AS and EXP experiments in one pair and the KUO and DRY experiments in the other. The AS and EXP both have a central pressure of just above 970 mb, and their isobars are very similar (Fig. 4.50a, b). The central pressures were 4 mb too weak compared to the analysis. Both experiments model the analyzed warm front well, and show the cold front and post-frontal trough. Neither experiment has any strong evidence of the frontal system to the west of the low, though there is some noise in the pressure fields in the correct area. The precipitation fields are very similar, with the exception of a larger areal extent of light rain in the AS experiment. The second pair of experiments, the KUO and DRY, were very similar to each other (Fig. 4.50c, d). Their central pressures were 1 mb apart at 978 mb

and 979 mb, respectively, about 7 mb less than the other experiments. Both of these experiments showed the warm front, and the KUO also showed evidence of the cold front and post-frontal trough. The precipitation patterns in these two forecasts were similar. Both show a larger area of precipitation over 1 cm than the other 2 forecasts, but had less precipitation in the immediate area of the low.

At 850 mb the AS and EXP forecasts were again similar (Fig. 4.51a, b). Their minimum heights were within 1 m, and both show a reflection of the surface warm front in a strong trough running southeast from the low. The KUO minimum height was 50 m higher than the AS and EXP, but it shows even sharper troughing than evident in the previous two experiments (Fig. 4.51c). The DRY 850 mb minimum height was another 13 m higher than the KUO. There was only a very faint reflection of the surface warm front in this field, and the whole height field was comparatively smooth (Fig. 4.51d). The locations of the low were very close in all four experiments. The temperature fields of all four experiments were also quite similar, with the exception of some perturbations near 38°N 60°W that were not in the DRY forecast. The area just southeast of the low center was also colder in the DRY forecast.

The 500 mb forecasts became more similar during this time period (Fig. 4.52a-d). The main vorticity maximum was associated with the 500 mb trough; the vorticity associated with the precipitation in the AS and EXP experiments earlier was much less noticeable now. The vorticity field in the DRY experiment was only slightly weaker than in the other three experiments. The height fields were virtually identical.

At 300 mb there were still separate jet streaks--one up-stream and one downstream of the surface low in all four experiments (Fig. 4.53a-d). The upstream section of the jet was increasing in intensity, while the downstream jet streak was decreasing in intensity with only a small area of greater than 70 m s^{-1} winds in the AS and

EXP cases and no winds over 70 m s^{-1} in the KUO and DRY cases. The increase in the upstream jet was particularly noticable in the DRY experiment, which now had the largest area of winds over 60 m s^{-1} of the four experiments.

Overall the two systems changed little other than in intensity and position over the past three hours. The most dramatic difference is the sudden increase in intensity in case 7.

There appears to be less precipitation in the forecasts for both cases, an indication that LHR is decreasing as the storms near maximum intensity. The forecsts at this time seem to show two storms with intensities headed in different directions. There had been minimal changes in the case 6 surface forecasts over the previous 3 hours. Precipitation and surface pressure fields remained relatively steady with little new precipitation and small drops in central pressure. Case 7 however, showed major decreases in central pressure and considerable precipitation associated with the low, even as the area of LHR and associated effects to the east of the low continued to decrease. Overall the forecast patterns continued, with the case 6 forecasts widely diverged based on parameterization, with the AS and EXP deeper than the forecast and KUO and DRY weaker. However, the case 6 AS and EXP forecasts have increased slightly in central pressure *while the analyzed pressure and KUO forecast continue to deepen thus there is a* pressure convergence occuring with the exception of the DRY experiment. The case 7 forecasts are all showing the same general forecast trend as the analyses, however, the analyzed storm is deeper than all forecsts. Aloft the case 6 system shows the indirect effects of LHR, with the enhancement of the downstream jet particularly illustrative of this. The case 7 forecasts aloft showed fewer differences than case 6, an indication that fewer indirect effects were involved in these forecasts of the storm.

8. 21 hour forecast

a. Case 6 synoptic situation

Over the three hours prior to 0900 UTC 7 Jan 1983, the case 6 low started deepening again. The analyzed central pressure deepened 6 mb in 3 h to 972 mb, after filling 2 mb in the previous 3 h. In this system the decrease in intensification took place in the local afternoon/evening, and rapid intensification started around local midnight. The surface center moved northeast at about 12 m s^{-1}, considerably slower than the 20 m s^{-1} it had been moving earlier. The occluded front continued to rotate cyclonically around the low, with the triple point located southeast of the surface center, and the warm front extended southeast from there (Fig. 4.54). The weak low pressure center that had previously been analyzed at the triple point had separated from the front, and had deepened to 998 mb. At this time it was located behind the cold front and at the northern end of the trailing trough. A stationary front was analyzed extending almost westward from the triple point toward the low, before turning southerly as a cold front near 55°W. The trough to the north maintained its continuity, with a small cyclonic rotation around the low noted. The strong pressure gradient between the low and the high continued. Useful maritime data were not available at this time.

b. Case 6 model results

The AS and EXP experiments (Fig. 4.55a, b) had central sea level pressures of 971 and 972 mb respectiveley, which compares well with the analyzed value of 972 mb. However the analyses showed the central pressure of the system still dropping, while the model results showed the system filling slightly. In the other two experiments, the KUO central pressure was 975 mb and the DRY central pressure was up at 992 mb

(Fig. 4.55c, d). The EXP experiment continued to model the cold front and the trailing tough, while the KUO experiment depicted the cold front and hinted at the trailing trough. The AS and DRY pressure fields were essentially featureless with little evidence of the frontal troughs. Locations of the low center in the AS and EXP experiments were very close to the analyzed position, with the KUO location again ahead of the others, and the DRY low center located well to the southwest. None of the experiments appear to duplicate the sharp bending of the frontal zone analyzed near the triple point. The precipitation fields have changed little over the previous 3 h.

c. Case 7 synoptic situation

The case 7 low continued to deepen very rapidly with a decrease of 6 mb in the previous 3 hours for a current minimum pressure of 960 mb at 2100 UTC 5 Jan 1985 (Fig. 4.56). The rapid variation in deepening rates continued to suggest problems with the analysis in what is a data sparse region. The final analysis did provide some smoothing over the 6 h periods. Forward motion has slowed to about 8 m s^{-1}, a sharp change from the previous 3 h period where motion had greatly increased from previous times. Storm positioning in the analyses is suspect in these rapid fluctuations. The system retained the characteristics of a bent-back occlusion, but the triple point remained close to the low. The overall structure of the system showed little change in the past 3 hours. The ridge to the east also changed little, and an increasing gradient existed between the low center and that ridge. The front that had been approaching from the west was undergoing frontolysis. Maritime data supported winds of 20-25 m s^{-1} and temperatures of 8-11°C south of the occluded front in the warm sector, and 25 m s^{-1} and 4°C behind the cold front.

d. Case 7 model results

The AS and EXP experiments were again almost identical for this forecast time. The minimum surface pressure was very close to 965 mb for both (Fig. 4.57a-d). These two experiments placed the low in the same location which was very close to the analyzed position. Both the warm and cold fronts were depicted, though the cold front is better defined in the EXP. The KUO and DRY experiments remained similar to each other with central pressures of 973 and 974 mb, respectively. The KUO and DRY pressure centers were a little south of the AS and EXP, with the KUO center being the farthest south. The KUO experiment clearly showed the warm and cold fronts, while the isobar pattern in the DRY case only showed the warm front. The precipitation pattern in all of the cases has changed little from the previous time. What little additional precipitation fell was concentrated near the storm center.

The two systems were becoming more and more alike by this time in their development. The ridge to the east of the case 7 system had increased the surface gradient in the same manner, though not magnitude, as the high in the case 6 system. The two occlusions were very similar in structure, though the case 7 system is about 12 mb deeper than the case 6 system. The dissipating frontal system in case 7 is analogous to the two troughs in case 6.

The forecasts in both cases were indicating much less precipitation. This resulted in reduced LHR, and the forecasts, with the exception of the case 6 DRY, were beginning to resemble each other. In fact the AS, EXP, and KUO forecasts of central pressure in case 6, were 970, 971 and 973 mb, respectively. The other forecast fields for those three experiments were also very similar. The situation was a little different in case 7, though all four forecasts were closer in central pressure to the analyses than they had been since early in the forecast period. Case 7 still had the forecasts split into two groups

based on central pressure, the AS and EXP forecasts were very close to the analysis with the KUO and DRY about 10 mb too weak. As in the case 6 forecasts, the model fields now more closely resembled each other. The difference is that the case 7 DRY forecasts was also similar.

9. 24 hour forecast

a. Case 6 synoptic situation

Over the previous 3 h, the case 6 low deepened another 8 mb to 964 mb at 1200 UTC 7 Jan 1983 (Fig. 4.58a). Forward motion was 20 m s^{-1} to the northeast, an increase to the rate of 6 hours prior. The system was located east of Newfoundland near 47°N 51°W. The analyses had the occlusion wrapping around the low for the first time, while the trough to the southwest and its associated low center were no longer analyzed. The trough to the north was also no longer analyzed. The intense gradient to the east has increased due to the decrease in central pressure of the low. The system now displays the characteristics of a very intense occluded storm. Maritime data were not available near the system center.

The 850 mb analysis showed little change in the overall patten during the previous 12 h. The closed low collocated with the surface center deepened to 1170 m and remained almost directly over the surface low (Fig. 4.58b). There is still a characteristic S-shaped pattern to the isotherms, with the 850 mb low located in the area of maximum temperature gradient. The temperature gradient tightened in the past 12 hours, but the overall orientation of the isotherms did not change much.

The 500 mb analyses showed that a main broad trough axis with two shortwaves still existed (Fig. 4.58c). The easternmost shortwave is associated with the case 6 low. The thermal wave lagged the wave in the height field sufficiently to yield

strong cold air advection just upstream of the trough and strong warm air advection just downstream. The jet streak pattern at 300 mb changed considerably in the previous 12 h (Fig. 4.58d). The jet streaks themselves have weakened and the very clear entrance/exit pattern has become harder to recognize since the two streaks have separated from each other .

b. Case 6 model results

The AS and EXP experiments decrease the storm's central pressure by only 1 mb in the past 3 hours (Fig. 4.59a, b) compared to the observed deepening of 8 mb. For the first time since initialization, the forecast central pressure of 970 mb for these two experiments was significantly higher than the analyses --about 6 mb. The essentially steady central pressure of these two forecasts was not matched by the KUO forecast (Fig. 4.59c), which continued to intensify the storm to 973 mb, less than 3 mb higher than the AS and EXP forecasts. The DRY case also had an essentially steady central pressure to finish the forecast period at 992 mb (Fig. 4.59d), 22 mb higher than the AS and EXP cases, and 28 mb higher than the analysis. The AS and EXP low center locations compared well with the analysis. The KUO location was slightly northeast of the analyzed low, while the DRY was well to the southwest. The cold front was represented in all four experiments, though in the DRY experiment the front was not evident until well south of the low. Very little change occured in the precipitation fields in the past three hours, except along the cold front in the AS, EXP and KUO cases.

At 850 mb, the AS and EXP experiments agreed with the analyzed location of the low center, although the forecast minimum height was about 100 m deeper than the analyzed (Fig. 4.60a, b). The analyzed value, however, may not be accurate since there are no observations in the immediate vicinity of the low center. The KUO experiment

position was too far northeast and about 50 m deeper than the analyzed (Fig. 4.60c). The low in the DRY experiment was too far to the southwest and 110 m weaker than analyzed (Fig. 4.60d). As before, the temperature fields at 850 mb were similar in the AS, EXP and KUO experiments. The DRY temperature field was much smoother than the others with less packing of the isotherms immediately north of the low and cooler temperatures east and south of the low center.

The 500 height fields for this time differ primarily in the troughing over the surface low (Fig. 4.61a-d). This enhanced troughing is very strong in the AS and EXP experiments, smaller in the KUO experiment, and nonexistent in the DRY. As at 850 mb, few observations exist in this region to confirm the actual structure of this feature. The strength of the vorticity maximum was related to the amplitude of the trough, as expected. The AS and EXP experiments had maxima approaching 40 units, the KUO about 28 units, and the DRY case had only a broad 16 unit maximum farther south.

The 300 mb height and windspeed fields were similar in all the experiments, with the DRY experiment a bit smoother, (Fig. 4.62a-d). The jet pattern was very weak in the area of the surface low, with no strong jets or speed gradients. This contrasts with the analyses which shows the surface low still under the influence of the right -rear quadrant of the downstream jet and the left-front quadrant of the upstream jet.

c. Case 7 synoptic situation

The case 7 surface low deepened two more millibars to 958 mb by 0000 UTC 6 Jan 85. The system's forward movement was analyzed at about 20 m s^{-1}, a sharp increase. The system's structure was a fairly classic example of a well developed occlusion with the point of occlusion remaining close to the storm center (Fig. 4.63a). There was still a ridge to the east of the system, and a high had started to build in behind

the system from the southeast. Significant maritime data were not available in the area of the system.

At 850 mb the closed low associated with the surface low had deepened to 1050 m, and was placed directly over the surface center (Fig. 4.63b). There had been little change in the isotherm pattern, indicating little increase in cold and warm air advection at this level. At 500 mb the trough pattern had broadened and rotated cyclonically so that the axis is oriented northeast/southwest (Fig. 4.63c). Overall there was little change in the heights associated with the trough. Ridging is now evident just downstream of the surface low location. The 300 mb pattern also showed a flattening of the trough (Fig. 4.63d). The jet streaks remained nearly stationary, with a weak secondary jet streak developing to the north of the exit region of the original jet streak. The surface low had also moved out from under the jet streak and was located to take some dynamic advantage of an exit/entrance jet streak pattern.

d. Case 7 model results

The forecast surface fields continued to portray the storm in two pairs of similar experiments. The AS and EXP central pressures were 960 and 962 mb respectively, close to the analyzed surface pressure of 958 mb (Figs. 4.64a, b). The location of these forecast lows agreed well with the analysis, as do the warm and cold frontal troughs. The KUO and DRY experiments were also similar to each other with central pressures of 969 and 971 mb respectively (Figs. 4.64c, d). These values are about 12 mb weaker than the analyzed system. The location of these lows was close to the analyzed position, though the KUO was a bit too far south. The KUO experiment depicted the warm and cold fronts well; however the DRY experiment only showed weak evidence of the fronts. The precipitation patterns in the four experiments had changed little

over this three-hour period. The 24 h accumulation of precipitation includes a band well south of the low center in all four forecasts associated with warm frontal precipitation early in the period. A second band associated with the low center itself is portrayed further north in the AS and EXP forecasts. Weaker amounts of precipitation were present near the low center in the KUO and DRY experiments.

At 850 mb the AS and EXP forecasts were again similar (Figs. 4.65a, b). Their minimum heights differed only a little, and the AS experiment was now about 5 m deeper than the EXP. Both showed a reflection of the surface warm front in a strong trough running southeast from the low. The KUO minimum height was about 78 m higher than the AS, but it showed even sharper troughing along the warm front than in the previous two cases (Fig. 4.65c). The DRY 850 mb minimum height was 15 m higher than the KUO experiment and 94 m higher than the AS (Fig. 4.65d). There was no reflection of the surface warm front, and the whole height field is comparatively smooth. The locations of the low were close in all four experiments. The temperature fields of all four experiments were quite similar, with the EXP being noisier than the others.

The 500 mb forecasts were becoming even more alike than earlier (Fig. 4.66a-d). The main vorticity maximum was associated with the 500 mb trough and was diminishing in magnitude. The height fields were virtually identical apart from enhanced troughing over the surface low center in the AS and EXP forecasts.

Enhanced ridging was present at 300 mb over Newfoundland in the AS and EXP forecasts compared to the KUO and DRY forecasts (Figs. 4.67a-d). The height forecasts were otherwise essentially identical. A northern extension of the jet was present in the AS and EXP forecasts associated with the ridging. The enhanced ridge and windspeeds were supported at least in part by the NMC analysis and plotted observations. There were still separate jet streaks up-stream and downstream of the surface low in all four

experiments. The downstream jet was strongest in the AS experiment and weakest in the DRY. The northward movement of the low had moved it away from the jet; the jet should therefore have little effect on the surface low.

The two surface systems were quite similar by this time; even their central pressures were within 6 mb of each other according to the analyses. Aloft the systems were still different, even so. At 850 mb both systems had a closed low, however the case 6 system had a tighter temperature gradient and a much clearer S-shaped isotherm pattern. At 500 mb the case 6 analysis again showed a much better developed isotherm pattern , and a somewhat sharper trough. The 300 mb analysis showed a sharper trough for case 6, but a much weaker jet streak pattern.

There was some change in the forecast comparison in the previous 3-h. Case 6 is interesting because the forecasts have started to diverge in their central pressure trends which actaully caused the AS, EXP, and KUO forecasts to become more similar. The AS and EXP cases are now holding approximately steady, while the KUO continues to deepen the cyclone, as does the analysis.

D. Conditions after Model Forecast Period

1. 3 hours after model forecast

The case 6 low pressure system started to fill extremely rapidly by 1500 UTC 7 Jan 1983. The analyzed central pressure was 972 mb, an increase of 8 mb in three hours (Fig. 4.68a). The system had also increased speed slightly to 22 m s^{-1}. The physical structure of the system remained essentially unchanged with the exception of a considerable weakening of the gradient to the east.

The case 7 central sea level pressure remained constant at about 958 mb over the three hours prior to 0300 UTC 6 Jan 85. The system continued to move northeast

though it had slowed again to about 15 m s^{-1} (Fig. 4.68b). If the propagation speeds, which varied between 8 and 22 m s^{-1} over the past 18 hours, were averaged over this period the average speed would be 17 m s^{-1}. The physical structure of the storm remained about the same, though the triple point was moving along the occlusion to a position southeast of the system center. The ridge to the east of the system had moved eastward, and there had been some relaxation of the pressure gradient.

At this time both systems seem to have reached their maximum intensity, and considering the collapse of upper-air support analyzed three hours ago, this is not surprising.

2. 6 hours after model forecast

At 1800 UTC 7 Jan 1983, 6 hours after the model run, the case 6 system had stopped filling and maintained a central pressure of 972 mb (not shown). Later analyses showed that the system actually deepened again as it moved south of Greenland. At this time the system had increased forward motion to 38 m s^{-1}.

By 0600 UTC 6 Jan 85 the case 7 system had started filling. The central pressure increased to 961 mb, an increase of 3 mb in 3 hours. The system had started to move very rapidly east-northeastward, with speeds approaching 30 m s^{-1}.

E. Summary

The case 6 system was considerably more affected by LHR than the case 7 system. The strong diabatic contribution to the system was associated with a precipitation maximum near the center of the cyclone. LHR effects included deepening the low-level cyclone, tightening the 850 mb temperature gradient near and south of the storm center, enhancing the development of the 500 mb shortwave trough and vorticity maximum, and altering the 300 mb jet structure. The latter included increases in windspeed in the jet streak

downstream from the surface cyclone, as well as decreases in windspeed in the jet streak upstream of the cyclone center.

The experiments in this case provided forecasts that both overestimated and underestimated the central pressure of the system compared to the analysis. The two experiments that had the most sophisticated cumulus parameterizations, the AS and EXP, consistently overdeveloped the case 6 cyclone system compared to the analyses through approximately the 15 h forecast. The KUO experiment was closest to the analysis through the 18 h forecast, though it was consistently too weak. The DRY experiment made a very poor forecast with an error of 28 mb in the 24 h forecast central pressure. At the end of the forecast period the AS, EXP, and KUO cases were producing similar forecasts as the cyclone lost its strongly diabatic component. In general the EXP case had the noisiest heating-induced effects, with small-scale perturbations apparent in the height, vorticity, and windspeed fields. The DRY forecast produced the smoothest fields.

The way the experiments handled the total moisture parameterization showed up in a comparison of the EXP precipitation with the other experiments. Once away from the LHR in the center of the system the EXP experiment produced very little precipitation, while the other experiments produced similar broad areas of light precipitation. This apparently reflected the inclusion of evaporation in the EXP parameterization but not in the others.

The case 7 cyclone was much less diabatically forced, though it did have a very strong area of LHR along the warm front through approximately the first twelve forecast hours. This area had very little effect on the cyclone's central pressure although the sea level pressure minimum in the AS case was briefly collocated with this feature early in the forecast period. Central pressures in the 12 h forecasts differ by less than 2.5 mb. The most striking differences at this time were associated with the very strong warm front,

which had a sharper low-level trough, a 500 mb vorticity maximum, and a 300 mb windspeed maximum in the forecast with LHR.

The diabatic influence increased after the 12 hour forecast, as a precipitation maximum formed near the storm center. The increase in the diabatic forcing caused a divergence among the forecasts, with an 11 mb spread in the 24 h forecasts. This storm apparently had much weaker diabatic forcing than case 6, since the DRY experiment, while weaker, made a much better forecast than in case 6. Differences in the 24 h forecast were also much weaker than for case 6.

V. RESULTS

The comparison of the model forecasts with the observed cyclonic systems, reviewed in Chapter IV, provided considerable insight into the influence of parameterization scheme on forecast accuracy. Of particular note were the enhanced central sea level pressure decreases, the increased troughing and vorticity at 500 mb, and the increase in the velocity of the downstream jet and the decrease in the velocity of the upstream jet at 300 mb in all of the case 6 experiments except the DRY case. The case 7 model runs were unique more for the strong precipitation, 500 mb vorticity maximum and 300 mb windspeed minimum generated at the warm front east of the surface low mainly in the AS and EXP cases. The shift in the location of the surface low to this position in the AS case indicates the importance of the heating. These changes can be tied in with latent heat release (LHR) through the vertical motion field. As shown by the generalized omega equation, a local heating maximum contributes to upward vertical motion. By continuity, upward motion is associated with convergence/divergence at lower/upper levels and therefore increases/decreases in relative vorticity and troughing/ridging. The latter implies height changes on isobaric surfaces and therefore changes the height gradient and therefore in the geostrophic wind. At the same time, the ageostrophic winds associated with the heating-induced divergence aloft have a cross-contour component toward lower/higher heights to the north/south of the heating maximum, leading to acceleration/deceleration of the flow in that region.

With the omega fields apparently playing a very large part in the system's development, this chapter will concentrate on the differences between the 700 mb model output total omega fields and the computed diabatic omega fields as described in Chapter III. A single representative level of omega was chosen based on visualizing the data in four dimensions using the software VIS-5D version 3.0, developed at the University of

Wisconsin - Madison's, Space Science and Engineering Center. Differences in the 700 mb omega fields will be used to examine the vertical motion resulting from LHR in each of the model experiments. The diabatic vertical motion fields are derived from the residual heating rates, so there is no initial field or 24 h forecast field. The discussion will therefore start at forecast hour 6, and values at forecast hour 23 will be used in place of hour 24.

The vertical motion fields clearly show the diabatic component of the total model forecast omega, and demonstrate in an empirical way the acceptability of the diabatic calculations. All of the experiments show the diabatic rising and sinking motions where they would be expected in storms of this type. One problem that shows up in both storms and every experiment is an area of significant diabatic rising motion over the Appalachian Mountains where the total vertical motion is negligible; at one point in the case 7 DRY experiment this is the area of maximum rising motion. This region varies slightly in size and occasionally location, and is generally weakest at the very end of the forecast period. This region of heating-induced upward motion is an artifact of either the model or the heating calculation that is not explained at this time.

Direct comparison of the model and diabatic omegas is difficult when the differences between the two are small, and when the values have steep gradients such as near maxima. As discussed in Chapter III, a small amount of smoothing in the heating field was required in all of the experiments to enable the diabatic omega calculations to run properly. The additional smoothing required in some cases was detailed in Chapter III. Because of this, a direct comparison of maximum values of diabatic and model omegas will not be presented in this thesis. The units of omega presented here are microbars per second, which gives values approaching -50 for the maximum rising motion.

A. Case 6

As discussed before, this case was characterized by large differences in the performance of the forecasts. The DRY forecast did poorly on forecasts of surface location and central pressure. The KUO experiment did a reasonable job on the forecast up through the final hours, while the AS and EXP experiments overdeepened the system through most of the 24 hour forecast period.

1. 6 hour forecast

Comparison of the DRY case with the others shows that near the surface cyclone center almost all of the upward vertical motion is generated by diabatic processes (Fig. 5.1a-d). As expected, in the DRY experiment there is no significant diabatic omega in the vicinity of the storm, and there is also a lack of strong model omega immediately around the storm. The strong rising motion in the other experiments can be seen to be almost entirely the result of diabatic processes. The AS and EXP experiments show very strong diabatic upward motion just to the north of the surface center. In this region, the -25 unit line in the model omega is nearly coincident with the -20 unit line in the diabatic omega, indicating that only about -5 units of vertical motion are driven by dry dynamics near the center of the storm. The omega values in the experiment KUO experiment fall between those in the DRY and the AS/EXP experiments, though the location and pattern of diabatic omega is similar between the three experiments. The model rising motion to the northeast of the low center outside the area of strong diabatic upward motion in all of the experiments is similar, though small differences relative to the DRY experiment, indicate some influence of LHR in this region of warm air advection and weak 500 mb PVA.

A second main area of model rising motion can be seen along the cold front. This activity is at least partially diabatic in the AS and EXP cases since diabatic upward motion is present. There is also likely a diabatic component in the KUO, though one below

the -5 threshold; the area of model rising motion enclosed by the -5 isopleth is much larger than in the DRY forecast. An anomaly occurs in the EXP forecast where the calculated diabatic omega is larger than the total omega, most likely a result of errors in either the heating rate or the diabatic omega calculation. The EXP model omega depicts the rising motion along the warm front extending to the southwest of the low center, while the other experiments only suggest its location.

The overdevelopment of the system at this point by the AS and EXP experiments is likely the direct result of LHR. The Chapter IV discussion showed that the upper level fields at this time were still similar in all of the cases, thus LHR had not yet started to effect the overall system itself. Since surface pressure is equal to the weight of the overlying atmosphere if conditions are hydrostatic, the release of LHR will warm the atmosphere and make it less dense. It also enhances upward motion and therefore low-level convergence (and spin-up) and upper-level divergence (and mass evacuation). The values of LHR generated by the cumulus parameterization used in the AS and EXP experiments are apparently too large at this time in this diabatically driven storm. The KUO experiment produces less LHR, and the resulting forecast is much closer to the analysis. The lack of LHR in the DRY forecast is quickly apparent in the omega fields and the very small central pressure drops.

2. 12 hour forecast

The EXP experiment's omega field at this time is very striking and complex (Fig. 5.2a). The area of largest rising motion running northeast out of the low is located along the trough in the analysis. The analyzed occluded and cold fronts are also depicted very well by the rising motion in the model forecast. However, there is little model representation of the analyzed warm front. The AS experiment depicts strong rising motion associated with the same features as the EXP, but with smaller magnitudes (Fig. 5.2b).

However, the AS forecast also shows some hint of the warm front. The difference between the cumulus parameterizations is evident along the cold front as a difference in diabatic omega. The diabatic omega and the model omega in the EXP case is approximately 10 units greater than the AS experiment. Despite differences in the vertical motion the central pressure in the AS and EXP forecasts is very similar. The precipitation generated by the EXP experiment is also no stronger than in the AS case, and as noted in Chapter IV the areal extent of precipitation is much smaller in the EXP experiment as compared to the others. The stronger LHR implied by the stronger diabatic omega values in the EXP forecast does not manifest itself as precipitation because of the inclusion of subcloud evaporation in this parameterization but not in the AS or KUO experiments.

The KUO experiment is still the closest to the actual system in central pressure at this time, and its omega field is still between that of the AS/EXP forecasts and the DRY (Fig. 5.2c). The KUO forecast rising motion depicts the trough, the occluded front, the cold front, and the warm front. With the exception of the warm front, which is more evident in the KUO experiment, the vertical motion is weaker than the AS/EXP. The DRY experiment depicts only an area of weak model omega in the general area of the trough (Fig. 5.2d).

The EXP experiment also shows much larger areas of downward motion than any of the other experiments, both model and diabatic. Along with reduced rising motions, the KUO experiment also has smaller sinking motions. The DRY case again only shows diabatic vertical motion over the Appalachians. In addition the adiabatic vertical motion associated with the trough extending northeast from the cyclone center at hour 6 has become more diabatic at this time in all experiments except the DRY. In the AS and EXP experiments diabatic omega has become a major component of rising motion along almost the entire trough. In the KUO experiment the diabatic omega is much smaller, and so is the

model omega. However, the DRY experiment model omega also increased along the trough.

The sharp vertical motion gradients, and the larger areas of subsidence in the EXP experiment may be the cause of the decreased areal extent of precipitation. As described before, the rainfall rate in the EXP experiment is also affected by the allowance for evaporation of raindrops in non-saturated layers, which would decrease the total precipitation. Despite the greater magnitude of rising motion near the low center in the in the EXP experiment the amounts of precipitation near the system center and along the cold front remain about the same as in the three non-DRY cases.

Initially the direct effects of LHR deepened the system but these direct effects modified the system so there are indirect effects influencing system intensification by the 12 h forecast. The evidence for this involves the LHR-induced differences in the 500 mb vorticity and 300 mb speed fields among the experiments discussed in Chapter IV. The overdevelopment of the system by the AS and EXP cases at this time is likely the result of a developing feed-back loop involving the 500 mb trough and the upper-level jet, which the models had developed more favorably for upper-level support than the analysis showed. The AS/EXP rising motion maximum northeast of the surface low center coincides with the strong 500 mb PVA downstream of the LHR enhanced trough. It is also located in the right-rear quadrant of the LHR-enhanced downstream jet streak. The additional rising motion generated by these LHR-enhanced features was associated with additional low-level convergence by continuity, and therefore spin up and increased low-level vorticity in the system. Continuity also requires additional upper-level divergence (and ageostrophic outflow) which accompanies the LHR-induced warming in the ridge just downstream of the surface low which increased the height of the ridge. As seen in Baker (1991) the LHR induced change in the height of the ridge can also change the vorticity

aloft, increasing the strength of the upstream trough. The ageostrophic outflow is oriented cross-contour toward lower isobaric heights north of the region of heating, yielding acceleration in the region of the downstream jet streak. The height gradient in this region was also enhanced by the LHR-induced ridging, strengthening the geostrophic wind. Both of these processes also worked to increase the speed of the jet, which in turn helped increase the divergence aloft and the vertical motion. Thus there is a link between the moisture parameterization and an increase in storm strength associated with both direct and indirect effects of LHR. The weaker omega in the KUO experiment that resulted from weaker LHR kept that experiment from overdeveloping the surface cyclone and 500 mb trough at this time. The DRY case with its non-existent LHR is already lagging quite a bit behind the others in intensifying the system.

3. 18 hour forecast

The surface cyclones continued to deepen even as the diabatic component of vertical motion had decreased in the *AS*, *EXP*, and *KUO experiments* (*Fig.* 5.3a-c). At this time the system appeared to be undergoing a conversion to a more dynamically driven system, even though there was still some feedback evident in a small increase in magnitude of the 500 mb vorticity maximum and the downstream jet. Despite the decrease in diabatic omega the model total omega is not greatly reduced, and an increase in maximum rising motion is even present in the EXP experiment. Both the model and diabatic omega maxima in all the experiments moved downstream away from the surface center, showing that the maximum rising motion is associated more with the point of occlusion than with the surface low as previously. This downstream movement of the omega maximum coincides with the downstream movement of the 500 mb PVA and the downstream jet streak. The maximum rising motion seems to be migrating with these features, or vice-versa.

The orientation of the omega values is also changing. The omega contours are now taking on the comma shape associated with an occluded system, even in the DRY case (Fig. 5.3d). The EXP case still clearly shows the cold frontal location and considerable areas of sinking motion around the rising motion. At this forecast time this is the only experiment that clearly identifies sinking motion associated with the storm. In some areas, the diabatic contribution to the sinking motion is dominant, while in others dynamic forcing is dominant. The AS and KUO cases still show a diabatic contribution to the cold front, and the overall model omega fields do compare well with the analysis concerning the position of the cold front.

4. 24 hour forecast

At the end of the forecast period the central pressure in the surface low in the AS and EXP experiments was almost steady and near the lowest recorded values. This contrasts sharply with the analyzed low which continued deepening right through the end of the forecast period. The KUO case did keep deepening through this last forecast period, though not as much as the analyzed system. The AS, EXP and KUO omega maxima show the classic signature of an occluded cyclone (Fig. 5.4a-c), and vertical motion has decreased near the surface center in all of the cases consistent with the occlusion process. However, along the cold front there had generally been an increase in organization and magnitude of the rising motion in other than the DRY case. The increase in the total and diabatic omegas were about the same, indicating most of the increase in rising motion along the cold front was due to an increase in the diabatic omega as would be expected. The EXP experiment also showed a larger area of descending motion than previously. As before the DRY case showed minimal vertical motion (Fig. 5.4d).

The lack of support for the surface low from aloft was now obvious. The main 300 mb jet streak, now well downstream of the surface low, and the weak upstream

jet were not providing any significant forcing except possibly in the KUO experiment. The more northerly position of the KUO low center may have put it a position to still be receiving some support from the downstream jet. At 500 mb the AS and EXP rising motion maximum appeared to be in an area of neutral or negative vorticity advection, while the KUO maximum appeared to be in a region of PVA. The greatly reduced upper-level support in the AS and EXP forecasts explains the lack of intensification in these systems. The stronger diabatic activity along the cold front is a product of the intensification of the front as continental polar air moving off the continent interacts with the subtropical air ahead of the cold front being advected into the front by the high to the east.

5. Case 6 summary

Case 6 was notable for the very strong diabatic omega in the cyclone. This system was very diabatic from the beginning, and direct LHR effects dominated the first 6 hours of intensification. As the system developed indirect LHR effects, initiated by the direct LHR, became more dominant in system development. The indirect effects became even more important late in the forecast period as the diabatic forcing of the system decreased and adiabatic forcing increased.

B. Case 7

The most obvious feature of the case 7 discussion in Chapter IV was the exceptionally strong area of vorticity and precipitation located generally to the east of the surface low. As will be seen in the 700 mb omega fields this is primarily a diabatic feature that had the largest omega magnitudes of either case. This feature was an integral part of a very strong warm front associated with this system.

1. 6 hour forecast

The 6 hour forecast shows the rising motion associated with the system broken into two parts -- a weak model maximum, with little diabatic contribution near the analyzed surface low, and a very intense area of diabatic rising motion along the analyzed warm front to the east of the low (Fig. 5.5a-d). The relatively weak rising motion near the surface low is surprising considering the rapid deepening discussed in Chapter IV. The minimal amount of precipitation in this area indicates that unlike the case 6 storm LHR is not an important factor in the development of the low center at this time. The very strong diabatic rising motion away from the analyzed low center was also surprising given that the surface analysis had no indication of this feature. The cause of this very strong area of diabatic upward motion and precipitation has not been identified but a region of static instability along the warm front is suspected. The upper-air analyses, both prior to and after this time also showed no sign of this feature, although the forecast fields show small-scale perturbations in the height, vorticity, and windspeed fields aloft. However, given the size of this feature and the lack of data in the area it could have gone undetected by conventional observations. The possibility also exists that this feature is unrealistic. In either case, the rising motion in this area of diabatic omega in the AS experiment was intense enough to cause the lowest surface pressures to be collocated with the rising motion. It should be noted that this does not mean that there is no low pressure center further west; it means that the plotting scheme used to mark the lows did not find a sufficiently significant minimum.

Descending motion in both diabatic and model output is evident in all of the experiments except the DRY. It appears that strength of the descending motion is directly related to the strength of the ascending motion. Further east along the warm frontal area there is a

second weaker area of upward motion in all of the experiments except the DRY. Based on the computed values in this eastern area the EXP experiment appears to have more diabatic than total omega, the AS experiment has about equal values of diabatic and total omega, and the KUO experiment more total than diabatic omega. The EXP experiment is interesting since it indicates that either there is adiabatic descending motion that is opposing the diabatic ascending motion, or that errors exist in the diabatic omega calculation introduced by the smoothing.

2. 12 hour Forecast

By the 12 h forecast, vertical motion had increased and become more organized around the surface low center in all of the experiments except the DRY (Fig. 5.6a-d). The AS and EXP experiments now have diabatic rising motion to the north of the low, as well as increased values of total omega. In these two experiment there is a mix of diabatic and adiabatic vertical motions in this region. The KUO and DRY experiments had smaller omega magnitudes than the other two forecasts, with the DRY experiment having less than 5 units. However, the central pressure forecasts for the KUO and DRY experiments were only about 3 mb weaker than the forecasts of the other two experiments. One notable factor in this case compared to case 6 is the considerably stronger temperature gradient and advections in the area of both the warm and cold front. This gradient provided the initial forcing needed to initiate the deepening of the low, and produced the large-scale precipitation that is beginning to add LHR to the system. Adding to the increase in adiabatic upward motion is the vertical alignment of the PVA max over the omega maximum, a forcing that was not present at the 6 h forecast. There also seems to be a relationship between the strength of the PVA and the strength of the rising motion. Thus there is a weak indirect effect of LHR appearing in this case. The increase in LHR as this system becomes more diabatic appears to be providing for some increase in the vorticity

over the location of the maximum rising motion.

The AS and EXP forecasts still showed an area of large omega values to the east along the warm front, though the diabatic components have decreased markedly since forecast hour 6. In these two experiments this omega maximum moved eastward in the preceding 6 hours, apparently along the warm front away from the main low. The amount of descending motion, and the way it is positioned almost completely around the low, particularly in the EXP case, indicates that a fairly-self contained circulation seems to have developed. A small-scale vorticity maximum associated with this heating maximum is present at 500 mb. However this vorticity is located in the large-scale ridge, roughly 1500 km away from the vorticity maximum associated with the trough. A weakening of the 300 mb jet is also collocated with this feature. The KUO experiment is still forecasting this omega maximum, and while the diabatic component decreased, there appears to be an increase in the extent of the maximum model omega. In the KUO experiment the model omega is also starting to elongate east/west indicating the existence of the warm front. These is also some indication of a cold front in all three forecasts incorporating LHR

3. 18 hour forecast

All four experiments showed an elongated omega pattern in the area of the surface low (Fig. 5.7a-d) and further increases in diabatic and total omega. The AS experiment had a model rising motion maximum north of the low exceeding -25 units with an area of diabatic motion imbedded in it. The diabatic omega made up roughly 2/3 of the total omega. This experiment also showed evidence of the cold front and the occluded front, though the latter had weak rising motion compared to the case 6 AS experiment, even though this case 7 forecast was very close to the case 6 AS forecast in central pressure.

The EXP experiment was also taking on the appearance of an occluded system, with stronger omega values evident near the low center than in the AS experiment

with the diabatic omega comprising only roughly half the total. The EXP experiment, however, did not produce as much rising motion associated with the warm front. The appearance of diabatic descending motion to the east and south of the rising motion is not confirmed by the model omega and may be an artifact of the relaxation technique.

The KUO experiment does a better job in detailing the position of the warm front, but the ascending motion near the low center is weak with no significant diabatic contribution. There is no indication of a cold front in the KUO forecast. The DRY experiment now shows a broad area of weak ascending motion wrapped in a rough comma shape around the system similar to the KUO. There was stronger precipitation in the vicinity of the low in the AS and EXP cases, which compared well with the greater rising motion and lower central pressure in these experiments. As discussed in Chapter IV, upper-level support was roughly equal in all four experiments.

At forecast hour 18 the area of diabatic rising motion to the east of the low had continued to decrease in magnitude in the three experiments incorporating LHR. The AS and KUO experiments were merging this maximum with the broad warm frontal ascent. The EXP experiment showed the maximum in the same location as in the AS and KUO forecasts, but more isolated from the primary ascent maximum. The signature of this heating maximum was present but weak in the 500 mb vorticity and 300 mb windspeed field.

In contrast to case 6 where strong upward motion and ageostrophic outflow and an increase in the ridge amplitude increased the velocity of the downstream jet, case 7 showed only a weak increase in the downstream jet streak well away from the surface low center. In addition, only small differences in the 500 mb height and vorticity fields are present in the vicinity of the surface low. A strong interrelated feedback mechanism between the surface and upper air was still not evident for case 7.

4. 24 hour Forecast

By the 24 hour forecast, the model forecasts continued to show only weak rising motion in the vicinity of the surface cyclone center (Fig. 5.8a-d). Despite this, the AS and EXP experiments produced good forecasts as far as central pressures and locations are concerned. The AS and EXP cases are fairly similar. Both predicted a long area of weak model rising motion along the warm front with a small diabatic component. By this forecast period both experiments also showed some indication of upward motion developing along the cold front. The EXP experiment output showed that the cold front omega was very much a result of diabatic processes, while the AS experiment showed some adiabatic processes were at work. The EXP case had an area of descending diabatic motion extending southeastward from the low partially down the cold front. This is hard to reconcile with cold frontal processes, though there is also a small area of descending model omega near the southern edge of the diabatic descending motion.

The KUO and DRY cases also showed similar omega patterns. The KUO case had a larger area of rising motion, and a small area of diabatic rising motion. The DRY experiment showed no evidence of the warm or cold front, while the KUO experiment does suggest both. The precipitation totals of the forecasts are correlated with the magnitude of the vertical motions, although there has been little new precipitation generated by any of the experiments in the last hours of the forecast.

5. Case 7 Summary

The case 7 system was characterized by primarily adiabatic vertical motion early in the forecast. There was considerably more support for the system from temperature and vorticity advection than in the case 6 cyclone. The initial adiabatic motion released latent heat which slowly increased diabatic activity through the first 12 h of the

forecast period. By forecast hour 12 there was weak indication of an indirect LHR effect increasing the vorticity max at 500 mb. In contrast with case 6 this system increased its diabatic activity through the forecast, though it never reached the levels of case 6. Overall, this cyclone had a much more balanced adiabatic/diabatic nature.

VI. CONCLUSIONS AND DISCUSSION

The model experiments described by this thesis clearly support the original assertion that LHR influences storm development. The systems chosen for this work are the extreme cases available from the experiments run by Kuo and Low-Nam (1990). These two storms represent the most sensitive to precipitation (case 6) and the least sensitive (case 7), as demonstrated by the minimum sea level pressure traces presented earlier. The investigation of results from the individual experiments shows in detail the interactions that resulted from the different parameterizations and lead to several main conclusions and numerous areas for further research.

A very important first conclusion is that the scheme used to calculate the diabatic omega values appears to work reasonably well. With the exception of the anomalous area of diabatic rising motion over the Appalachians, the diabatic vertical motions, both ascending and descending agreed well with known conceptual models. This is noteworthy, considering the smoothing that was required, particularly in the case 7 KUO and AS experiments. In the form used with this data the diabatic omega calculation appears to be very susceptible to sharp vorticity gradients; smoothing must be used in these regions. The calculation is also very susceptible to the value used to replace negative values. A number too large or small can produce very sharp small-scale gradients that will cause the calculation to "blow up". However, the use of smoothing leaves in doubt the actual magnitude of the calculated omegas. Further research in this general area could include an averaging scheme to determine the best value of vorticity to replace the negatives with rather than trying to find a single number. Another area to investigate is to determine what is causing the area of diabatic motion over the Appalachians, and whether the factor creating that anomaly affects other parts of the model output. Finding a way to determine

the accuracy of the calculated diabatic omega is also very important before an comparison of absolute values can be considered.

The case 6 storm was found to be much more responsive to moisture parameterizations. The forecasts produced by the individual experiments were different in all of the fields investigated, not just mean sea-level pressure. Of particular note is the influence that strong vertical motion appeared to have on the jet streak patterns. The increase in the downstream jet, and decrease in the upstream jet were greatest in the cases with the most diabatic vertical motion, while the speed changes were nonexistent in the DRY case. The AS and EXP experiments overbuilt the case 6 jet compared to the analysis early in the forecast period. These cases also had the strongest vorticity, vertical motion, and precipitation near the system center. Since the only difference between the experiments was the parameterization, a broad conclusion is that LHR was too large in these two systems, thus creating too much rising motion near the center of the storm which increased upper-level ageostrophic outflow and low-level inflow which aided storm spin-up. The upper-level ageostrophic outflow, and increased amplitude of the ridge from the excessive heating, increased the jet streak forcing to the system, and set up positive feedback. In the AS and EXP cases this feedback was stronger than in the atmosphere, and the forecast cyclone was too intense. The KUO experiment had less of all of the above parameters, and the feedback loop was sustained at a weaker level that was nearer to the analyzed system intensity. A calculation of the full vertical circulation, with associated ageostrophic winds could provide insight into these upper level effects, and allow a direct comparison of the effects of the upper-level ageostrophic outflow.

In both cases 6 and 7 the EXP experiment had a greatly reduced areal coverage of light precipitation, while maintaining among the highest values in regions of maximum precipitation. Most likely this was due to the parameterization, which allowed evaporation

of precipitation in non-saturated layers. This appeared to reduce the precipitation in areas of light rain where presumably the air is much less saturated. However, in the areas of heavy rain it is likely that the atmosphere is more nearly saturated in the subcloud layer so less evaporation occurs. Given the differences in the way the two cases reacted to the parameterizations it is interesting that the resulting precipitation patterns, i.e., reduced areal coverage of the EXP experiment, were nearly the same.

The case 7 forecasts, with the exception of the DRY experiment, all showed a very strong area of vertical motion, vorticity and relatively low central pressure to the east of the main low. The development of this area was almost strictly diabatic, and it was isolated from the primary dynamic forcing of the cyclone system. The case 7 low center itself showed very little vertical motion at 700 mb when compared to case 6, and what motion it did exhibit was mainly adiabatic. Four-Dimensional visualization showed that there was very little diabatic motion near the system center at any level until late in the forecast period, but that the total omega reached very close to -25 units through a large vertical extent by hour 12. Thus, though the contour values used for total omega do not indicate it well there was actually quite a bit of dynamic omega near the system center. This evidence supports the contention that case 7 was much more dynamically driven than case 6.

Case 7 lacked the LHR-induced feedback from the surface to upper levels present in case 6. This was due to the lack of LHR in the immediate vicinity of the low center until late in the forecast period. What case 7 did have was an extremely strong warm front, which was highly diabatic in character. Near the system center dynamic lifting and the resulting broad area of light rain triggered the LHR noticeable later in the forecast period. This change from a mostly dynamic system is noticeable in the surface pressure traces. Early in the forecast period when dynamic processes dominated the case 7 cyclone the experiments were all producing similar output since the convective parts of the

parameterizations were minimally triggered. Once LHR started occurring the AS and EXP experiments exhibited their stronger LHR responses and deepened the system more than the other experiments. The fact that this system is much more dynamic in nature is derived from the idea that if the DRY case makes a reasonable forecast then little precipitation is occurring. The precipitation fields described in chapter IV also support this. The case 7 precipitation fields tend to be weak in the area of the low until later in the forecast period.

Investigation of other storms is needed to determine if the character of the case 7 storm with its large strong warm front is somewhat of a normal condition associated with dynamic systems. Comparing other Kuo and Low-Nam storms that were not as extreme in their response to LHR would help greatly in determining the importance of the warm front in the dynamic type of system. Comparison of the other less "extreme" storms could also answer questions concerning the reasons a particular parameterization works best in each case and would provide a database of information concerning the degree of diabatic or dynamical forcing in each system. Further investigation should focus on the reason for the spin-up of the case 7 cyclone. The LHR in case 6 is an obvious generation mechanism for that system, but the cause of the initial cyclogenesis is not so clear in case 7, but it was not LHR.

The use of four dimensional visualization to get a direct time lapse comparison of any available field at all levels played a very important role in determining the results to display in the 2-D graphics presented in this thesis. Being able to compare any of the fields to each other, for example, watching the surface low move under the right-rear quadrant of a jet streak and then deepen as the rising motions increase substantially improves the understanding of the interactions in a cyclone. The ability to display data in many forms with the click of a mouse allows quick comparisons, and provides the ability to rapidly get needed information, in the form required.

The classification of a storm as diabatically or dynamically driven was easy in the two cases studied here. The nature of the cyclone had a profound effect on the success of the forecasts produced by the various parameterizations used in the "extreme" cases studied. In diabatically driven systems the AS and EXP experiments, with more sophisticated handling of cumulus parameterizations, tended to over-intensified the systems during the periods when there was very strong diabatic forcing. The KUO experiment had a less complex LHR scheme, that produced less LHR, and handled the forecast the best during the early diabatically dominated part of the forecast. By the end of the case 6 forecast when diabatic forcing had decreased the AS and EXP experiments were the most accurate in their central pressure forecast, though their forecast trend, steady, did not agree with the analysis trend of deepening. The KUO experiment, though still too weak in intensity at the end of the forecast period, was still forecasting deepening. In the dynamically driven case 7 cyclone the AS and EXP experiments produced a forecast very close to the KUO and DRY experiments near the beginning of the forecast when there was little LHR. The AS and EXP experiments produced a better forecast than the KUO and DRY experiments near the end of the storm when LHR became stronger. The lower levels of direct LHR in case 7, compared to case 6, appeared to greatly improve the success of the forecasts in the experiments with complex moisture parameterizations. The part that the indirect effects of LHR played in the differences in the forecasts between the two cases needs further investigation. The AS and EXP forecasts did produce a very strong area of vertical motion and precipitation along the warm front in case 7. The existence in the real world of this feature is unknown, but was likely not as intense as the forecasts.

Parameterizations greatly affect model output. The degree of that effect is very dependant on the system being modeled. Using the samples in this work it can be generalized that parameterizations with complex moisture components tend to over-deepen

systems while they are strongly diabatic in character. A parameterization with a moderate diabatic component tends to be too weak forecasting systems when they are strongly diabatic in character.

APPENDIX: FIGURES

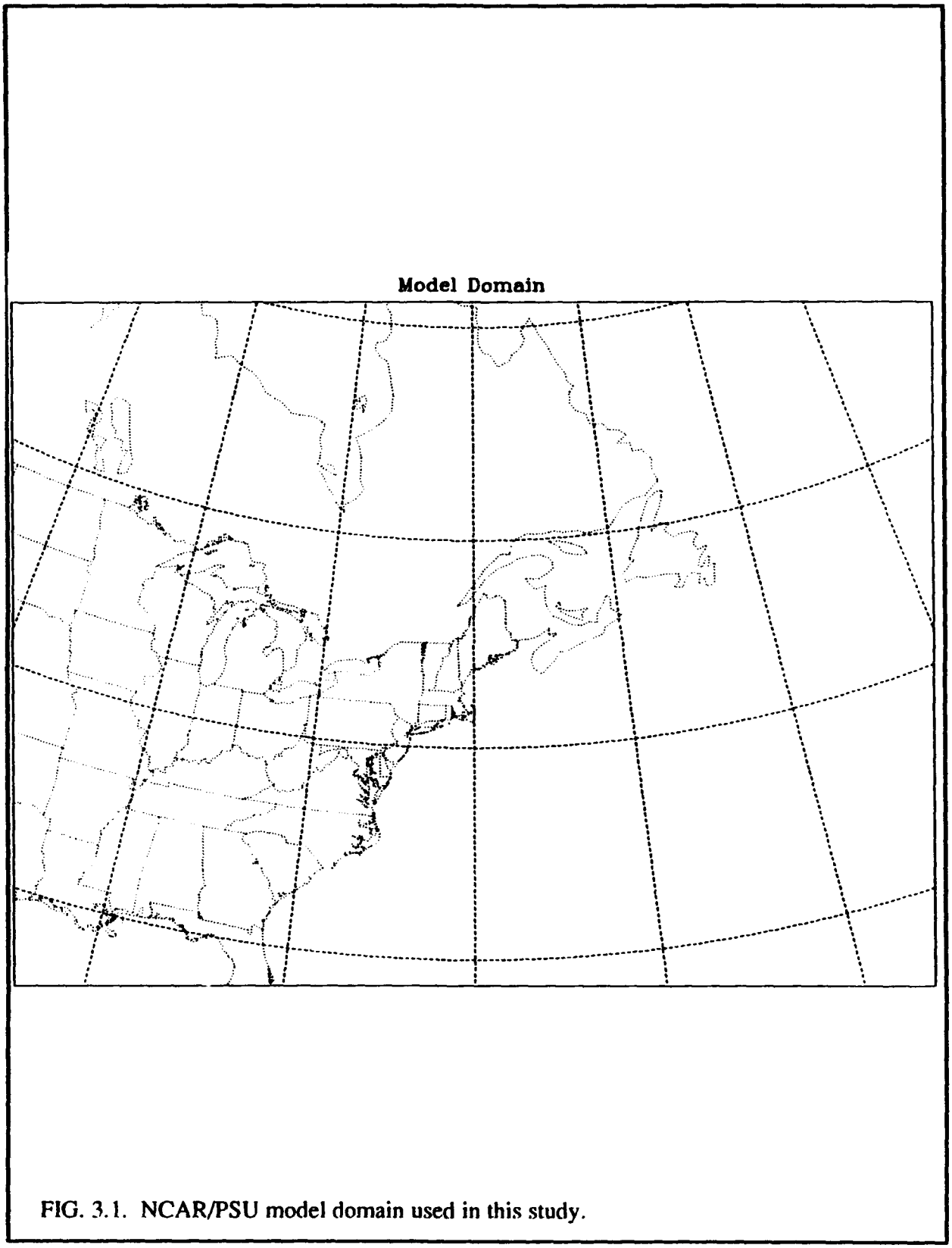

FIG. 3.1. NCAR/PSU model domain used in this study.

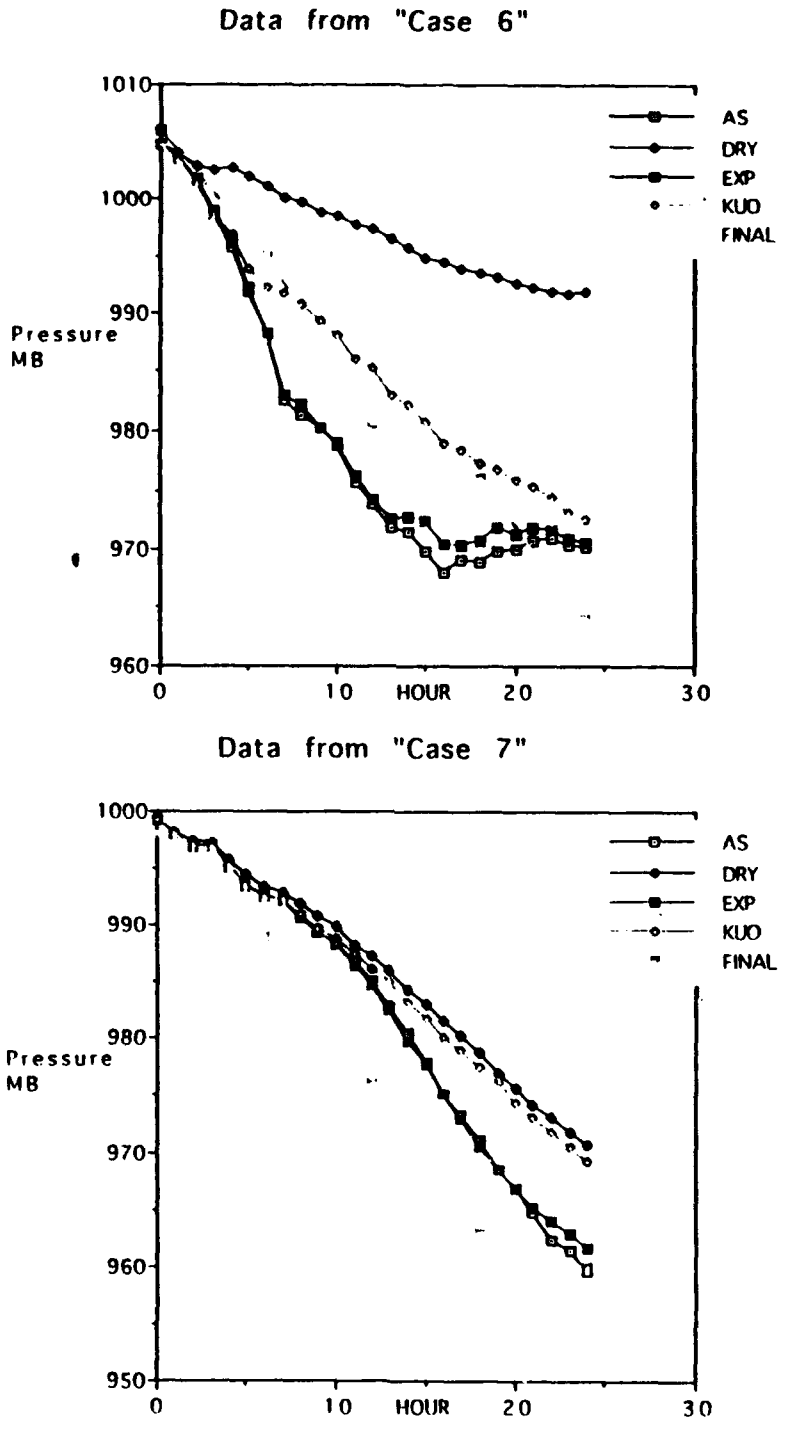

FIG. 4.1. Comparison of minimum sea level pressure between the four model experiments and the NMC final analysis for cases 6 and 7.

a.

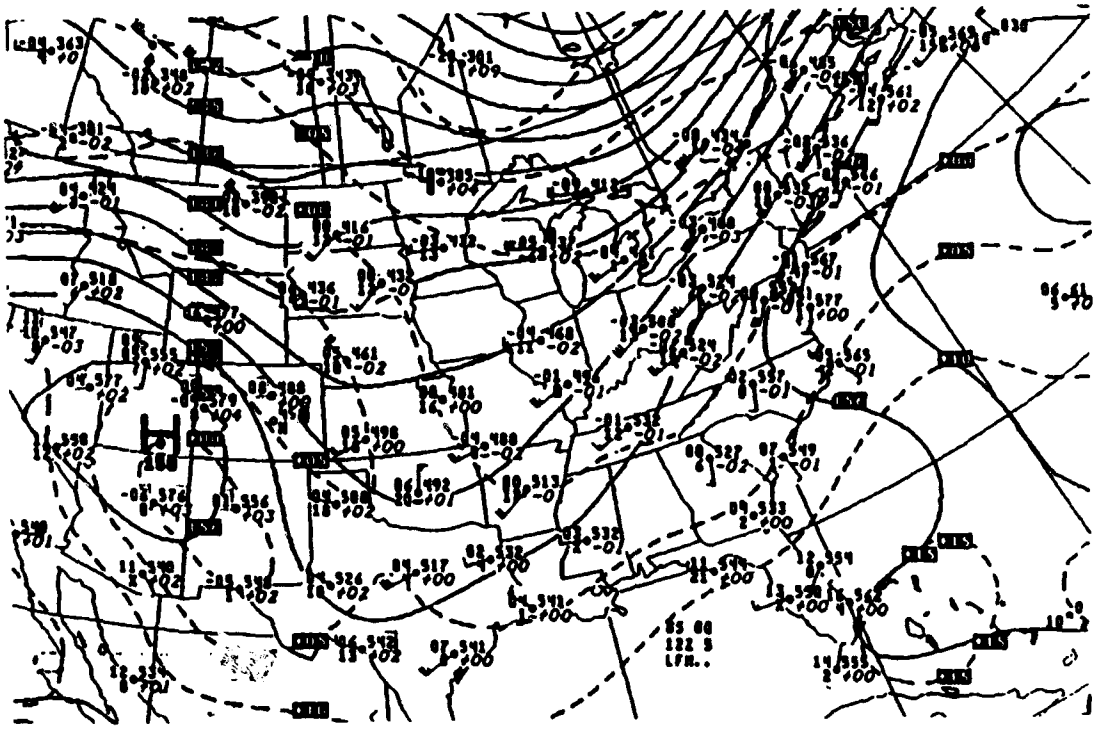

FIG. 4.2. 1200 UTC 5 Jan 1983 NMC analysis of case 6 (a) 850 mb heights (solid, 3 dm increment) and temperatures (dashed, 5°C increment), (b) 500 mb heights (solid, 6 dm increment) and temperatures (dashed, 5°C increment), and (c) 300 mb heights (solid, 12 dm increment) and isotachs (dashed, 20 kt/hr increment).

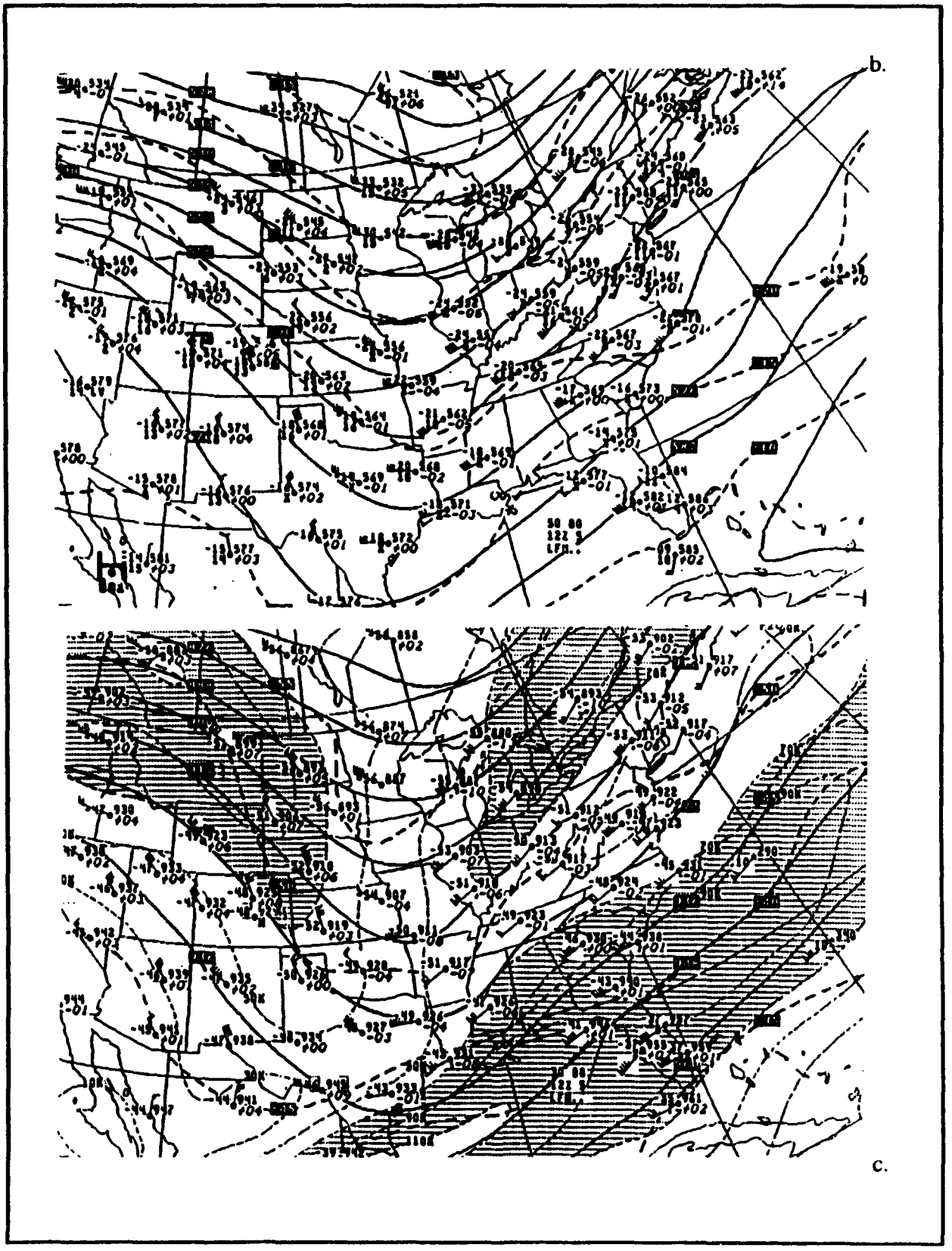
b.
c.

a.

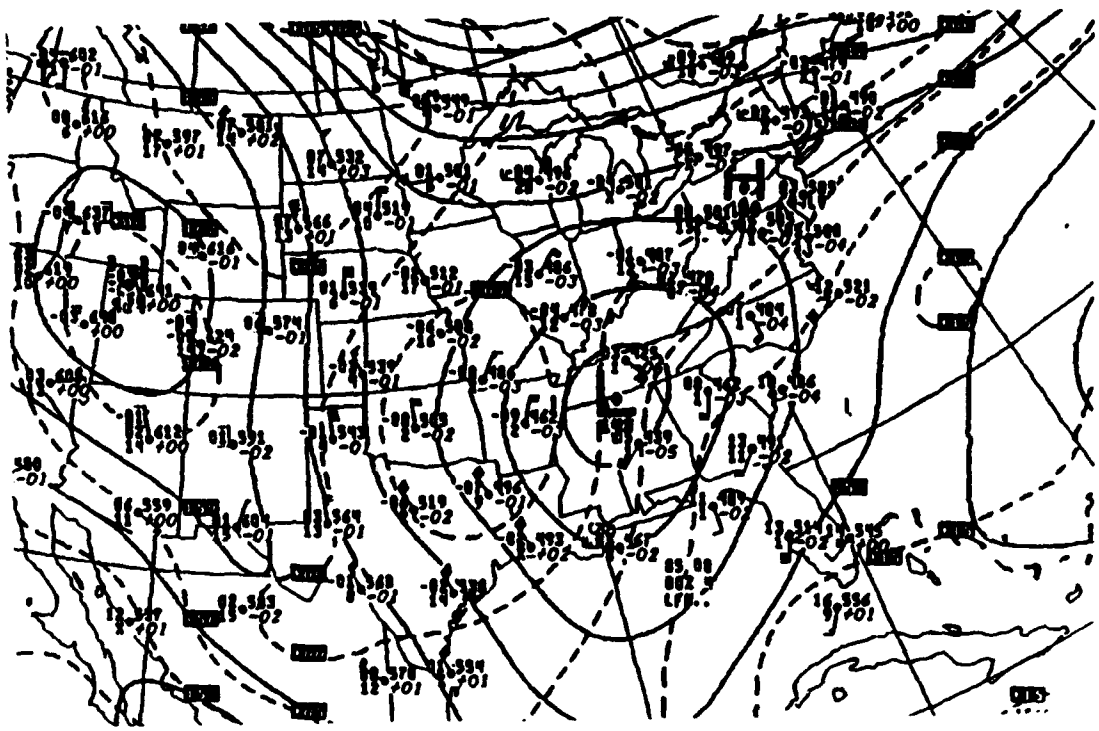

FIG. 4.3. Same as Fig. 4.2 except for 0000 UTC 4 Jan 1985 NMC analysis of case 7.

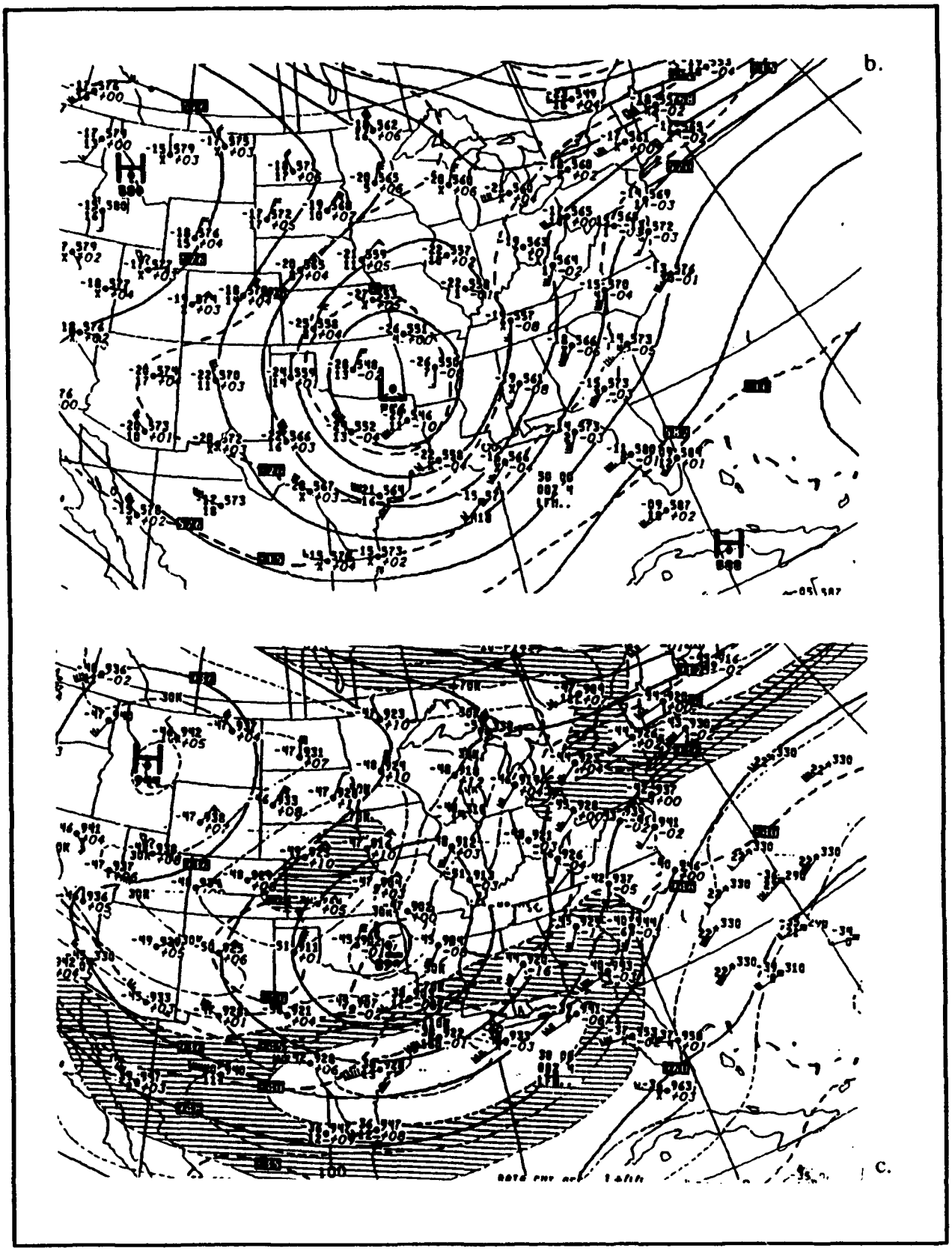
b.
c.

a.

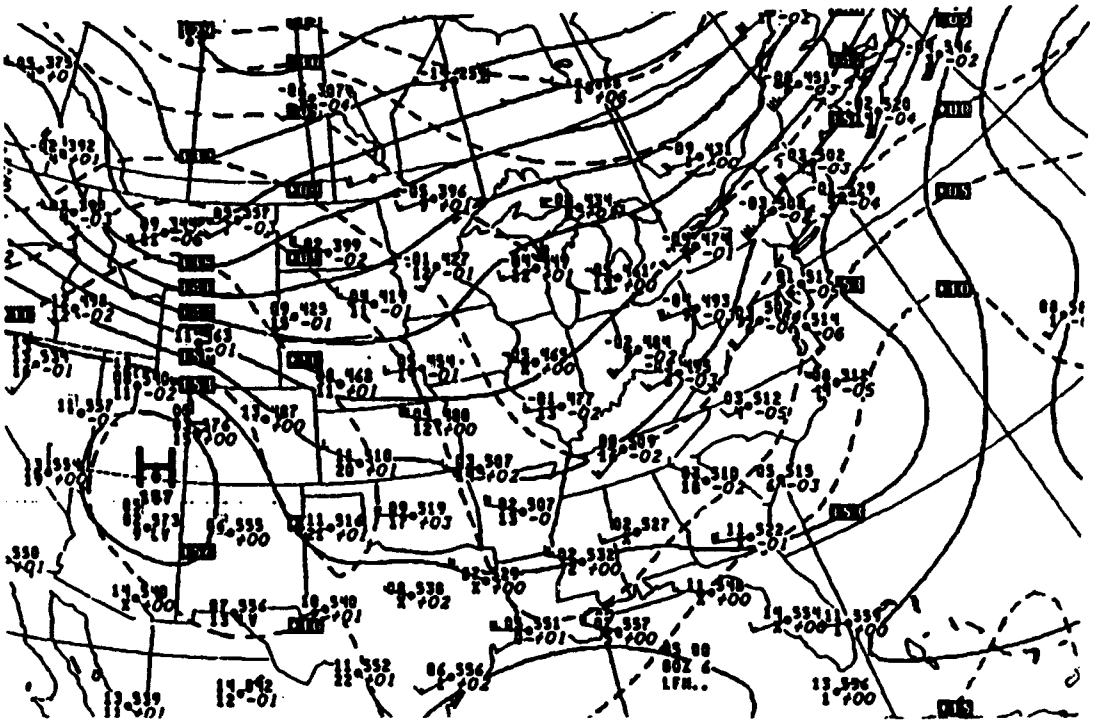

FIG. 4.4. Same as Fig 4.2 except for 0000 UTC 6 Jan 1983 NMC analysis of case 6.

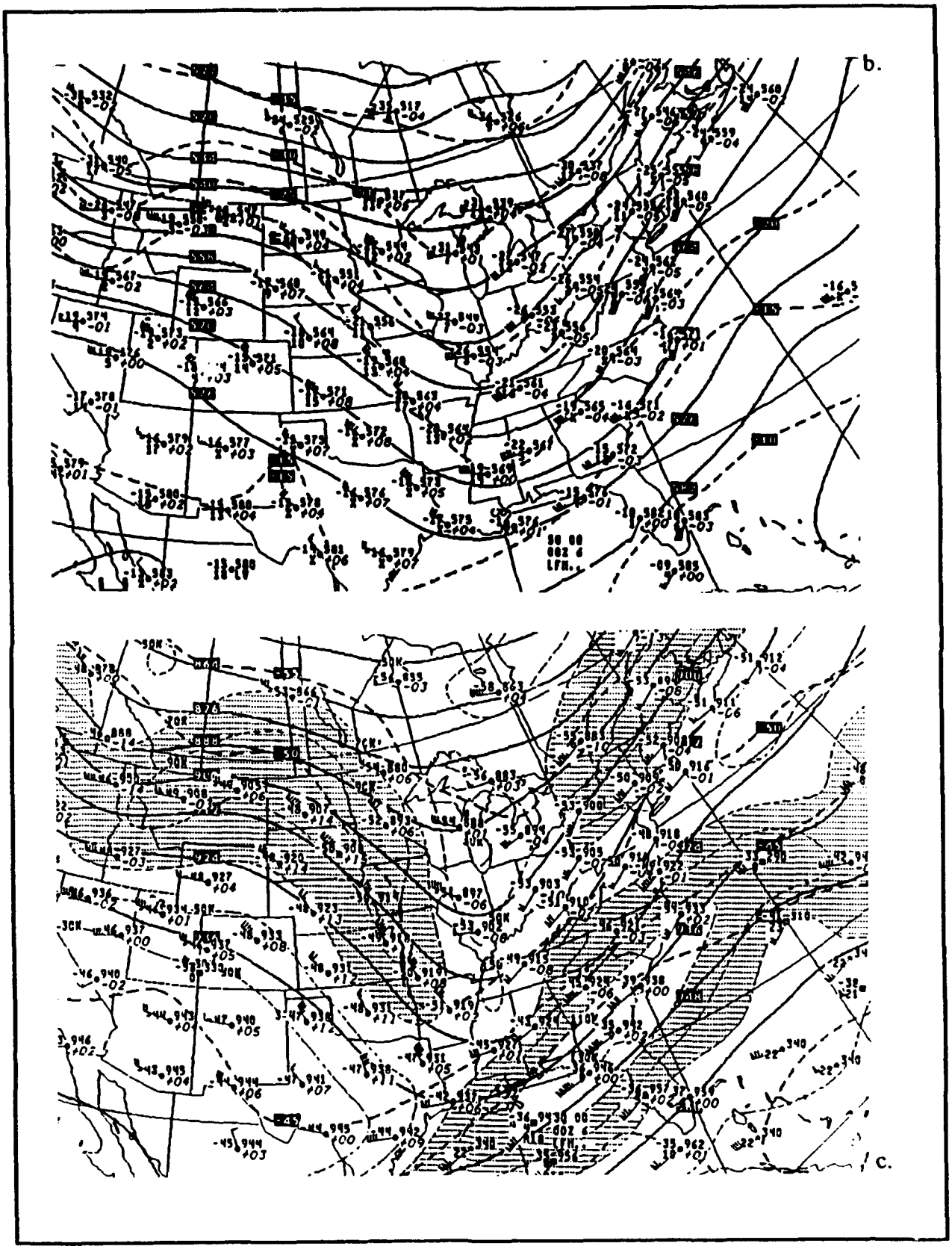
b.
c.

a.

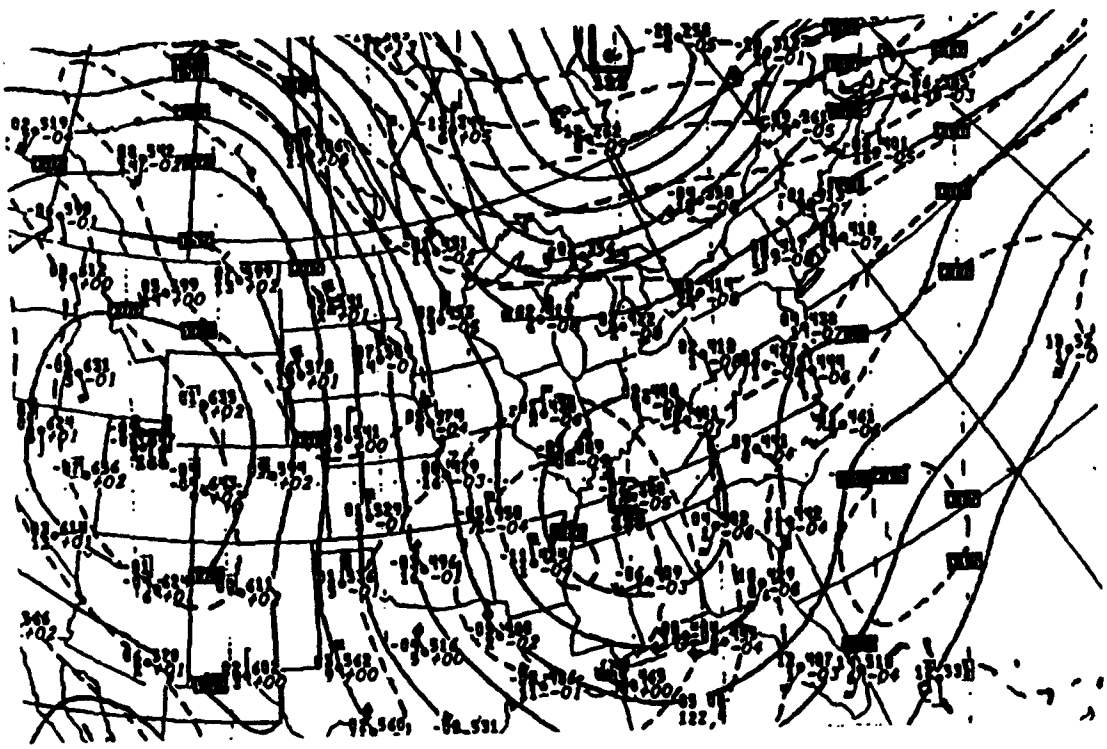

FIG. 4.5. Same as Fig. 4.2 except for 1200 UTC 4 Jan 1985 NMC analysis of case 7.

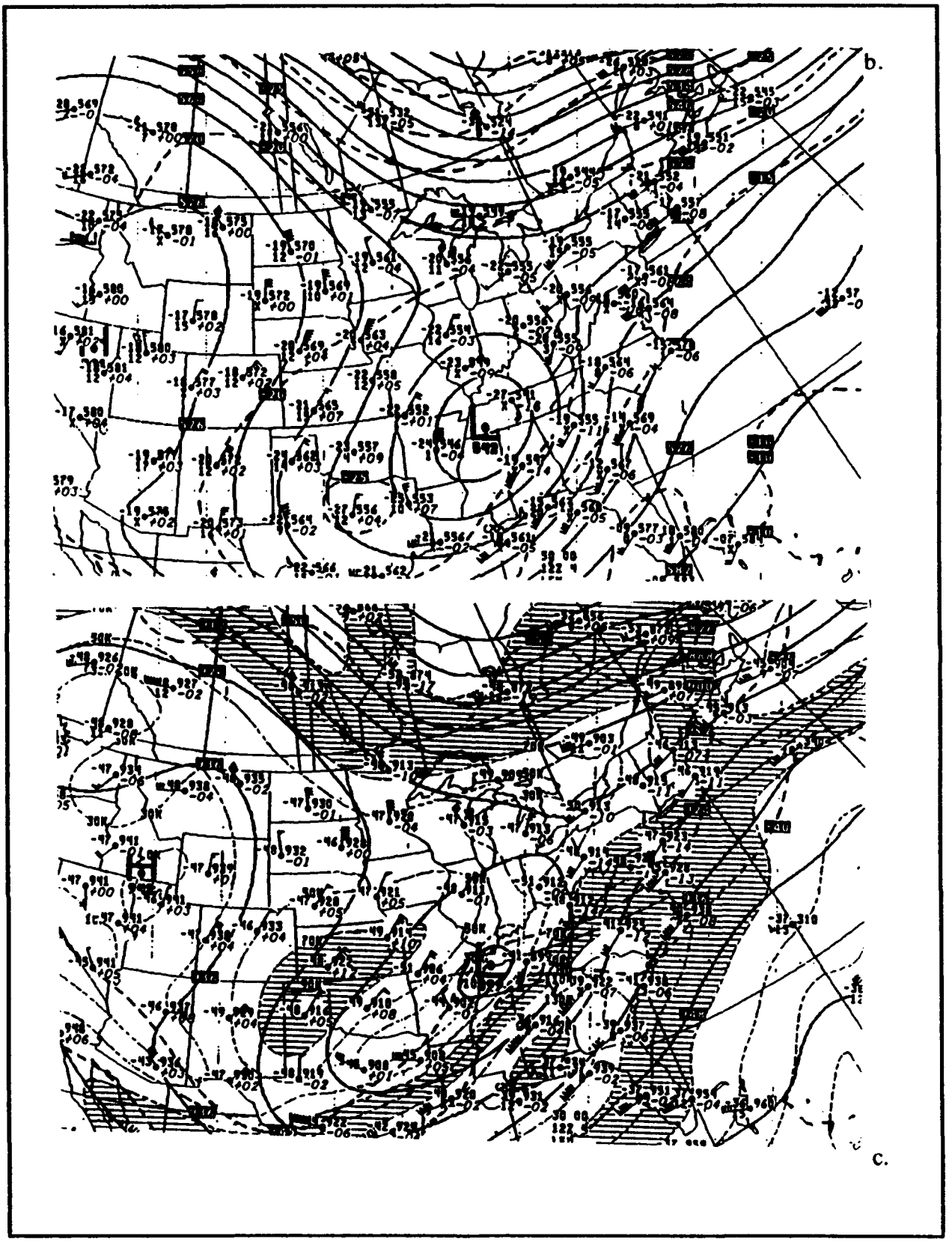
b.
c.

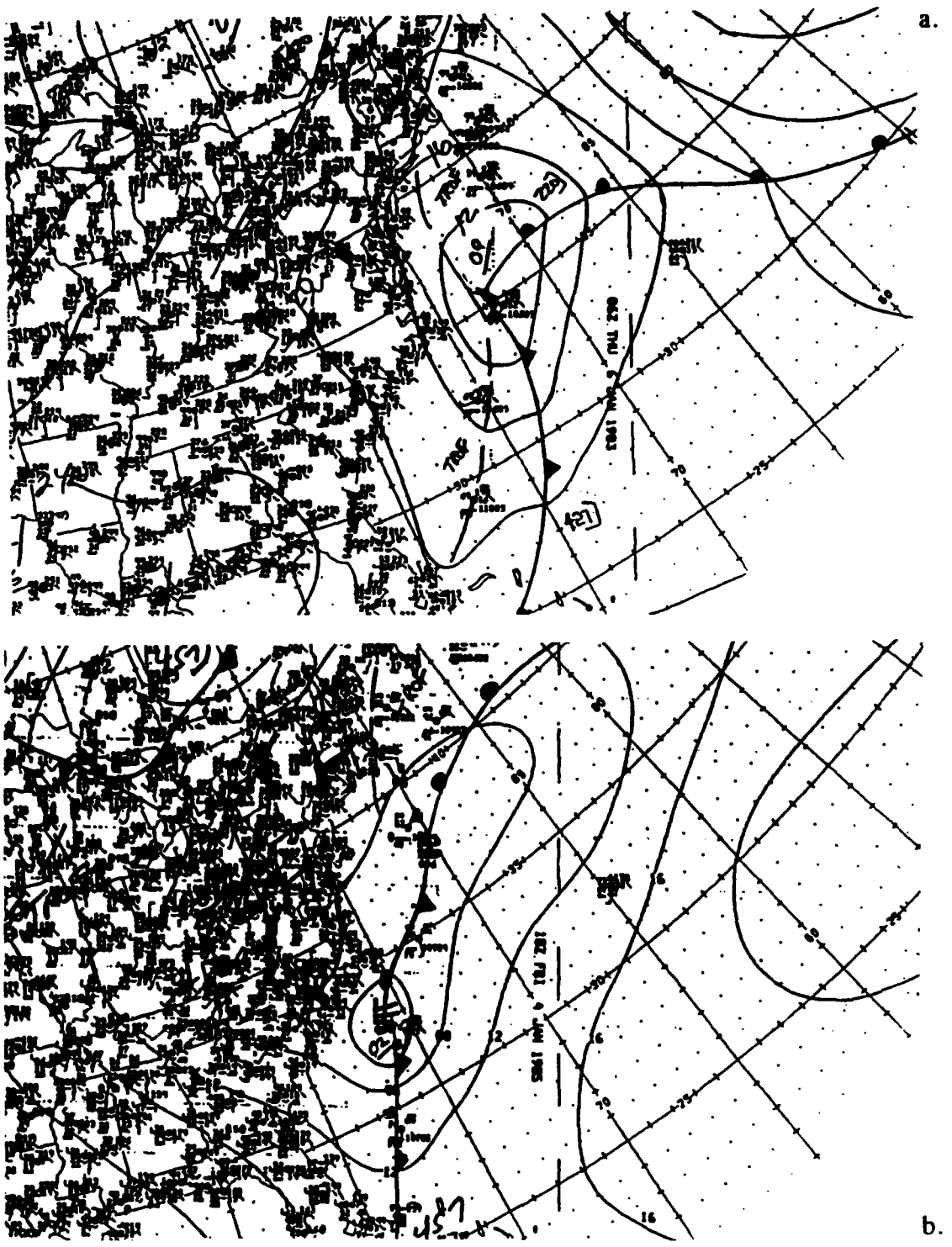

FIG. 4.6. NMC sea level pressure (4 mb increment) and frontal analyses for (a) case 6 - 0600 UTC 6 Jan 1983 and (b) case 7 - 1800 UTC 4 Jan 1985.

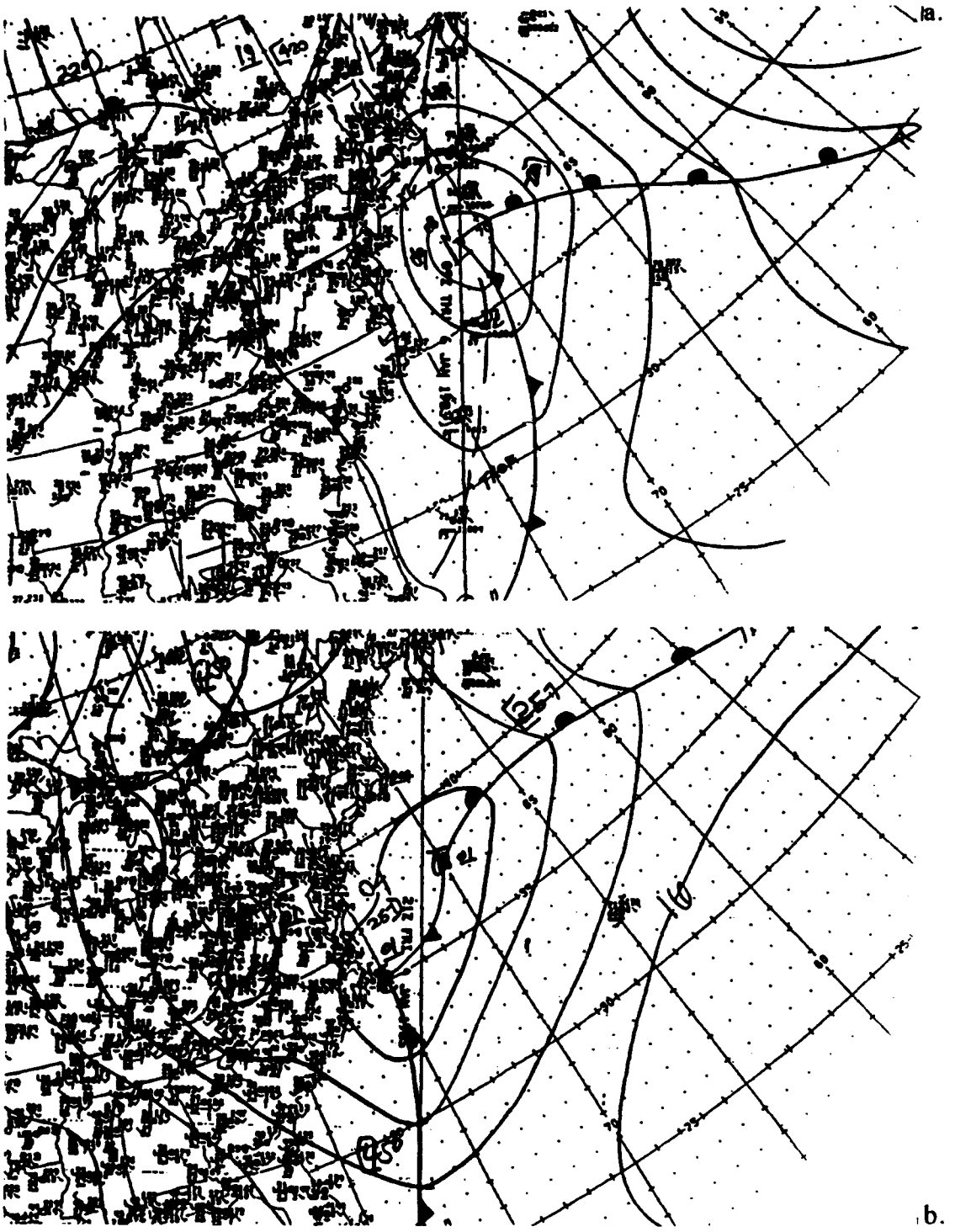

FIG. 4.7. NMC sea level pressure (4 mb increment) and frontal analyses for (a) case 6 - 0900 UTC 6 Jan 1983 and (b) case 7 - 2100 UTC 4 Jan 1985.

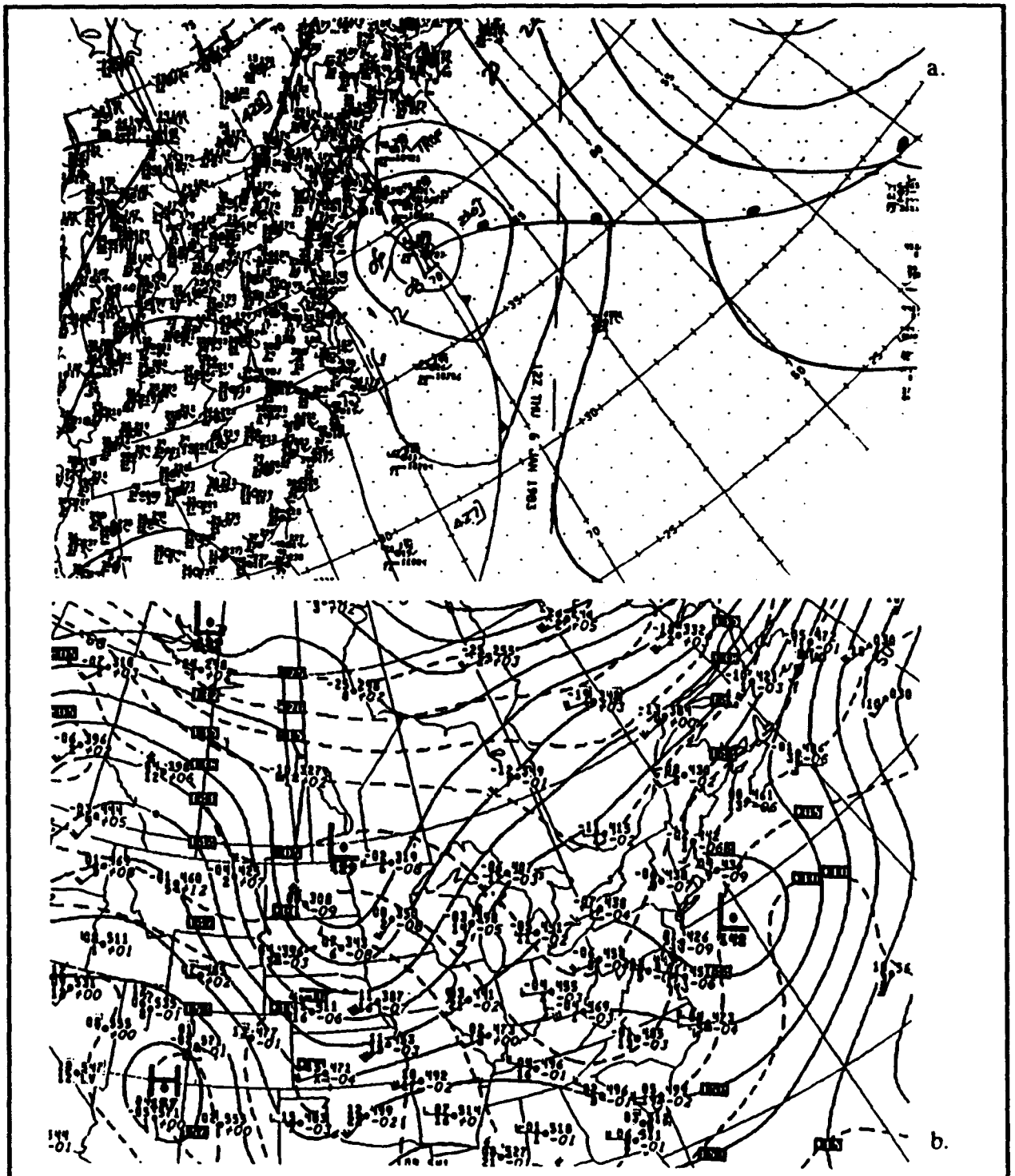

FIG. 4.8. 1200 UTC 6 Jan 1983 NMC analysis of case 6 (a) surface heights (4 mb increment) and fronts, (b) 850 mb heights (solid, 3 dm increment) and temperatures (dashed, 5°C increment), (c) 500 mb heights (solid, 6 dm increment) and temperatures (dashed, 5°C increment), and (d) 300 mb heights (solid, 12 dm increment) and isotachs (dashed, 20 kt/hr increment).

c.

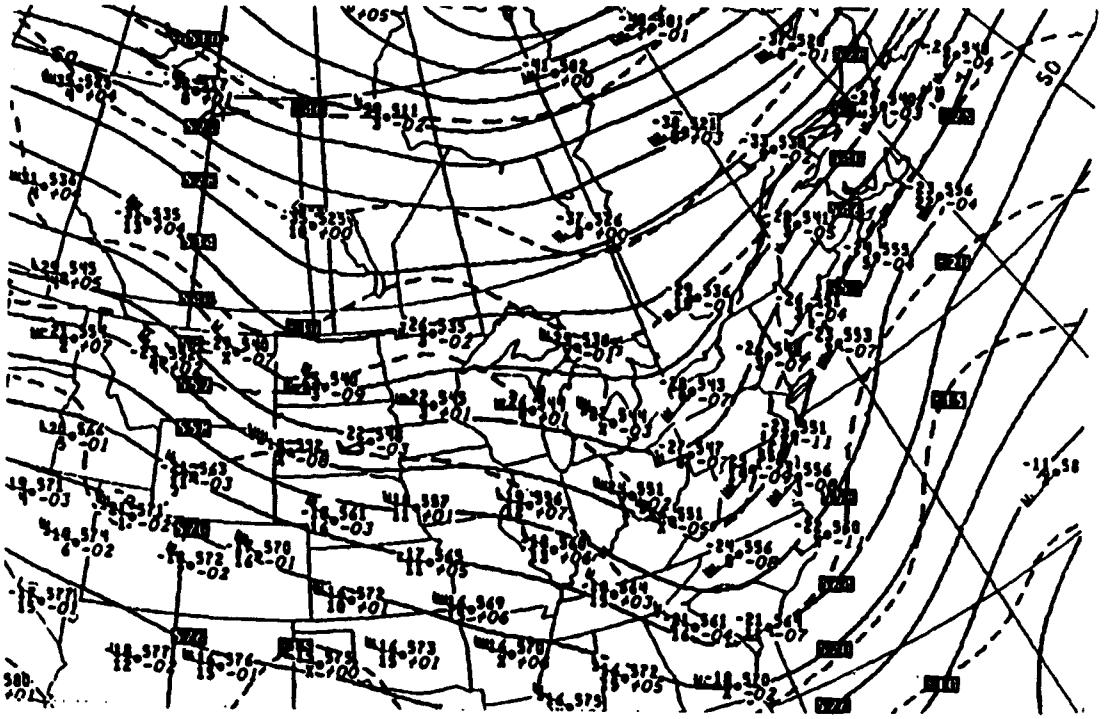

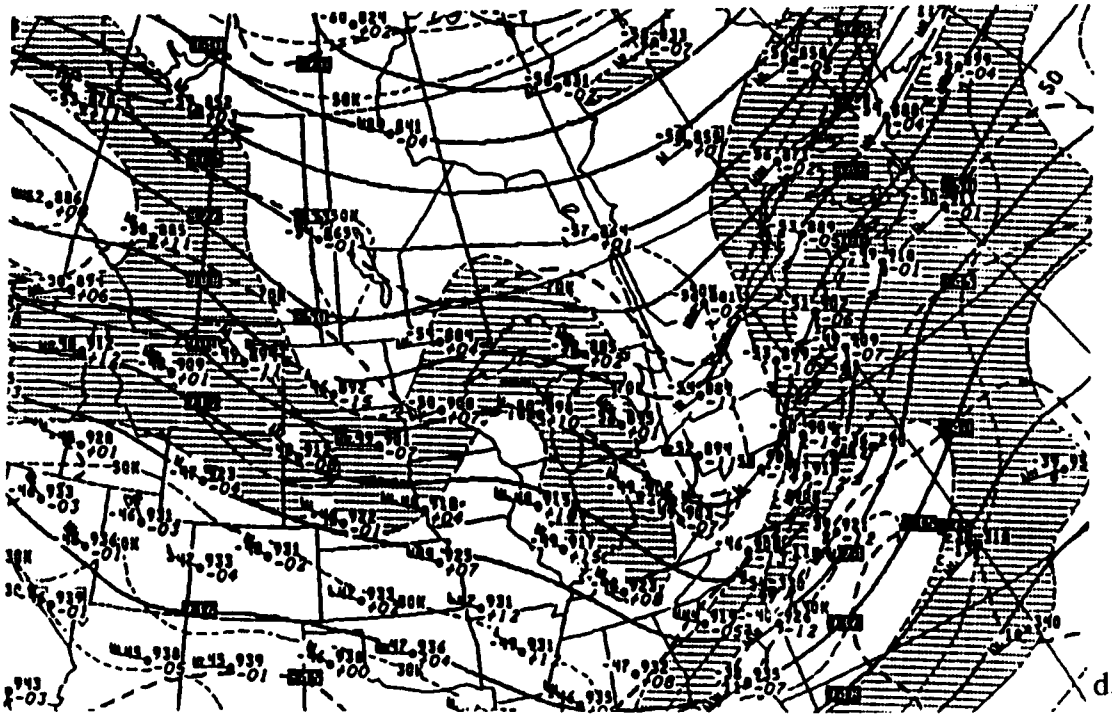

d.

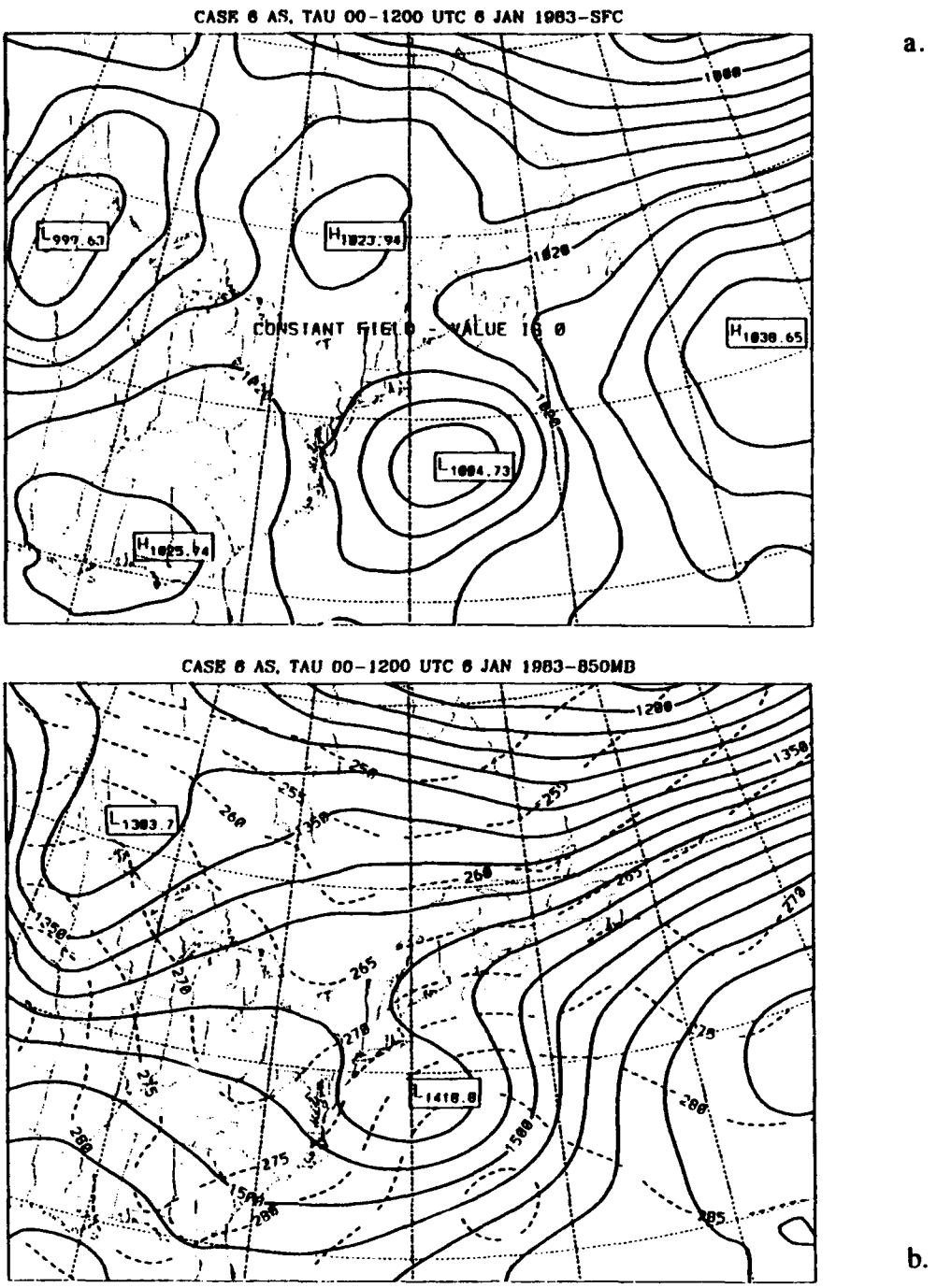

FIG. 4.9. 1200 UTC 6 Jan 1983 AS model initialization field for case 6 (a) sea level pressure (4 mb increment) and total precipitation (.025, .1, 1, and 2.5 cm), (b) 850 mb heights (solid, 3 dm increment) and temperatures (dashed, 5°C increment), (c) 500 mb heights (solid, 6 dm increment) and absolute vorticity (dashed, 2×10^{-5} s^{-1} increment), and (d) 300 mb heights (solid, 12 dm increment and isotachs (10 m s^{-1} increment). Initial fields were identical so only one experiment is included.

c.

CASE 6 AS. TAU 00-1200 UTC 6 JAN 1993-500 MB

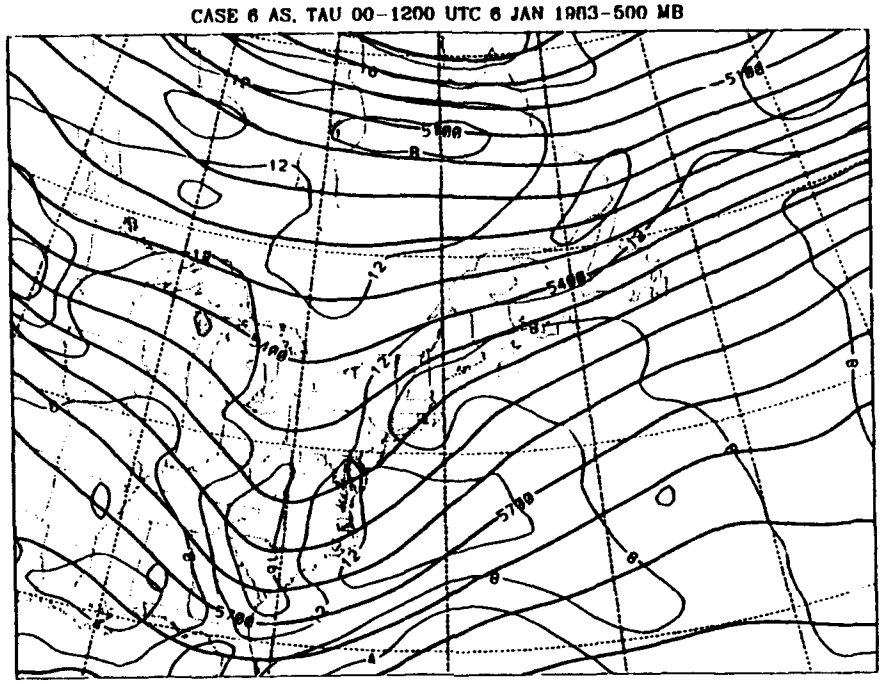

CASE 6 AS. TAU 00-1200 UTC 6 JAN 1993-300MB

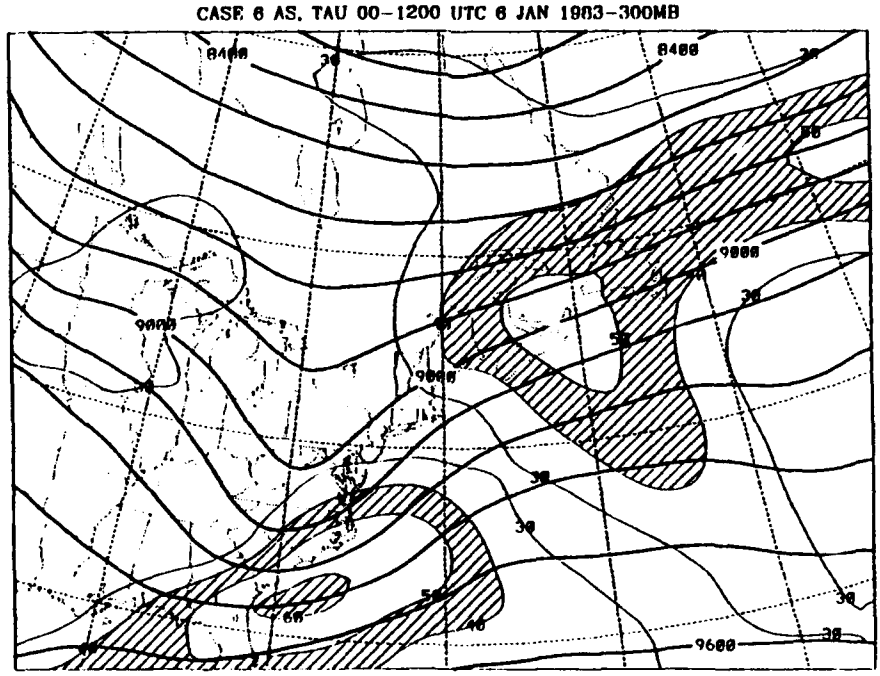

d.

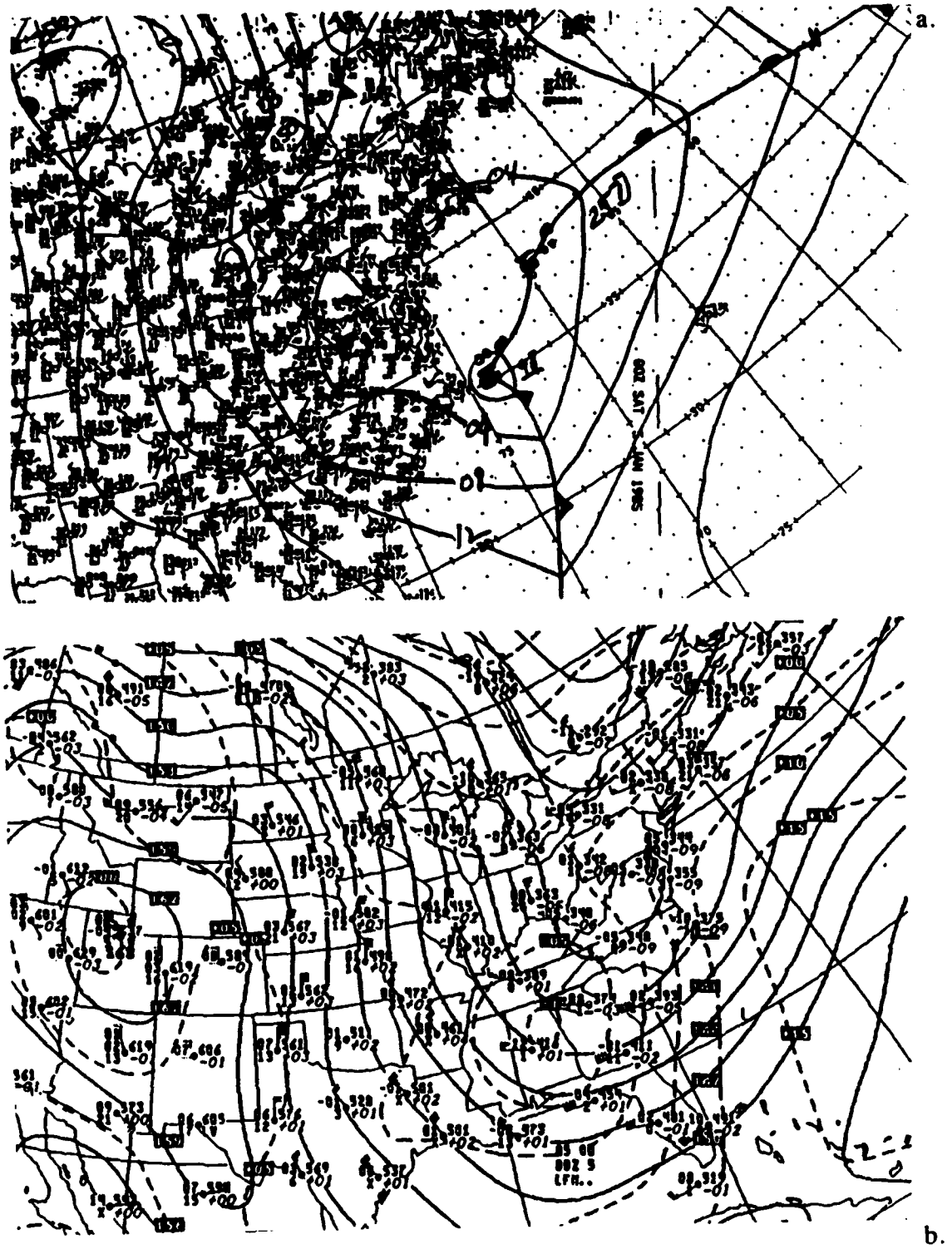

FIG. 4.10. Same as Fig. 4.8 except for case 7, 0000 UTC 5 Jan 1985.

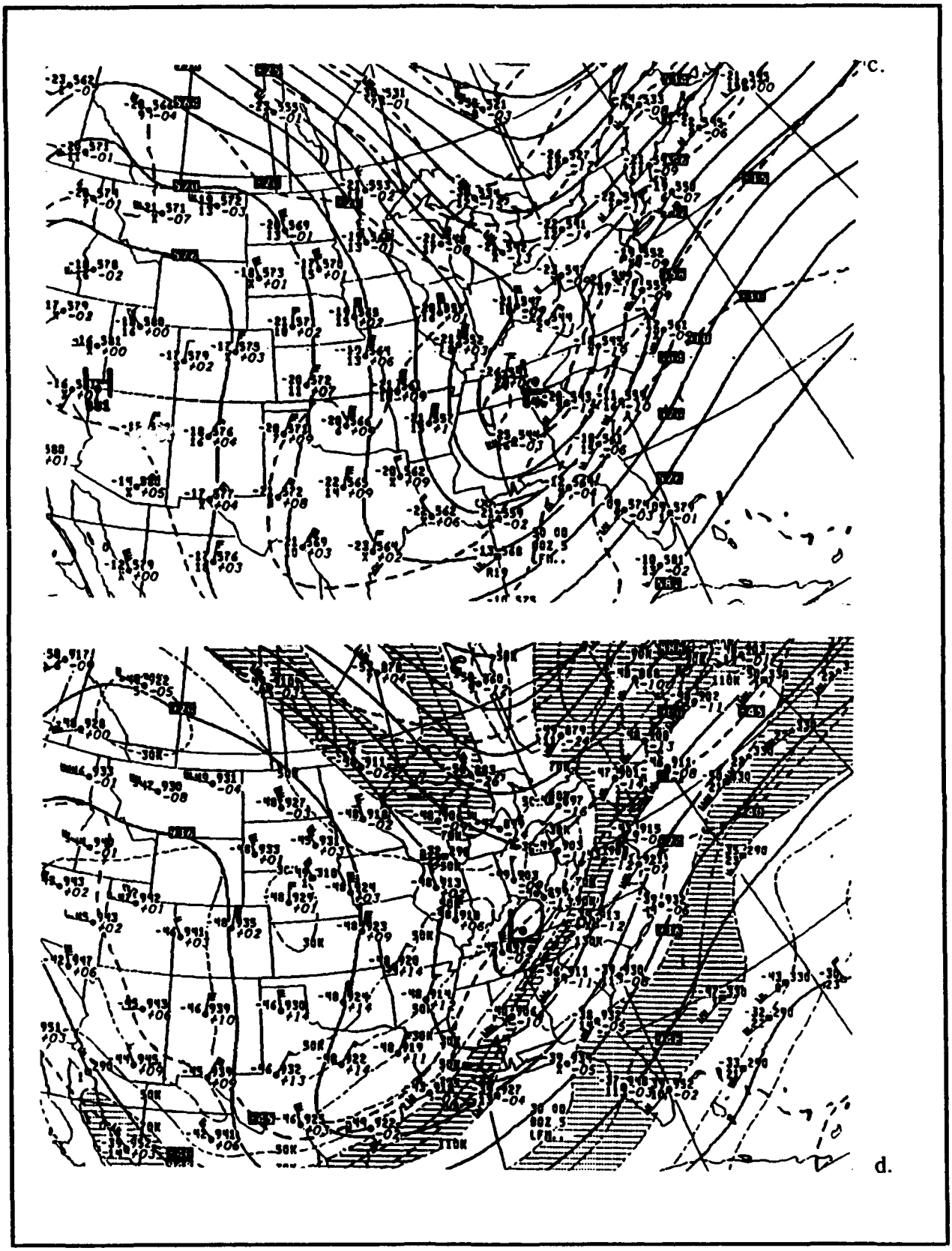

c.

d.

a.

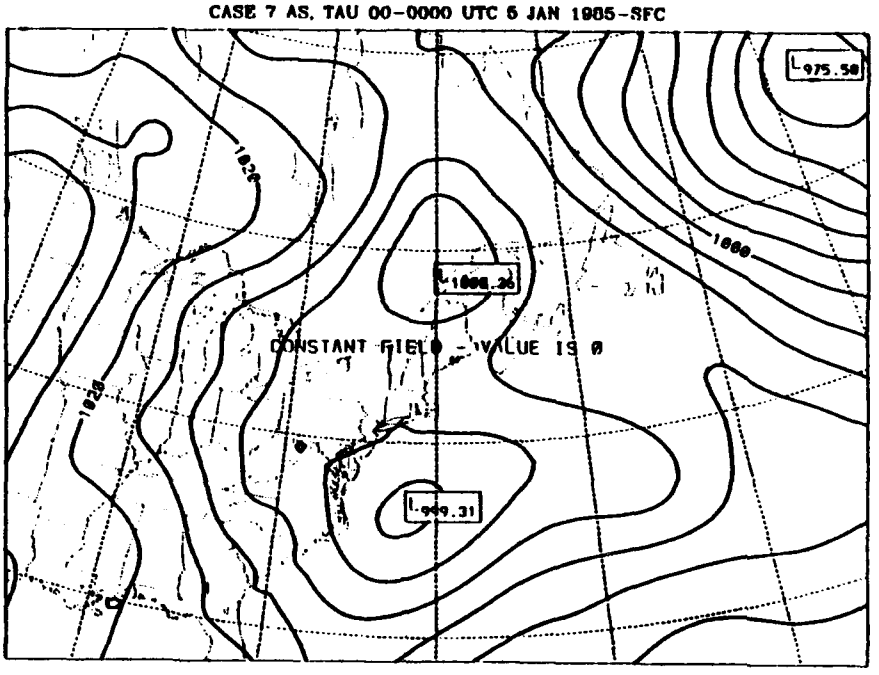

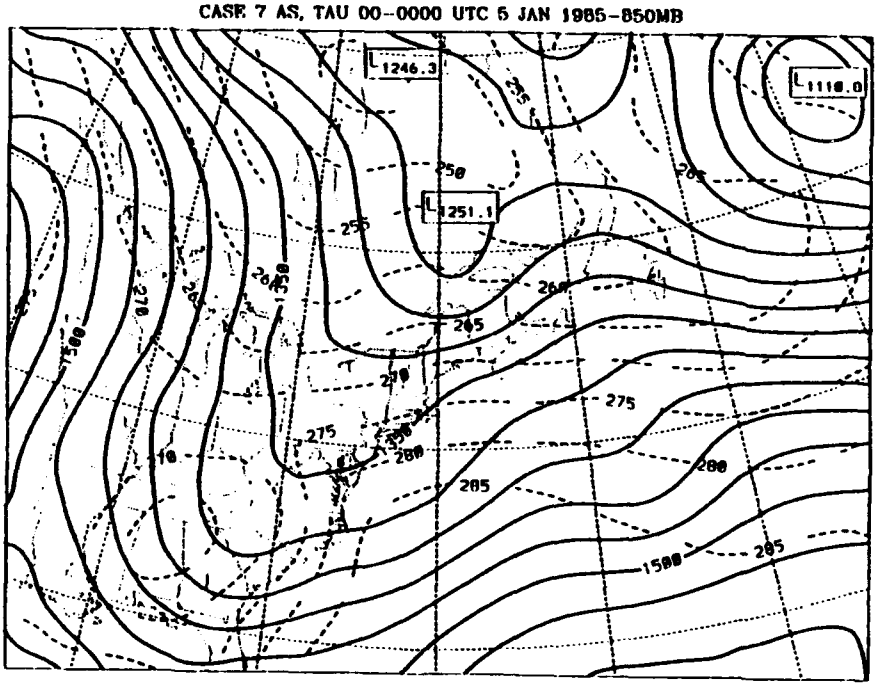

b.

FIG. 4.11. Same as Fig. 4.9 except for case 7, 0000 UTC 5 Jan 1985.

c.

CASE 7 AS, TAU 00-0000 UTC 5 JAN 1985-500 MB

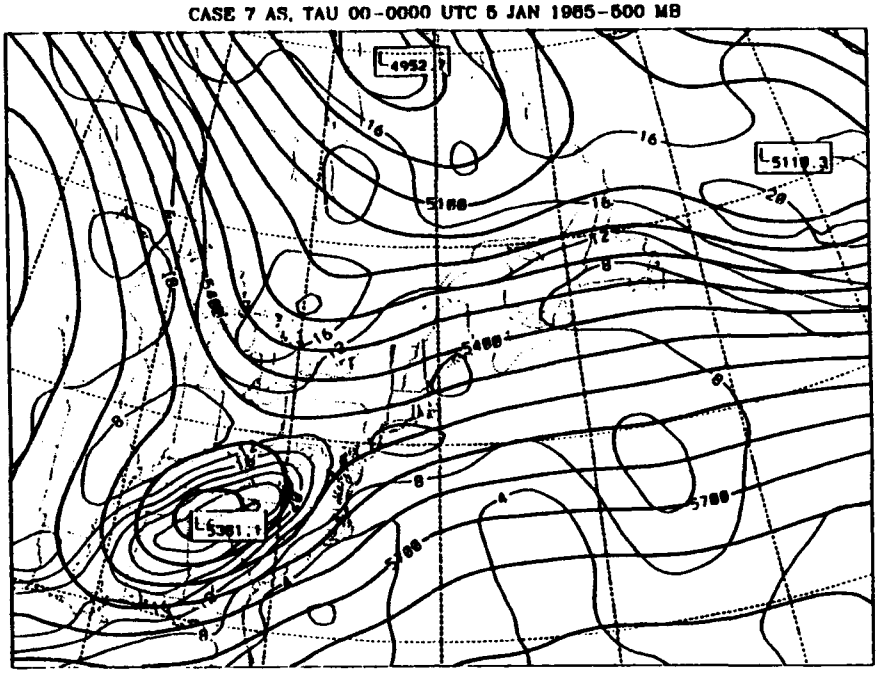

CASE 7 AS, TAU 00-0000 UTC 5 JAN 1985-300MB

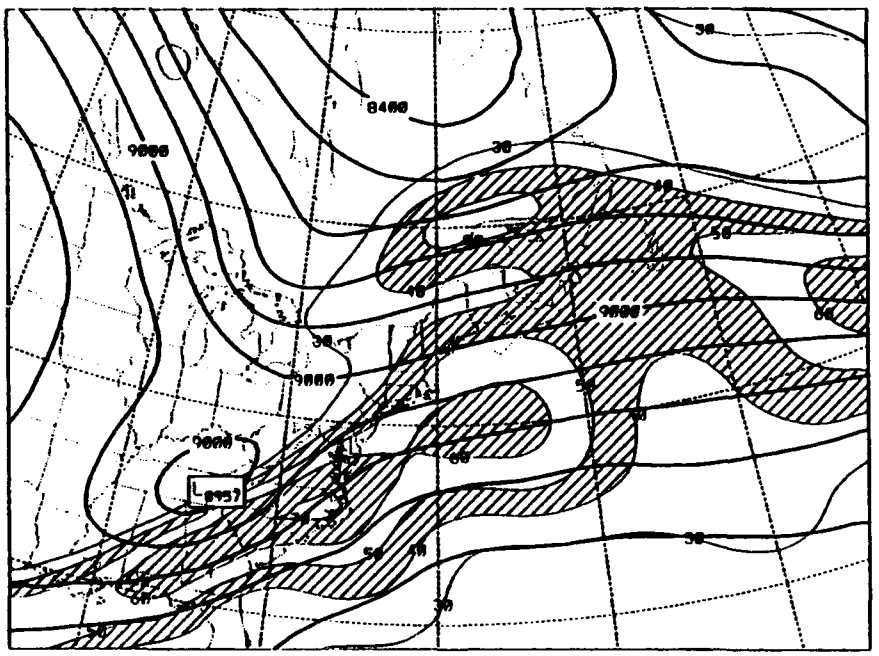

d.

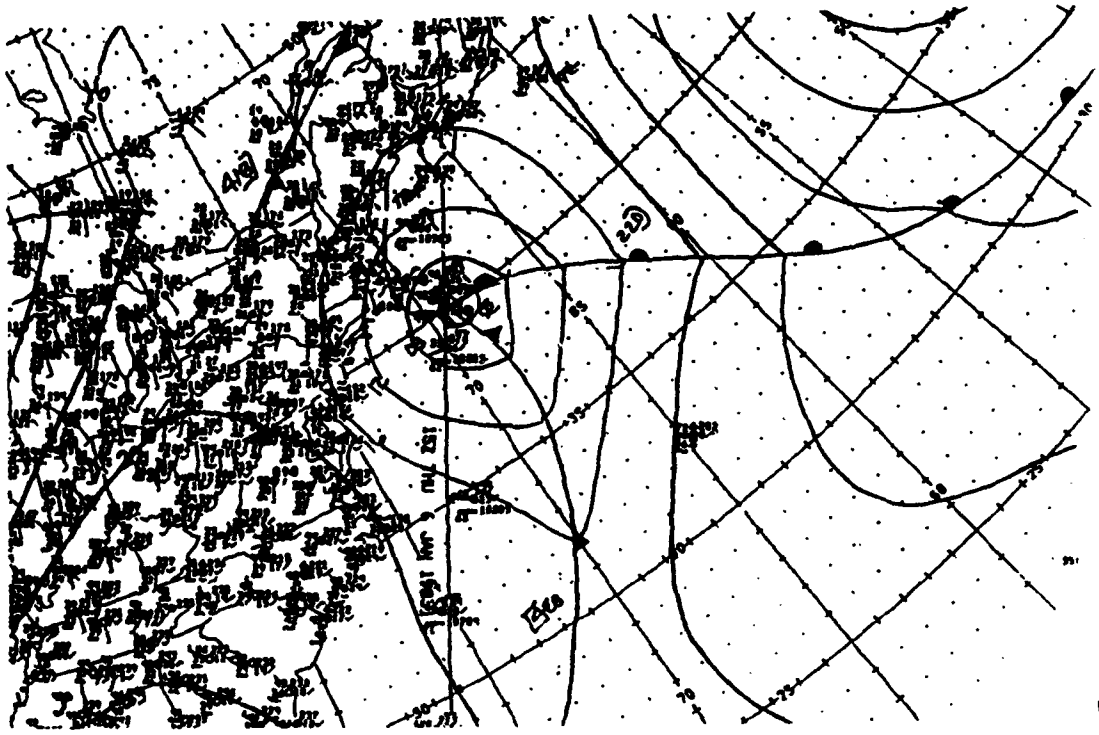

FIG. 4.12. 1500 UTC 6 Jan 1983 NMC sea level pressure (4 mb increment) and frontal analyses for case 6 .

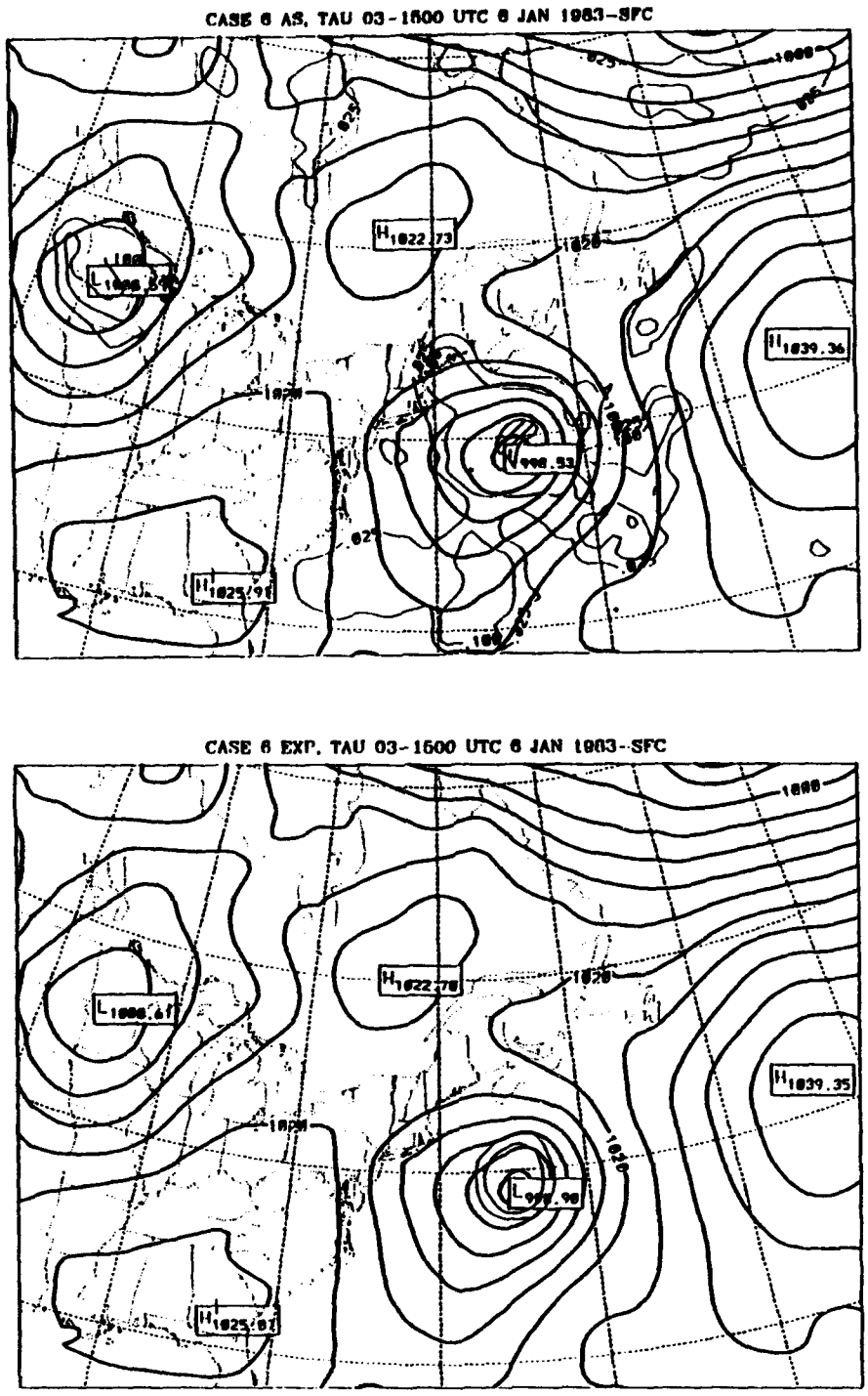

FIG. 4.13 1500 UTC 6 Jan 1983 case 6 model forecast fields of sea level pressure (4 mb increment) and total precipitation (.025, .1, 1, and 2.5 cm) for (a) AS experiment, (b) EXP experiment, (c) KUO experiment, and (d) DRY experiment.

c.

CASE 6 KUO, TAU 03-1500 UTC 6 JAN 1983-SFC

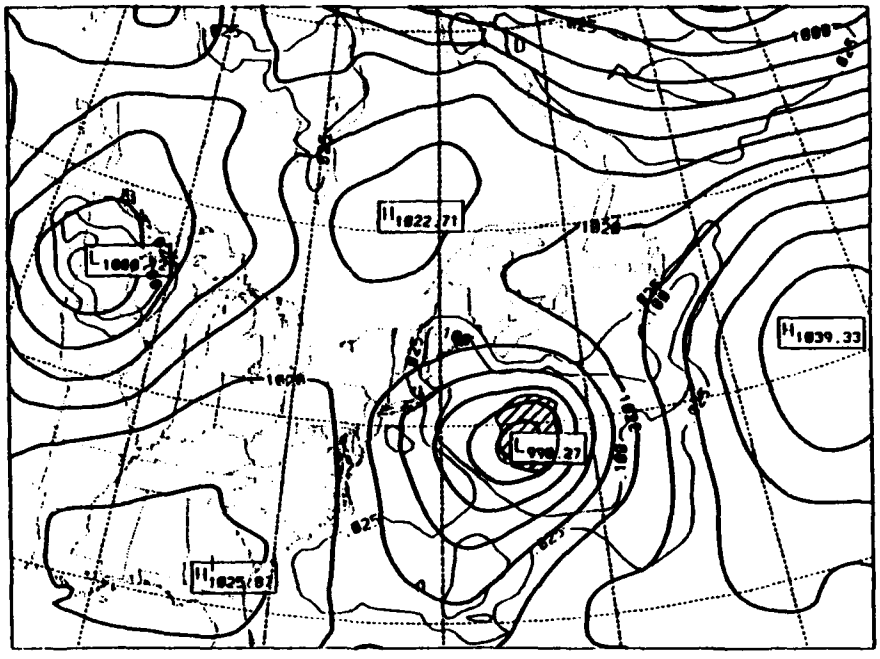

CASE 6 DRY, TAU 03-1500 UTC 6 JAN 1983-SFC

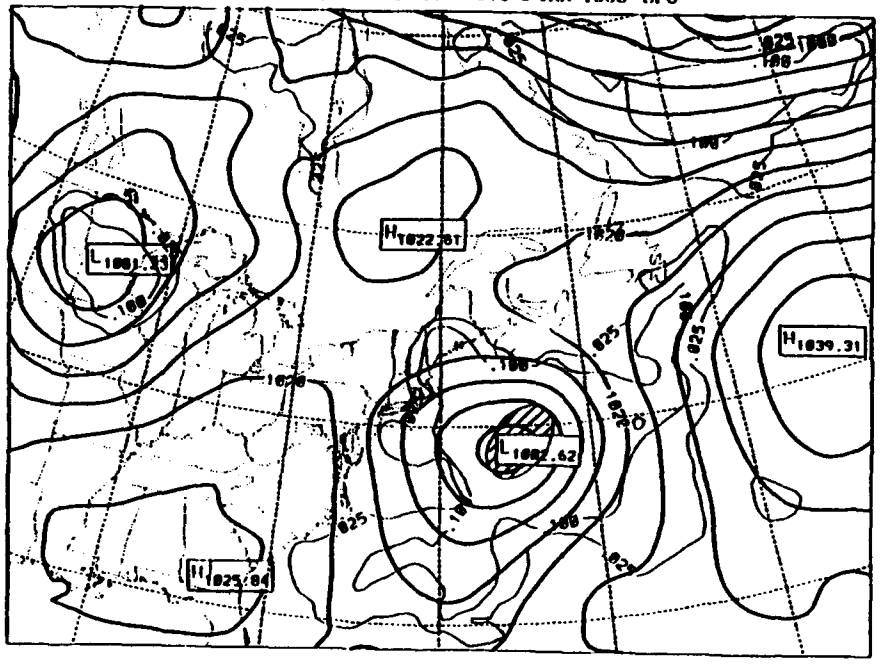

d.

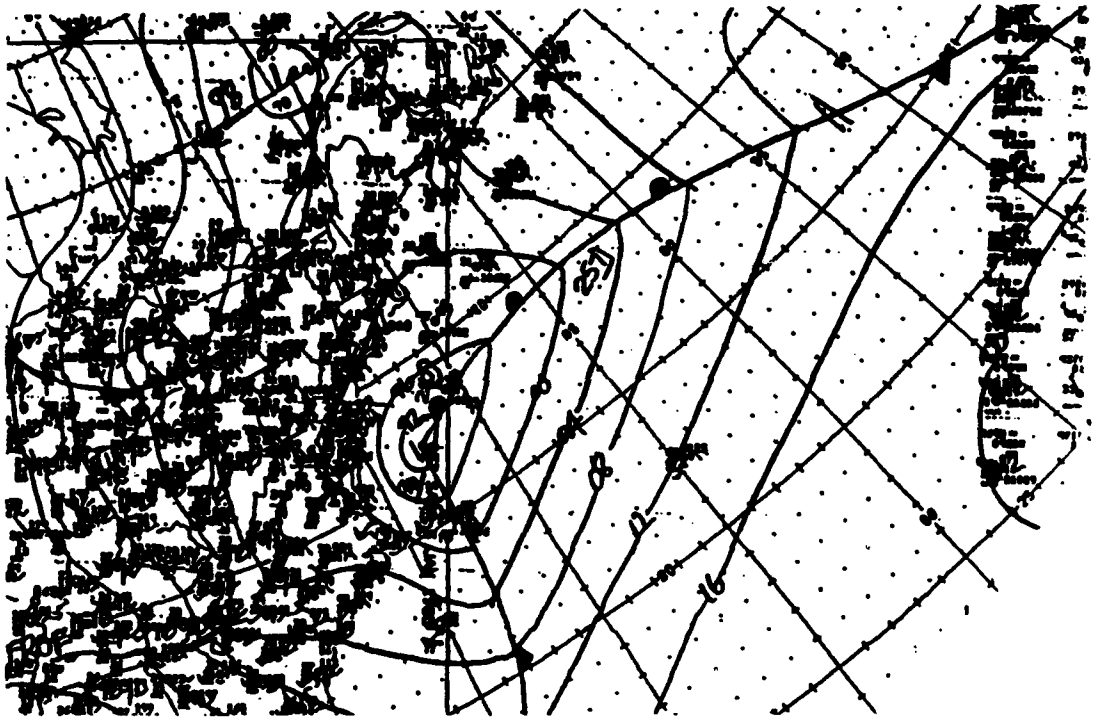

FIG 4.14. Same as Fig. 4.12 except for case 7 0300 UTC 5 Jan 1985.

a.

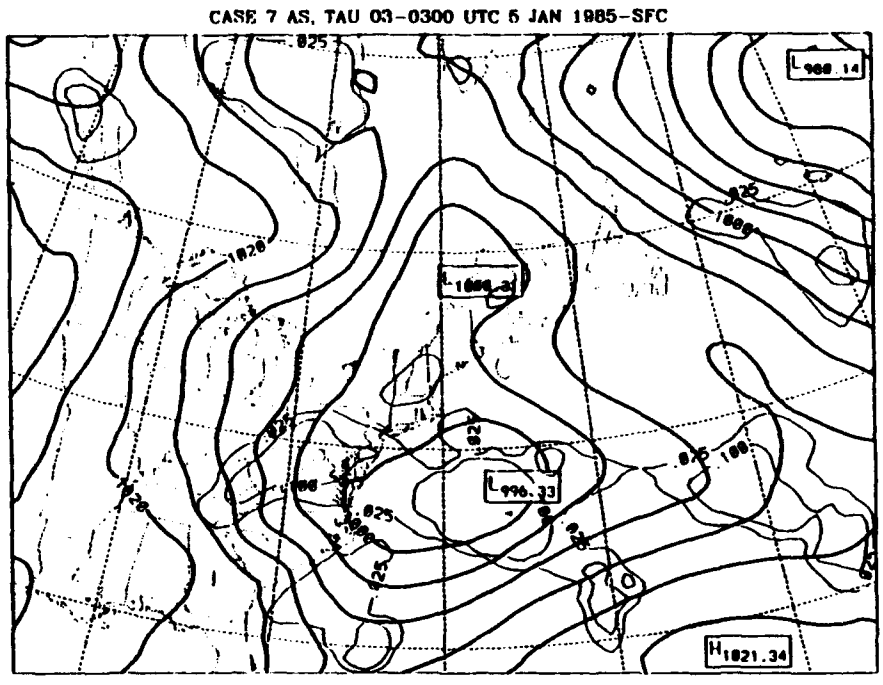

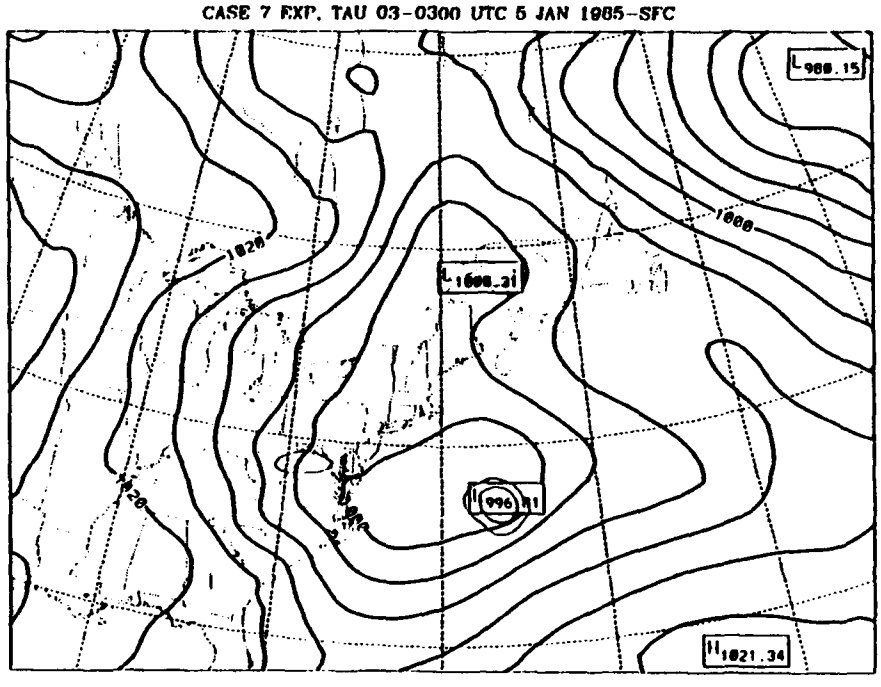

b.

FIG. 4.15. Same as Fig. 4.13 except for case 7 0300 UTC 5 Jan 1985.

c.

CASE 7 KUO, TAU 03-0300 UTC 5 JAN 1985-SFC

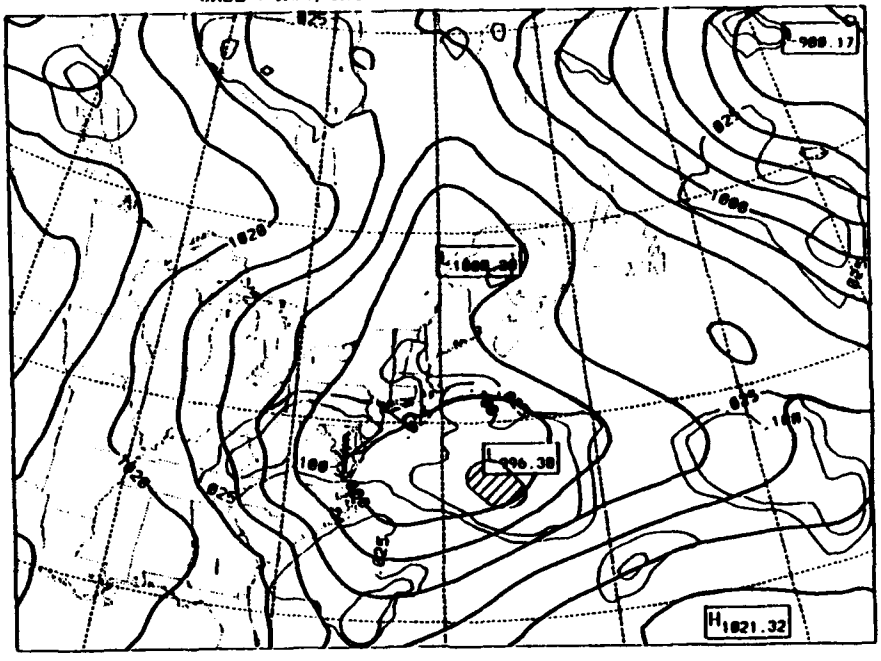

CASE 7 DRY, TAU 03-0300 UTC 5 JAN 1985-SFC

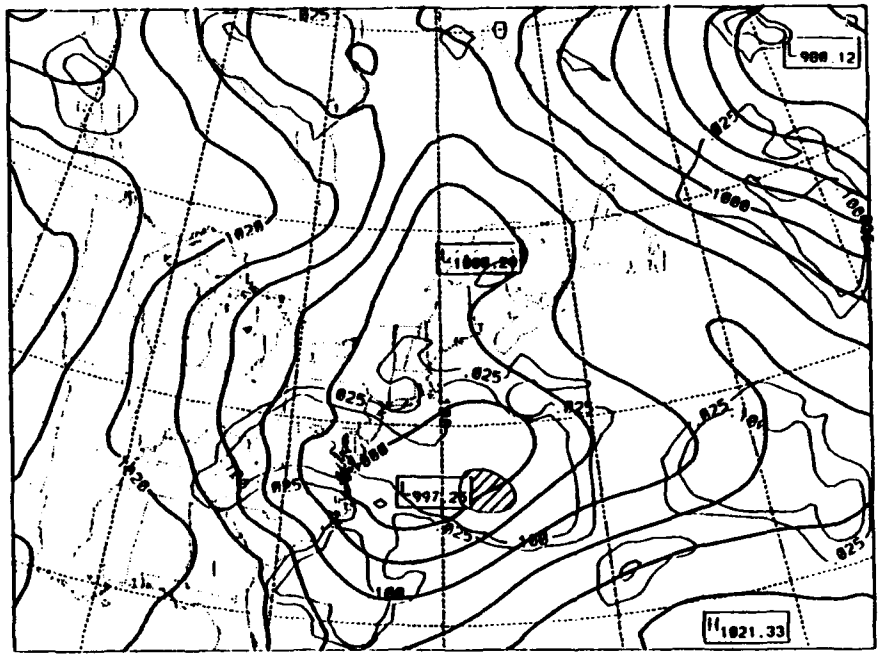

d.

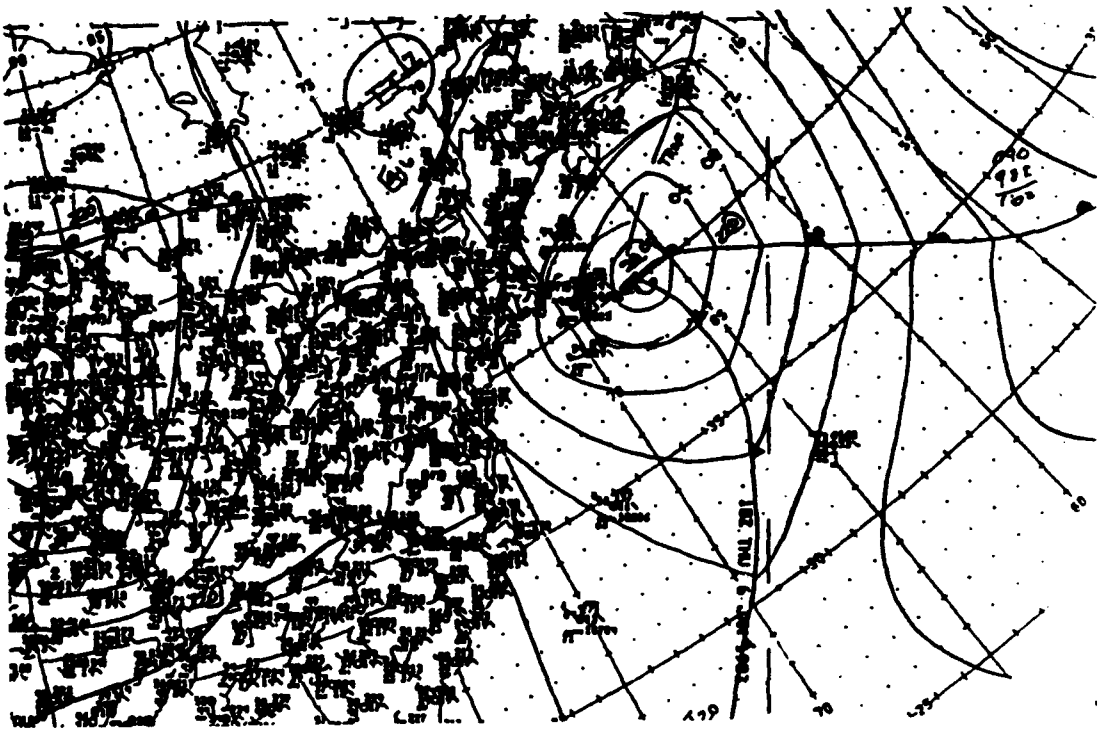

FIG. 4.16. Same as Fig. 4.12 except for 1800 UTC 6 Jan 1983.

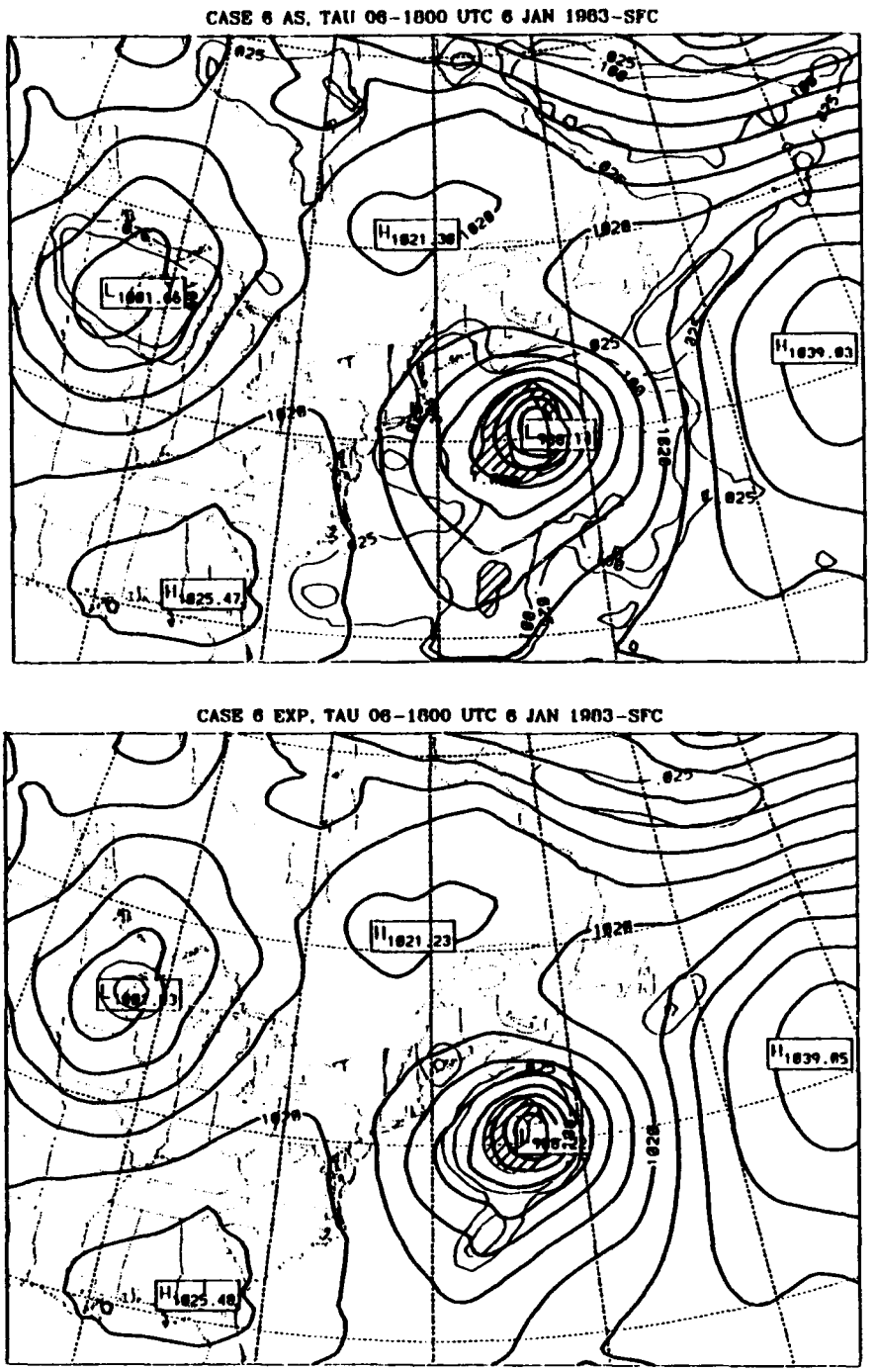

FIG. 4.17. Same as Fig. 4.13 except for 1800 UTC 6 Jan 1983.

c.

CASE 6 KUO, TAU 06-1800 UTC 6 JAN 1983-SFC

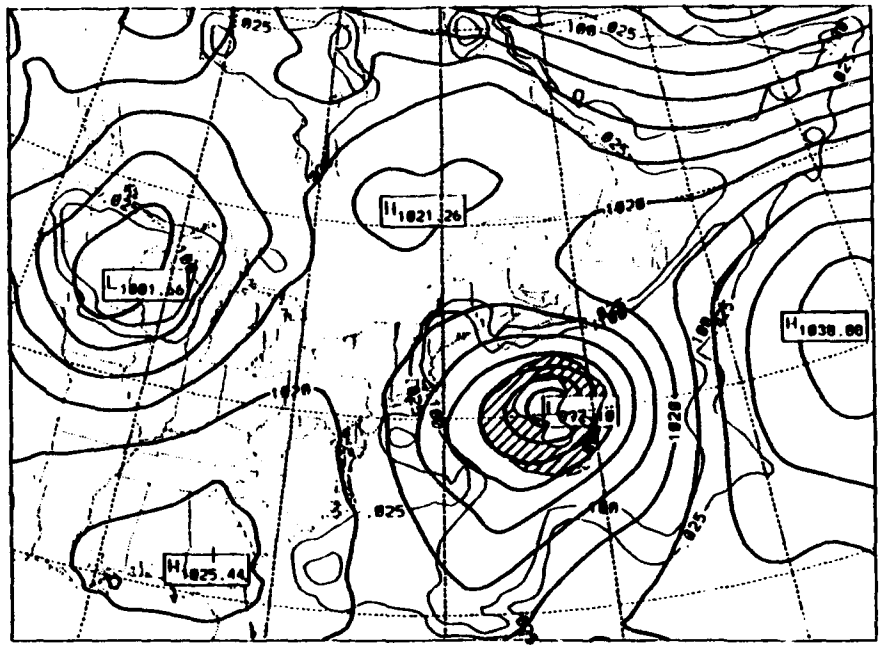

CASE 6 DRY, TAU 06-1800 UTC 6 JAN 1983-SFC

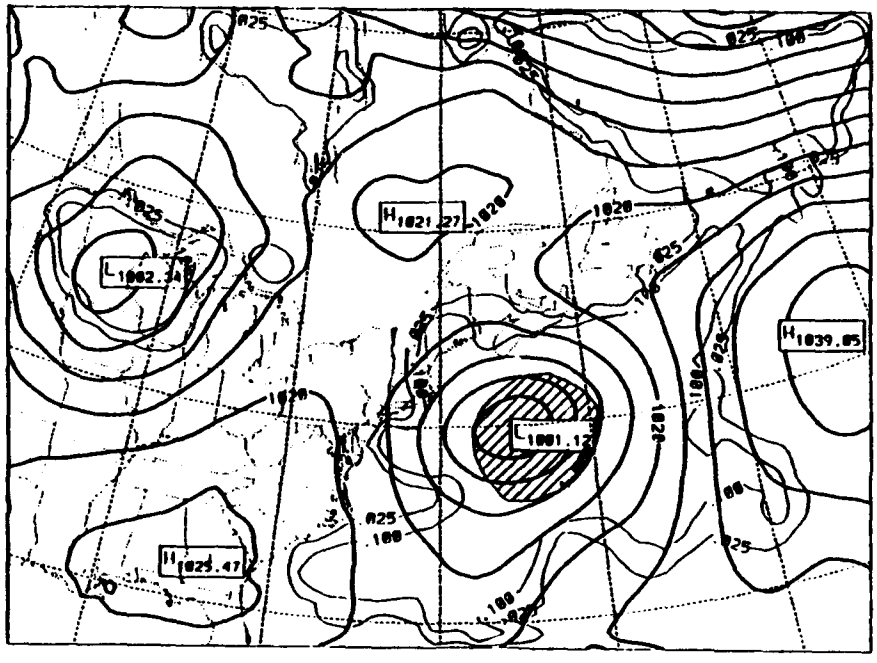

d.

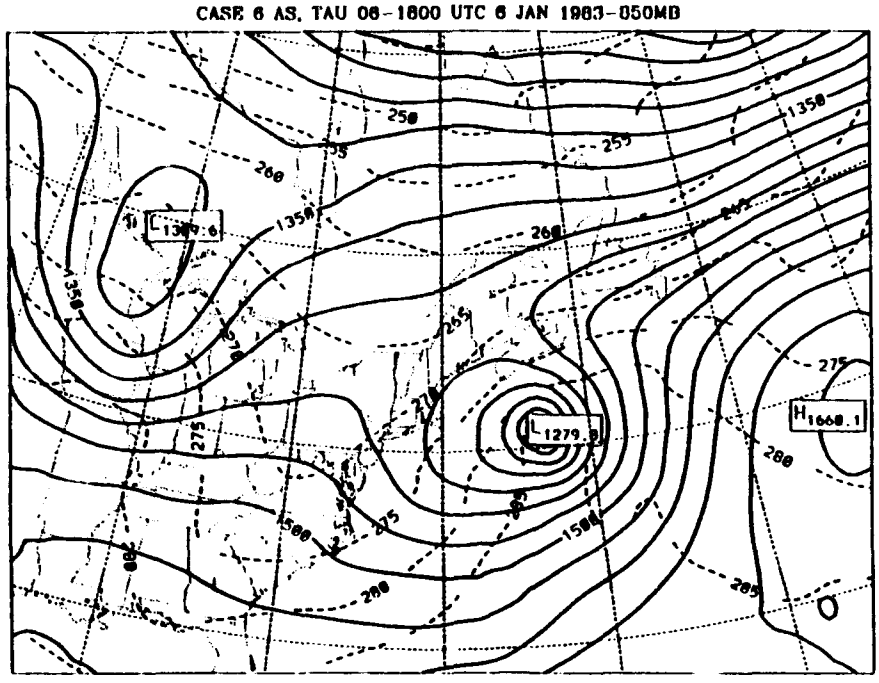

FIG. 4.18 1800 UTC 6 Jan 1983 case 6 model forecast fields of 850 mb heights (solid, 3 dm increment) and temperatures (dashed, 5°C increment) for (a) AS experiment, (b) EXP experiment, (c) KUO experiment, and (d) DRY experiment.

c.

CASE 6 KUO, TAU 06-1800 UTC 6 JAN 1963-850MB

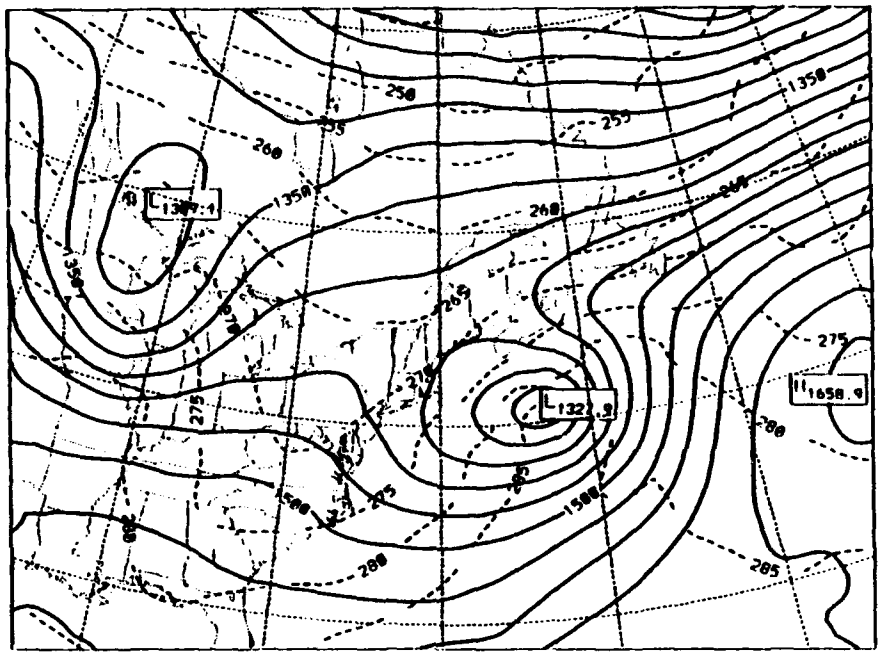

CASE 6 DRY, TAU 06-1800 UTC 6 JAN 1963-850MB

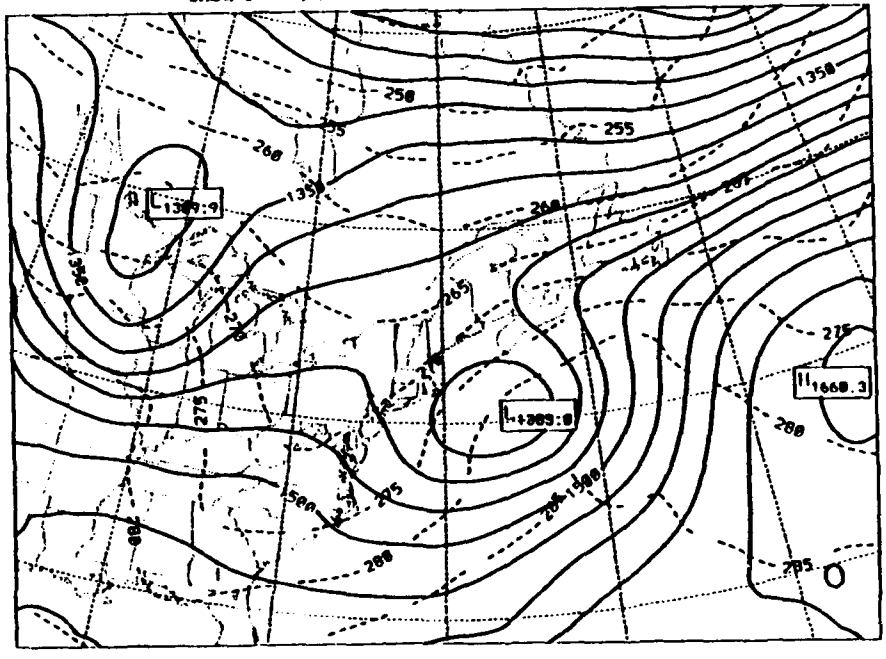

d.

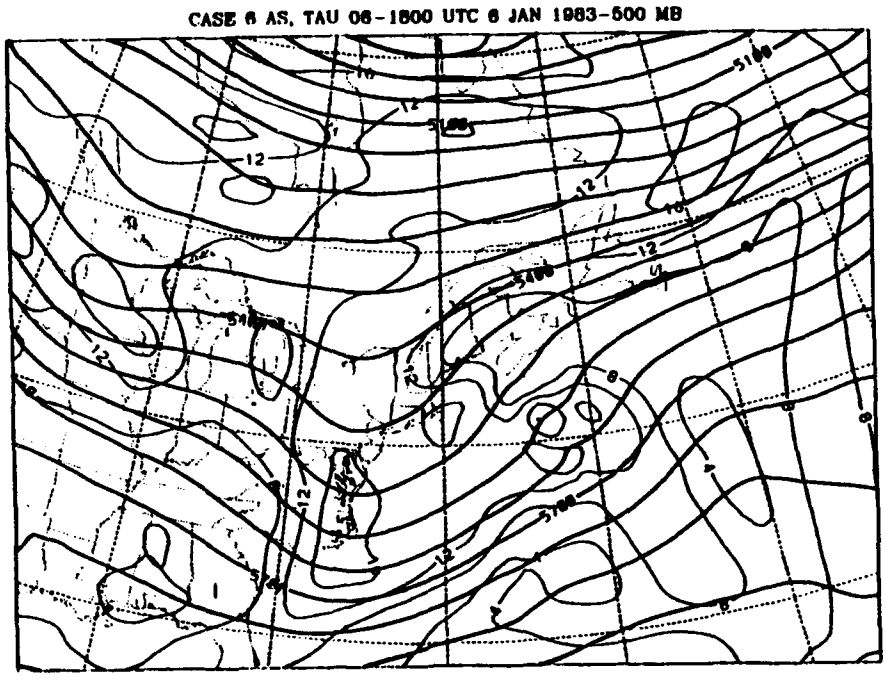

a.

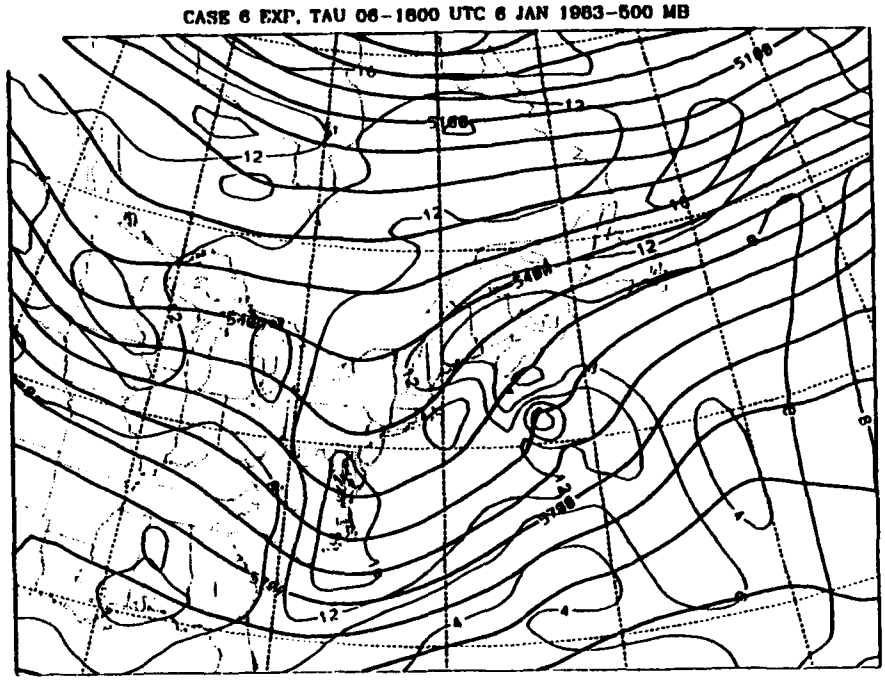

b.

FIG. 4.19 1800 UTC 6 Jan 1983 case 6 model forecast fields of 500 mb heights (solid, 6 dm increment) and absolute vorticity (dashed, 2×10^{-5} s^{-1} increment) for (a) AS experiment, (b) EXP experiment, (c) KUO experiment, and (d) DRY experiment.

c.

CASE 6 KUO, TAU 06-1800 UTC 6 JAN 1983-500 MB

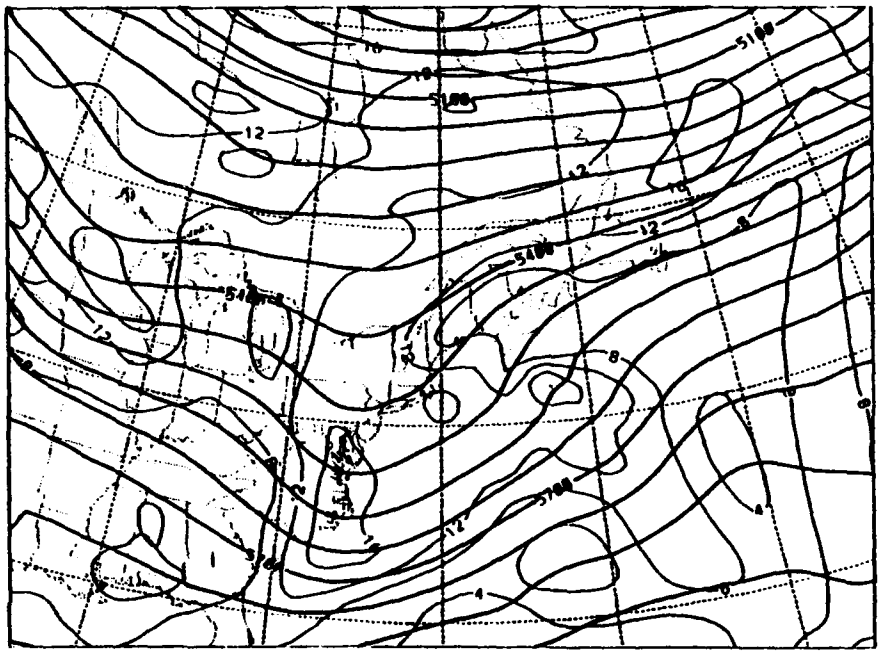

CASE 6 DRY, TAU 06-1800 UTC 6 JAN 1983-500 MB

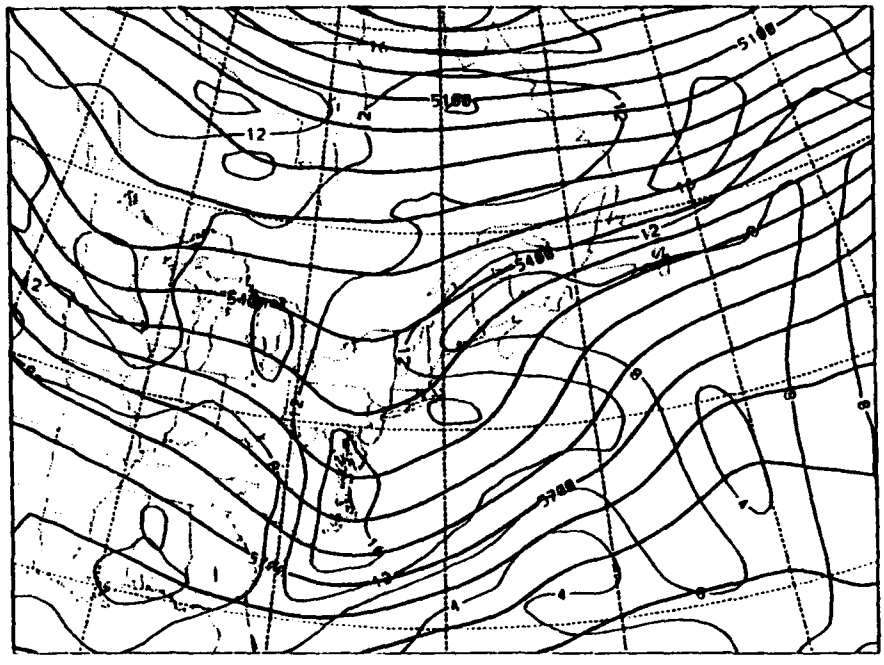

d.

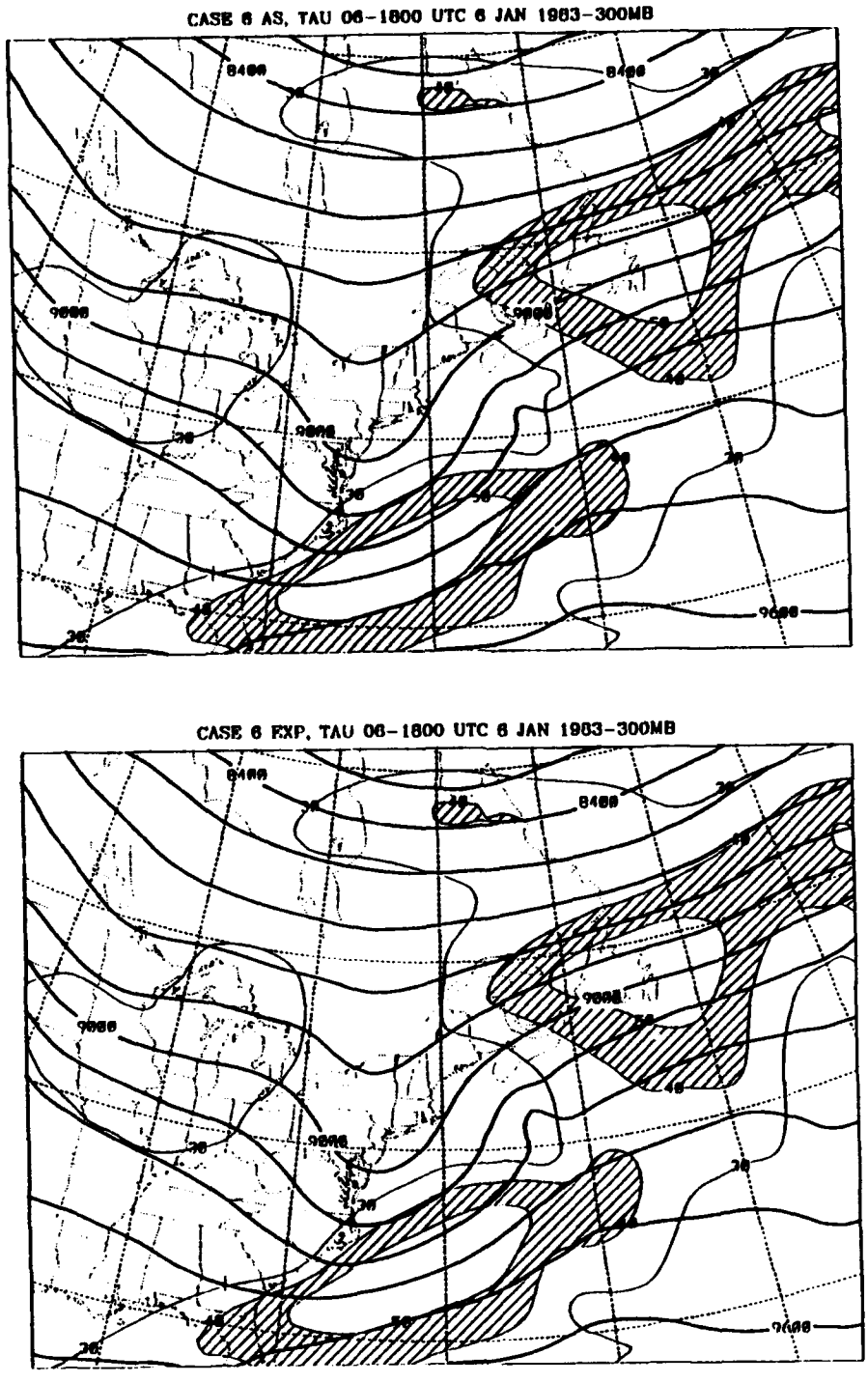

FIG. 4.20 1800 UTC 6 Jan 1983 case 6 model forecast fields of 300 mb heights (solid, 12 dm increment and isotachs (10 m s^{-1} increment)(a) AS experiment, (b) EXP experiment, (c) KUO experiment, and (d) DRY experiment.

c.

CASE 6 KUO, TAU 06-1800 UTC 6 JAN 1983-300MB

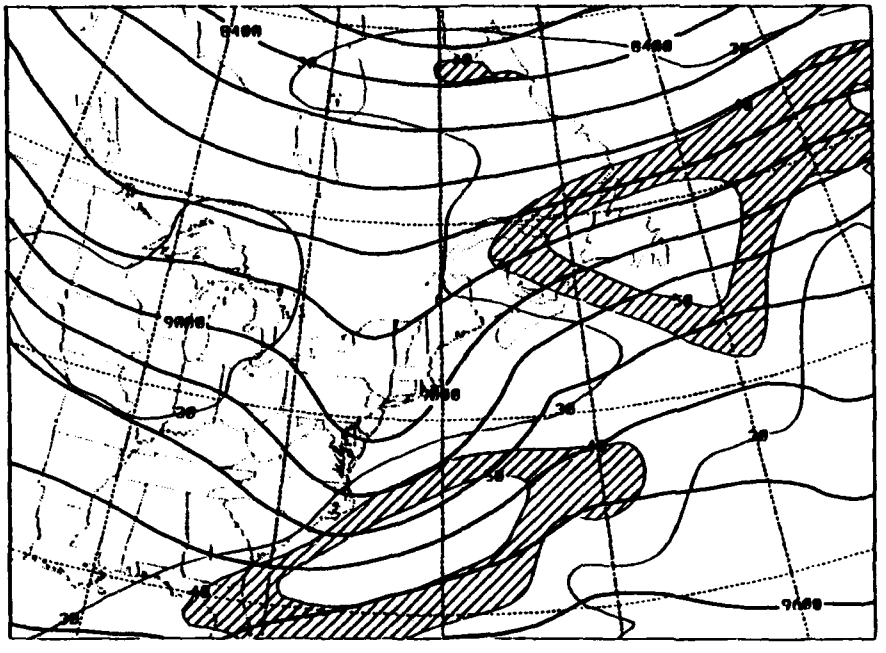

CASE 6 DRY, TAU 06-1800 UTC 6 JAN 1983-300MB

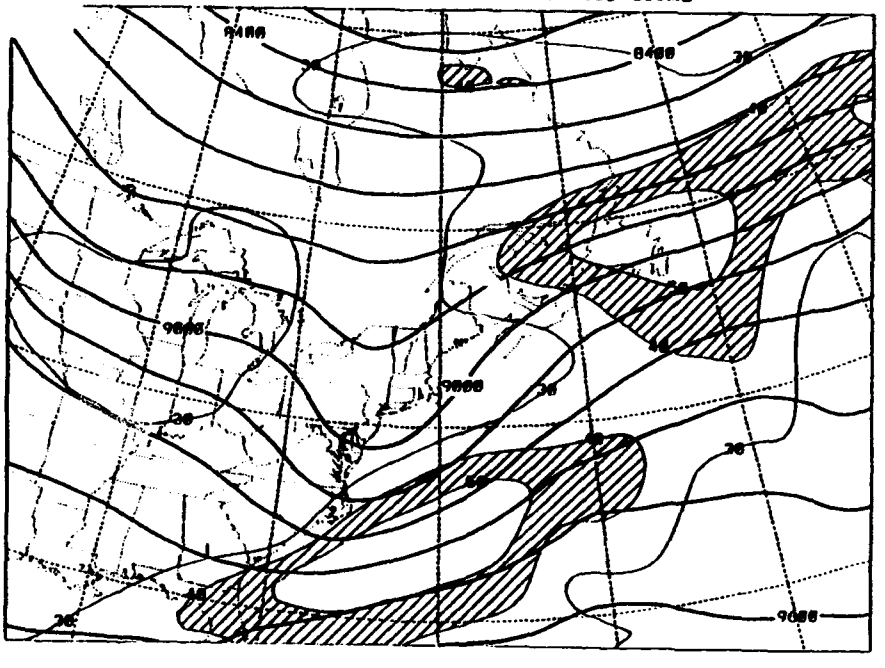

d.

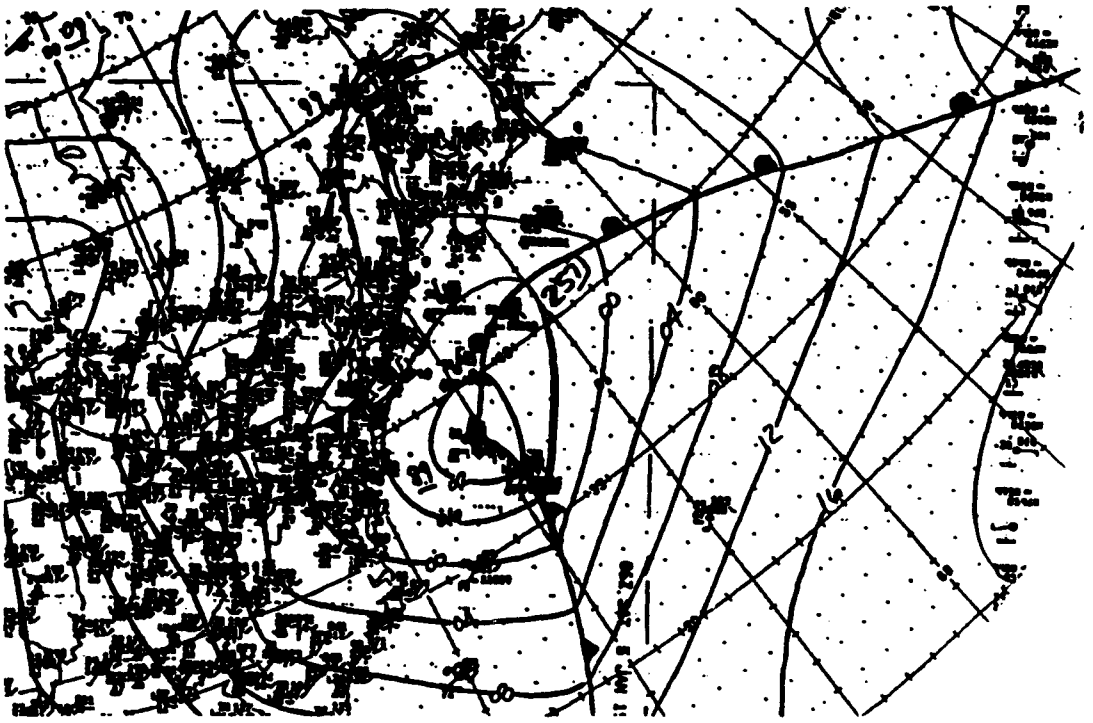

FIG. 4.21. Same as Fig. 4.12 except for case 7, 0600 UTC 5 Jan 1985.

a.

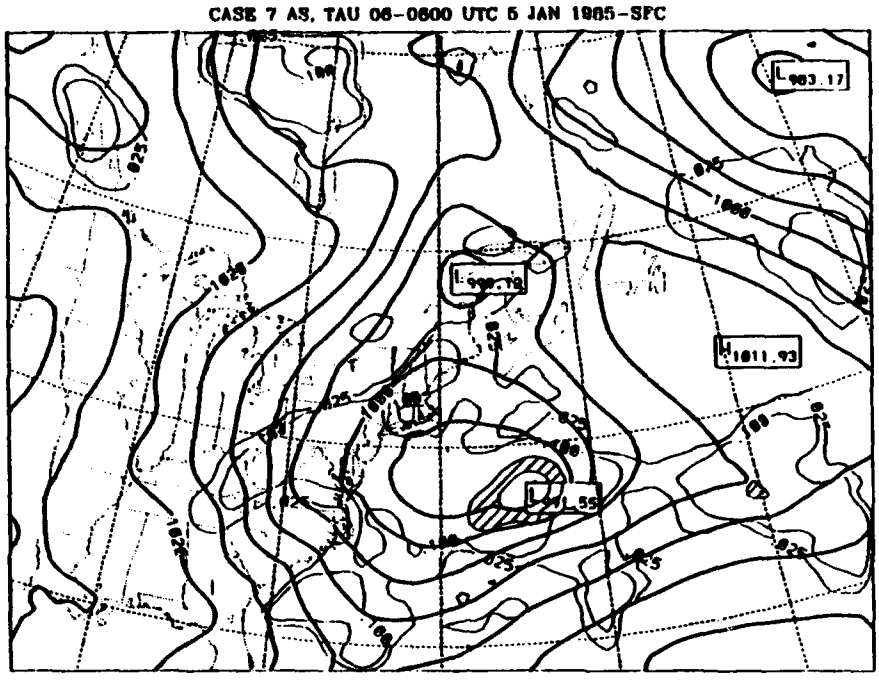

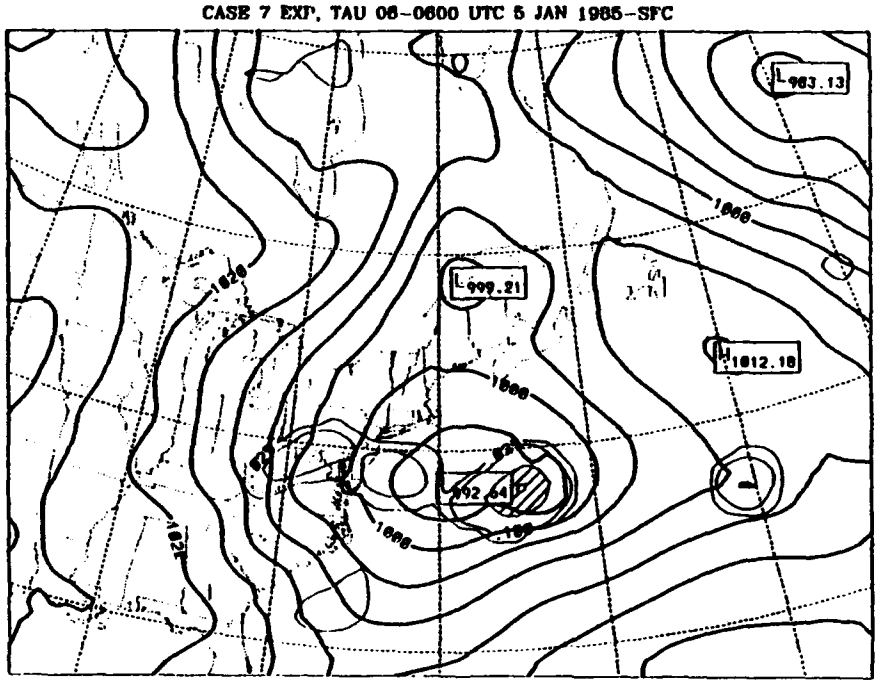

b.

FIG. 4.22. Same as Fig. 4.13 except for case 7, 0600 UTC 5 Jan 1985.

c.

CASE 7 KUO, TAU 06-0600 UTC 5 JAN 1985-SFC

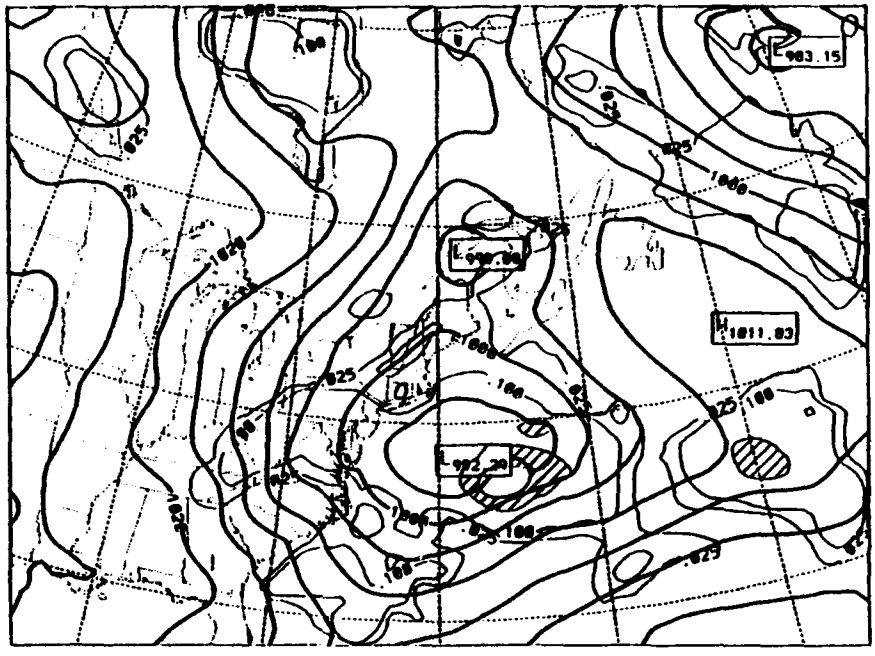

CASE 7 DRY, TAU 06-0600 UTC 5 JAN 1985-SFC

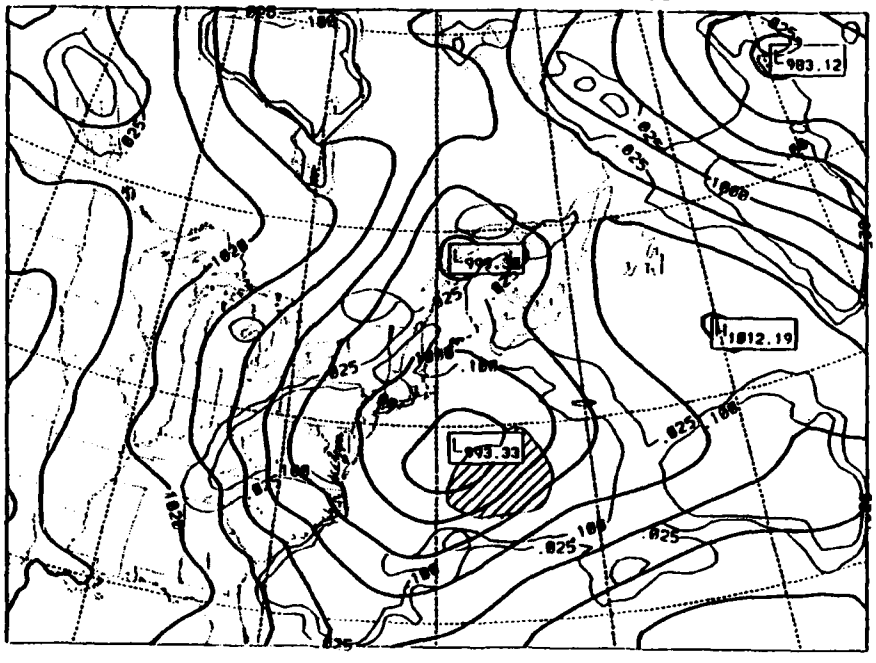

d.

a.

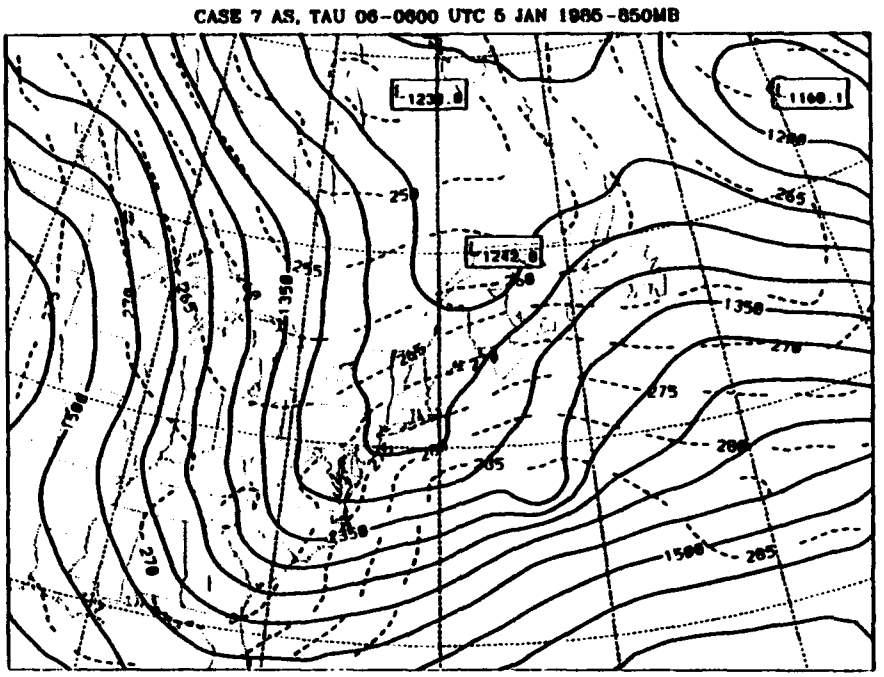

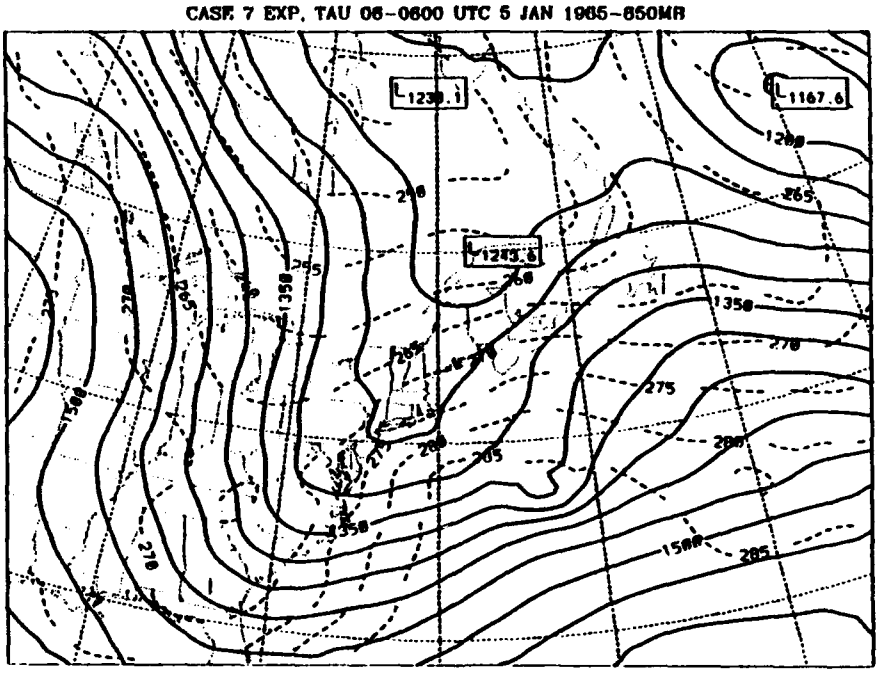

b.

FIG. 4.23. Same as Fig. 4.18 except for case 7, 0600 UTC 5 Jan 1985.

c.

CASE 7 KUO, TAU 06-0600 UTC 5 JAN 1985-850MB

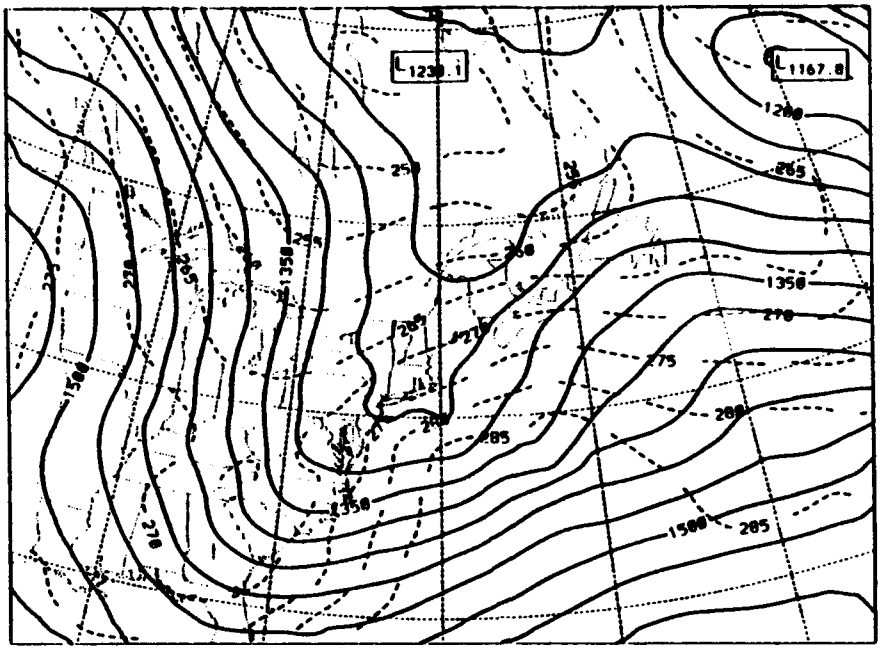

CASE 7 DRY, TAU 06-0600 UTC 5 JAN 1985-850MB

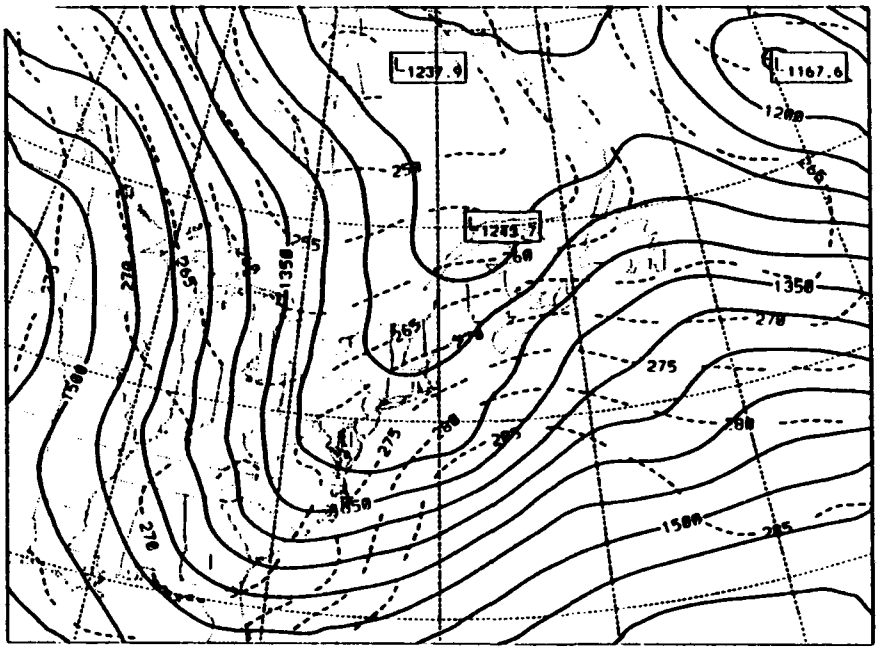

d.

a.

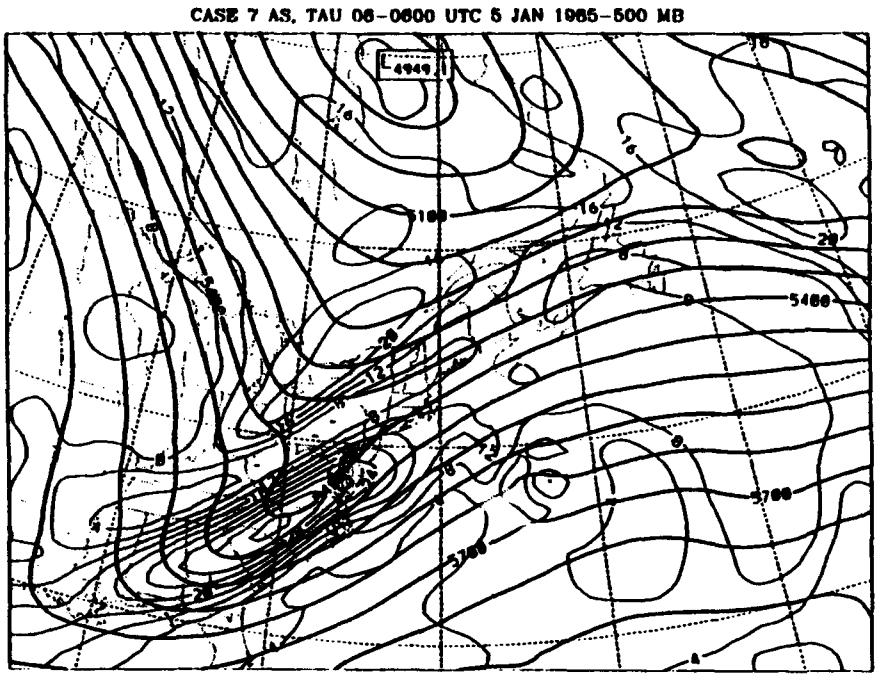

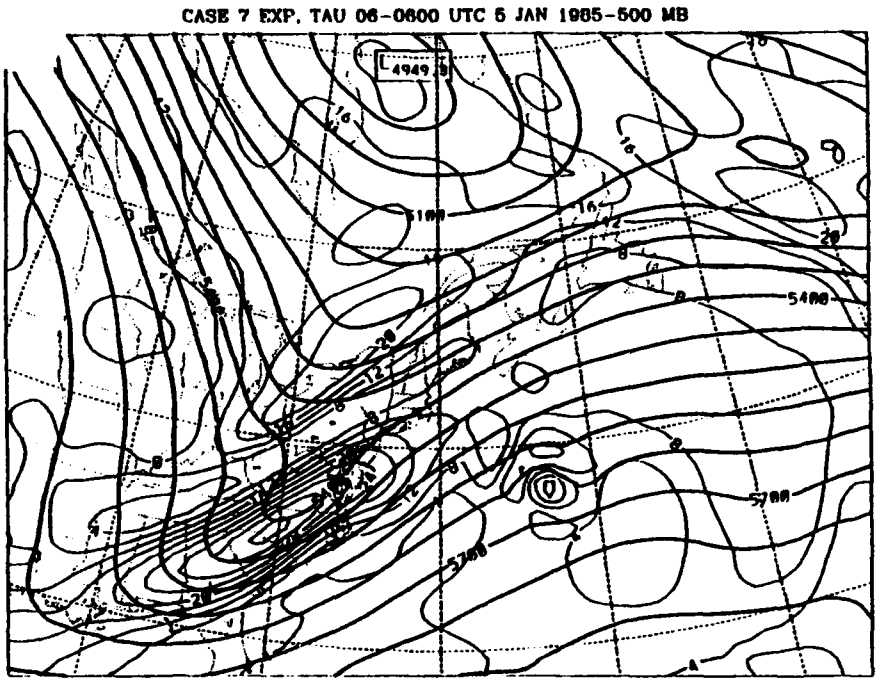

b.

FIG. 4.24. Same as Fig. 4.19 except for case 7, 0600 UTC 5 Jan 1985.

c.

CASE 7 KUO, TAU 06--0600 UTC 5 JAN 1985-500 MB

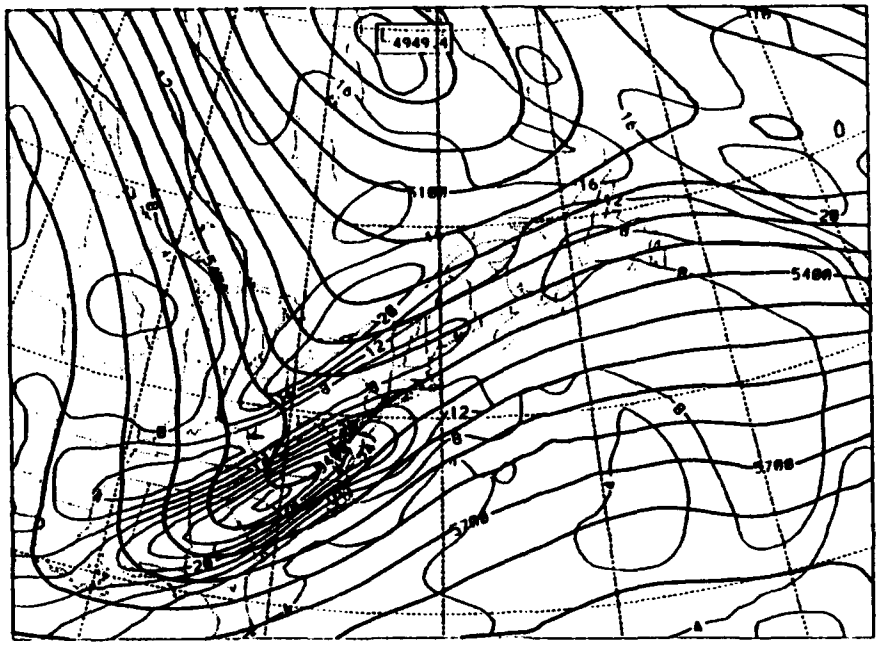

CASE 7 DRY, TAU 06-0600 UTC 5 JAN 1985-500 MB

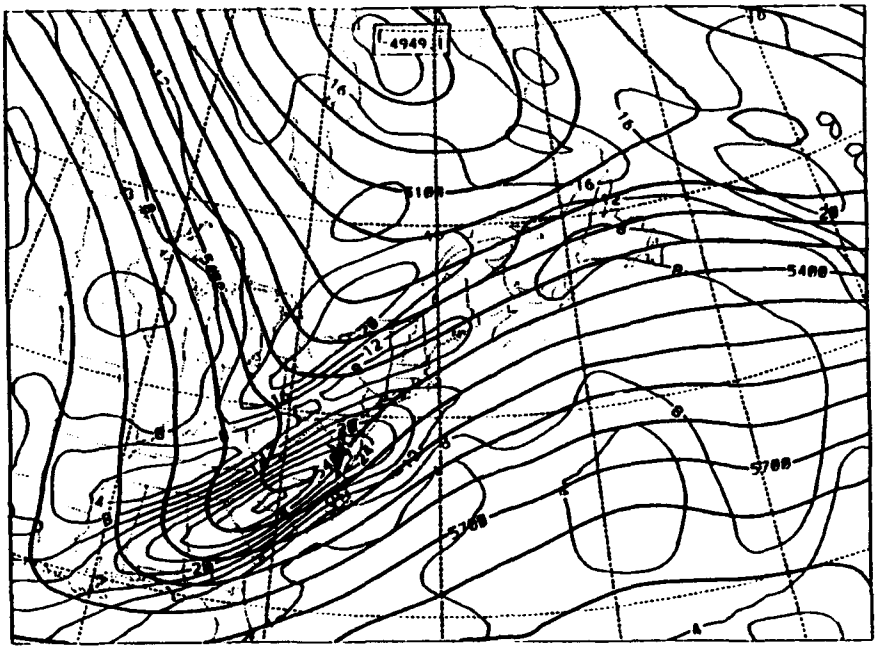

d.

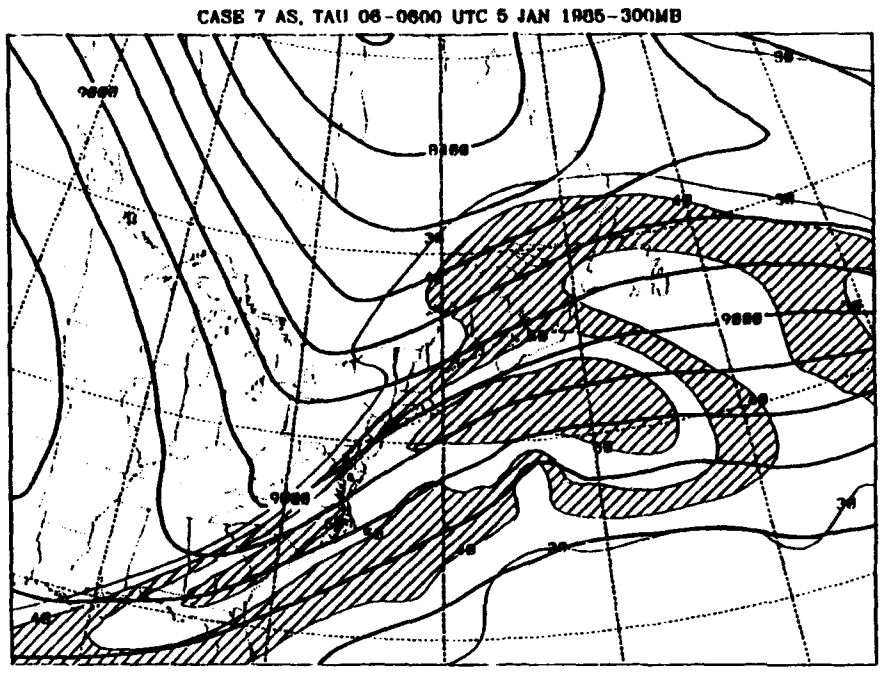

a.

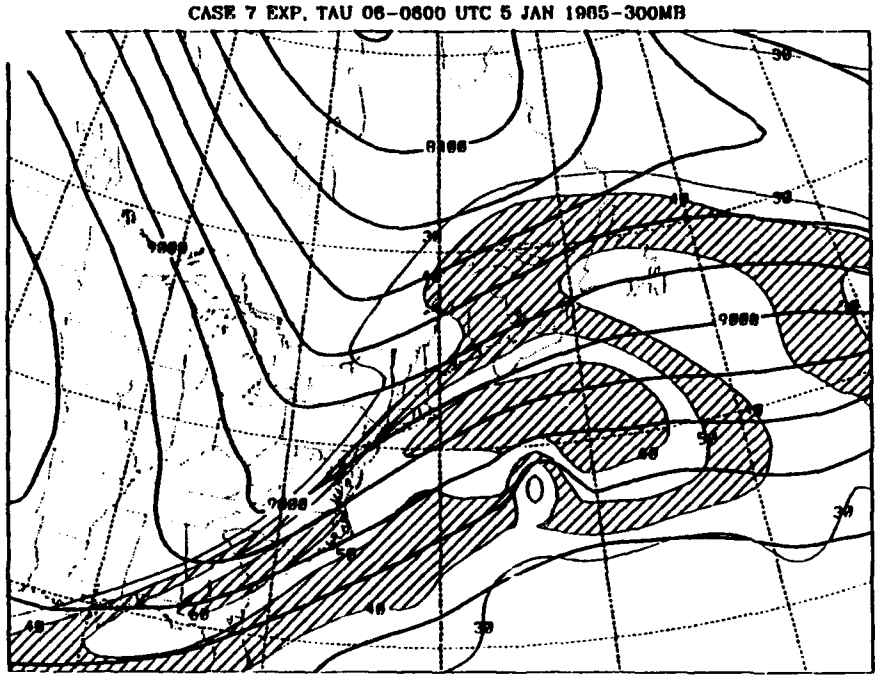

b.

FIG. 4.25. Same as Fig. 4.20 except for case 7, 0600 UTC 5 Jan 1985.

c.

CASE 7 KUO, TAU 06-0600 UTC 6 JAN 1985-300MB

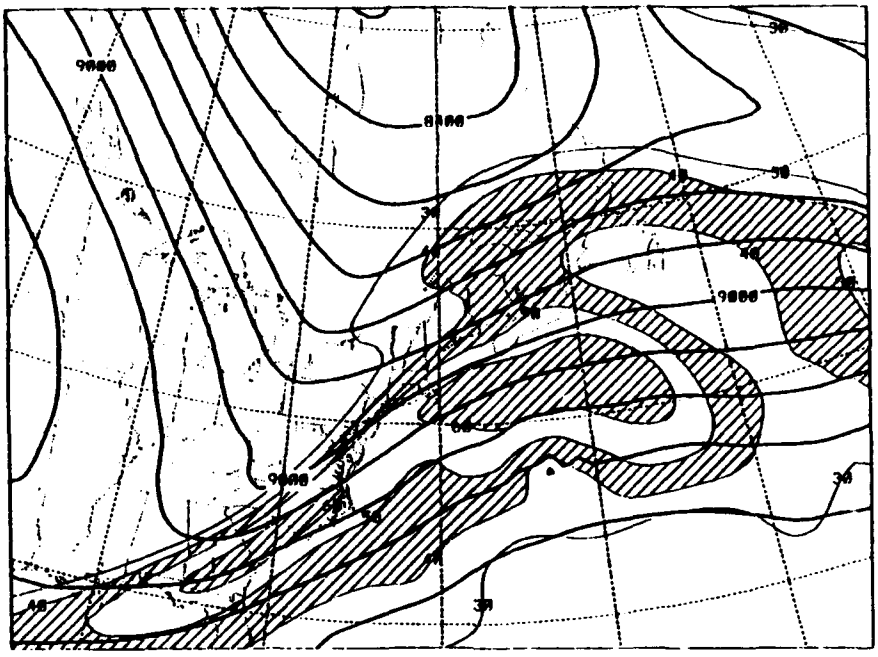

CASE 7 DRY, TAU 06-0600 UTC 5 JAN 1985-300MB

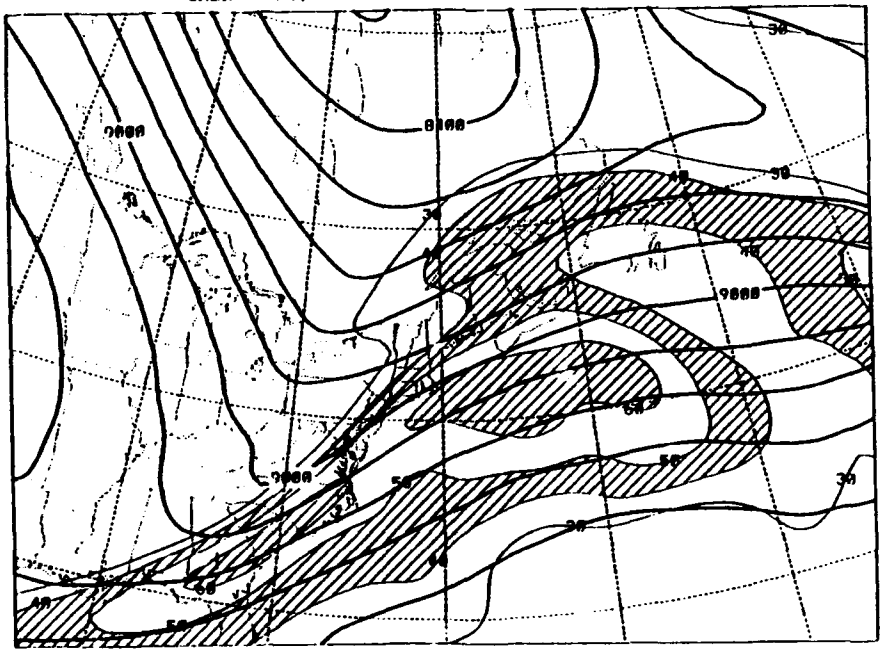

d.

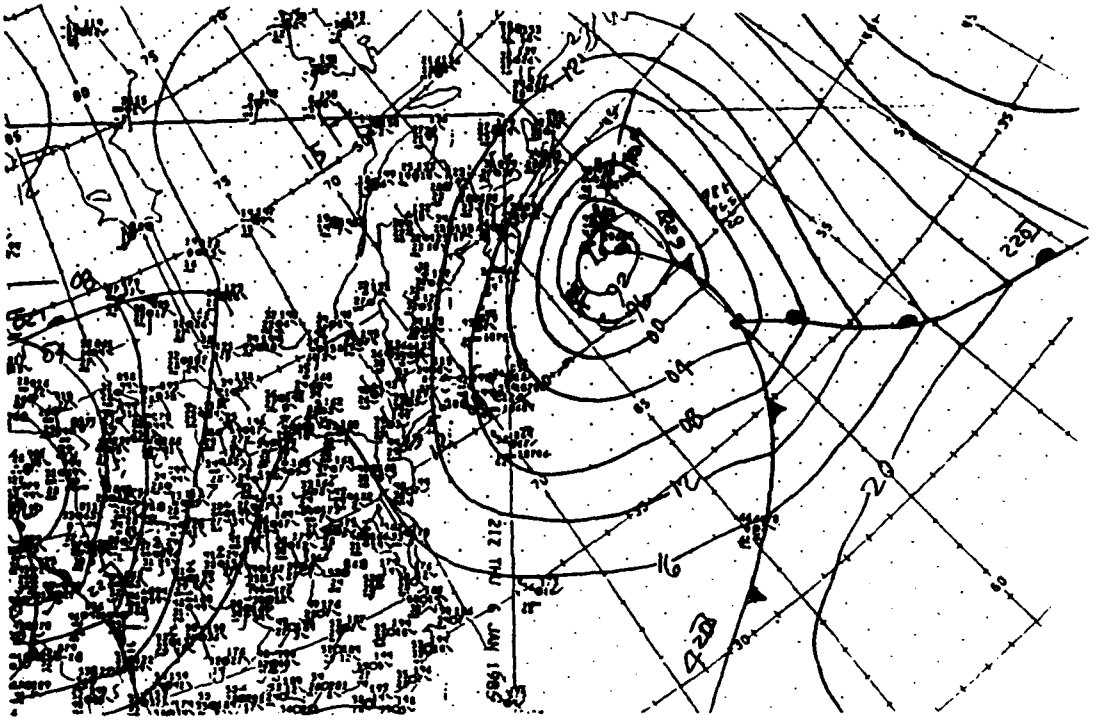

FIG. 4.26. Same as Fig. 4.12 except for 2100 UTC 6 Jan 1983.

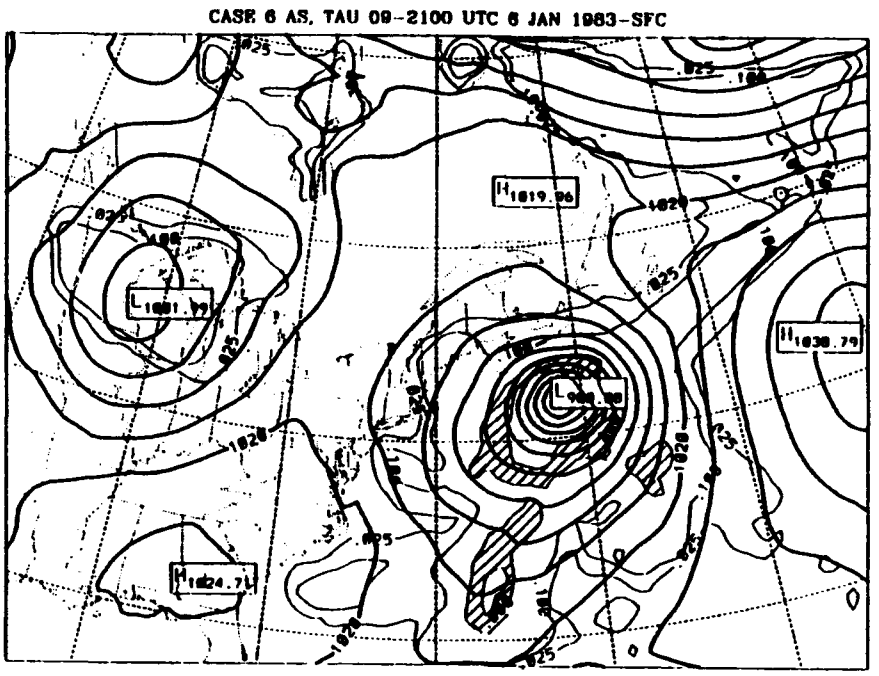

FIG. 4.27. Same as Fig. 4.13 except for 2100 UTC 6 Jan 1983.

c.

CASE 6 KUO, TAU 09-2100 UTC 6 JAN 1983-SFC

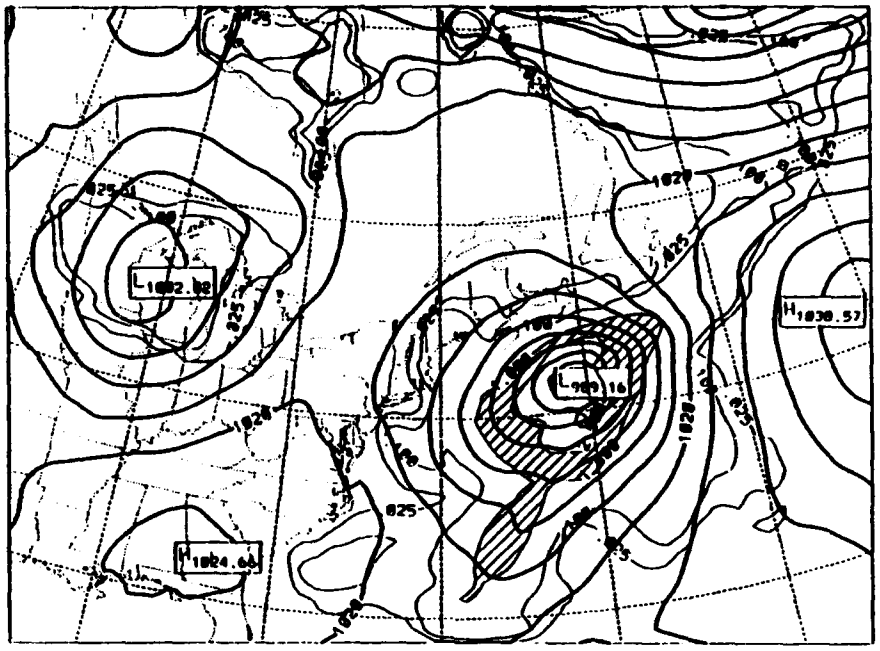

CASE 6 DRY, TAU 09-2100 UTC 6 JAN 1983-SFC

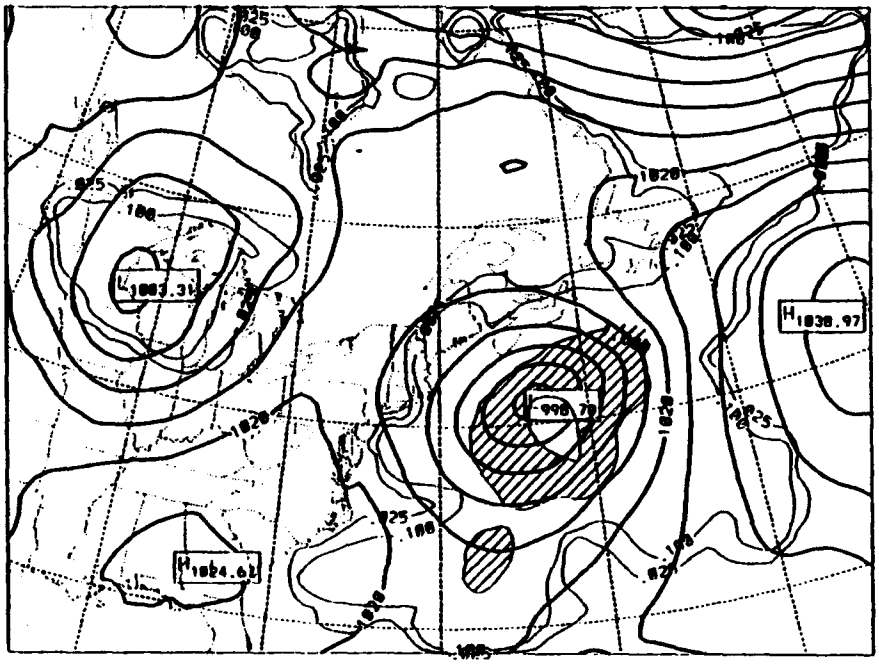

d.

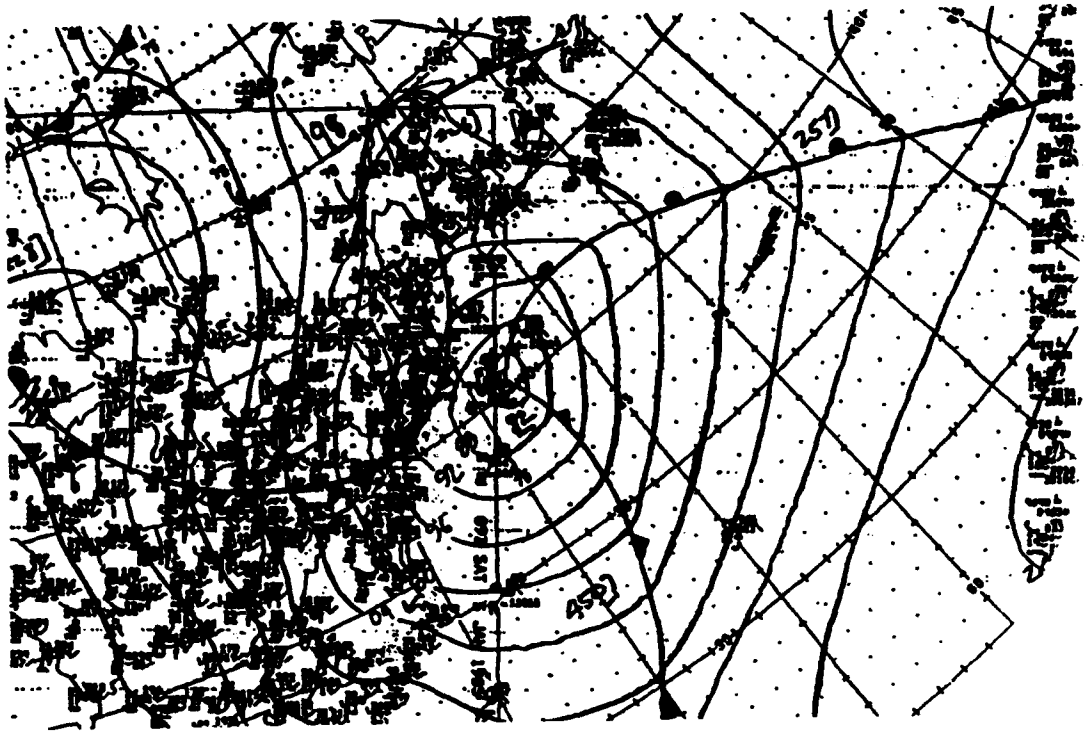

FIG. 4.28. Same as Fig. 4.12 except for case 7, 0900 UTC 5 Jan 1985.

a.

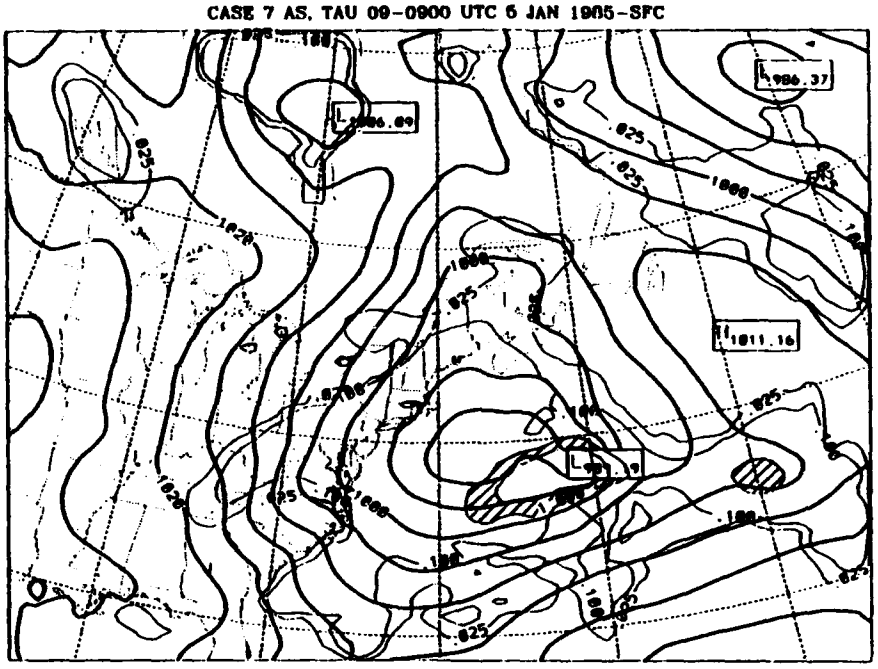

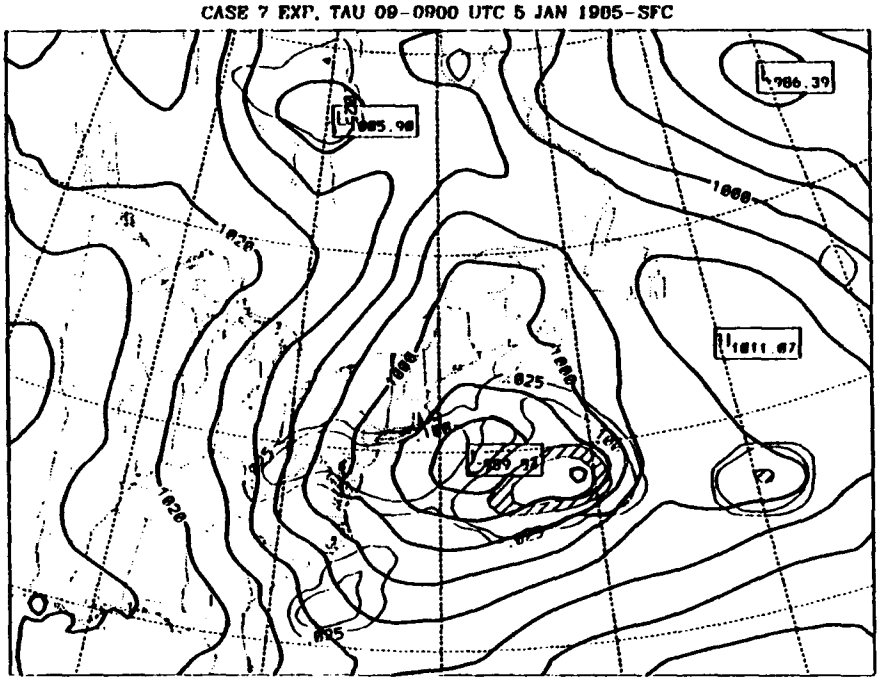

b.

FIG. 4.29. Same as Fig. 4.13 except for case 7, 0900 UTC 5 Jan 1985.

c.

CASE 7 KUO, TAU 09-0900 UTC 5 JAN 1985-SFC

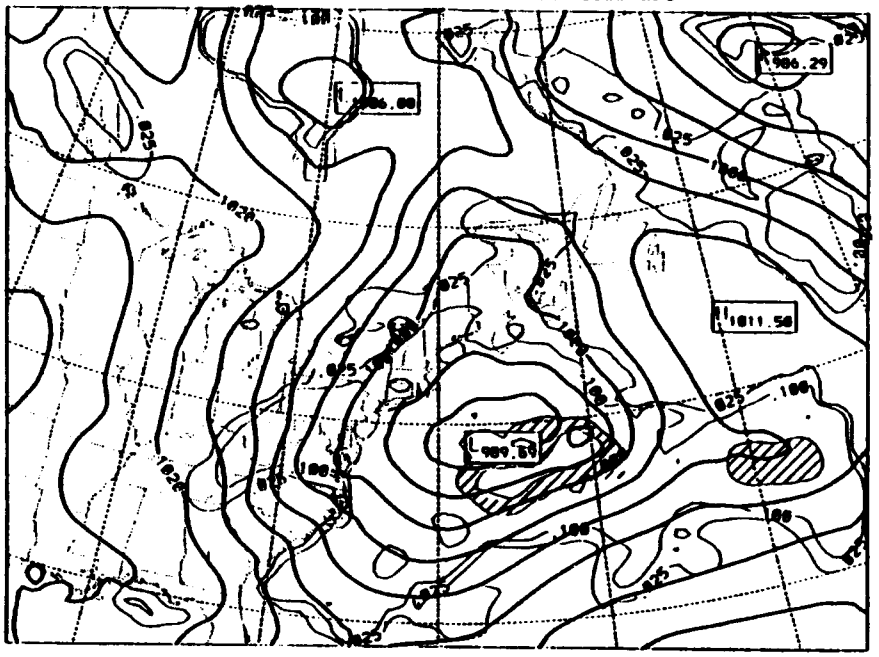

CASE 7 DRY, TAU 09-0900 UTC 5 JAN 1985-SFC

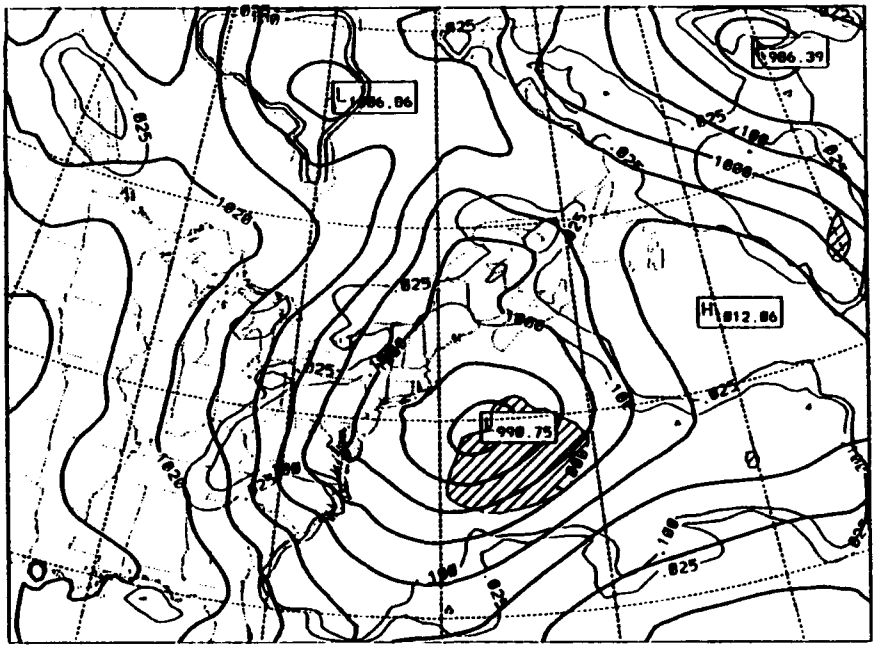

d.

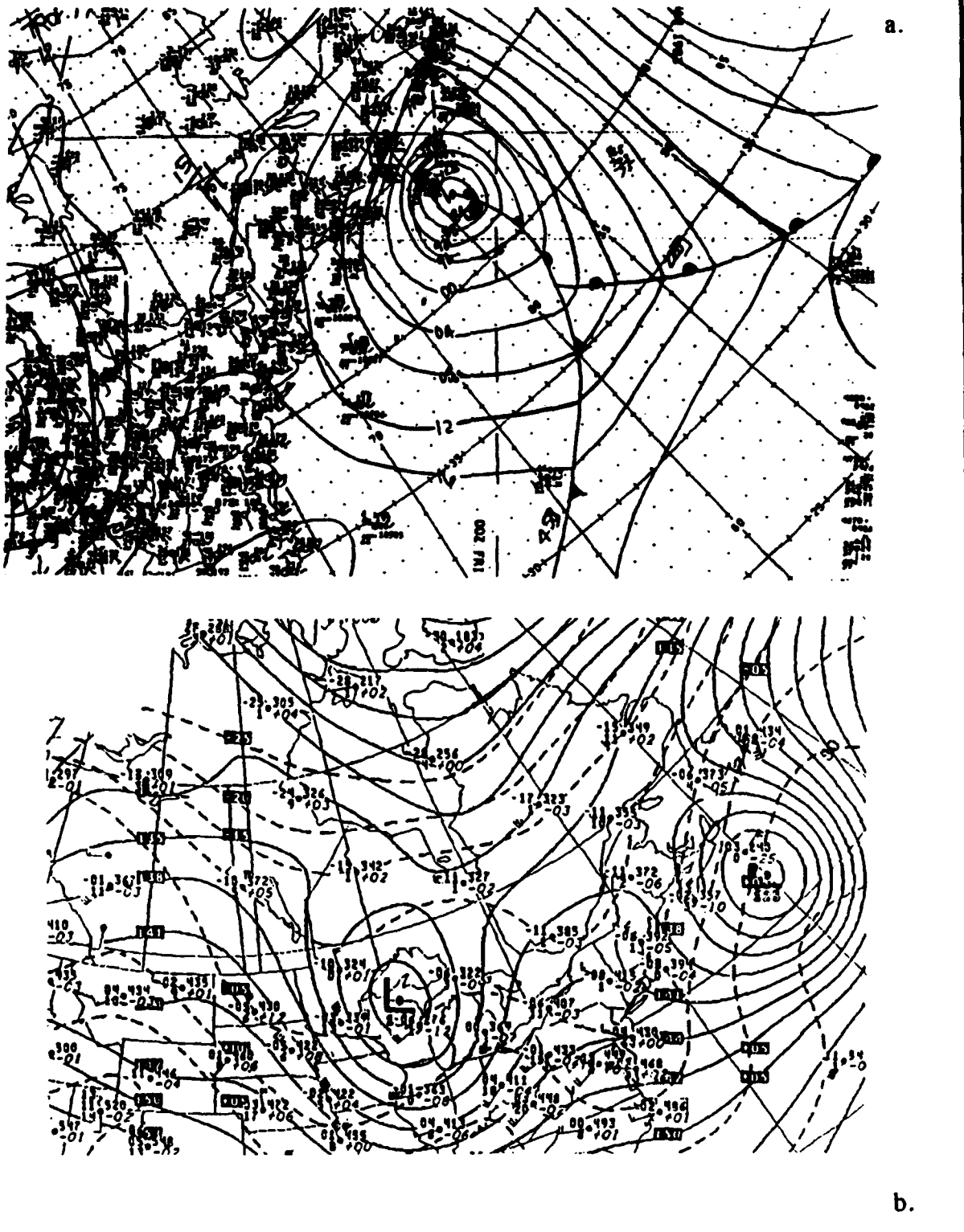

FIG. 4.30. Same as Fig. 4.8 except for 0000 UTC 7 Jan 1983.

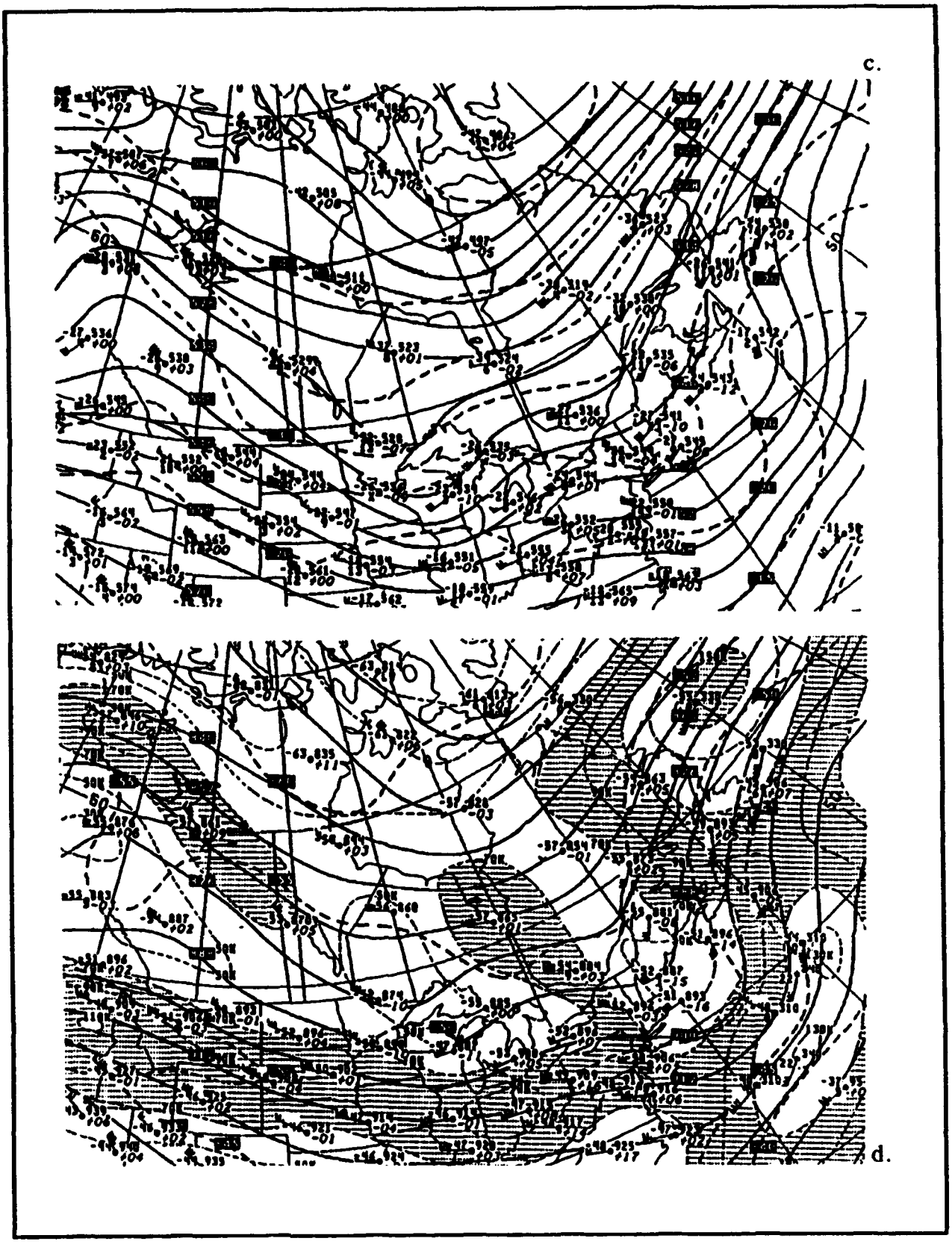
c.
d.

a.

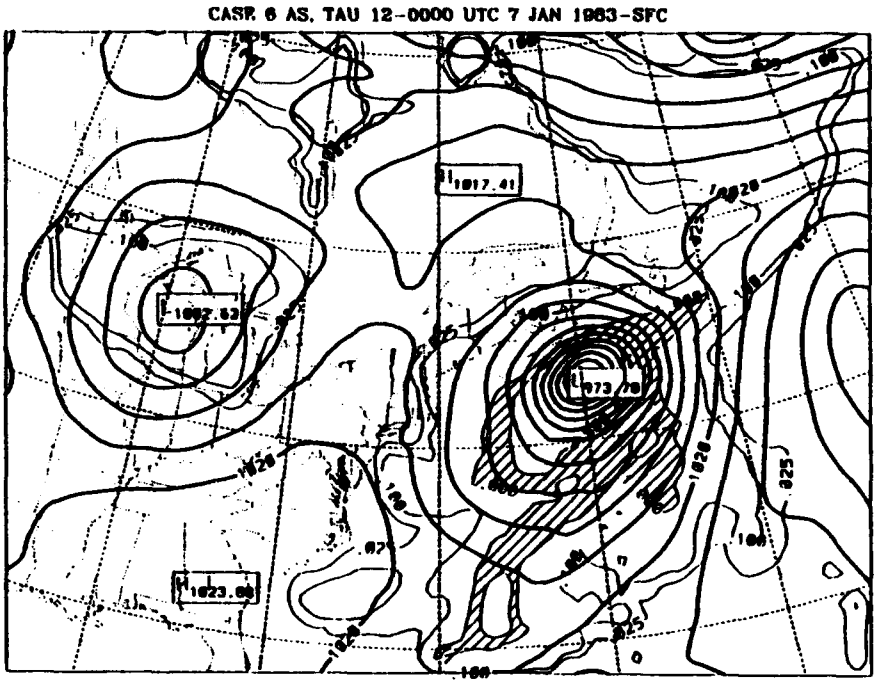

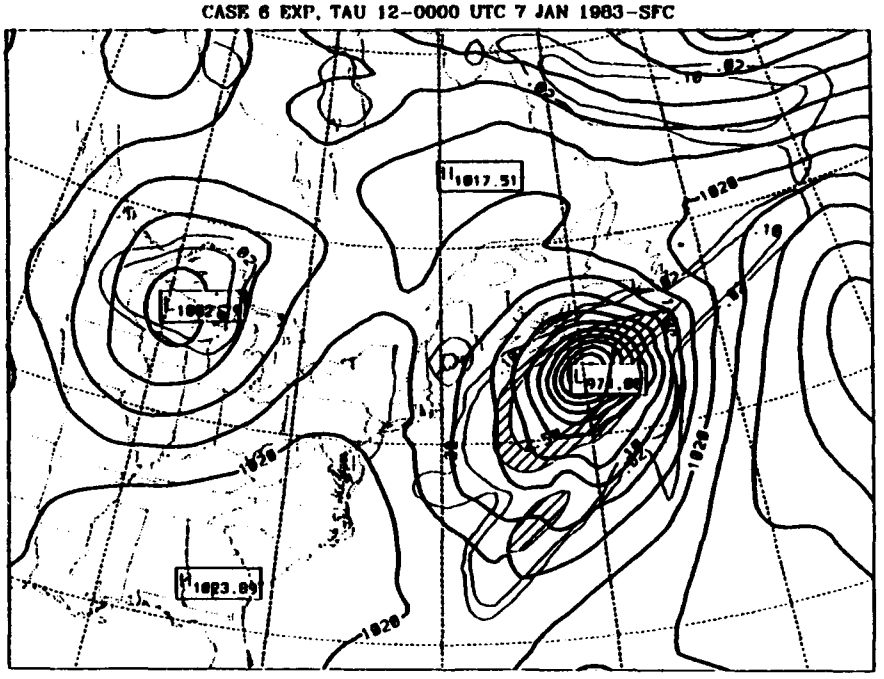

b.

FIG. 4.31. Same as Fig. 4.13 except for 0000 UTC 7 Jan 1983.

c.

CASE 6 KUO, TAU 12-0000 UTC 7 JAN 1983-SFC

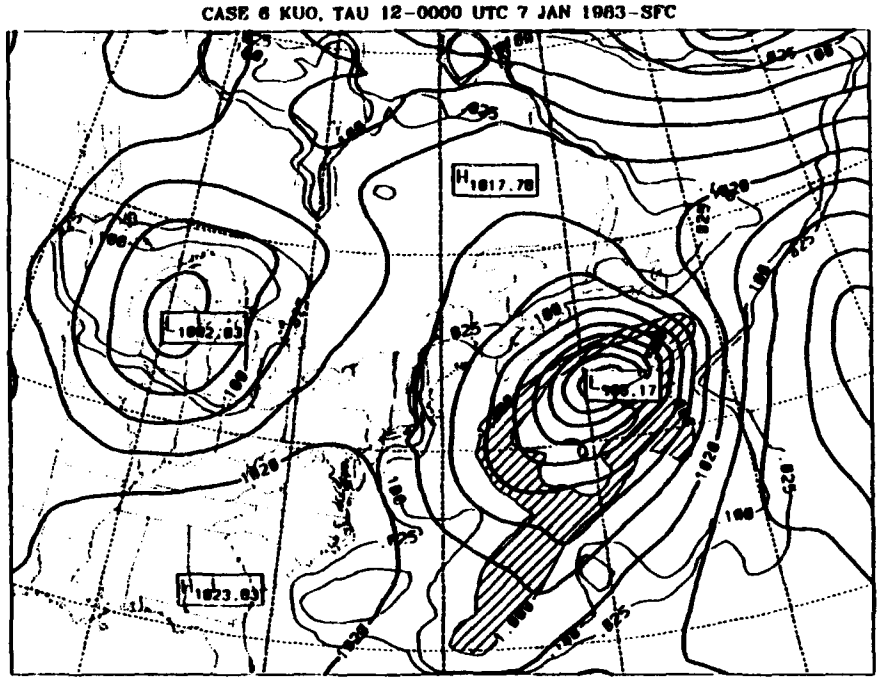

CASE 6 DRY, TAU 12-0000 UTC 7 JAN 1983-SFC

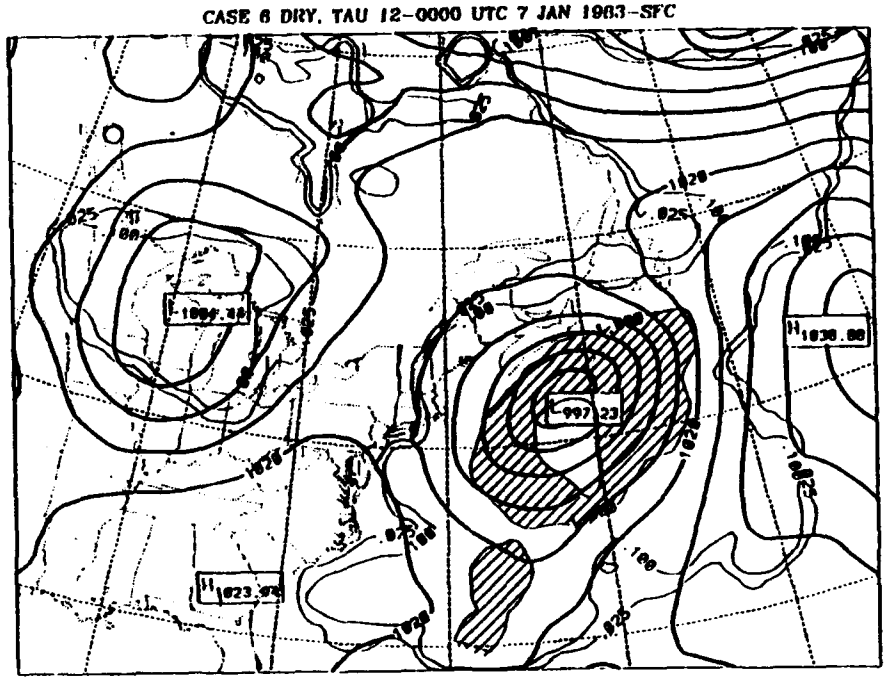

d.

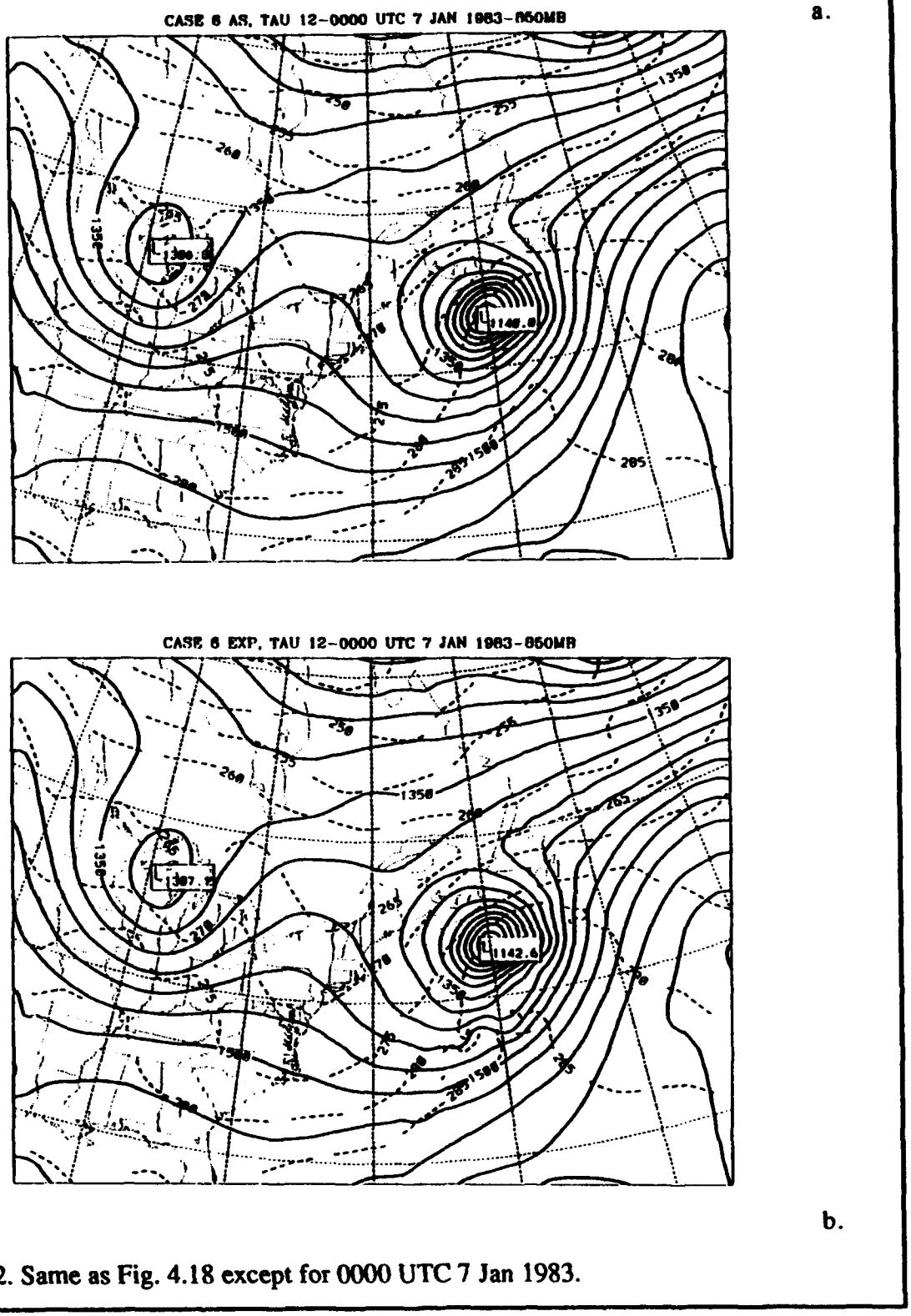

FIG. 4.32. Same as Fig. 4.18 except for 0000 UTC 7 Jan 1983.

CASE 6 KUO, TAU 12-0000 UTC 7 JAN 1983-850MB

c.

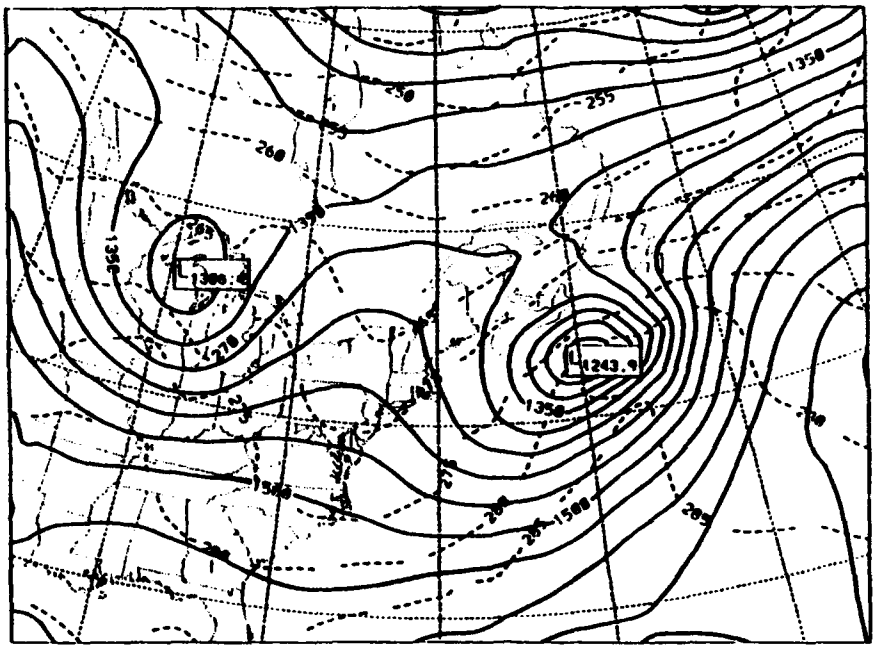

CASE 6 DRY, TAU 12-0000 UTC 7 JAN 1983-850MB

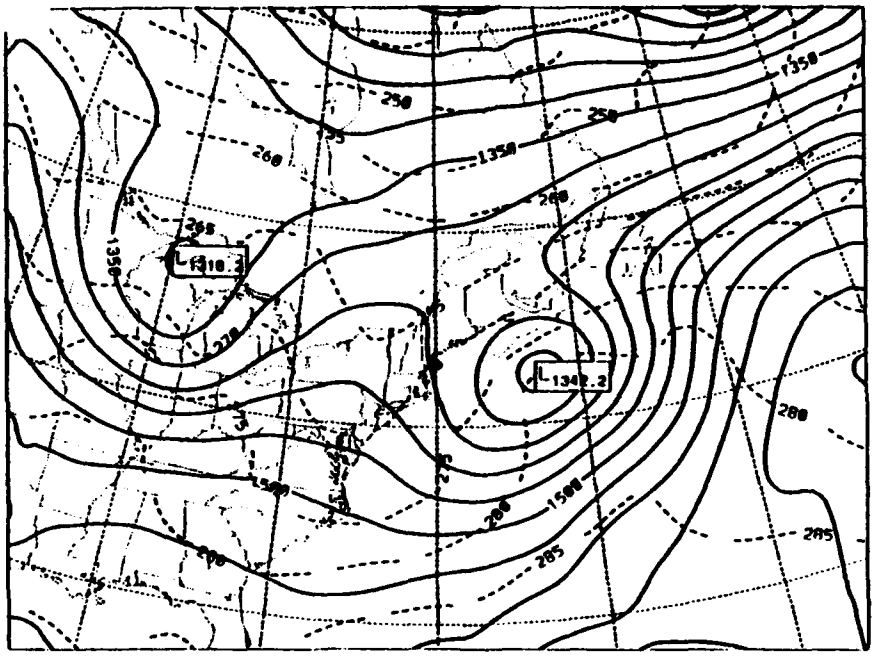

d.

a.

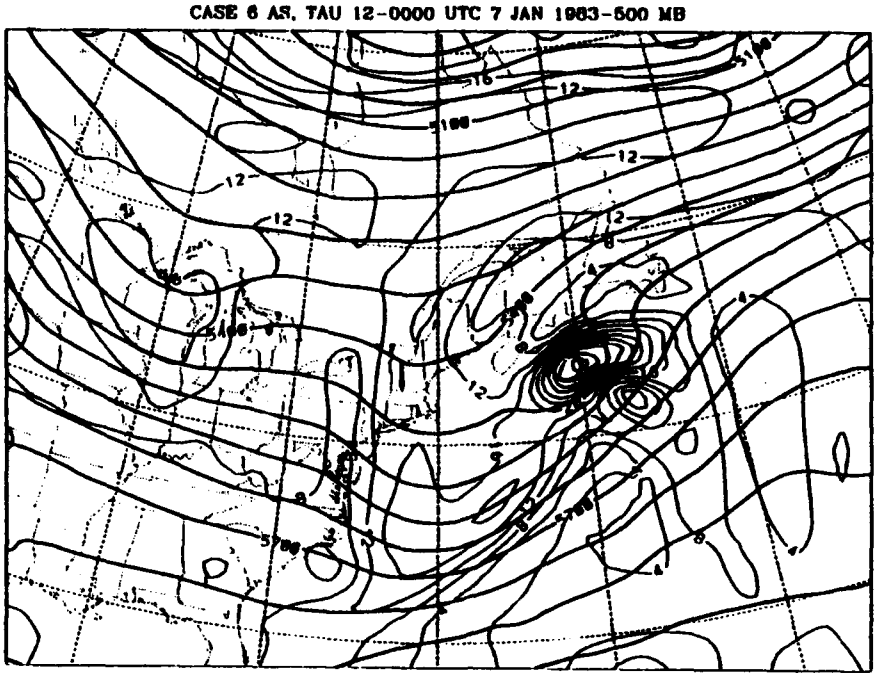

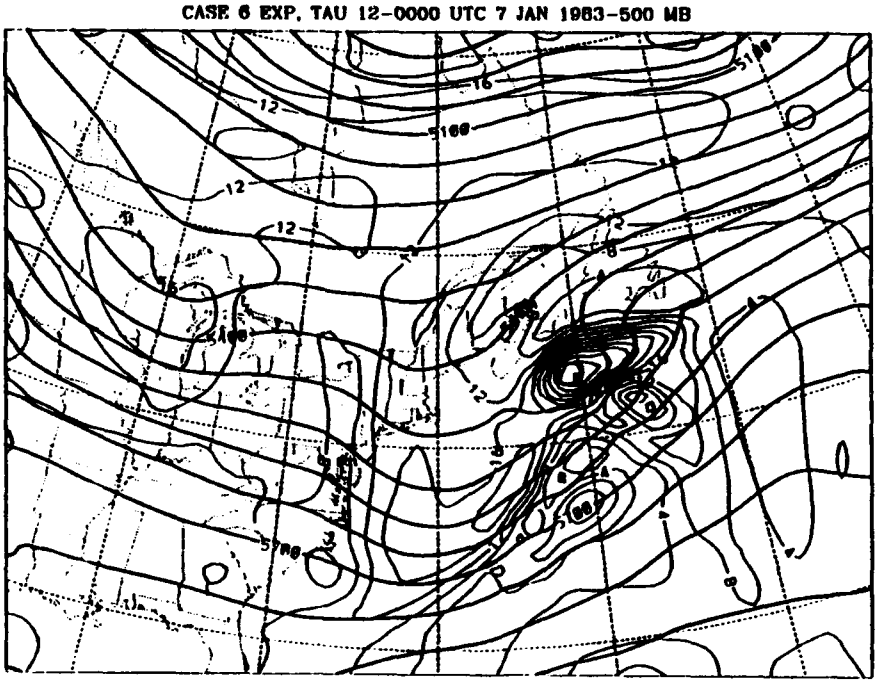

b.

FIG. 4.33. Same as Fig. 4.19 except for 0000 UTC 7 Jan 1983.

c.

CASE 6 KUO, TAU 12-0000 UTC 7 JAN 1983-500 MB

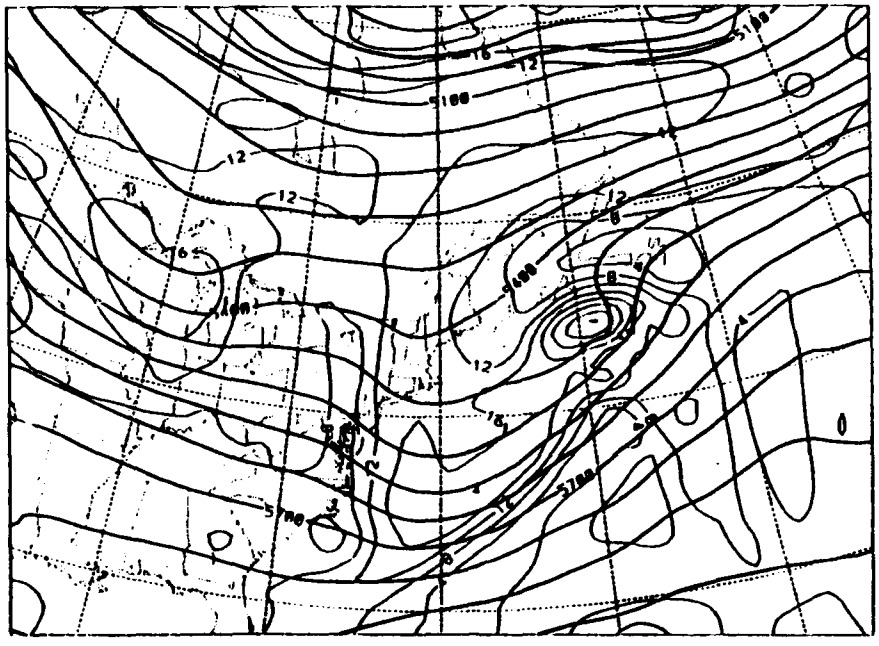

CASE 6 DRY, TAU 12-0000 UTC 7 JAN 1983-500 MB

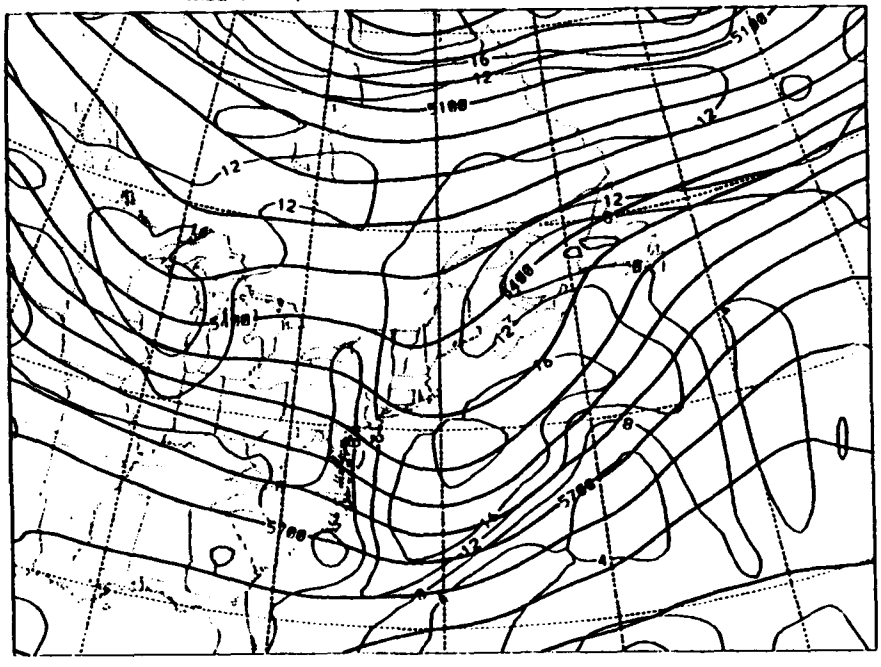

d.

a.

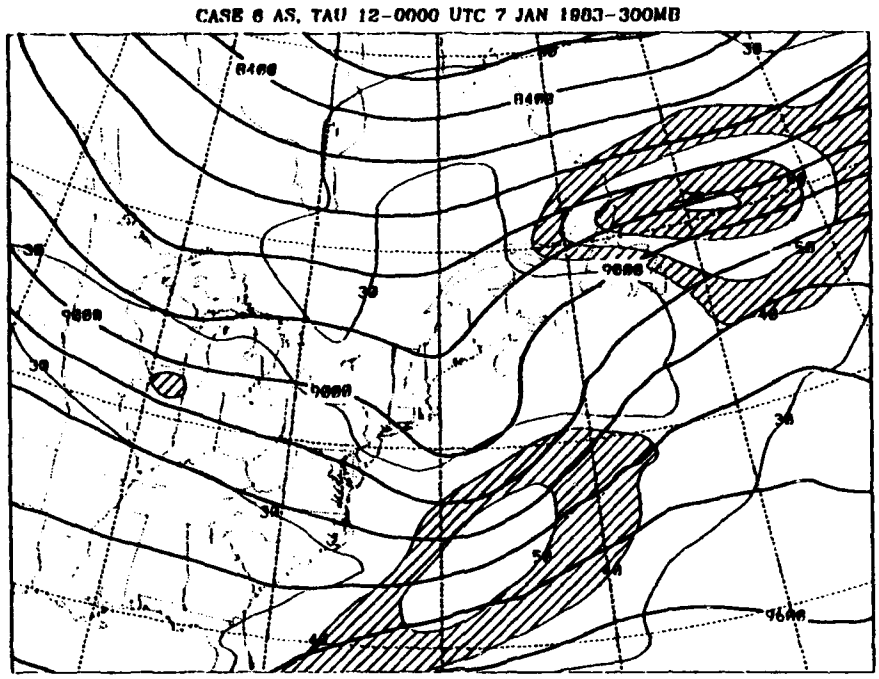

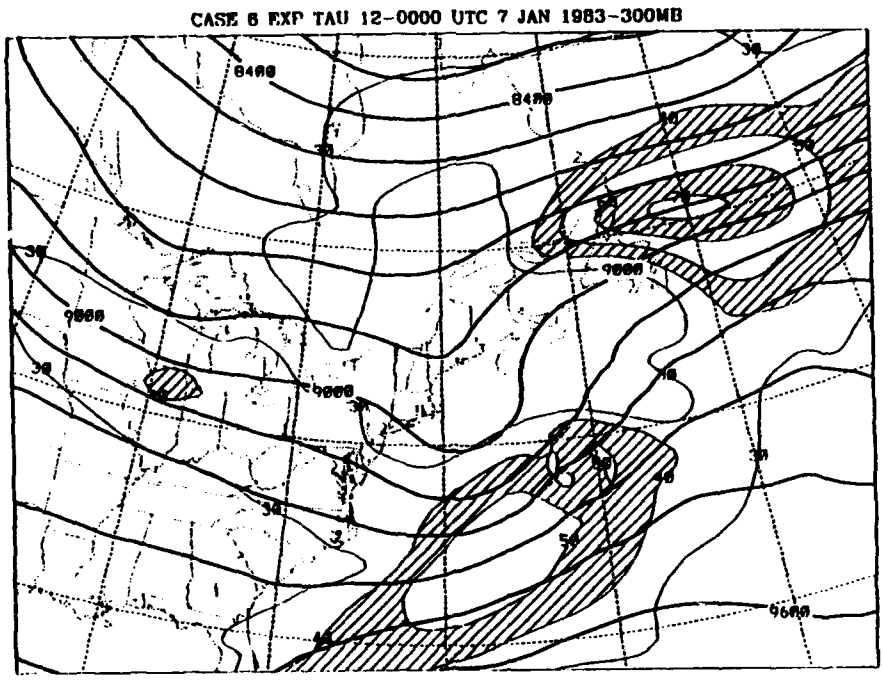

b.

FIG. 4.34. Same as Fig. 4.20 except for 0000 UTC 7 Jan 1983.

c.

CASE 6 KUO, TAU 12-0000 UTC 7 JAN 1983-300MB

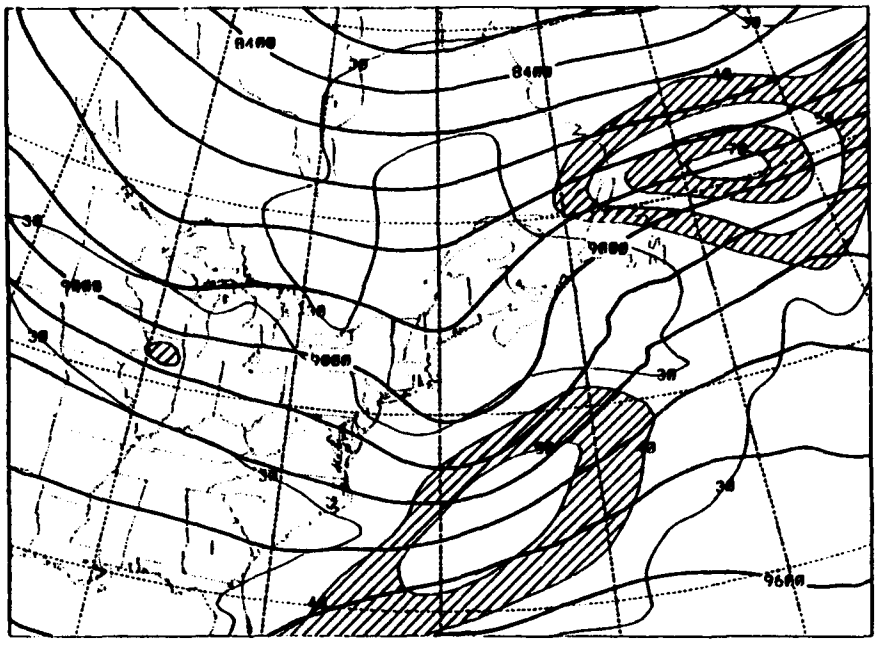

CASE 6 DRY, TAU 12-0000 UTC 7 JAN 1983-300MB

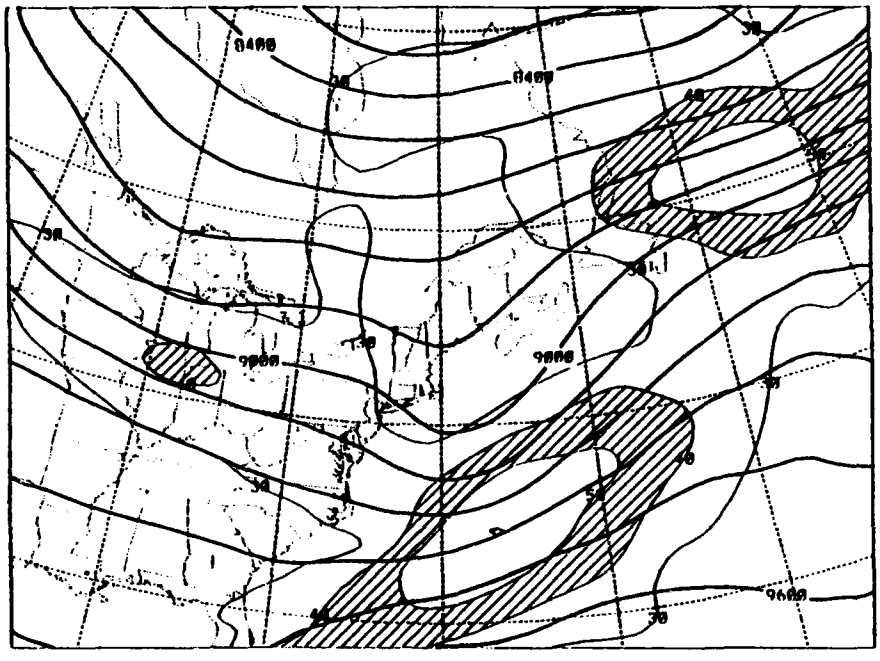

d.

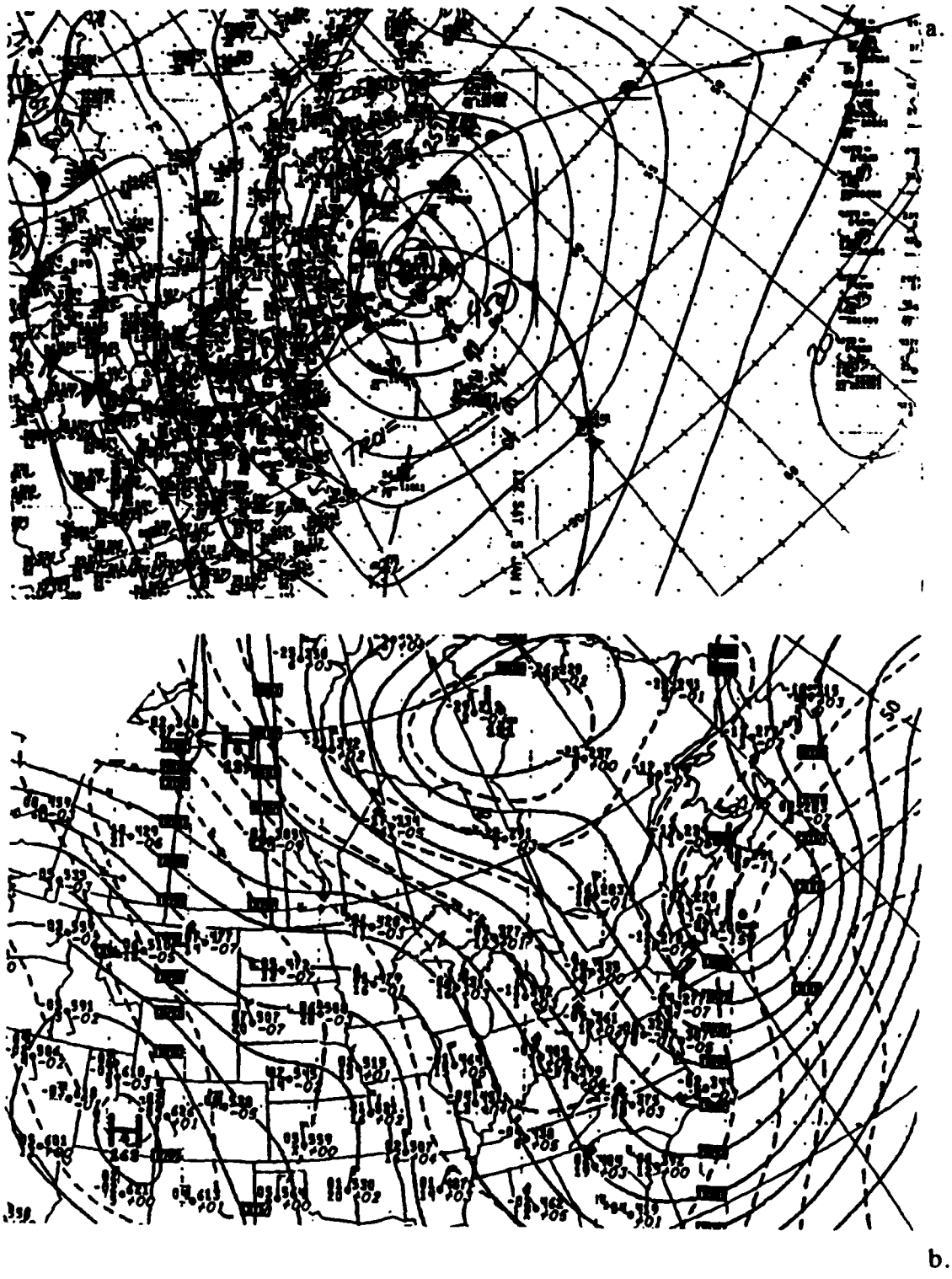

FIG. 4.35. Same as Fig. 4.8 except for case 7, 1200 UTC 5 Jan 1985.

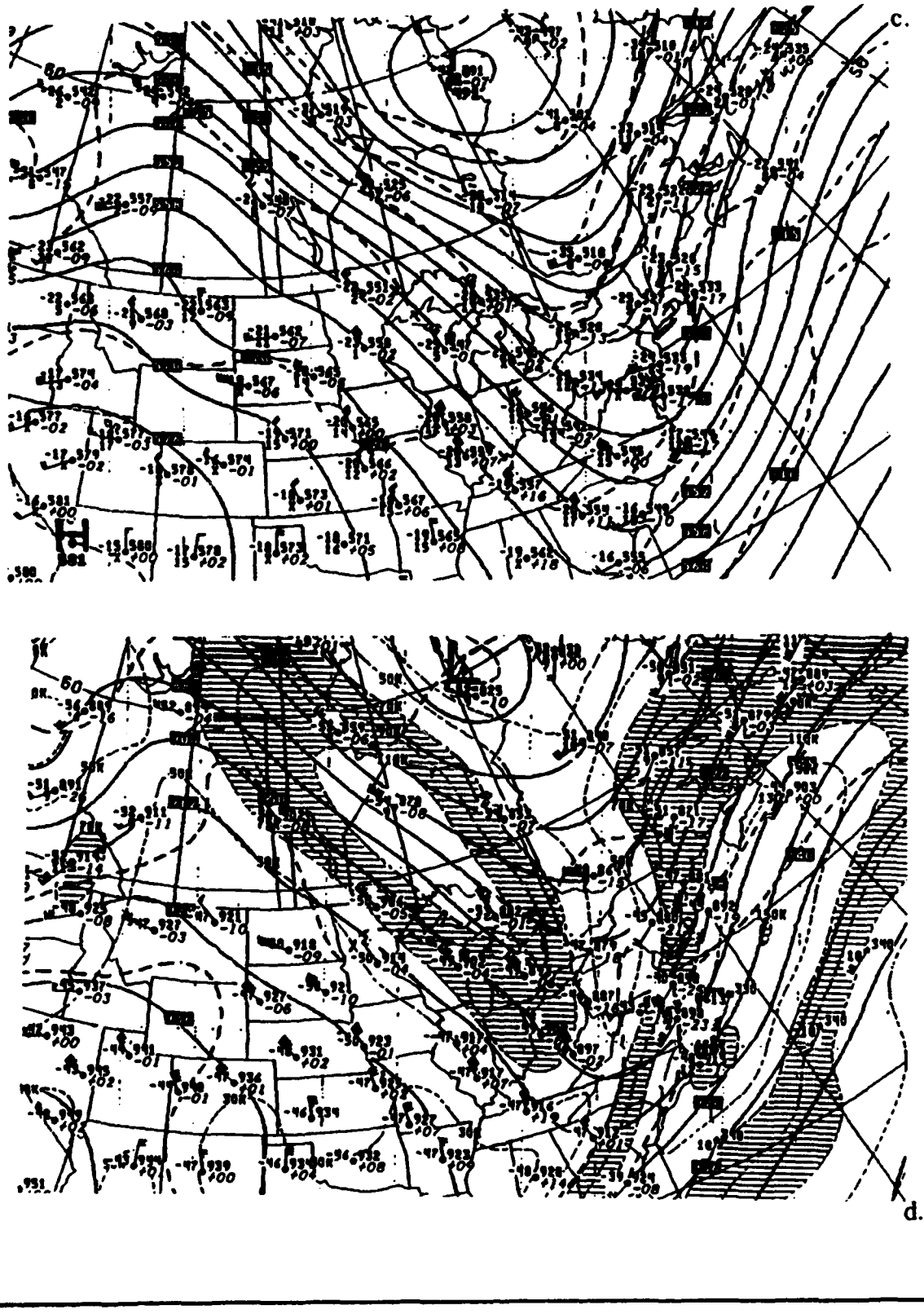
c.
d.

a.

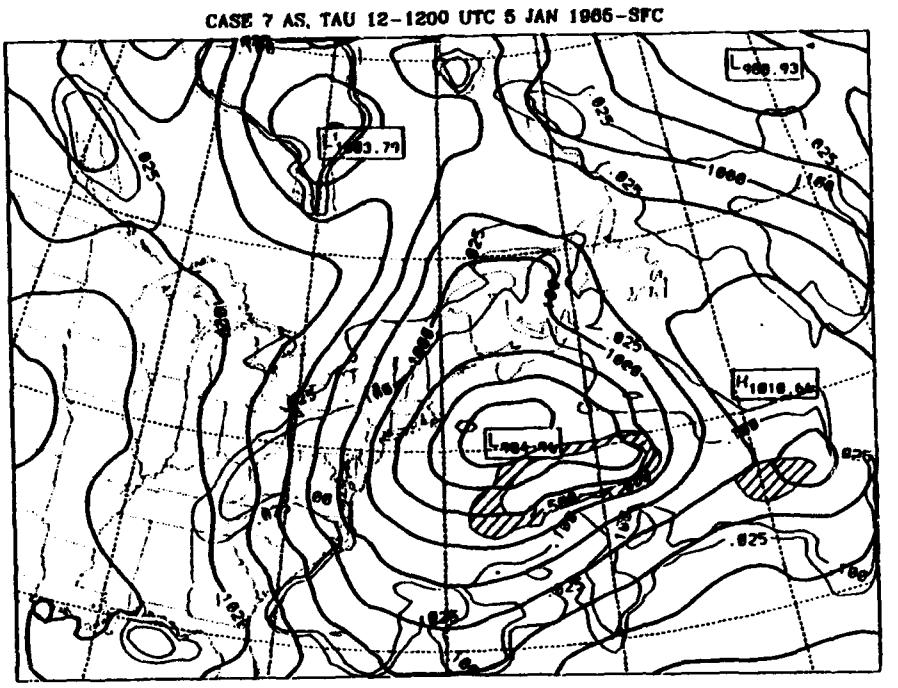

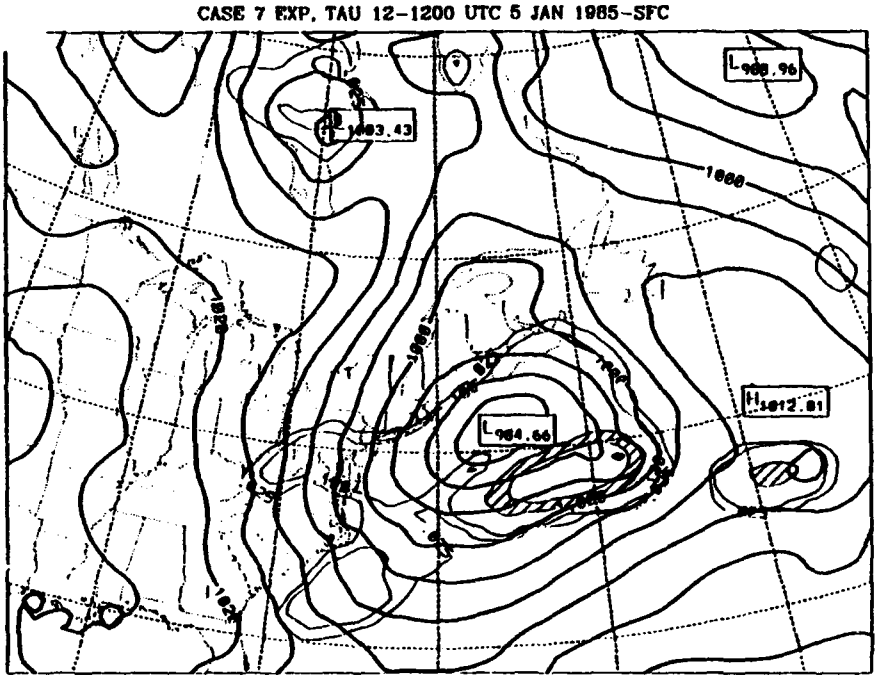

b.

FIG. 4.36. Same as Fig. 4.13 except for case 7, 1200 UTC 5 Jan 1985.

c.

CASE 7 KUO, TAU 12-1200 UTC 5 JAN 1985-SFC

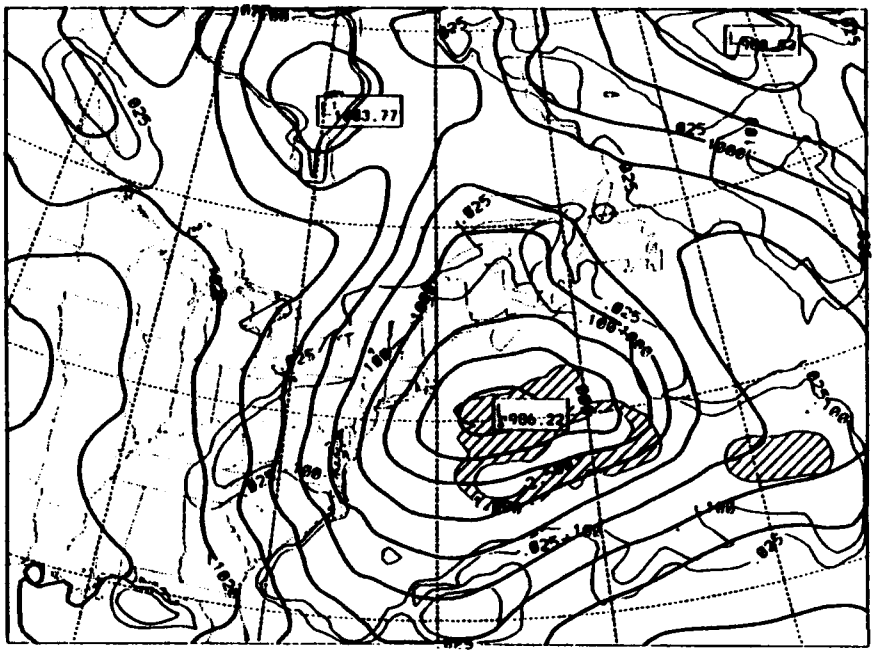

CASE 7 DRY, TAU 12-1200 UTC 5 JAN 1985-SFC

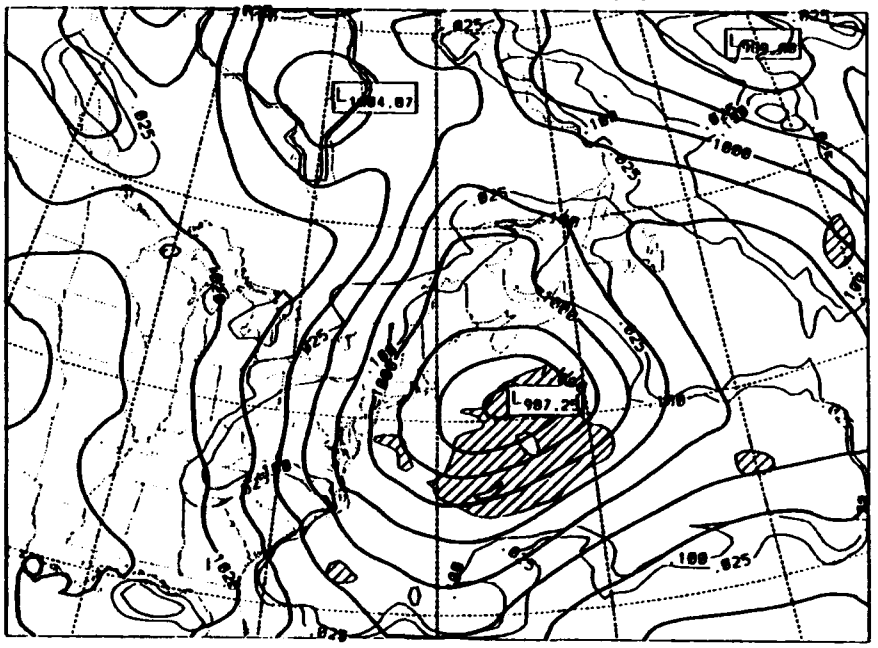

d.

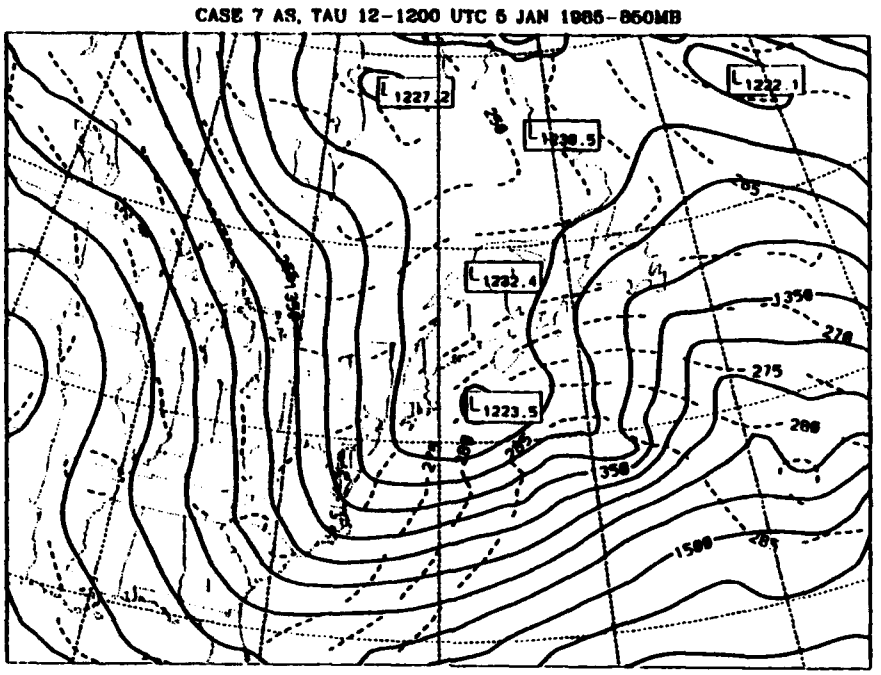

a.

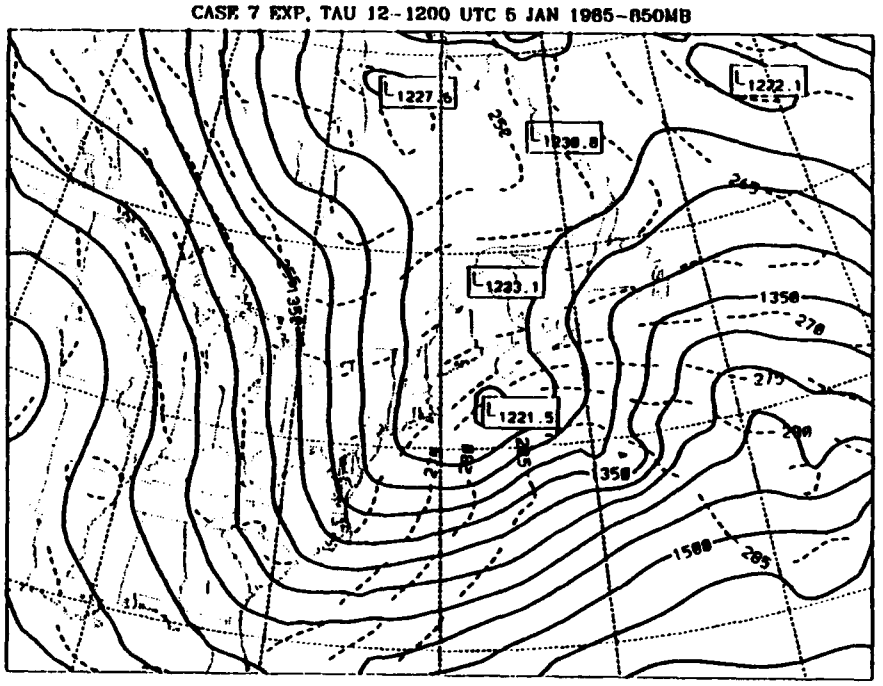

b.

FIG. 4.37. Same as Fig. 4.18 except for case 7, 1200 UTC 5 Jan 1985.

c.

CASE 7 KUO, TAU 12-1200 UTC 5 JAN 1985-850MB

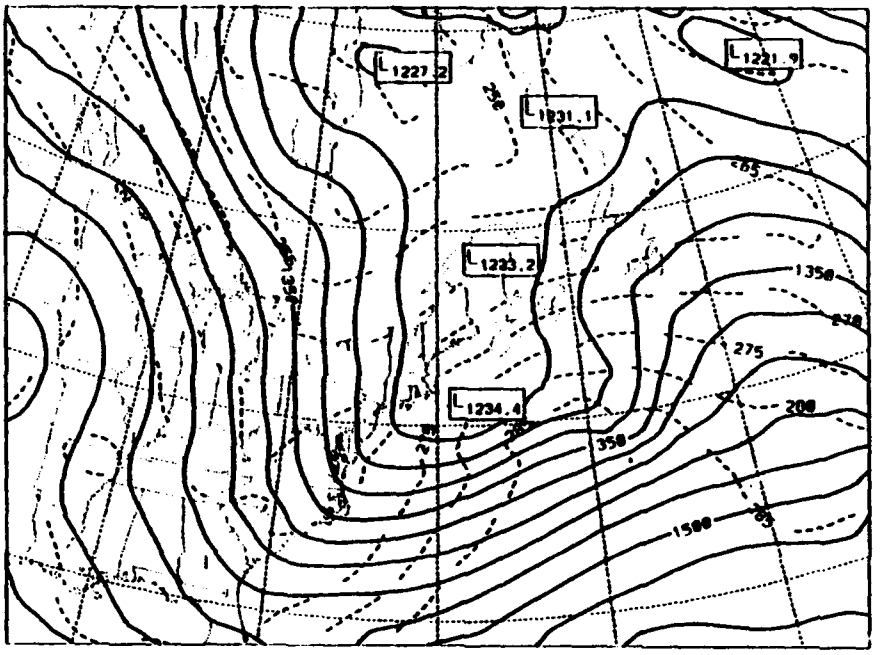

CASE 7 DRY, TAU 12-1200 UTC 5 JAN 1985-850MB

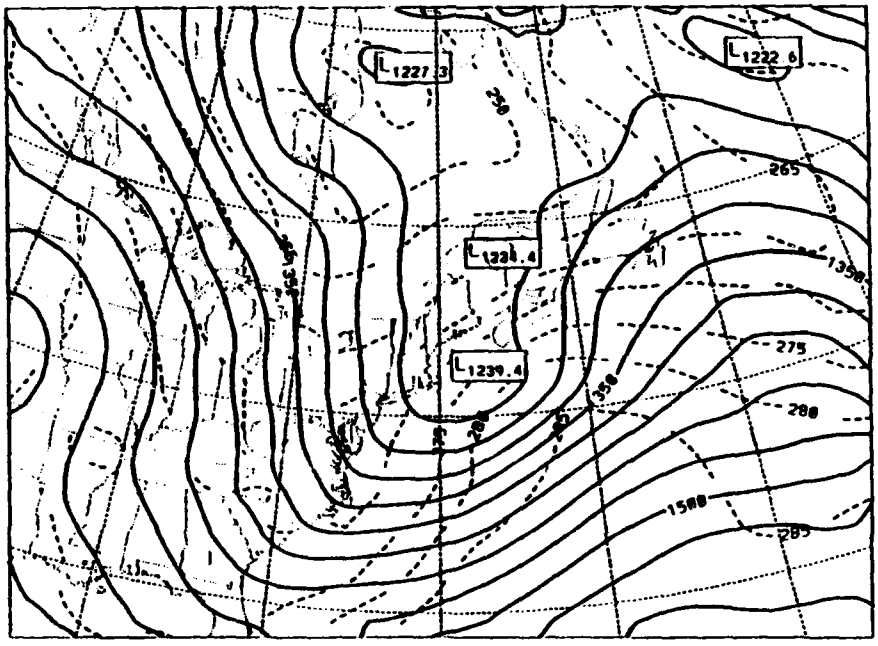

d.

a.

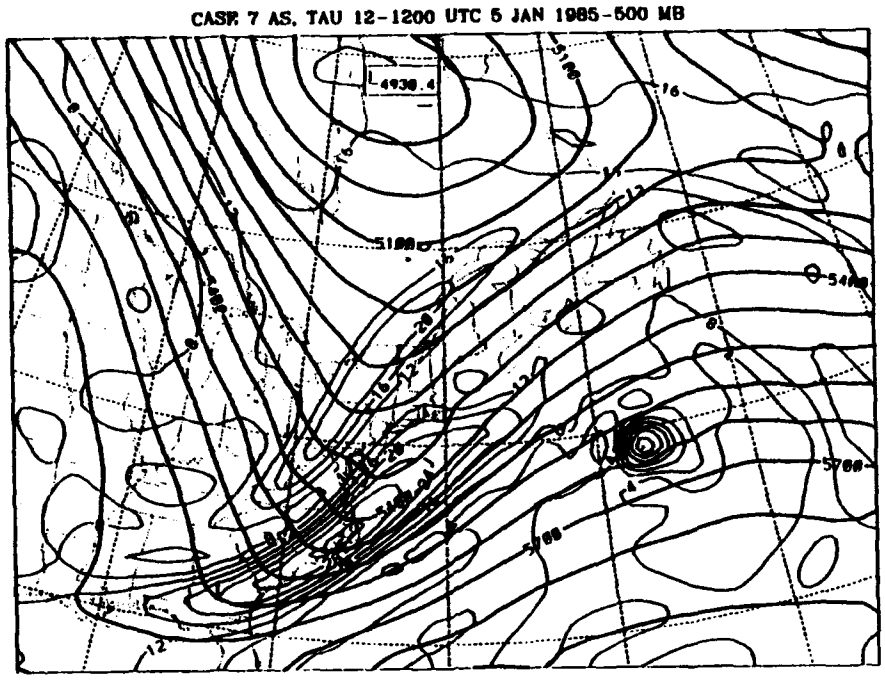

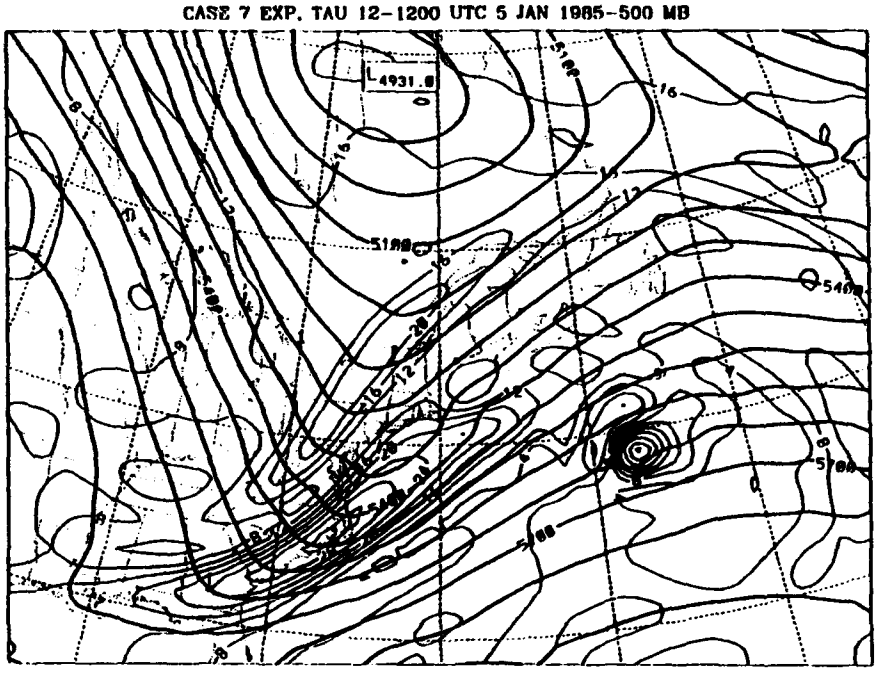

b.

FIG. 4.38. Same as Fig. 4.19 except for case 7, 1200 UTC 5 Jan 1985.

c.

CASE 7 KUO, TAU 12-1200 UTC 5 JAN 1985-500 MB

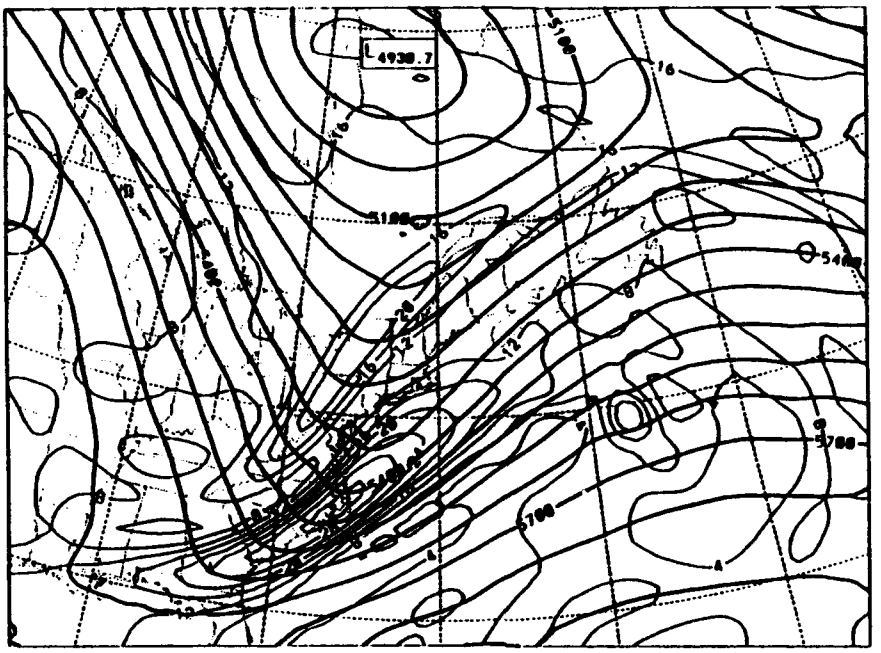

CASE 7 DRY, TAU 12-1200 UTC 5 JAN 1985-500 MB

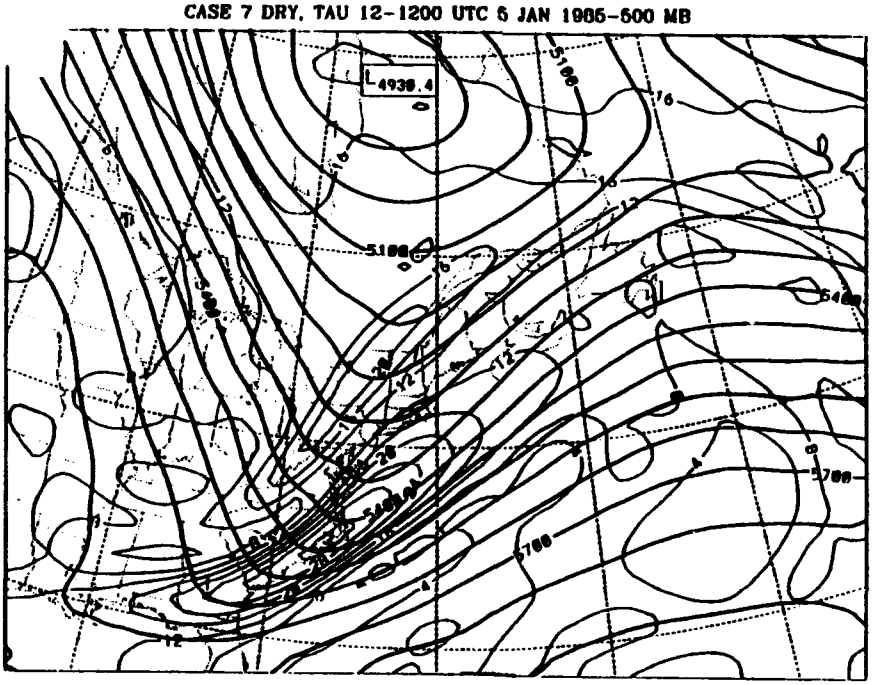

d.

a.

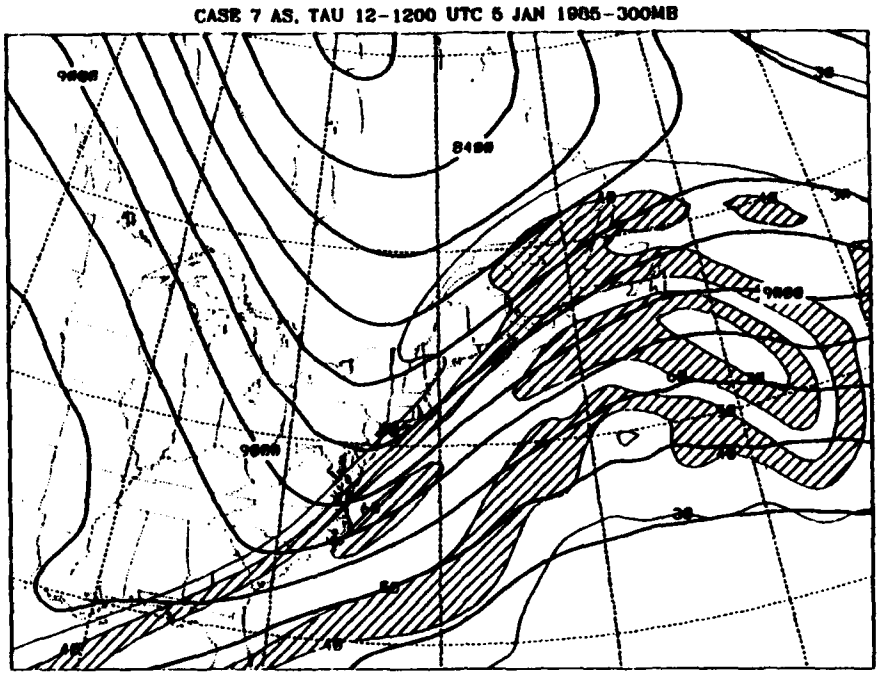

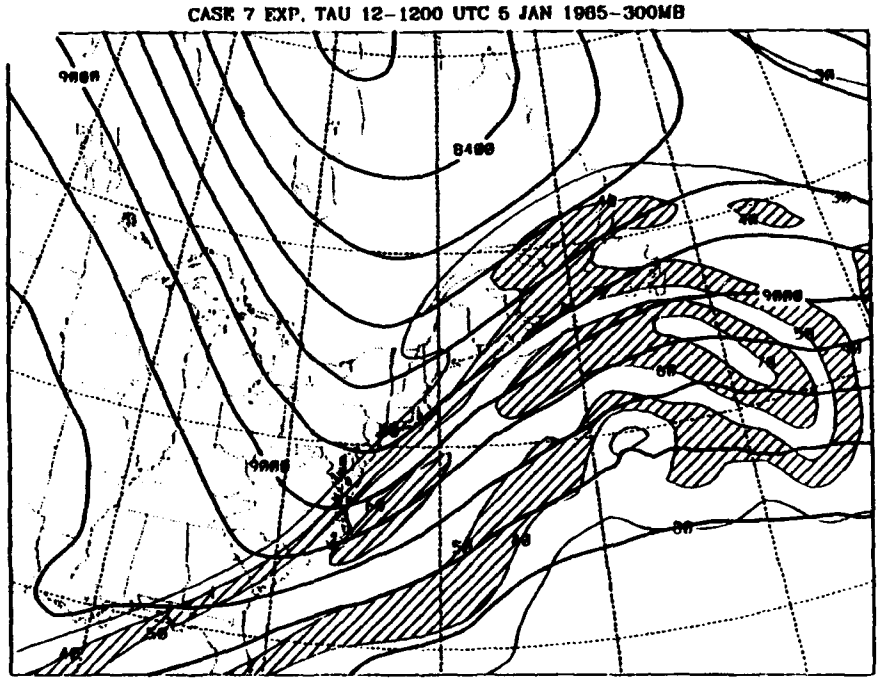

b.

FIG. 4.39. Same as Fig. 4.20 except for case 7, 1200 UTC 5 Jan 1985.

c.

CASE 7 KUO, TAU 12-1200 UTC 5 JAN 1985-300MB

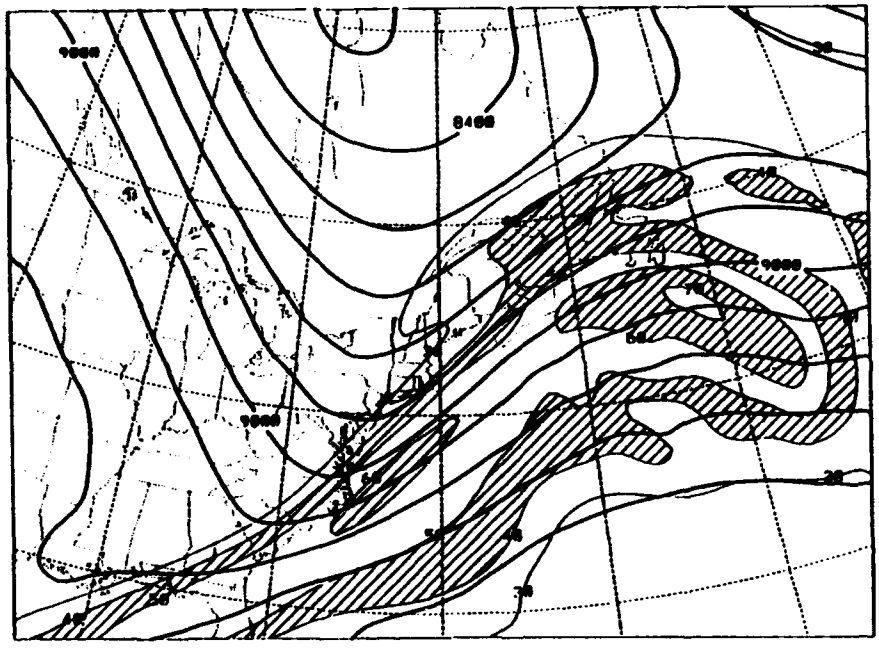

CASE 7 DRY, TAU 12-1200 UTC 5 JAN 1985-300MB

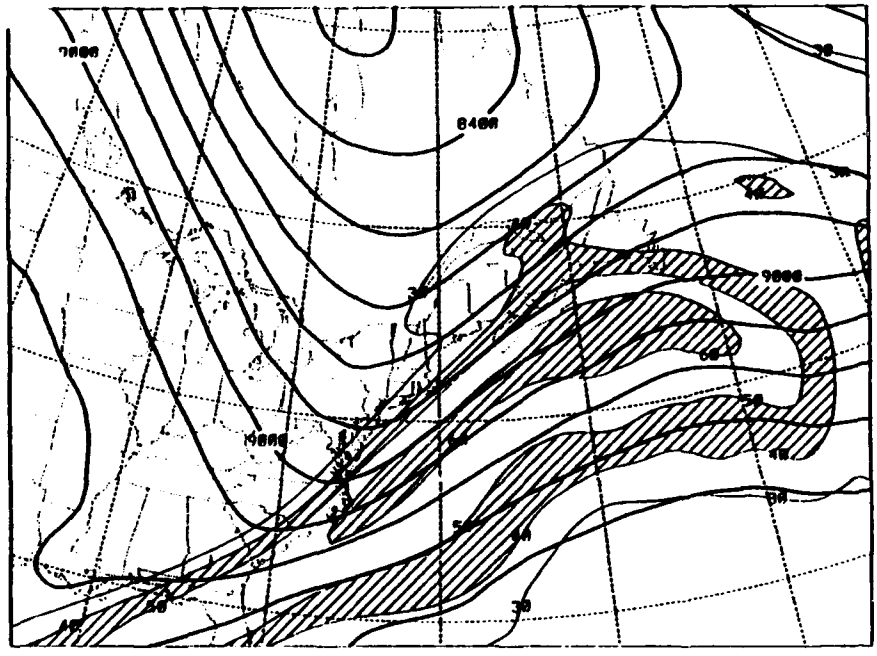

d.

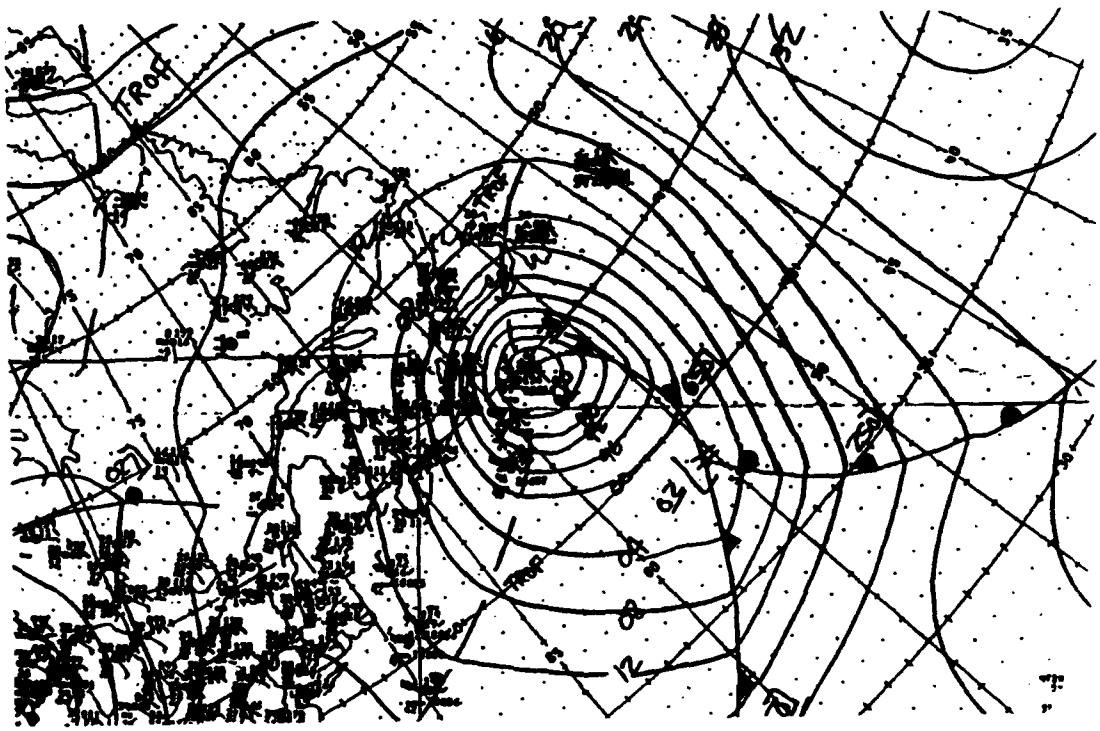

FIG. 4.40. Same as Fig. 4.12 except for 0300 UTC 7 Jan 1983.

a.

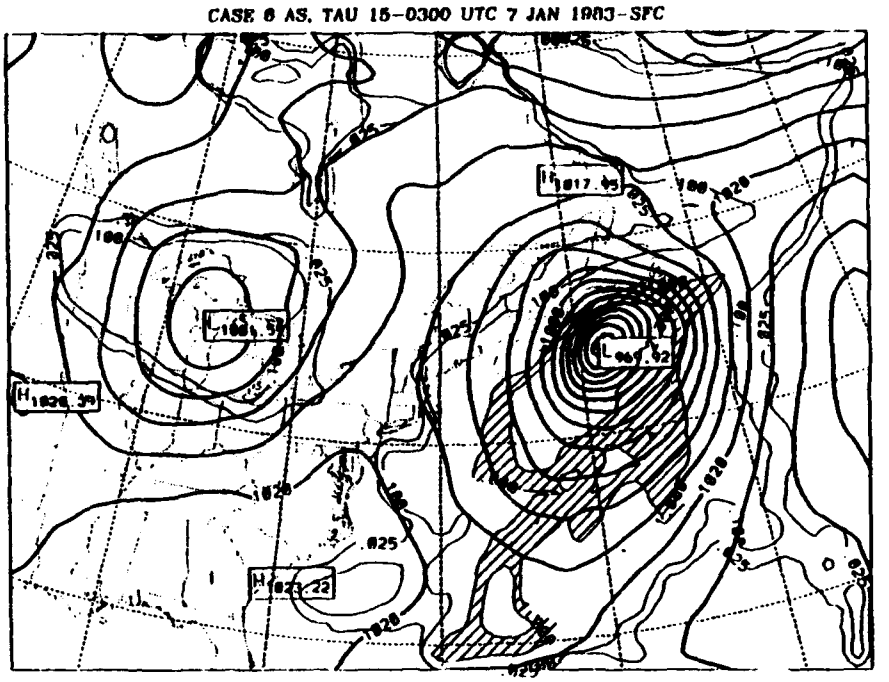

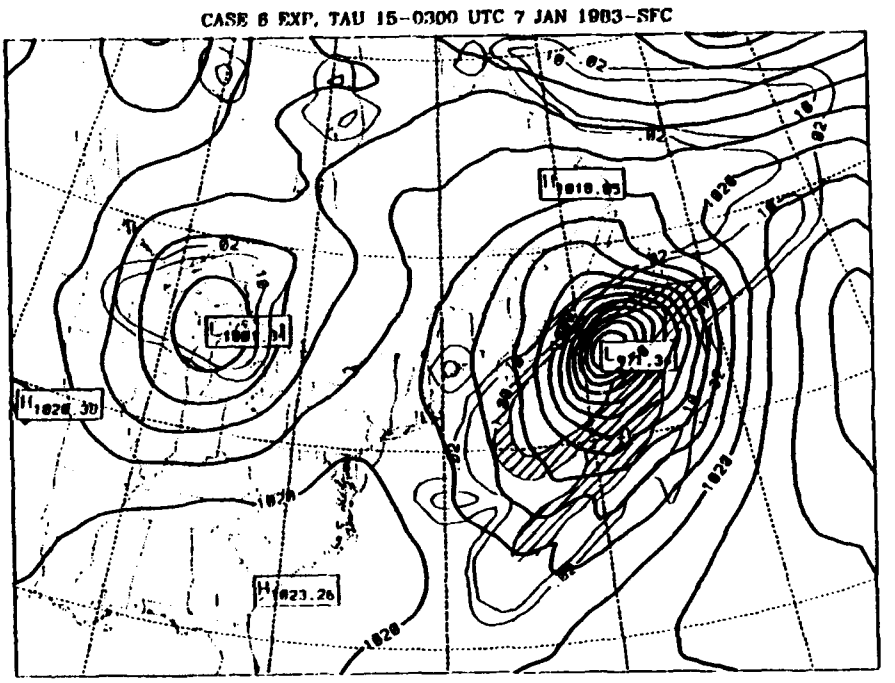

b.

FIG. 4.41. Same as Fig. 4.13 except for 0300 UTC 7 Jan 1983.

c.

CASE 6 KUO, TAU 15-0300 UTC 7 JAN 1983-SFC

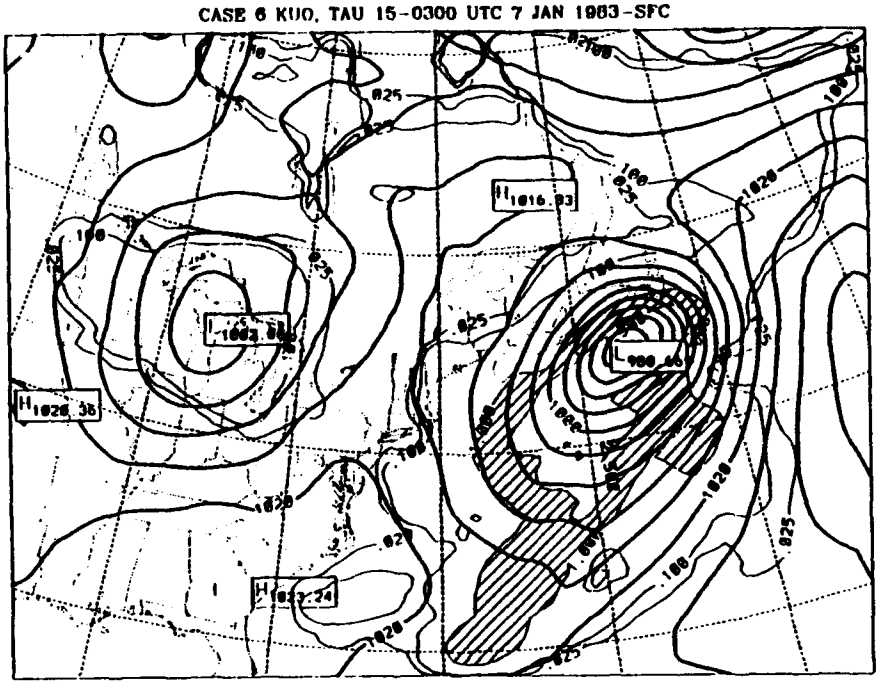

CASE 6 DRY, TAU 15-0300 UTC 7 JAN 1983-SFC

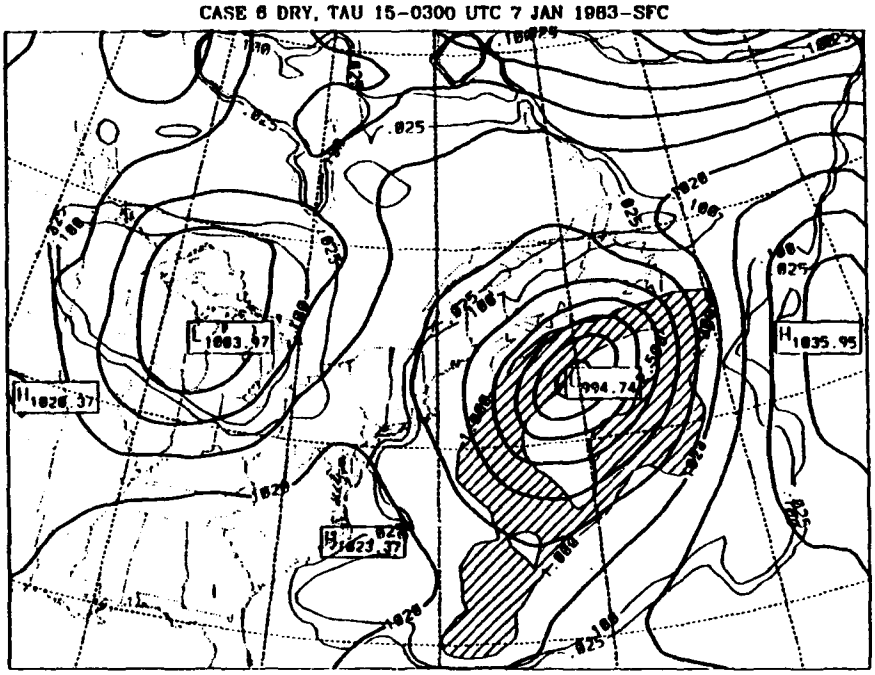

d.

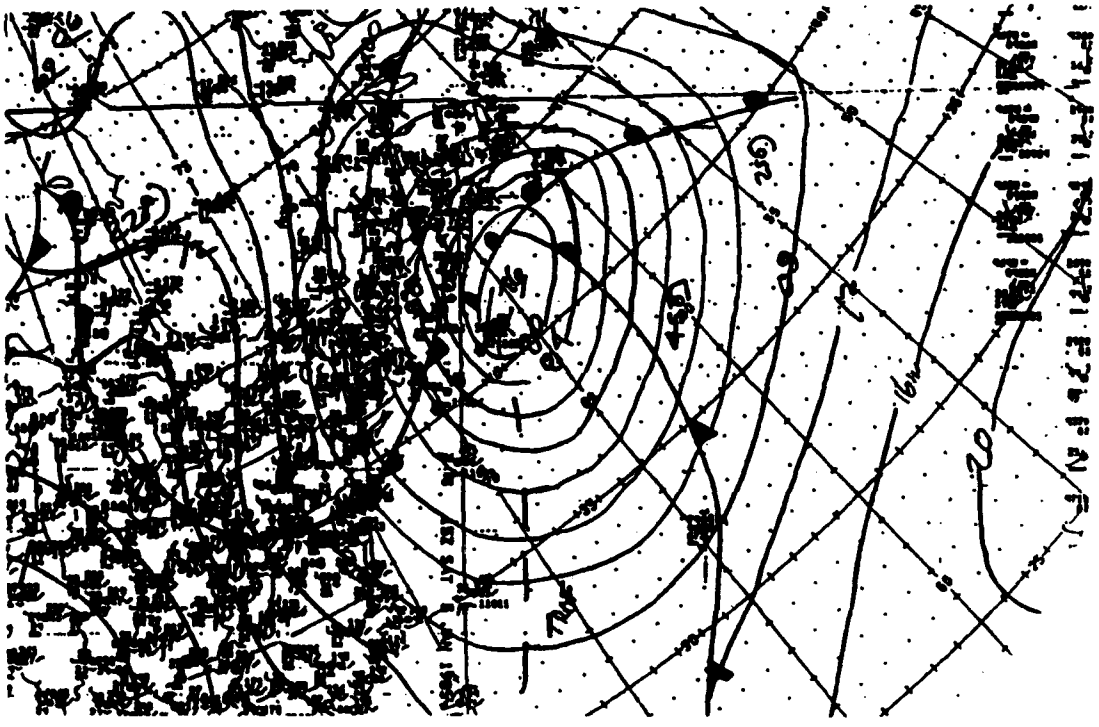

FIG 4.42. Same as Fig. 4.12 except for case 7, 1500 UTC 5 Jan 1985.

a.

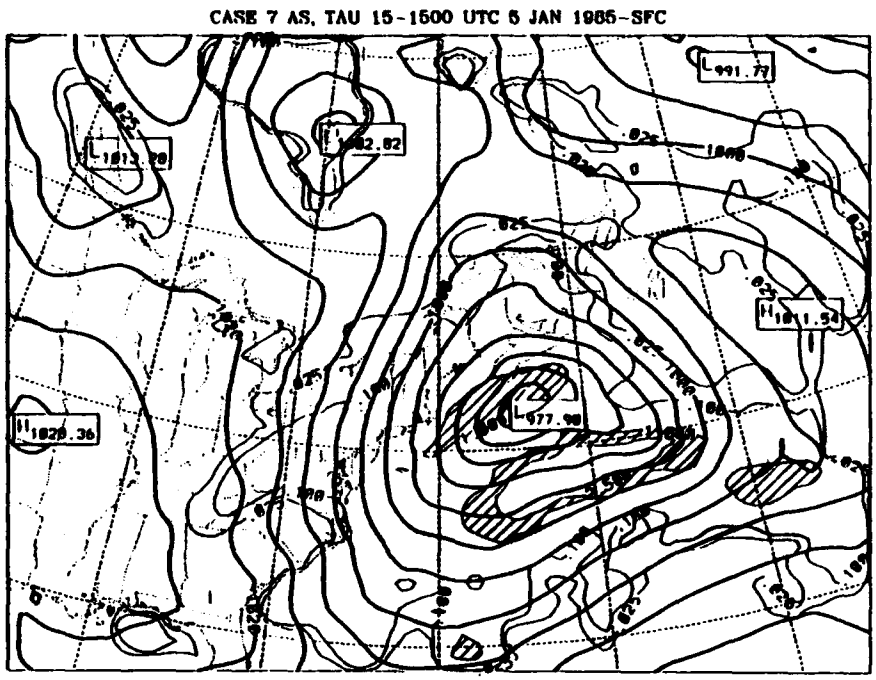

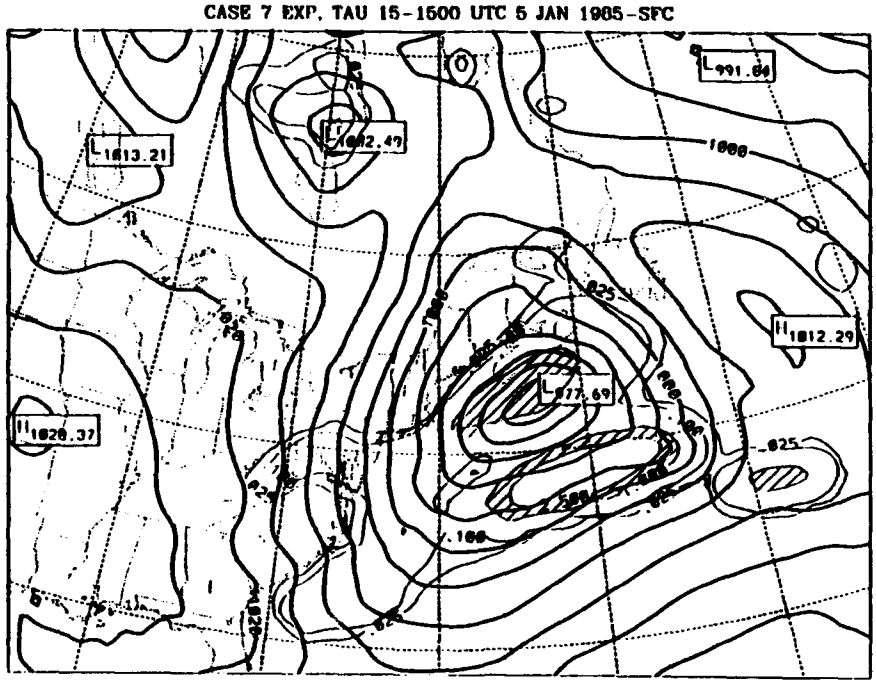

b.

FIG. 4.43. Same as Fig. 4.13 except for case 7, 1500 UTC 5 Jan 1985.

c.

CASE 7 KUO, TAU 15-1500 UTC 5 JAN 1985-SFC

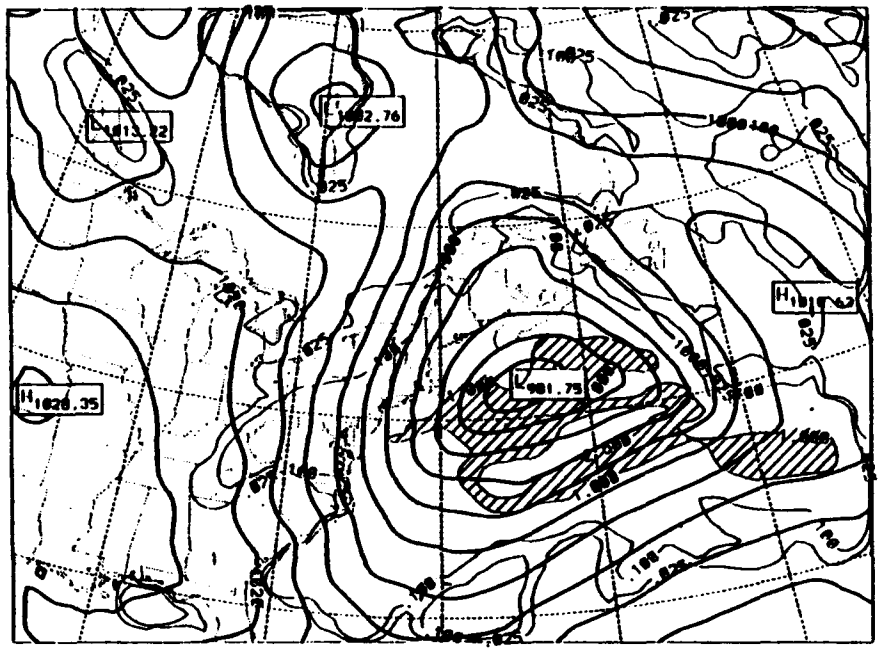

CASE 7 DRY, TAU 15-1500 UTC 5 JAN 1985-SFC

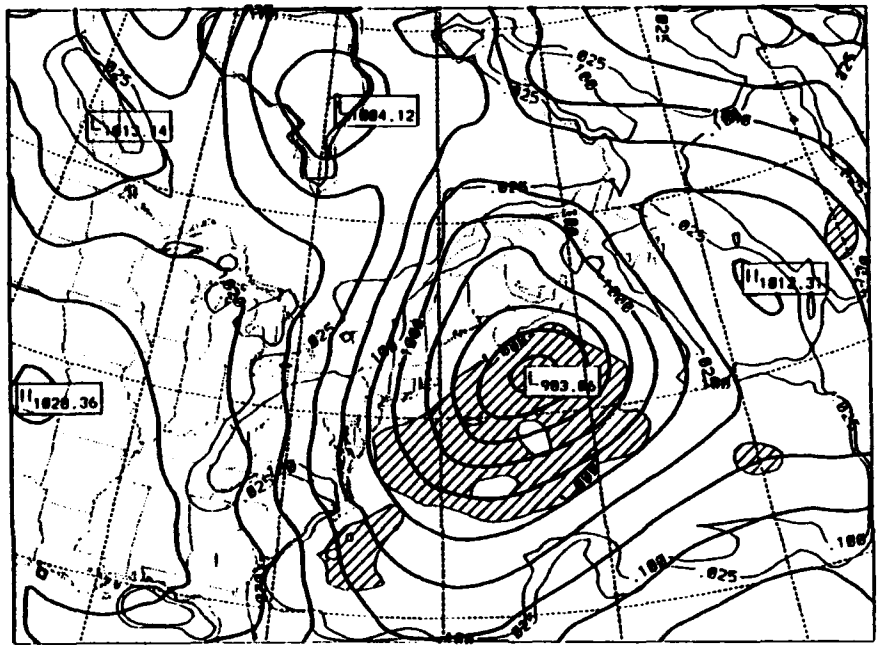

d.

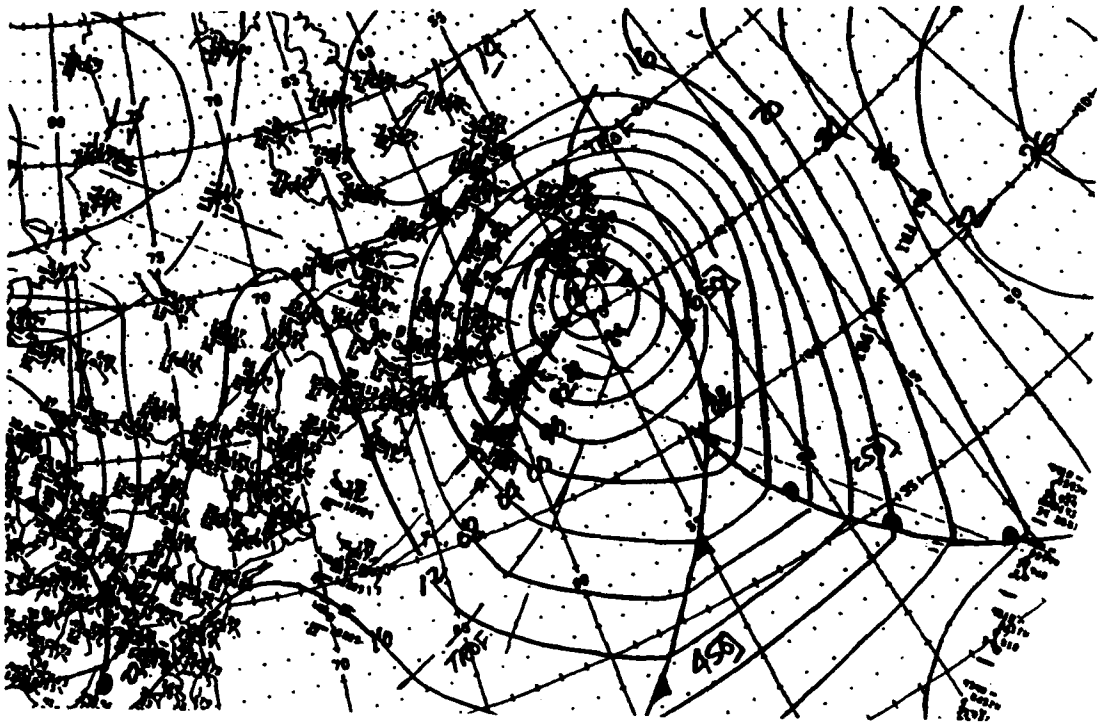

FIG. 4.44. Same as Fig. 4.12 except for 0600 UTC 7 Jan 1983.

a.

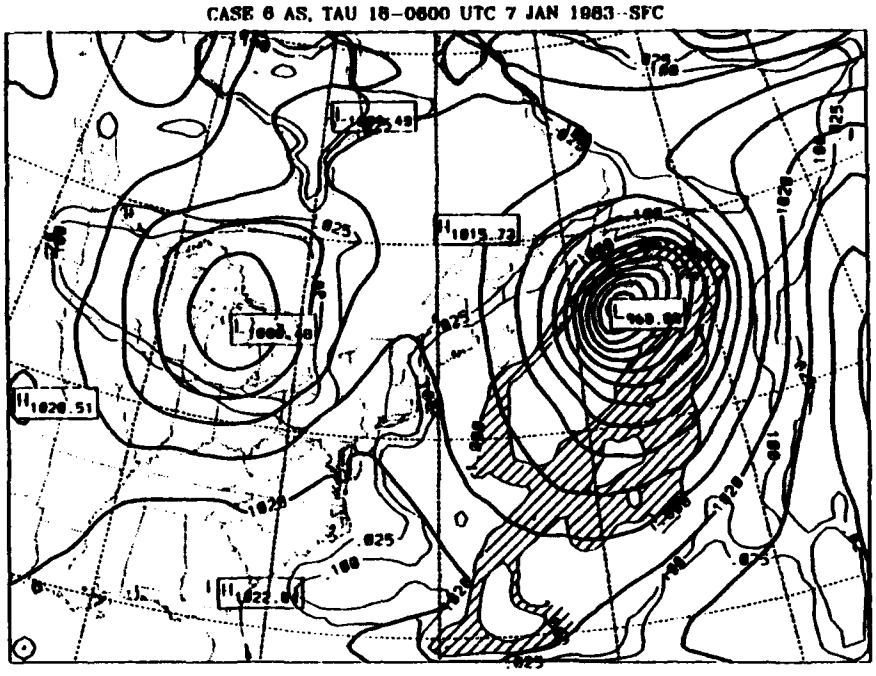

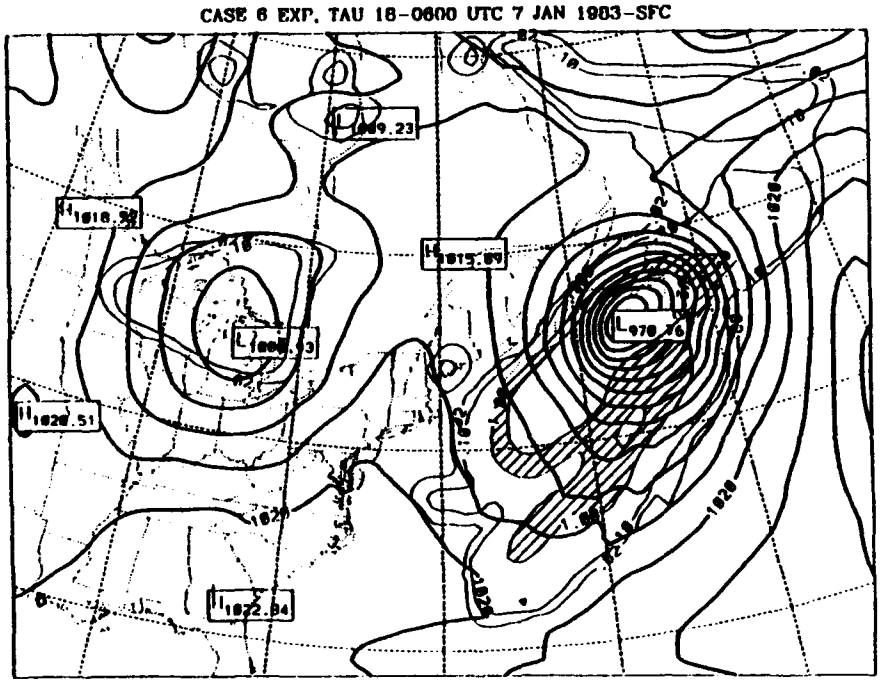

b.

FIG. 4.45. Same as Fig. 4.13 except for 0600 UTC 7 Jan 1983.

c.

CASE 6 KUO, TAU 18-0600 UTC 7 JAN 1983-SFC

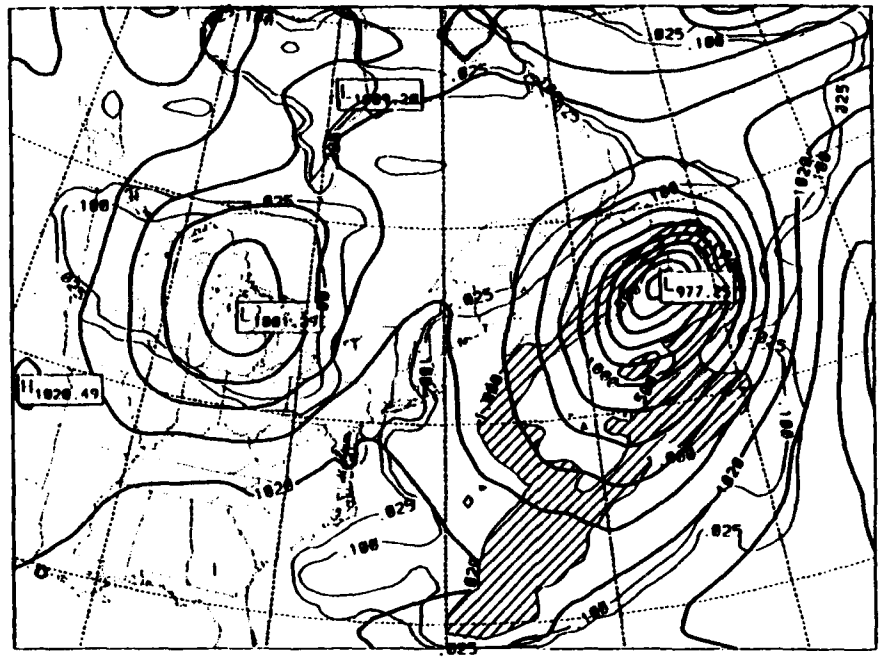

CASE 6 DRY, TAU 18--0600 UTC 7 JAN 1983-SFC

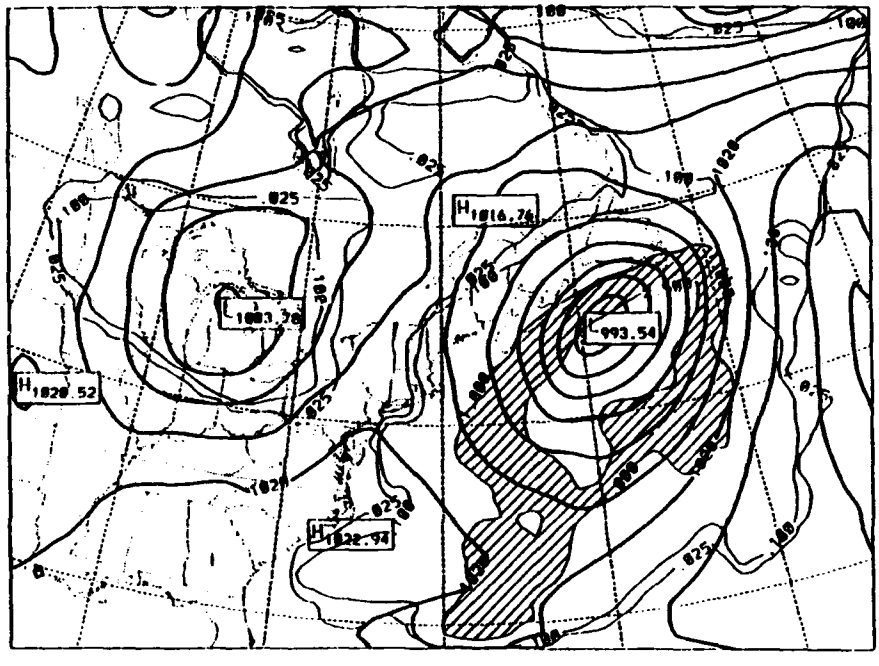

d.

a.

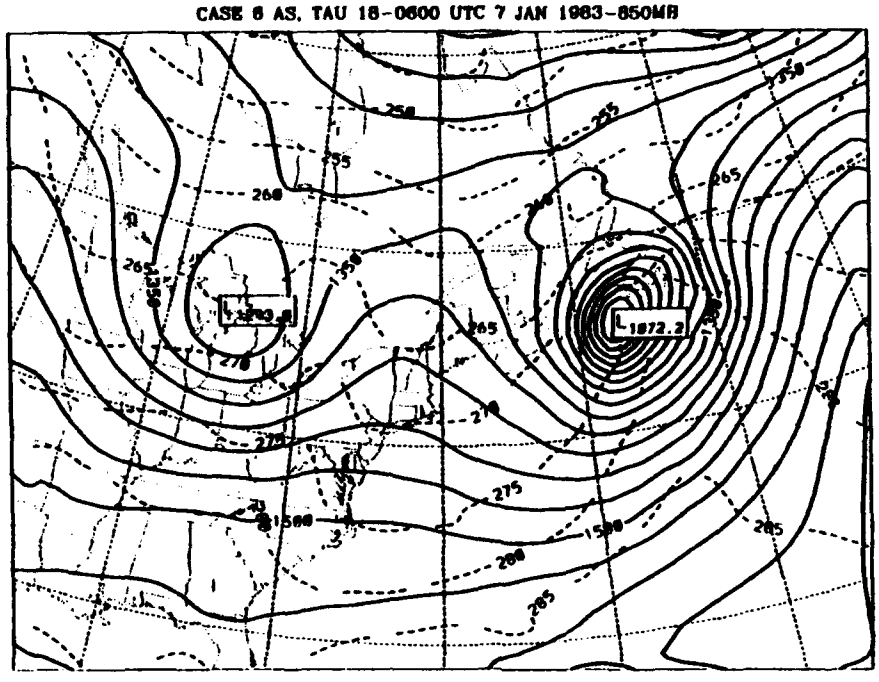

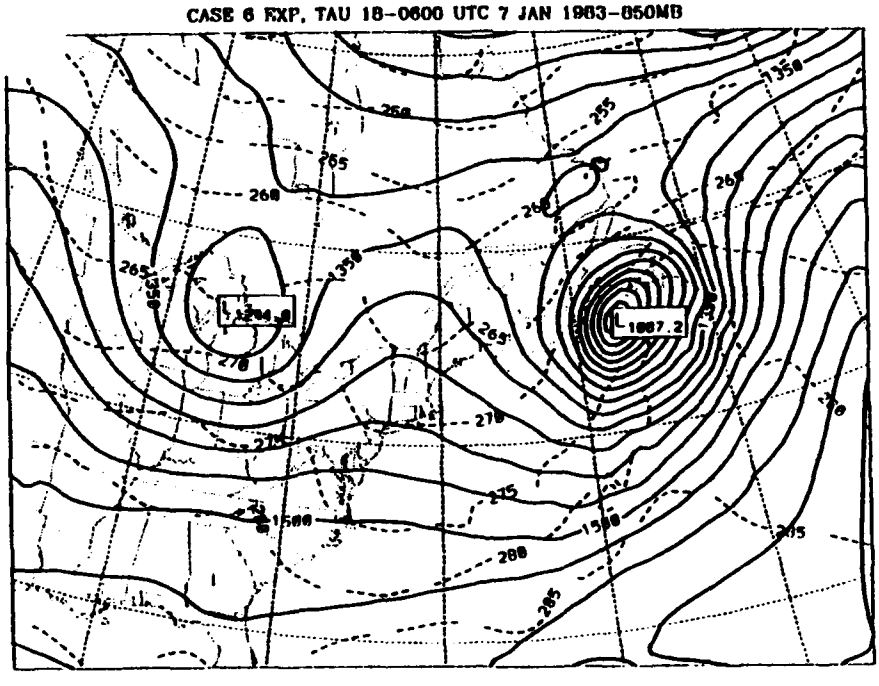

b.

FIG. 4.46. Same as Fig. 4.18 except for 0600 UTC 7 Jan 1983.

c.

CASE 6 KUO, TAU 18-0600 UTC 7 JAN 1983-850MB

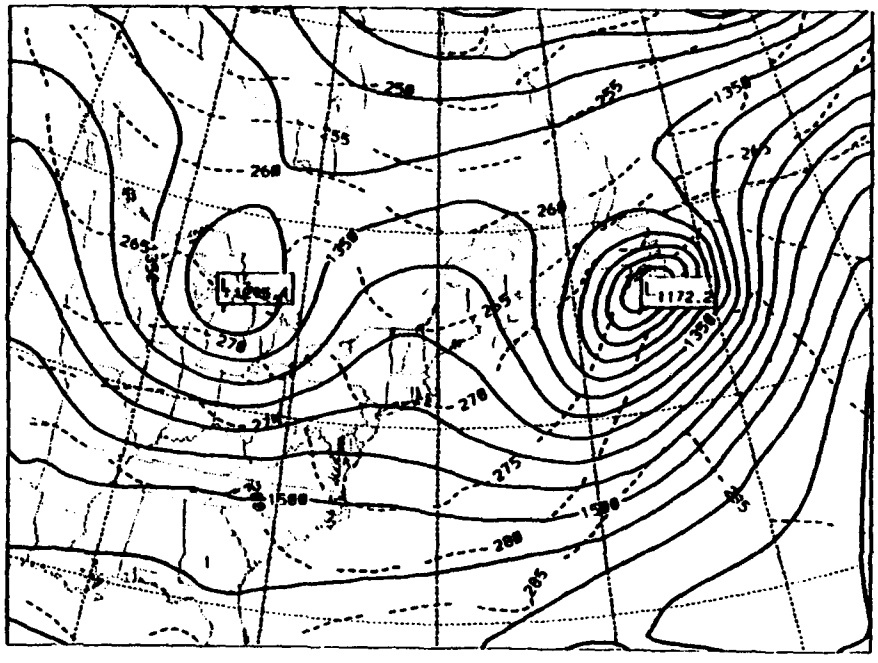

CASE 6 DRY, TAU 18-0600 UTC 7 JAN 1983-850MB

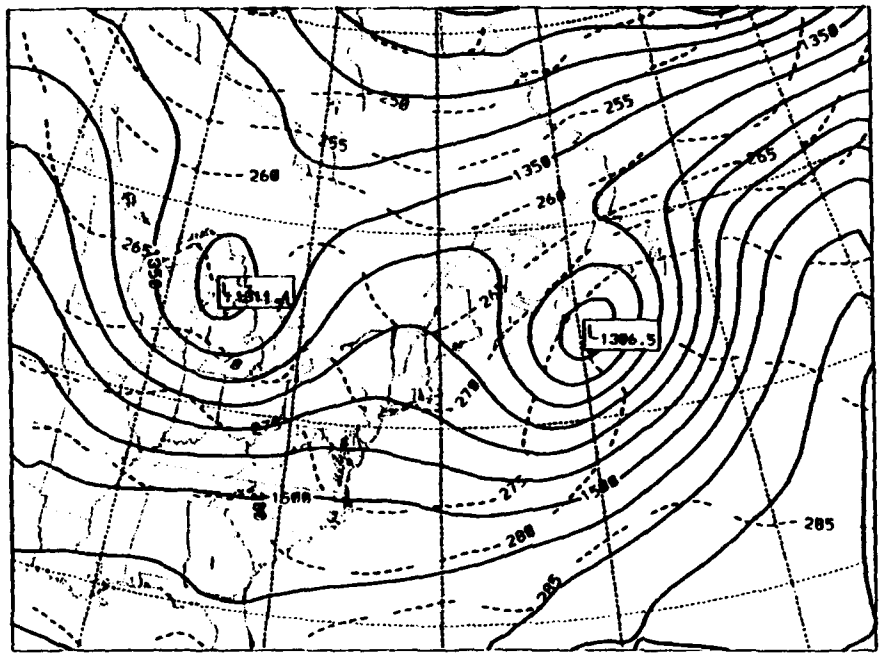

d.

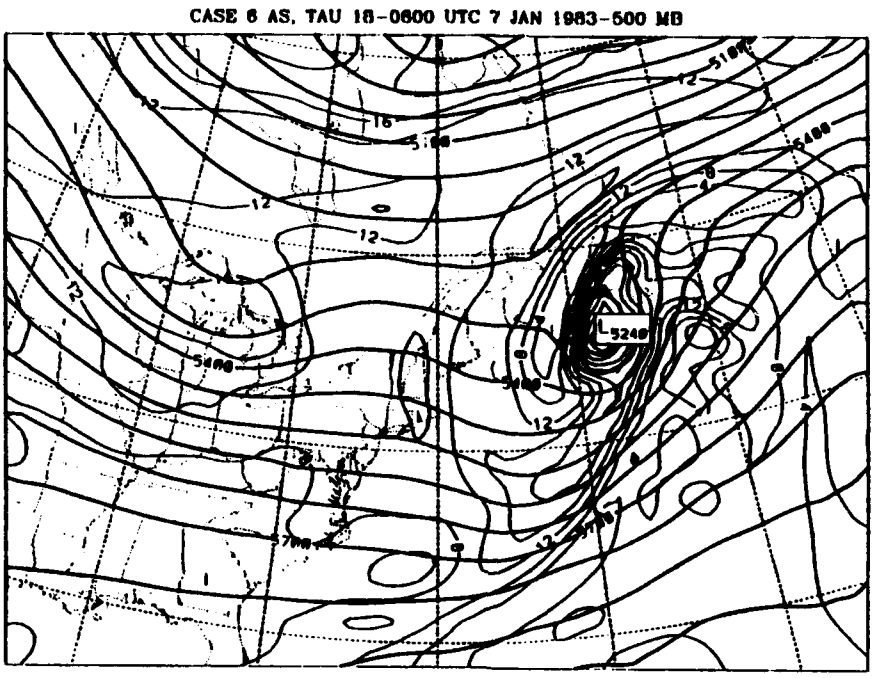

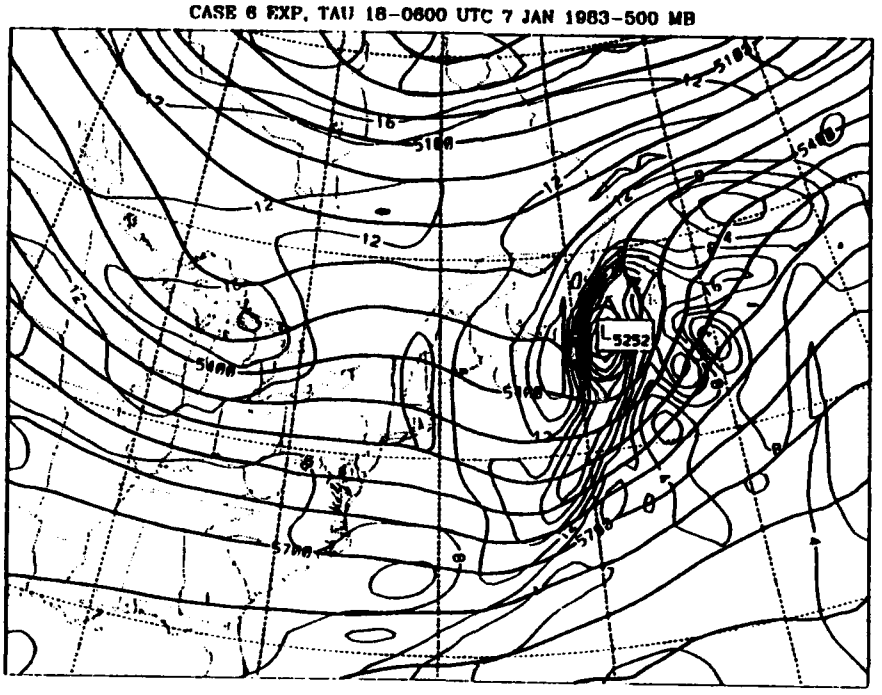

FIG. 4.47. Same as Fig. 4.19 except for 0600 UTC 7 Jan 1983.

c.

CASE 6 KUO, TAU 18-0600 UTC 7 JAN 1963-500 MB

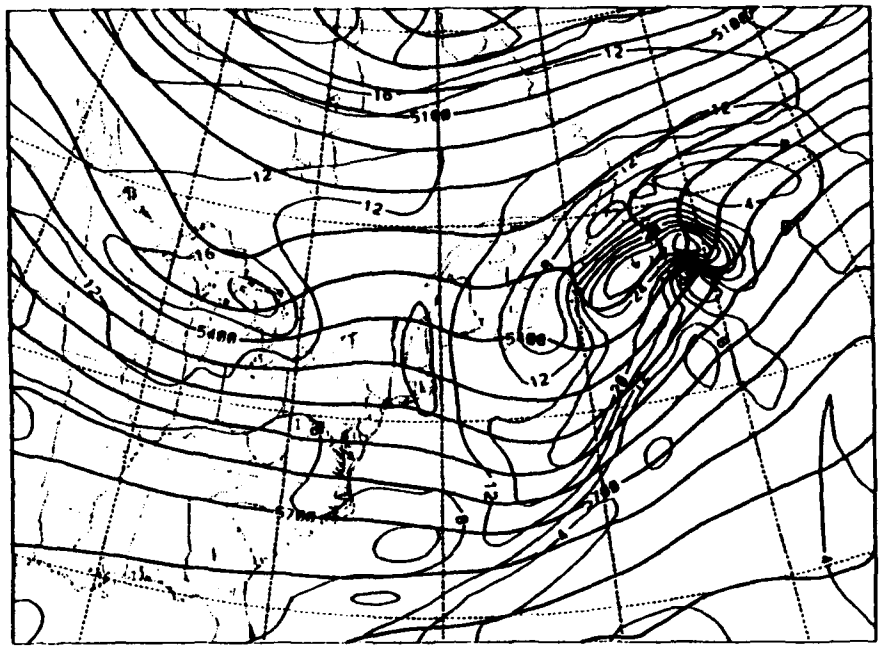

CASE 6 DRY, TAU 18-0600 UTC 7 JAN 1963-500 MB

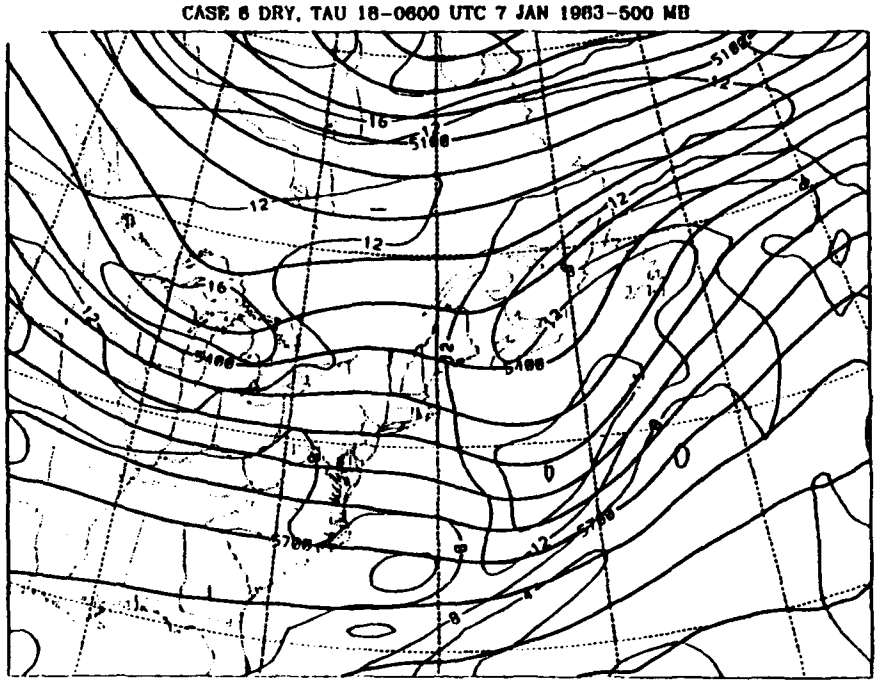

d.

a.

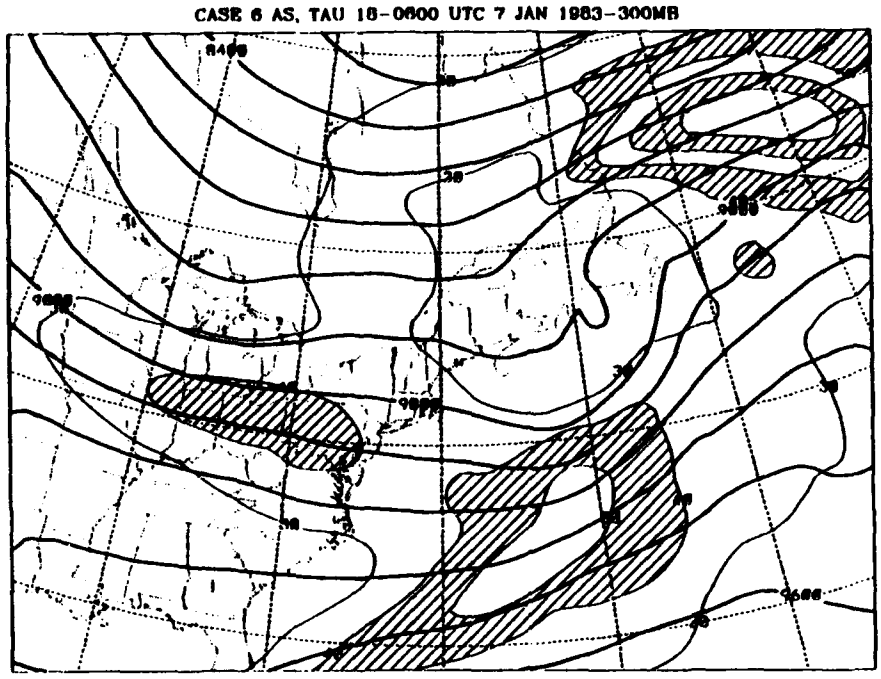

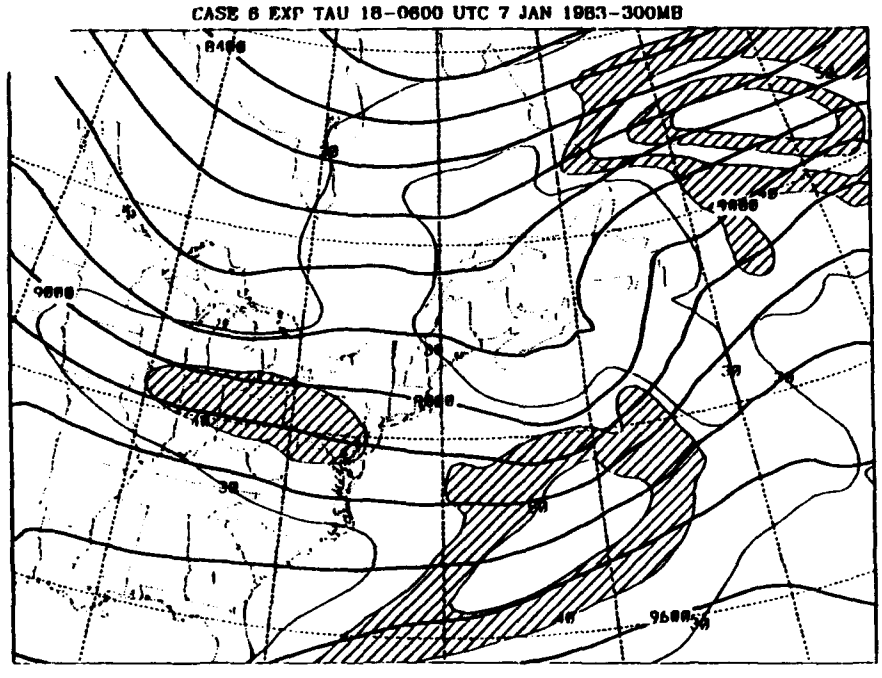

b.

FIG. 4.48. Same as Fig. 4.20 except for 0600 UTC 7 Jan 1983.

c.

CASE 6 KUO, TAU 18-0600 UTC 7 JAN 1983-300MB

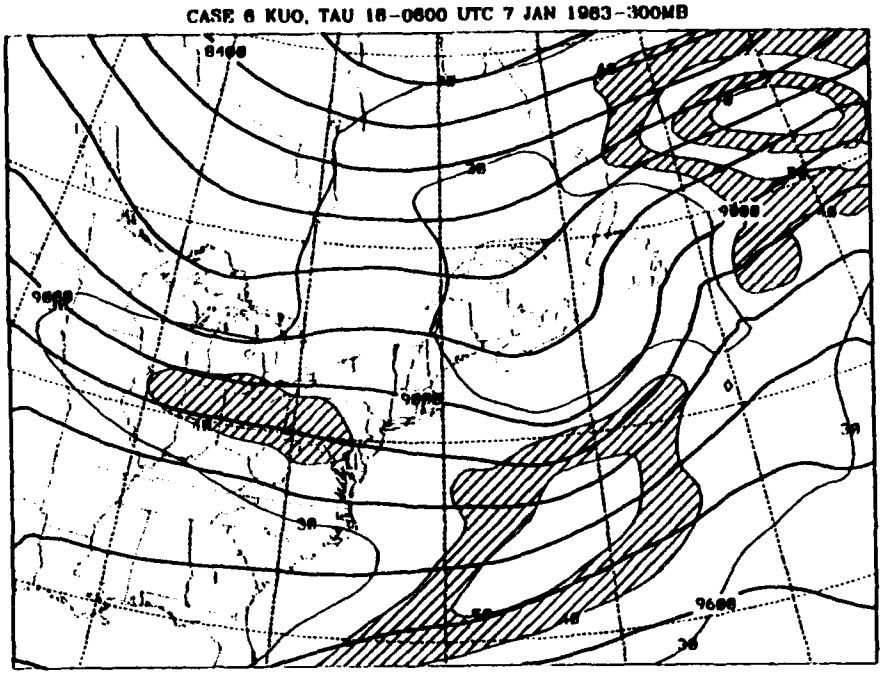

CASE 6 DRY TAU 18-0600 UTC 7 JAN 1983-300MB

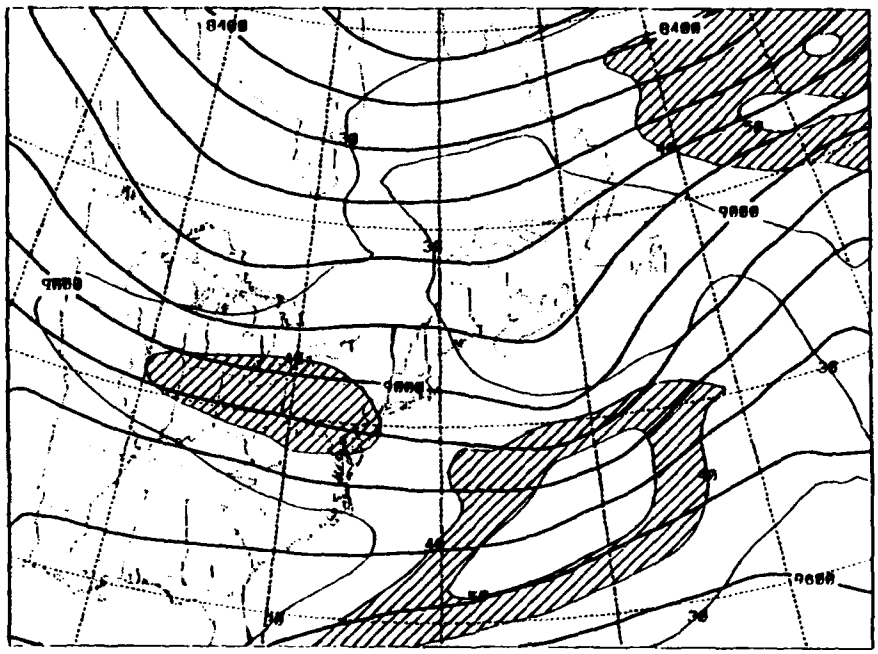

d.

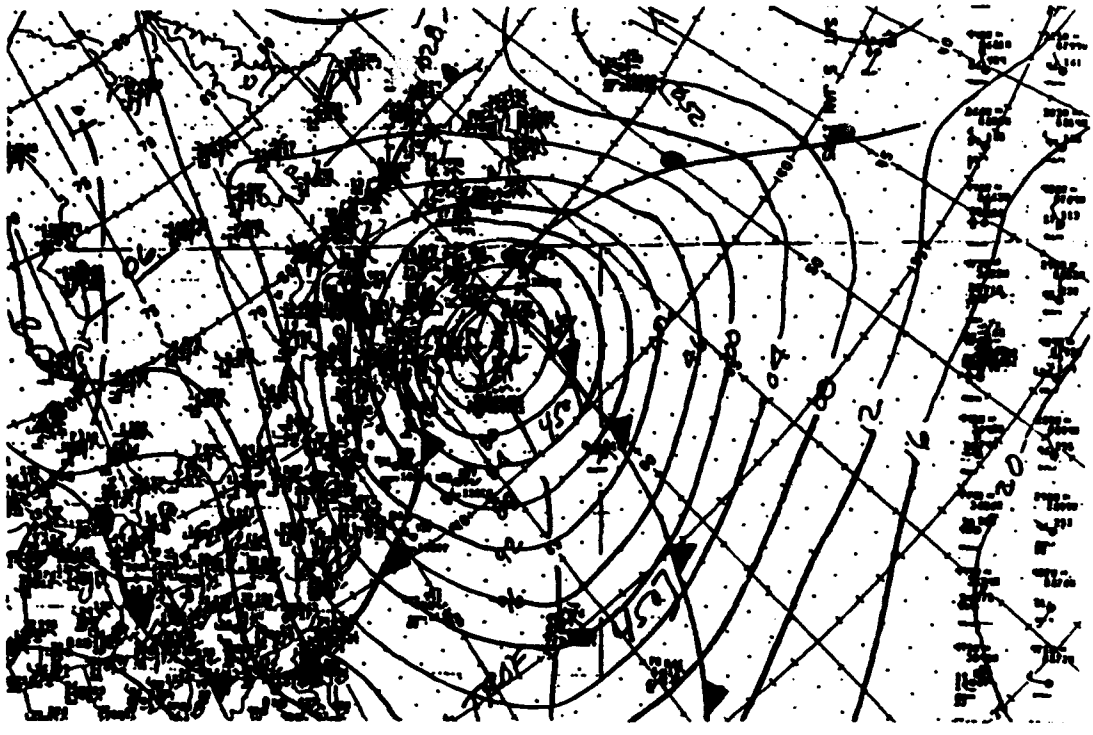

FIG 4.49. Same as Fig. 4.12 except for case 7 1800 UTC 5 Jan 1985.

a.

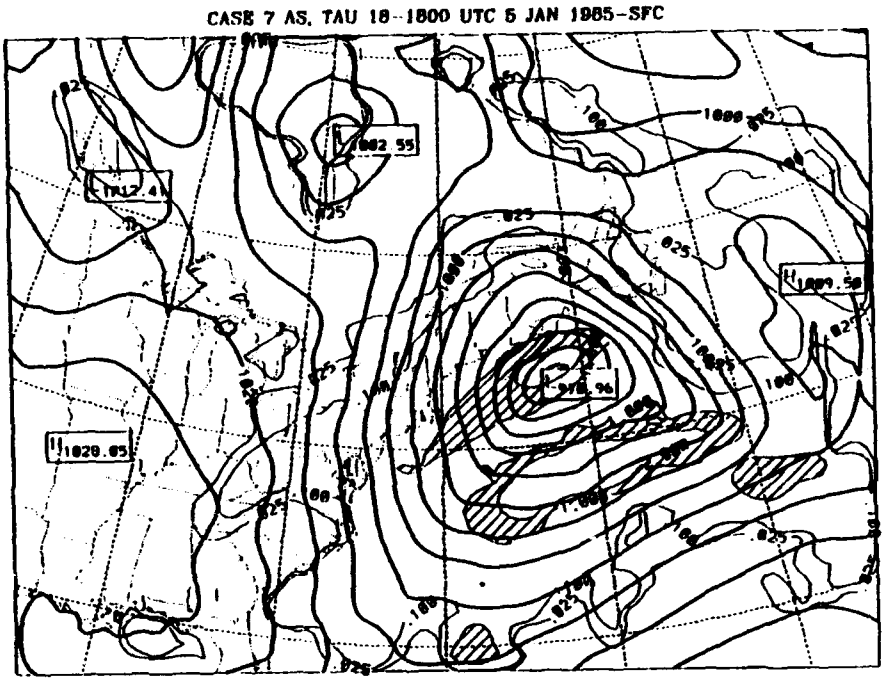

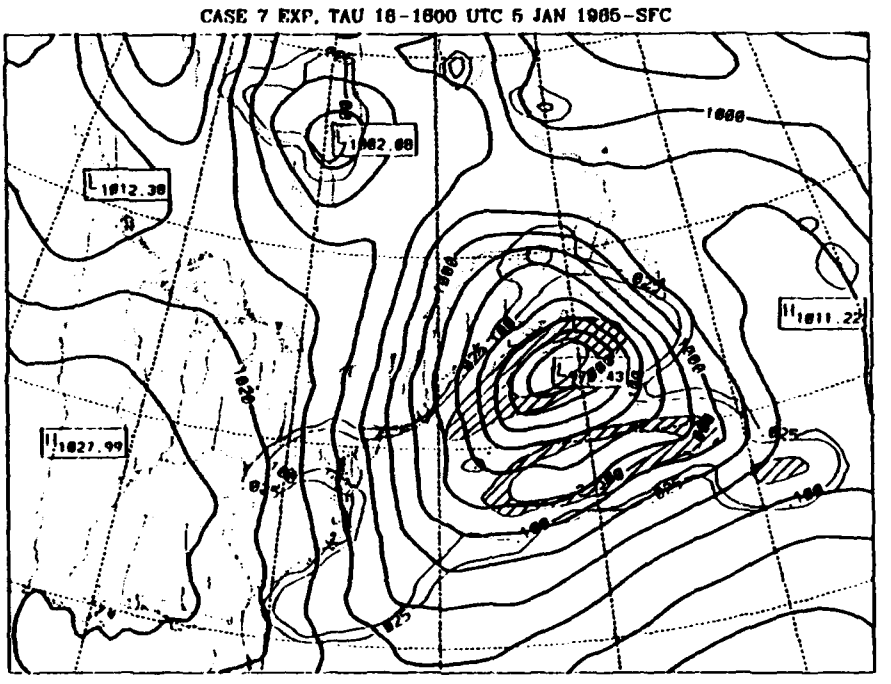

b.

FIG. 4.50. Same as Fig. 4.13 except for case 7, 1800 UTC 5 Jan 1985.

c.

CASE 7 KUO, TAU 18-1800 UTC 5 JAN 1985-SFC

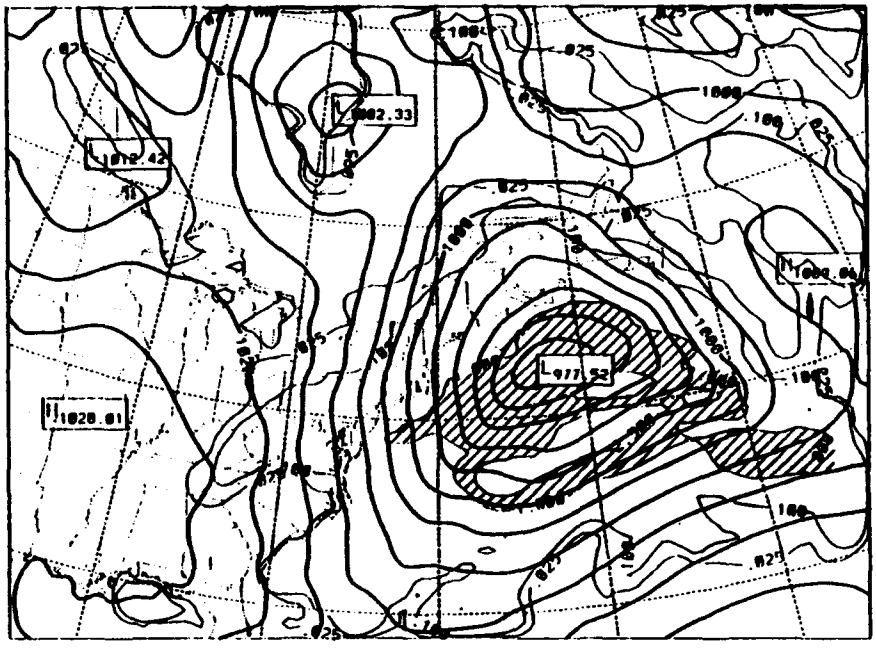

CASE 7 DRY, TAU 18-1800 UTC 5 JAN 1985-SFC

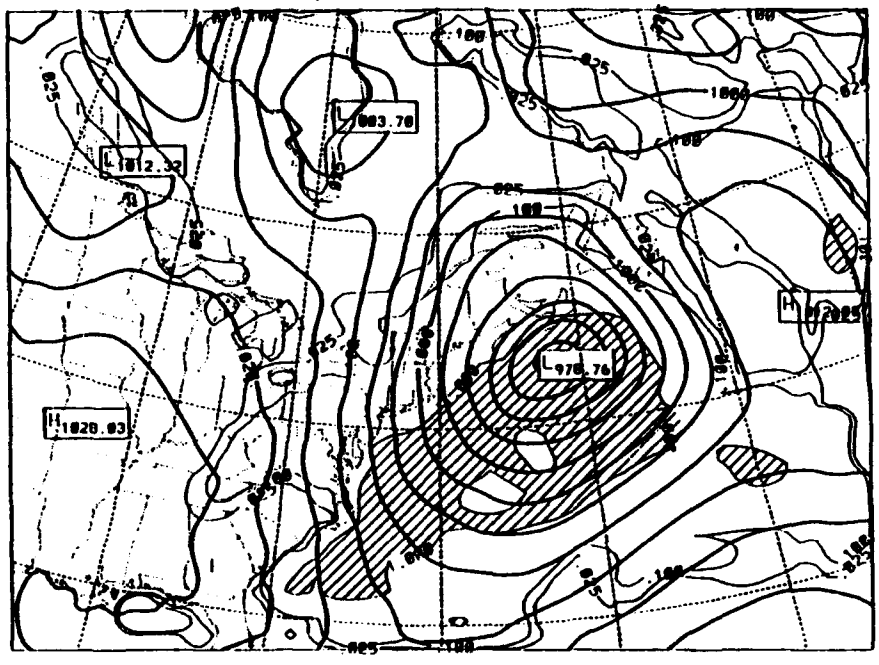

d.

a.

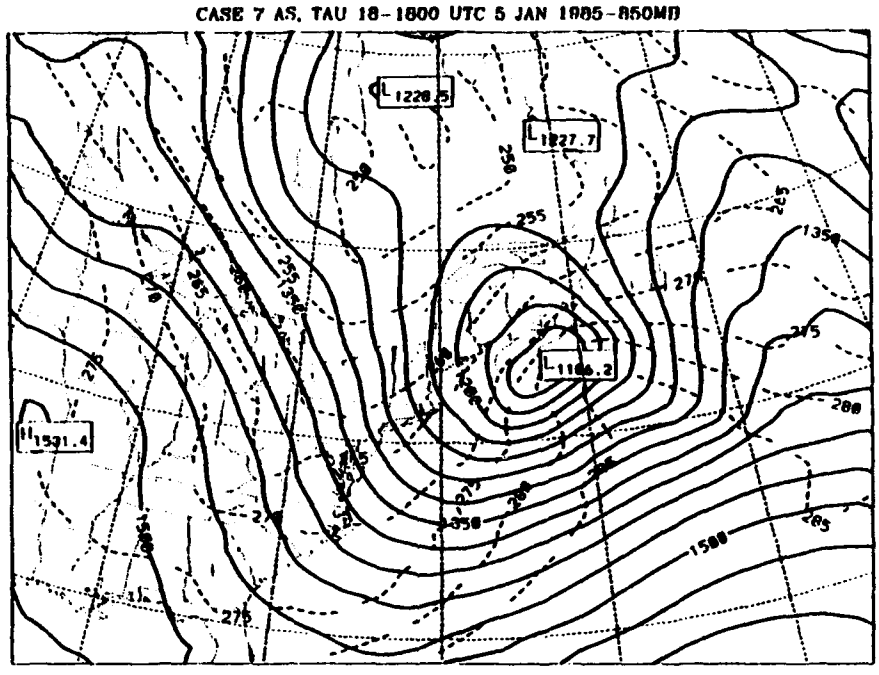

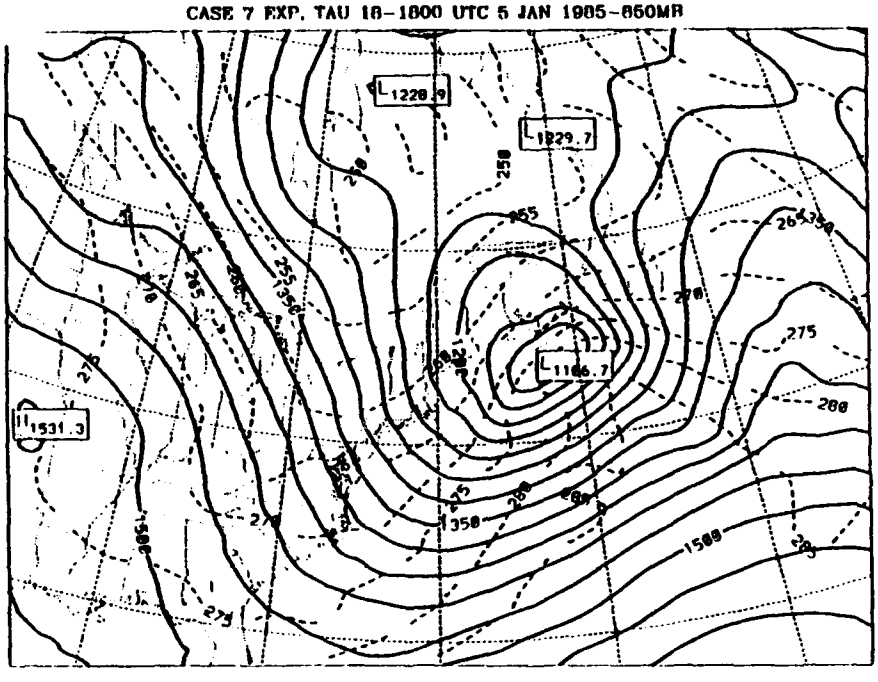

b.

FIG. 4.51. Same as Fig. 4.18 except for case 7, 1800 UTC 5 Jan 1985.

c.

CASE 7 KUO, TAU 18-1800 UTC 5 JAN 1985-850MB

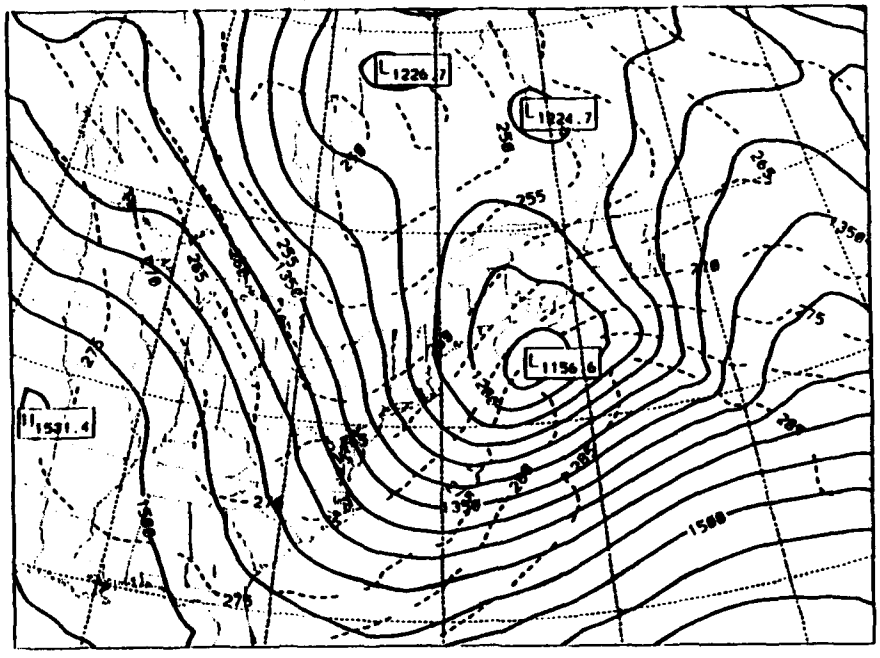

CASE 7 DRY, TAU 18-1800 UTC 5 JAN 1985-850MB

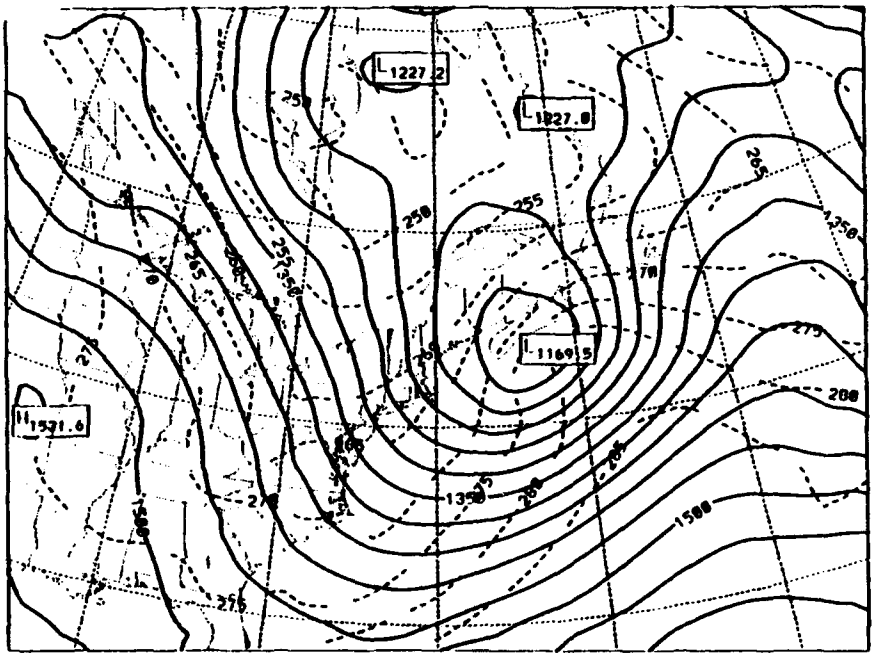

d.

a.

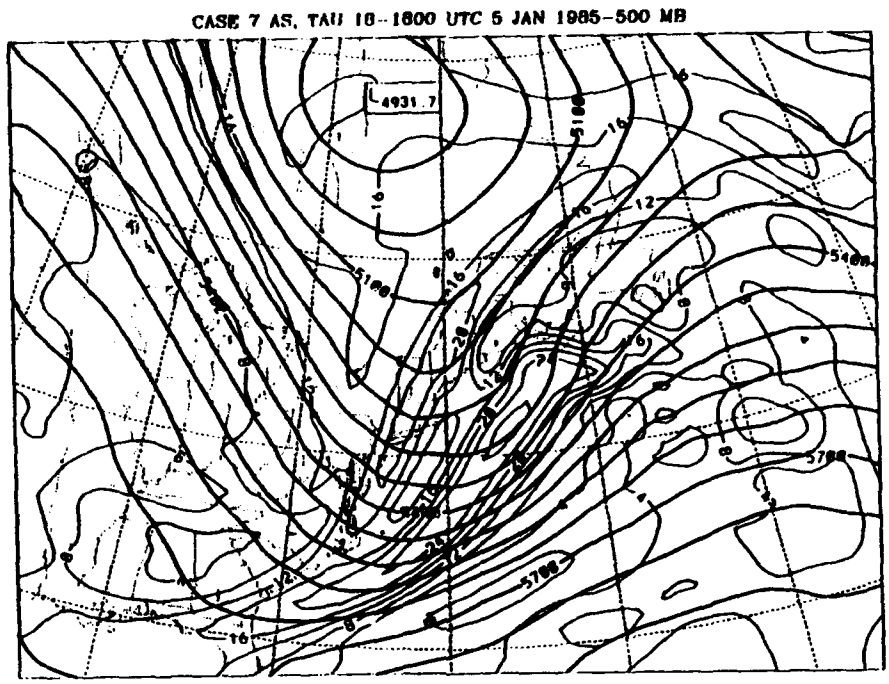

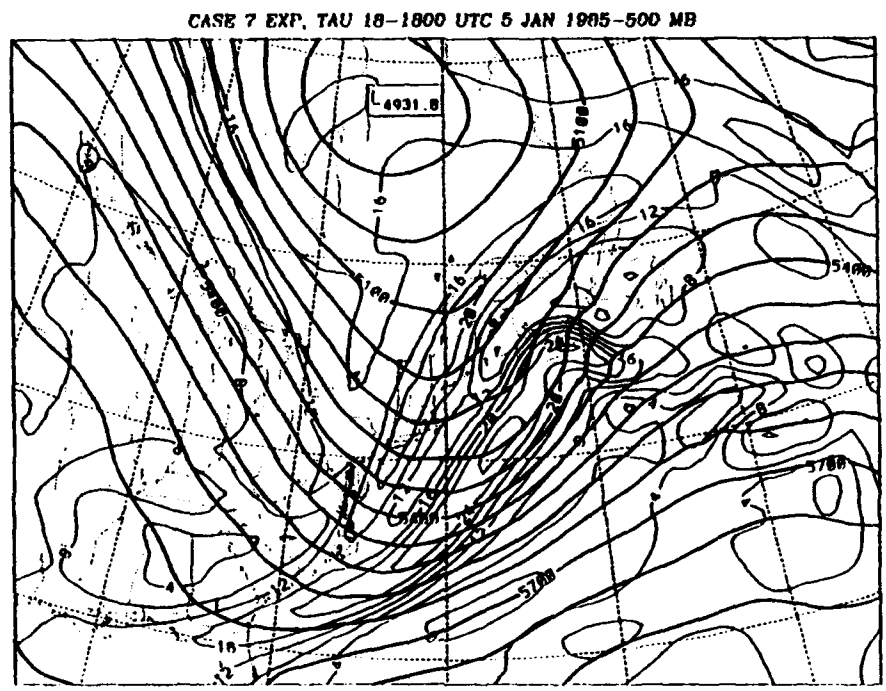

b.

FIG. 4.52. Same as Fig. 4.19 except for case 7, 1800 UTC 5 Jan 1985.

c.

CASE 7 KUO, TAU 18-1800 UTC 5 JAN 1985-500 MB

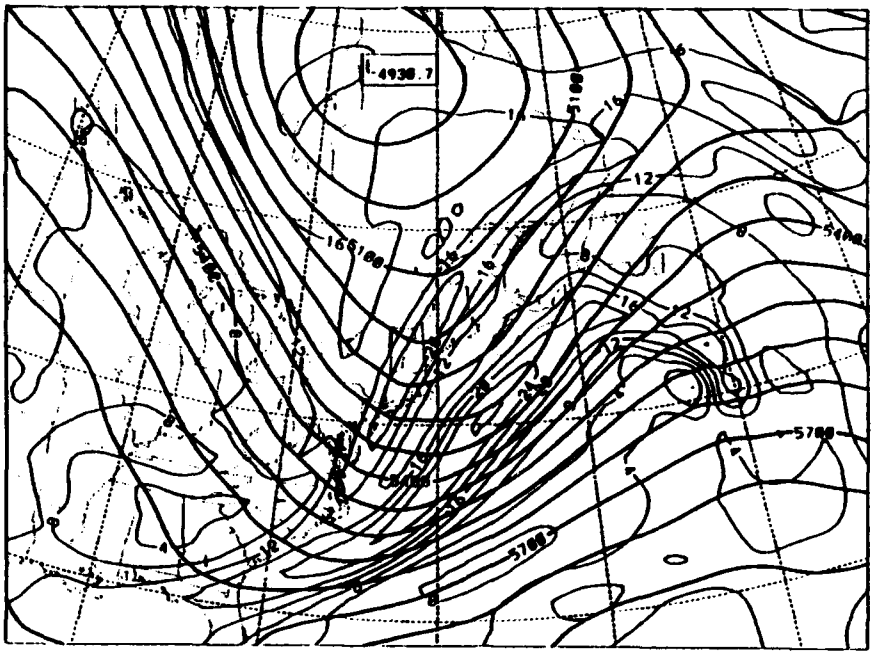

CASE 7 DRY, TAU 18-1800 UTC 5 JAN 1985-500 MB

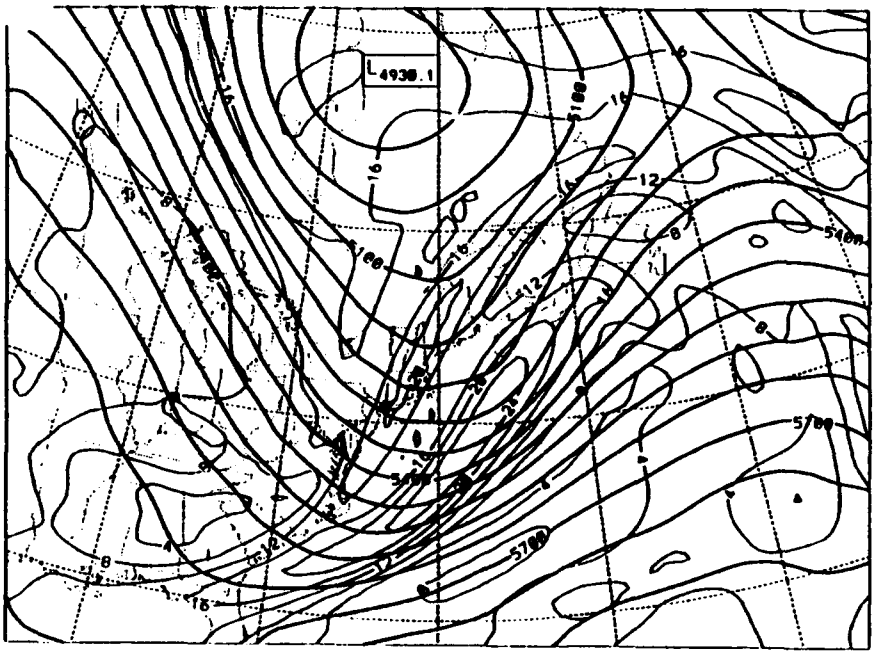

d.

a.

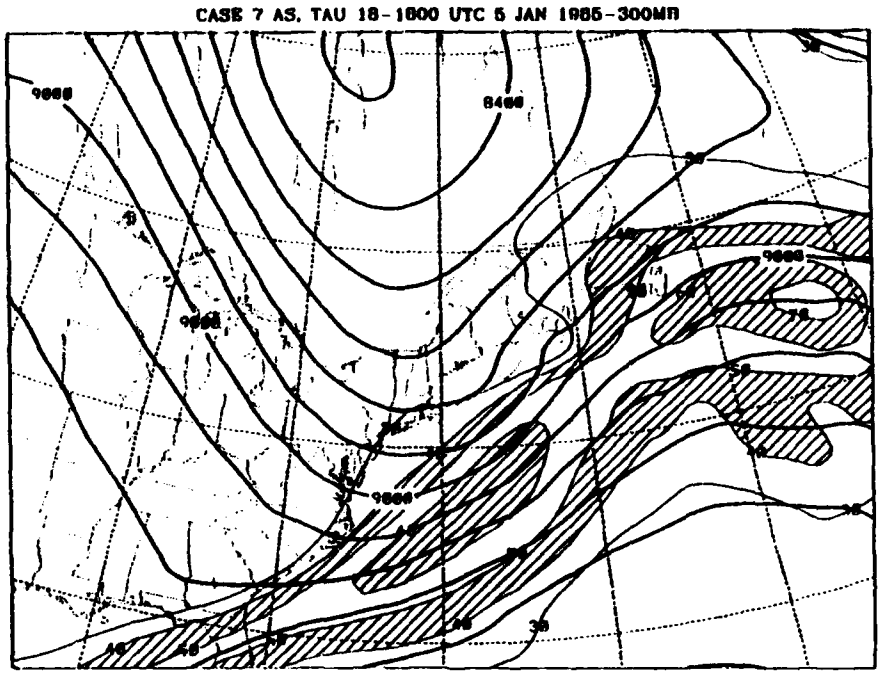

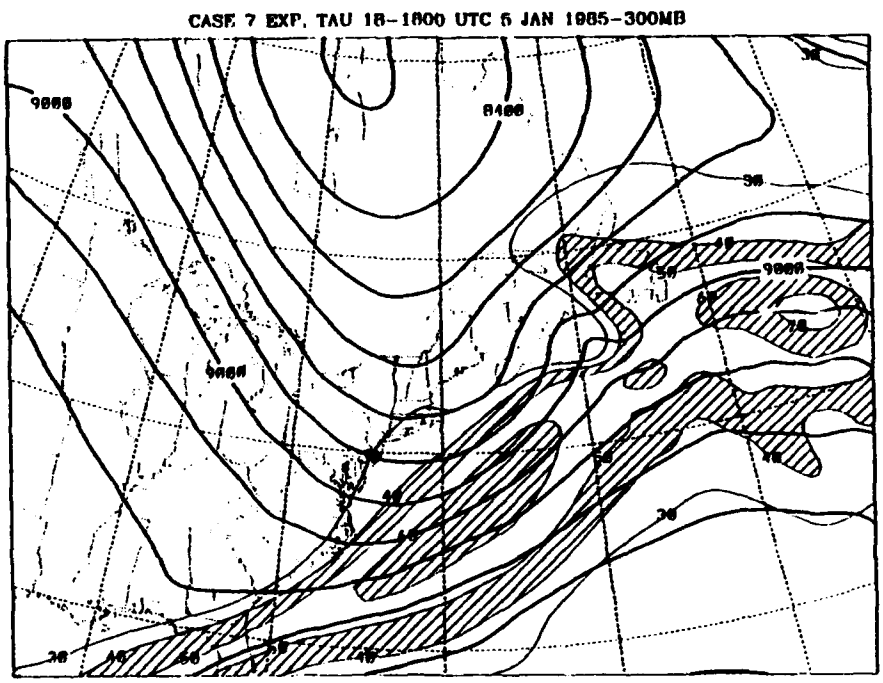

b.

FIG. 4.53. Same as Fig. 4.20 except for case 7, 1800 UTC 5 Jan 1985.

c.

CASE 7 KUO, TAU 18-1800 UTC 5 JAN 1985-300MB

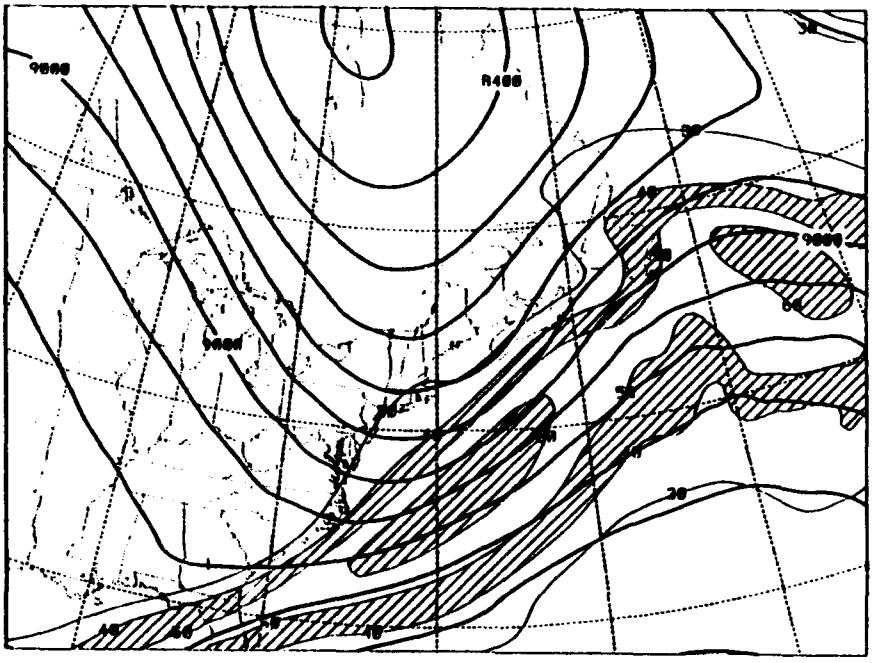

CASE 7 DRY TAU 18-1800 UTC 5 JAN 1985-300MB

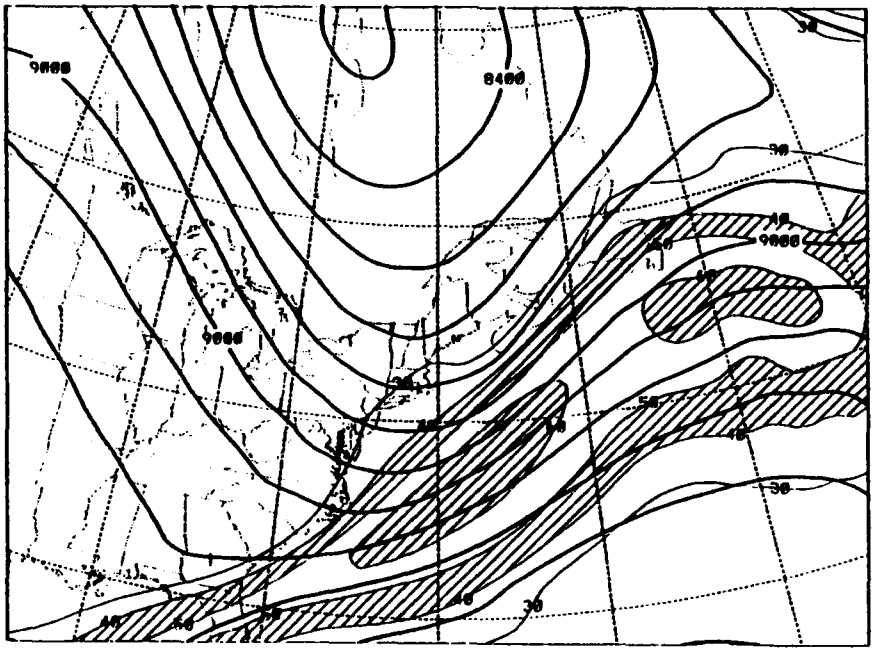

d.

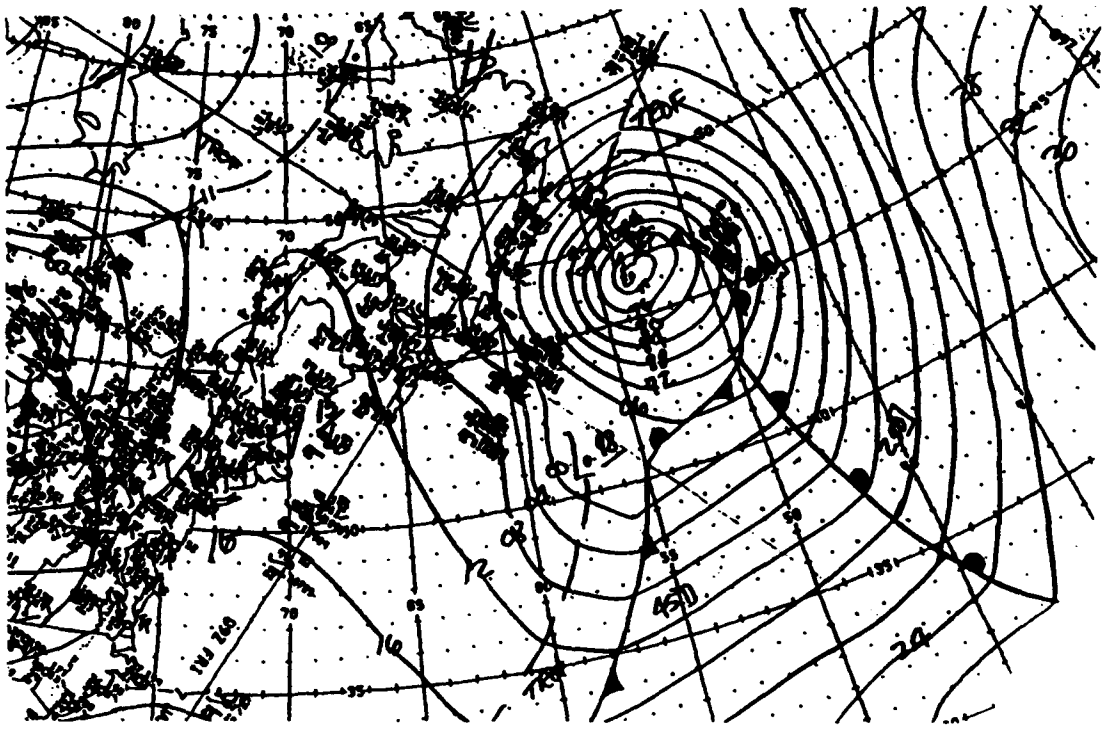

FIG. 4.54. Same as Fig. 4.12 except for 0900 UTC 7 Jan 1983.

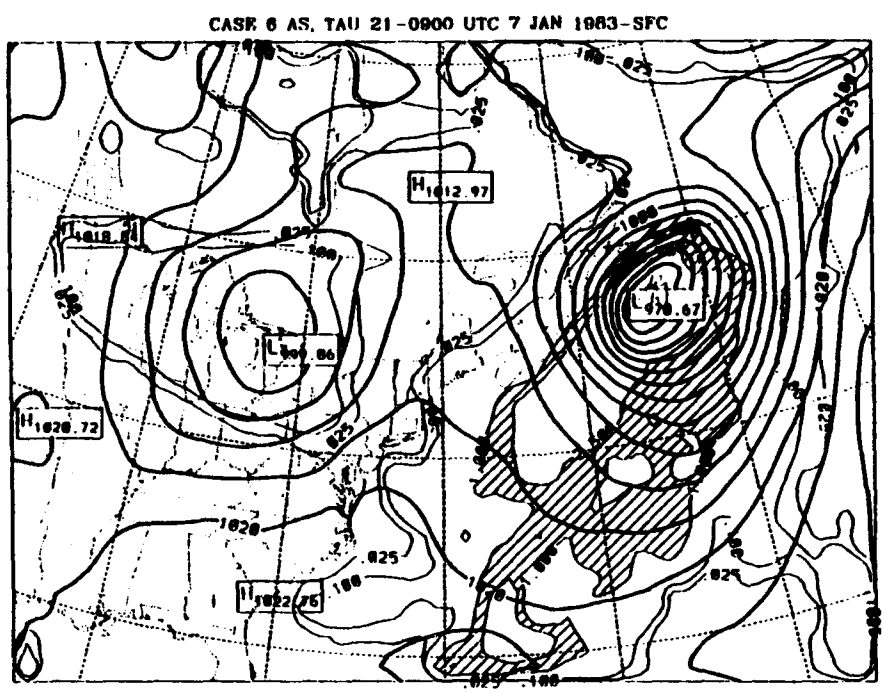

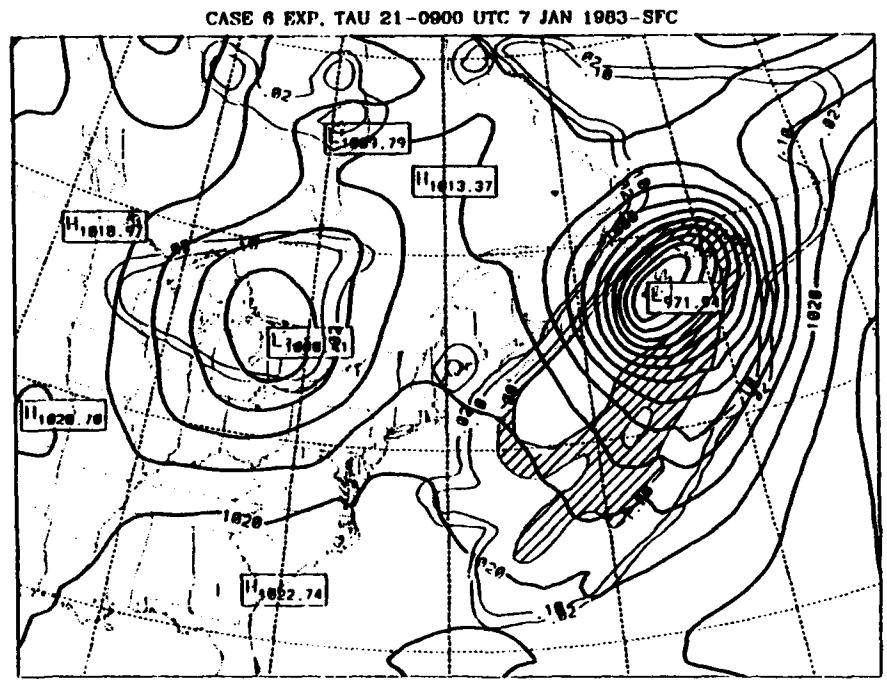

FIG. 4.41. Same as Fig. 4.13 except for 0900 UTC 7 Jan 1983.

c.

CASE 6 KUO, TAU 21-0900 UTC 7 JAN 1983-SFC

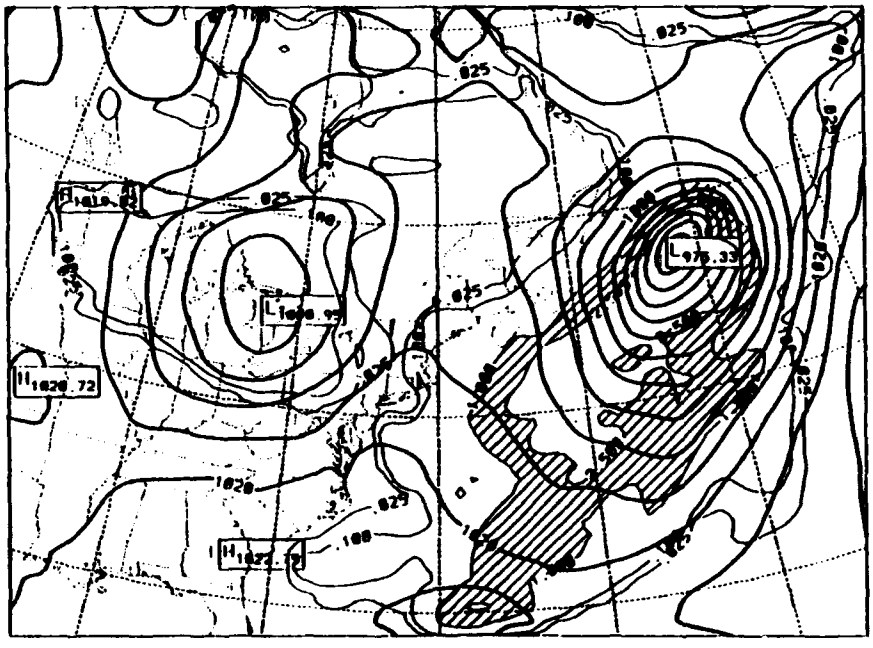

CASE 6 DRY, TAU 21-0900 UTC 7 JAN 1983-SFC

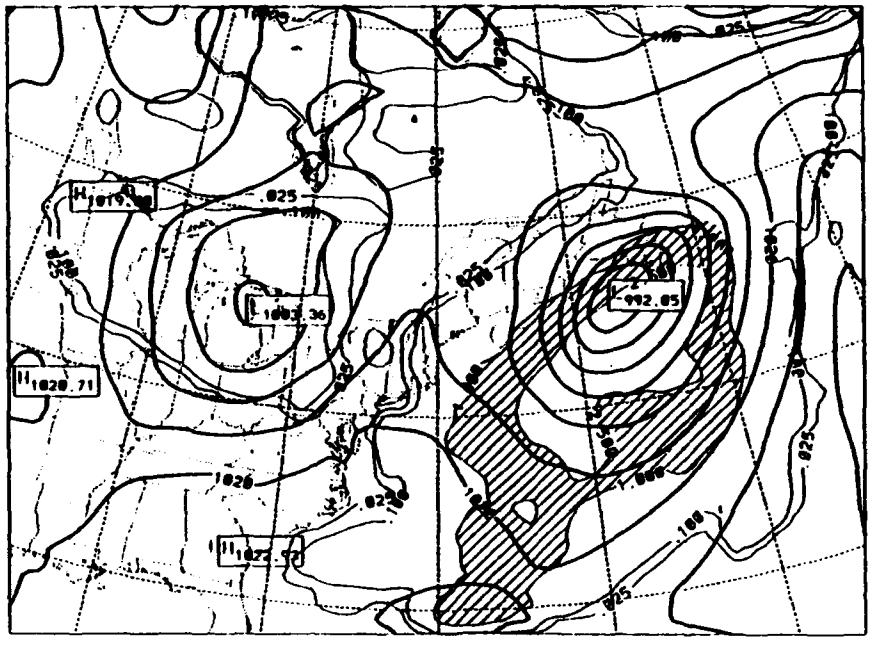

d.

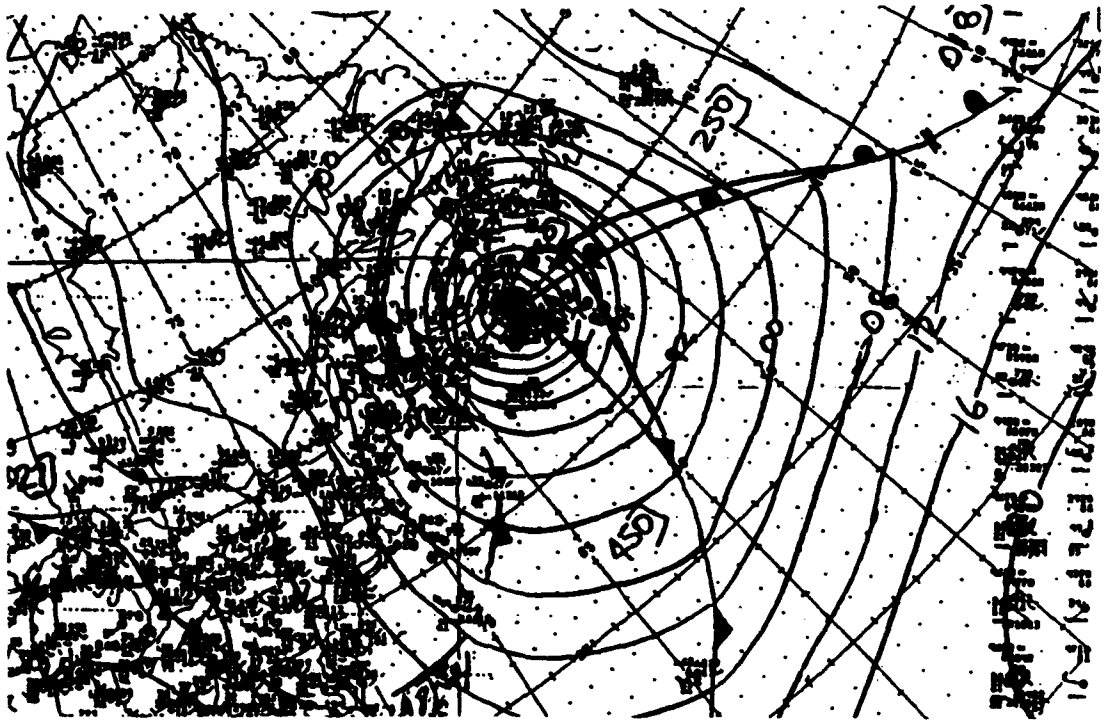

FIG 4.56. Same as Fig. 4.12 except for case 7, 2100 UTC 5 Jan 1985.

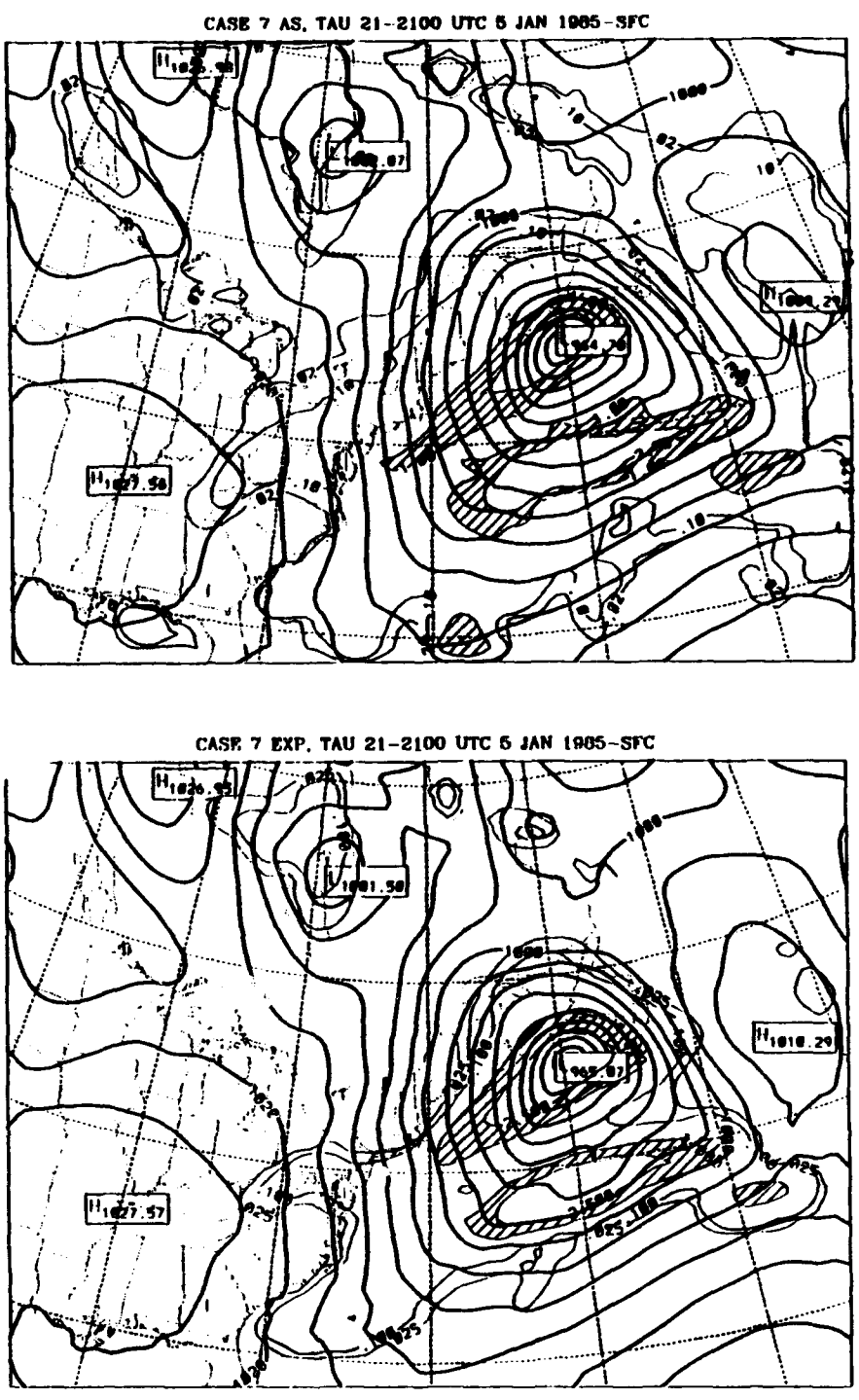

FIG. 4.57. Same as Fig. 4.13 except for case 7, 2100 UTC 5 Jan 1985.

c.

CASE 7 KUO, TAU 21-2100 UTC 5 JAN 1985-SFC

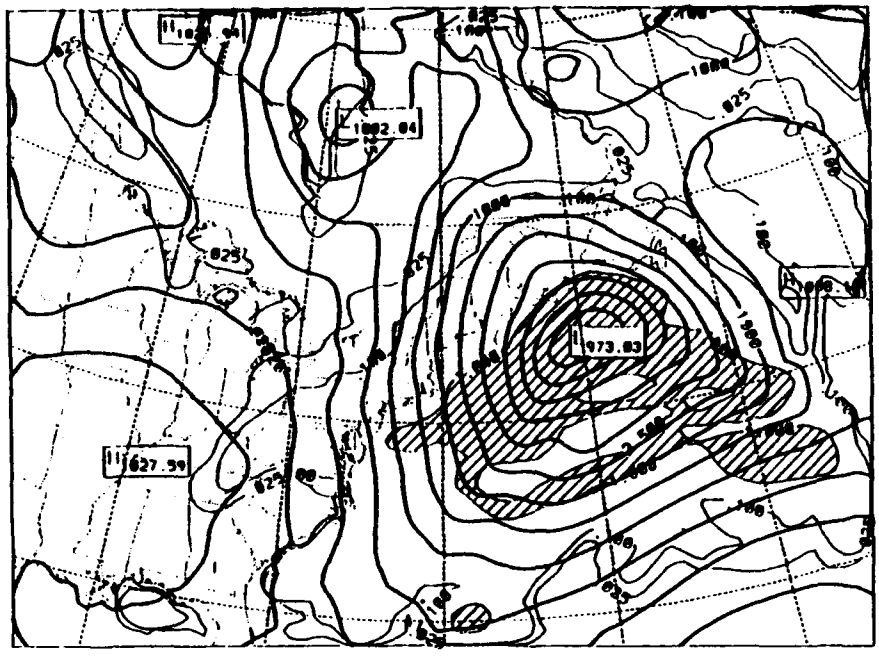

CASE 7 DRY, TAU 21-2100 UTC 5 JAN 1985-SFC

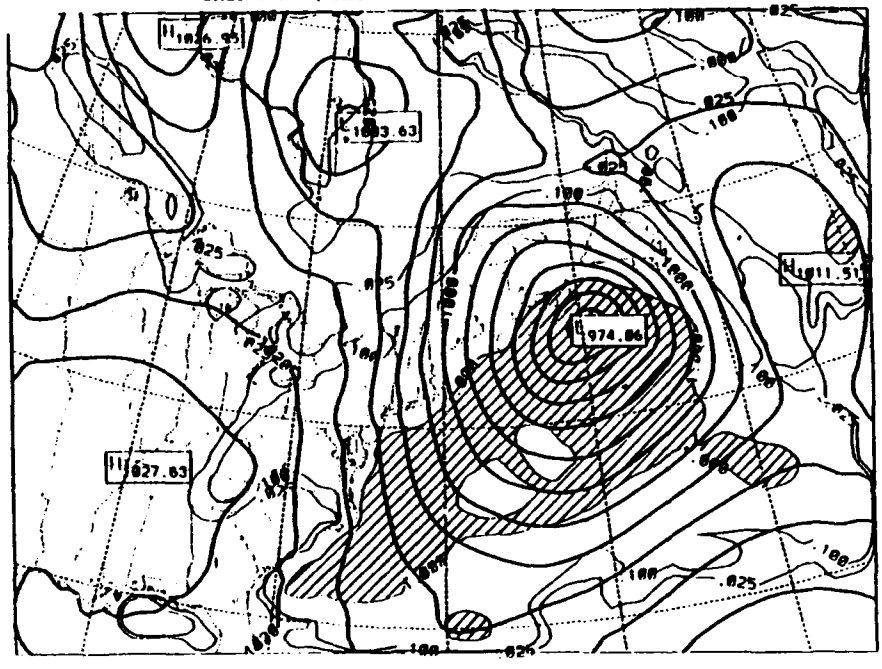

d.

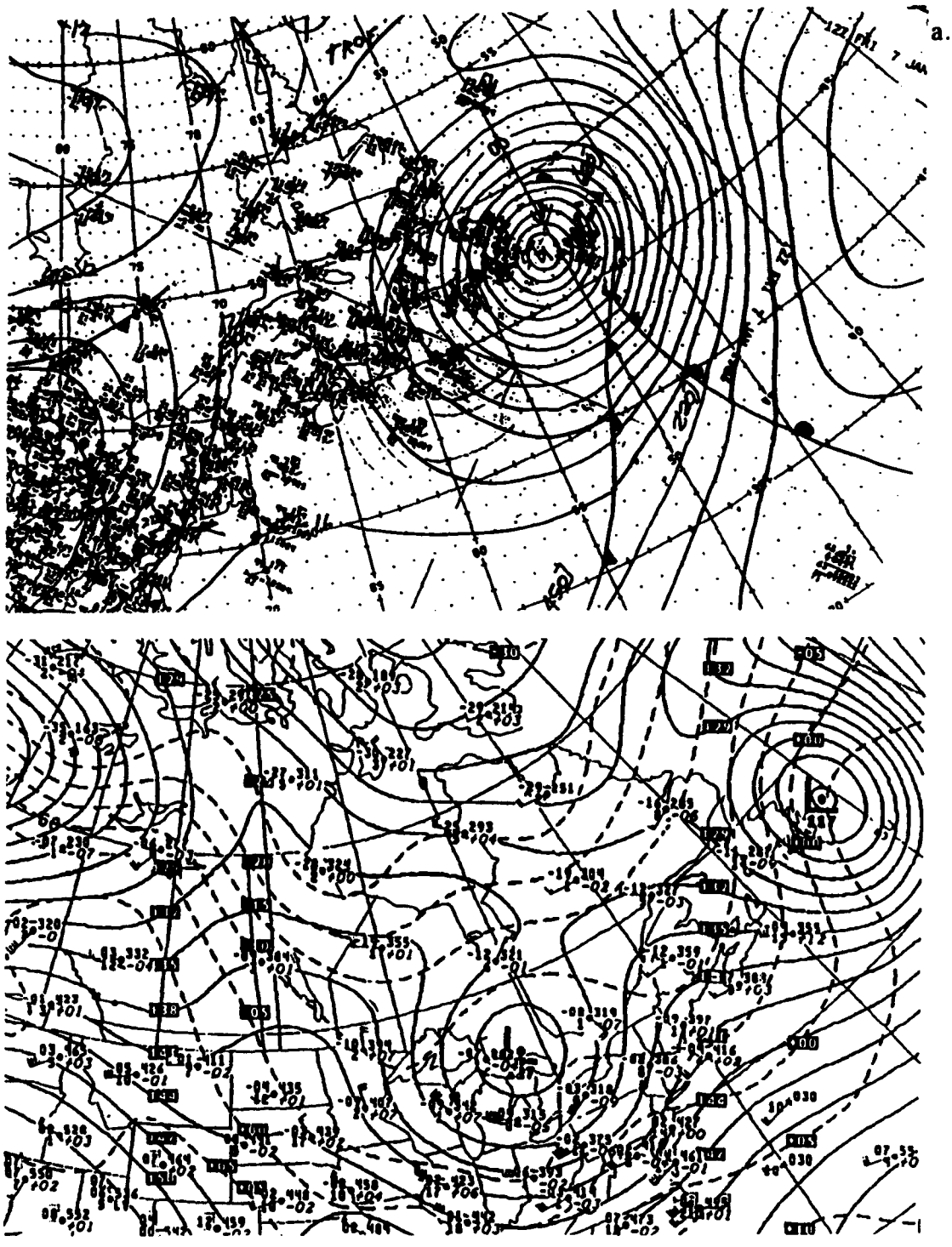

FIG. 4.58. Same as Fig. 4.8 except for 1200 UTC 7 Jan 1983.

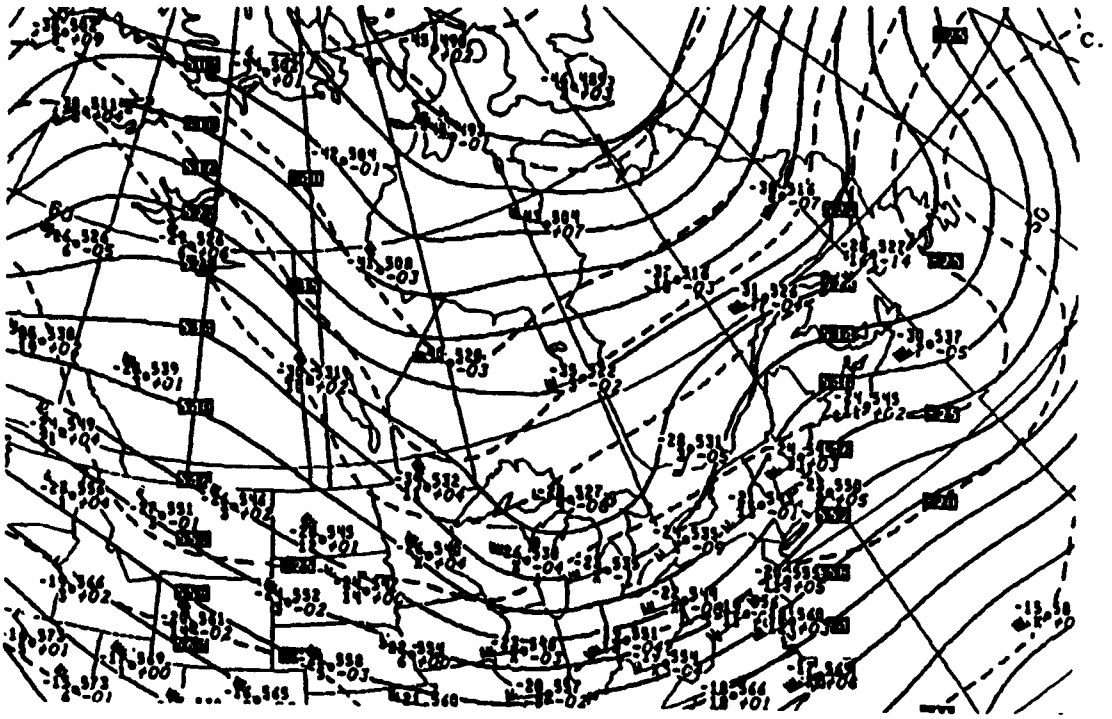

c.

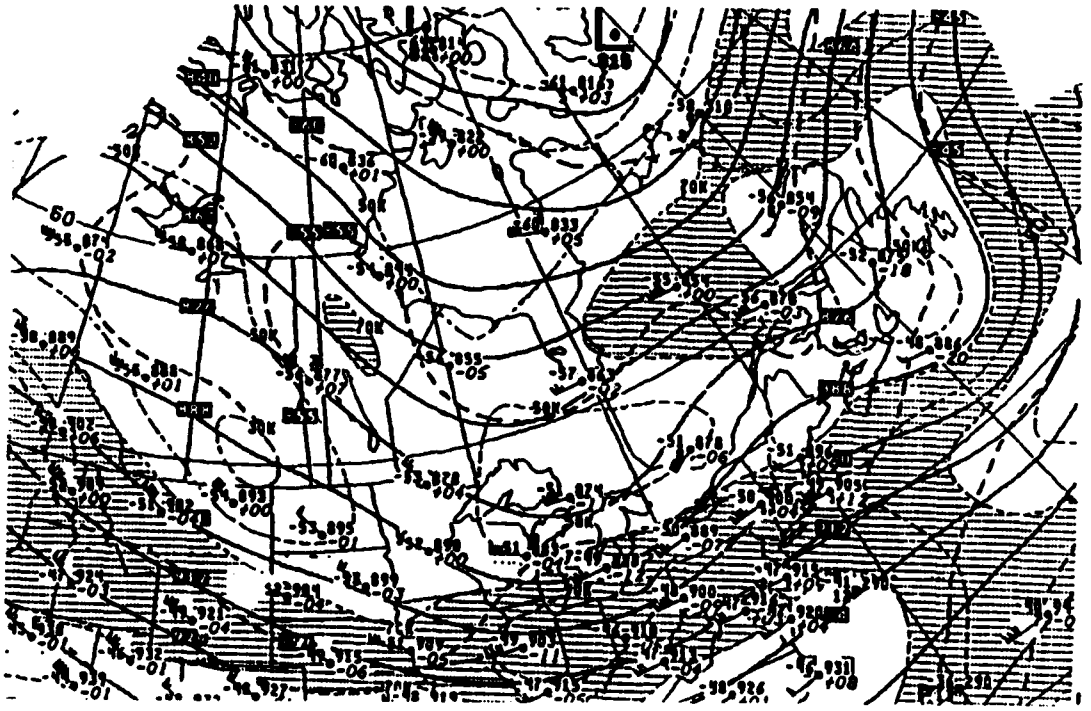

d.

a.

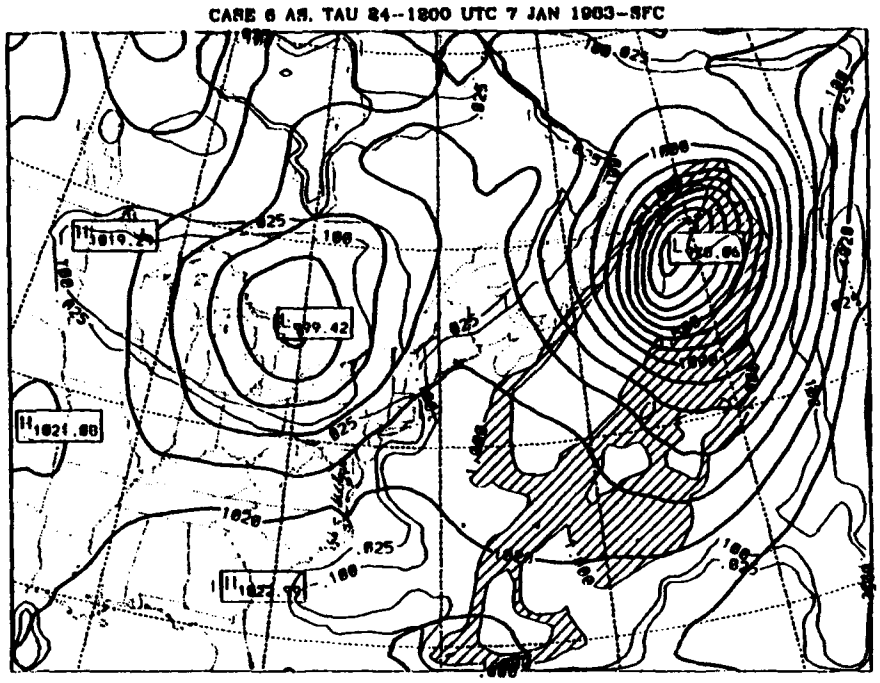

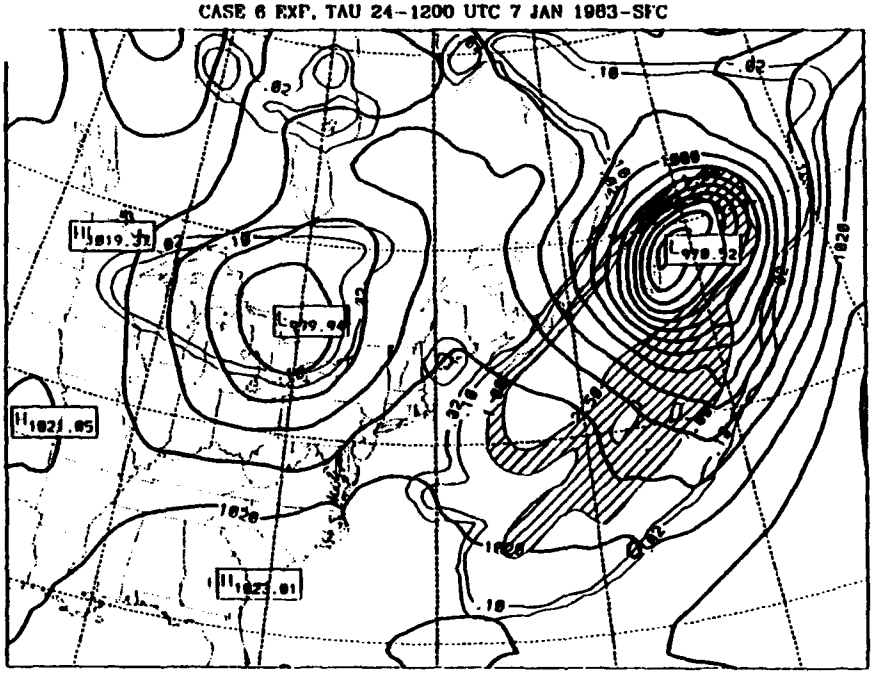

b.

FIG. 4.59. Same as Fig. 4.13 except for 1200 UTC 7 Jan 1983.

c.

CASE 6 KUO, TAU 24--1200 UTC 7 JAN 1983-SFC

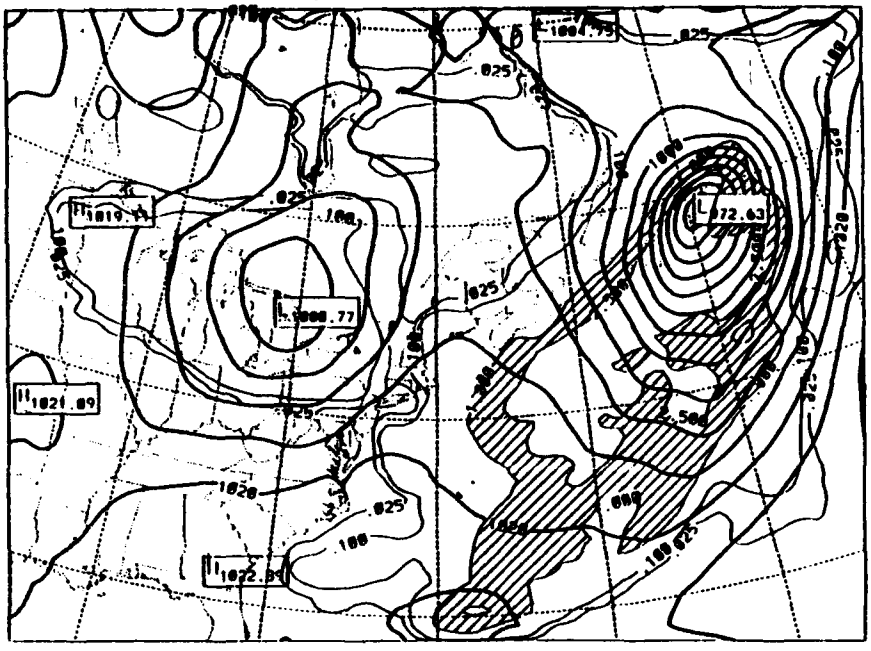

CASE 6 DRY, TAU 24-1200 UTC 7 JAN 1983-SFC

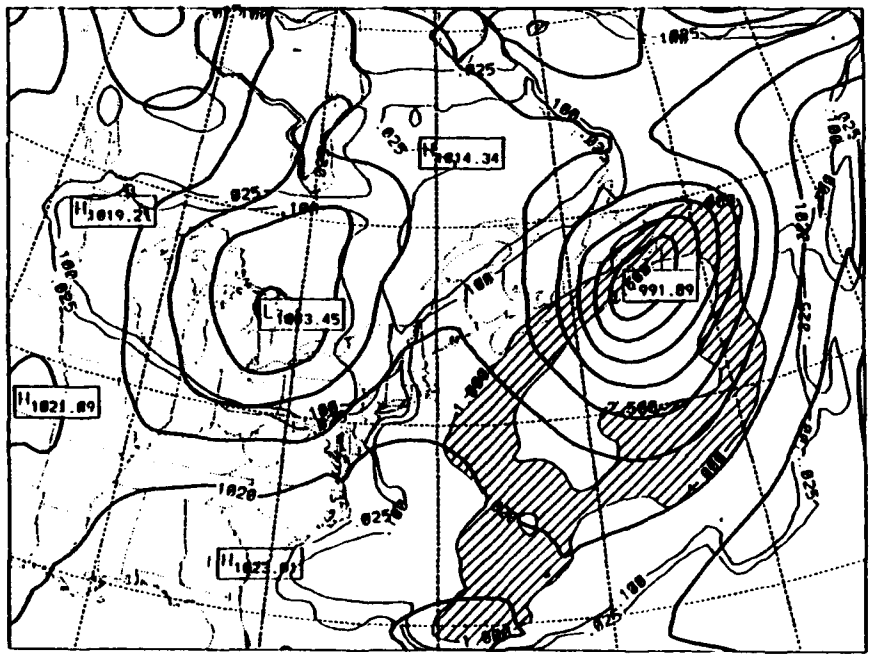

d.

a.

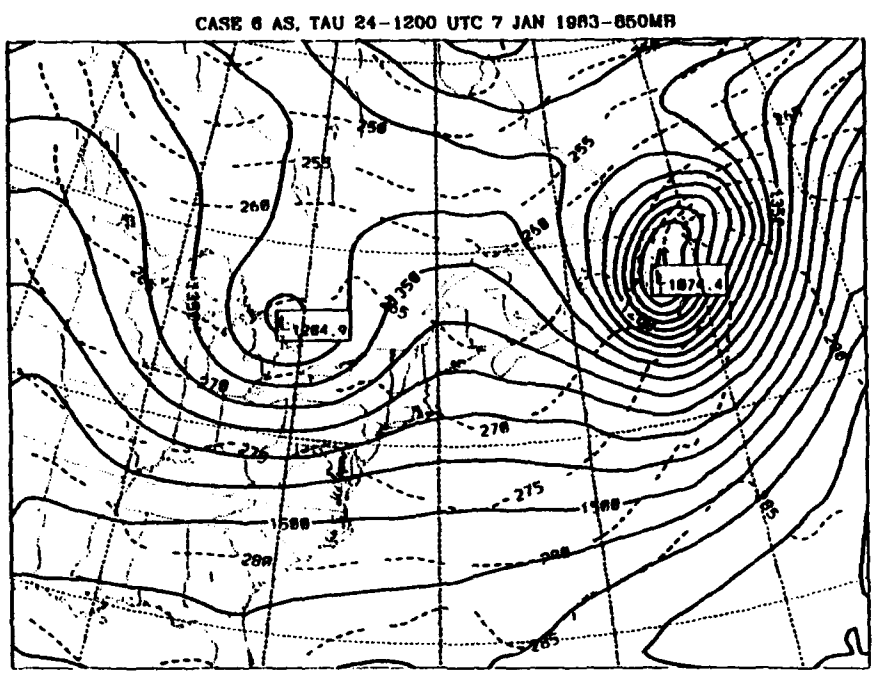

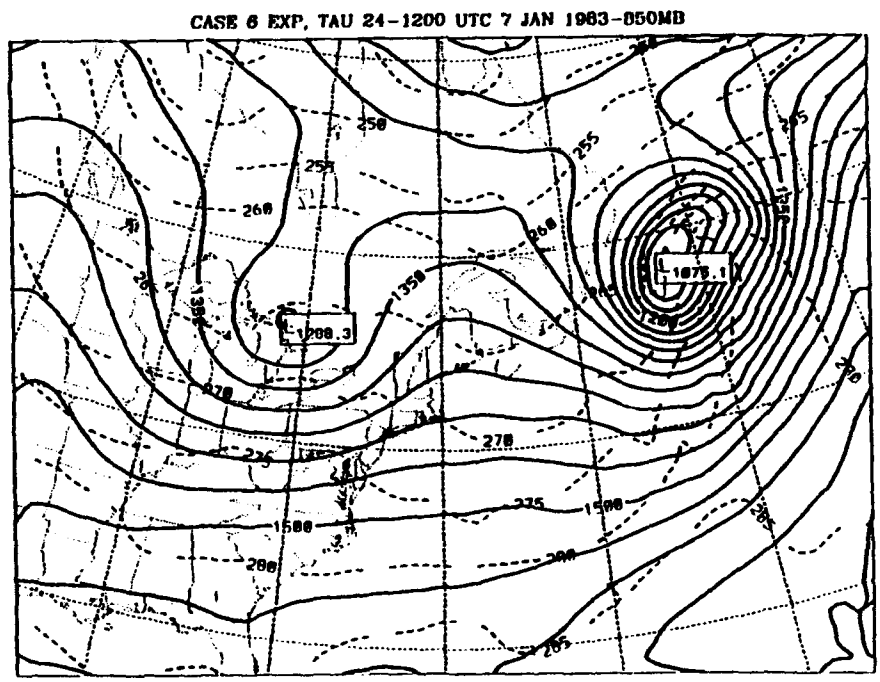

b.

FIG. 4.60. Same as Fig. 4.18 except for 1200 UTC 7 Jan 1983.

c.

CASE 6 KUO, TAU 24-1200 UTC 7 JAN 1983-850MB

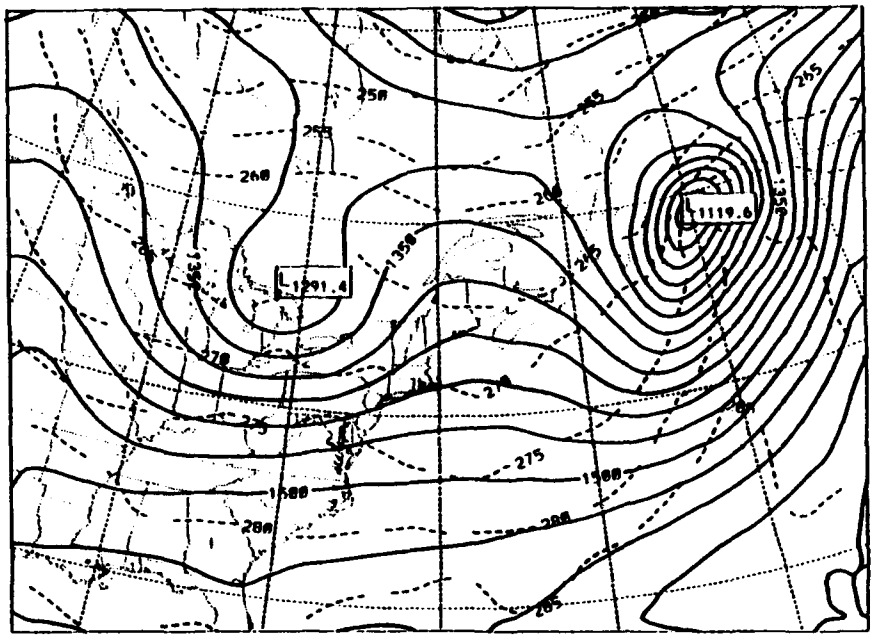

CASE 6 DRY, TAU 24-1200 UTC 7 JAN 1983-850MB

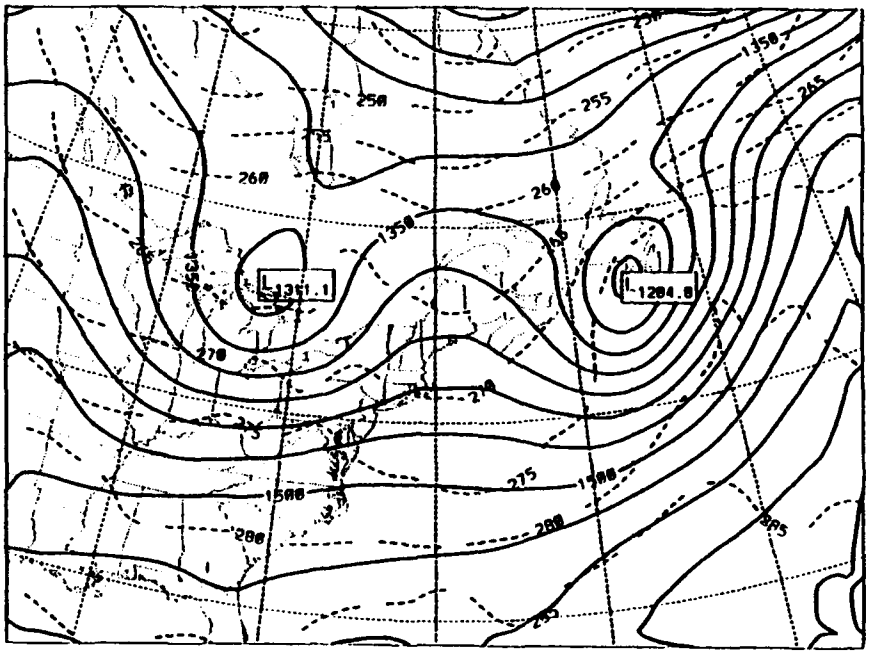

d.

a.

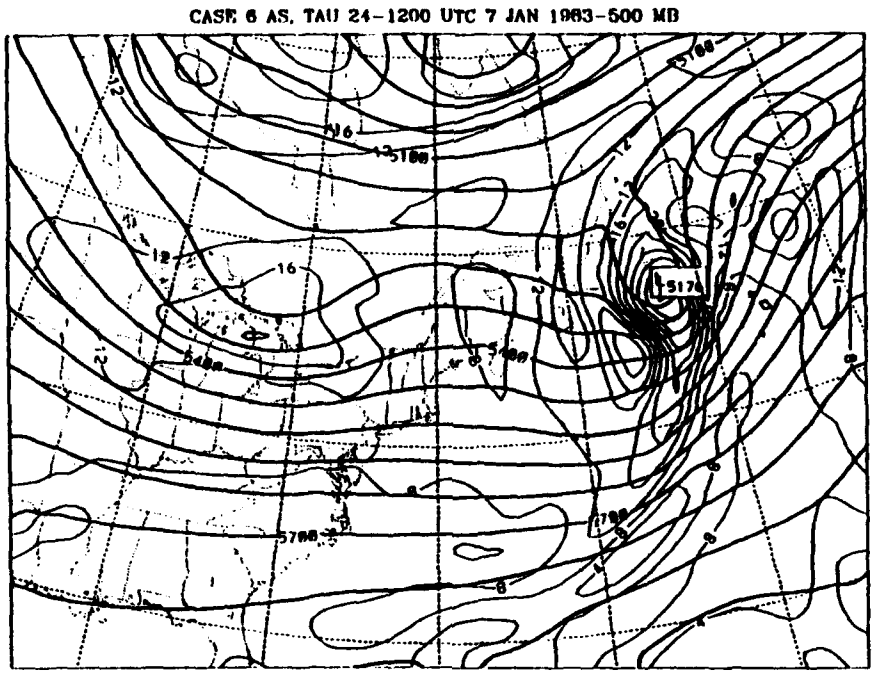

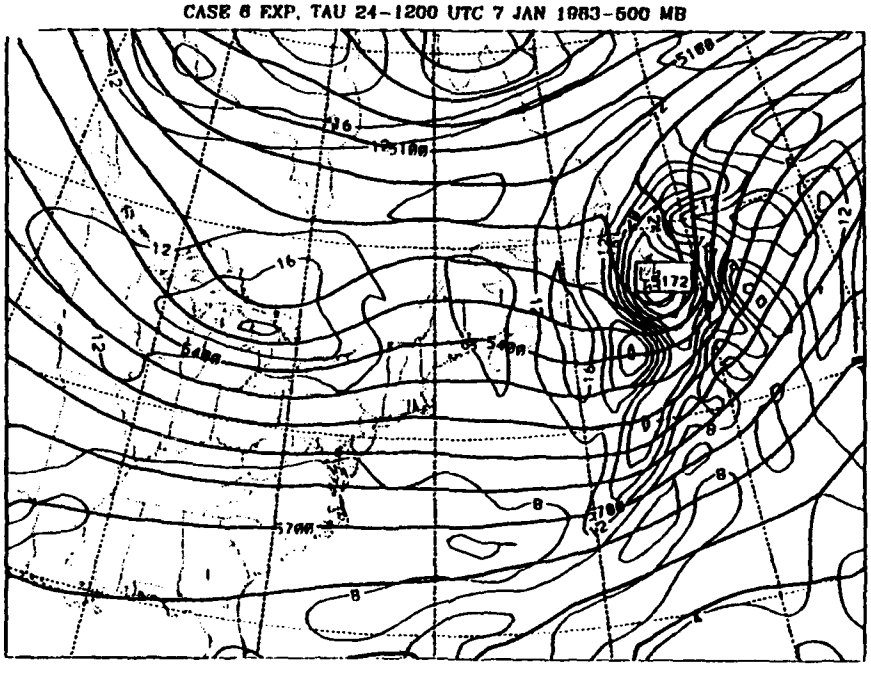

b.

FIG. 4.61. Same as Fig. 4.19 except for 1200 UTC 7 Jan 1983.

c.

CASE 6 KUO, TAU 24-1200 UTC 7 JAN 1983-500 MB

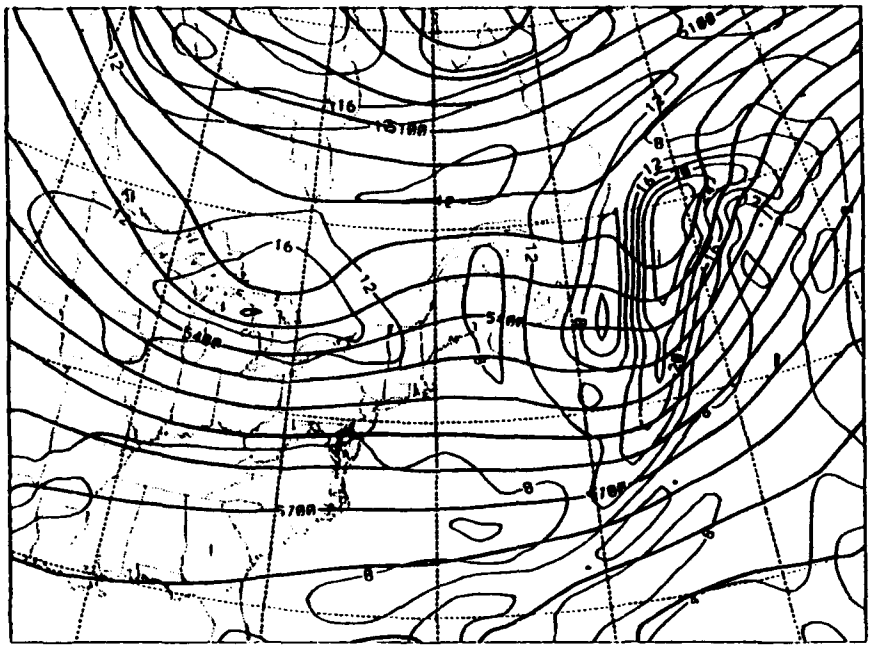

CASE 6 DRY, TAU 24-1200 UTC 7 JAN 1983-500 MB

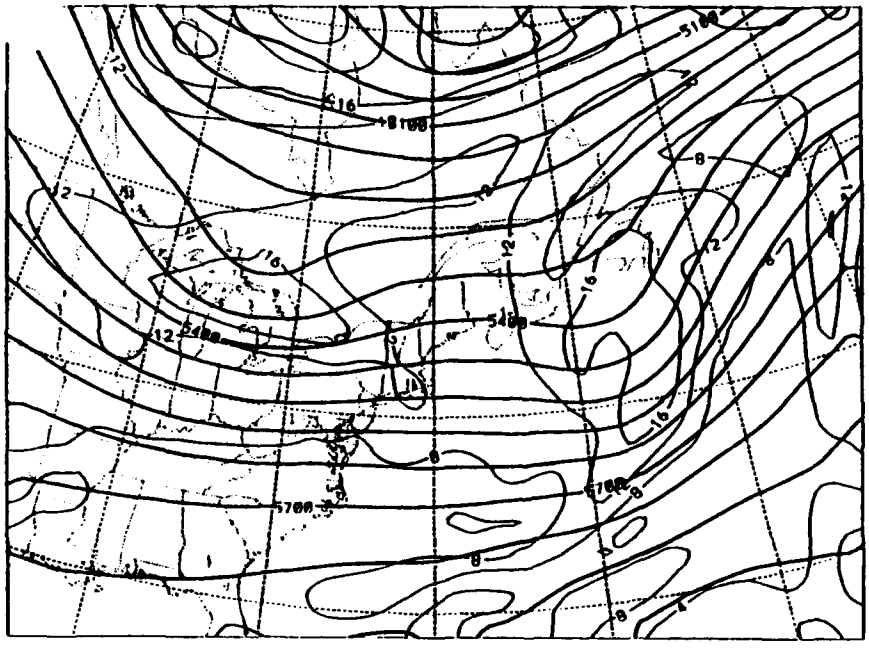

d.

a.

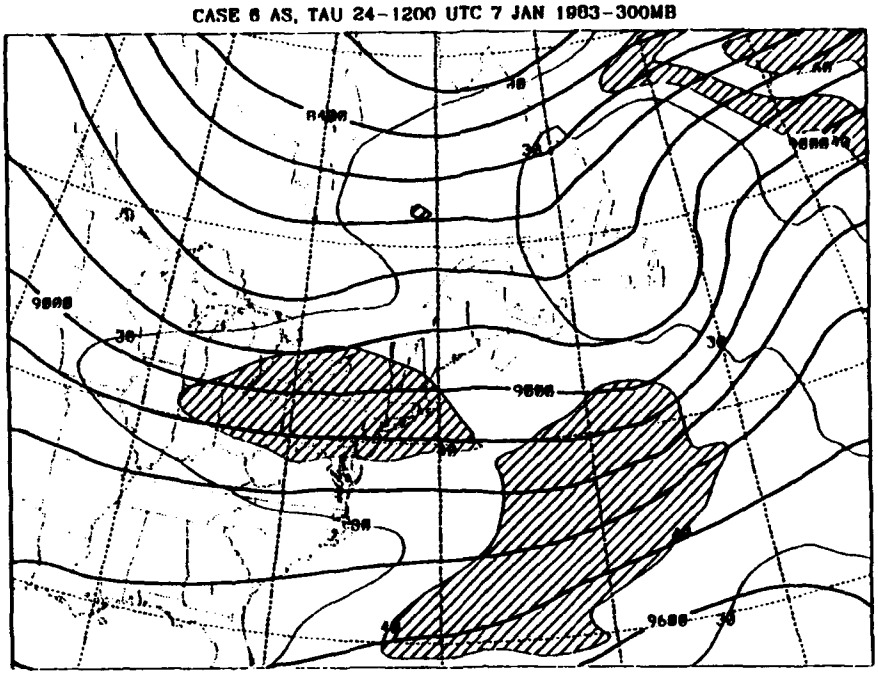

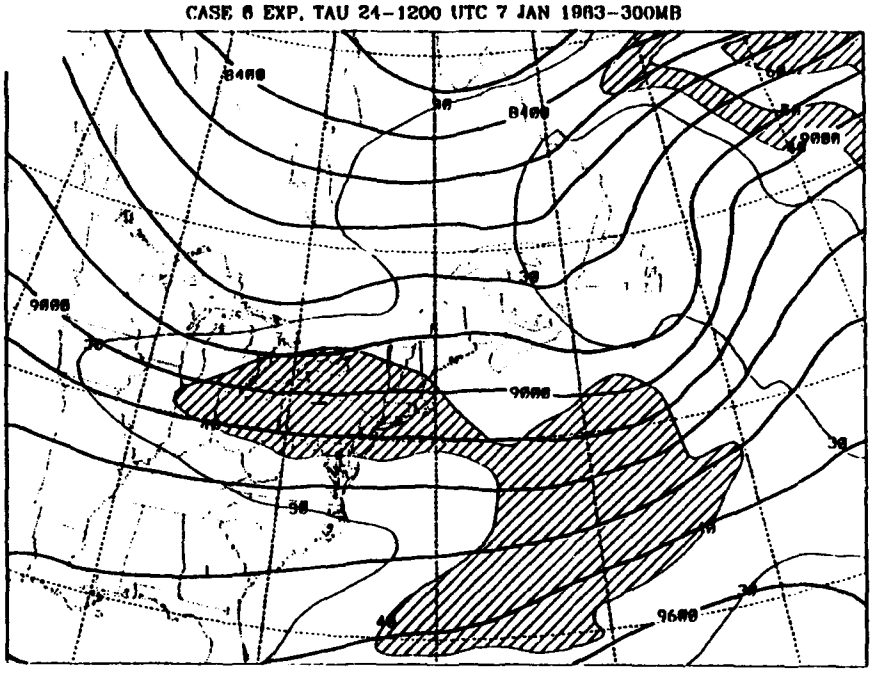

b.

FIG. 4.62. Same as Fig. 4.20 except for 1200 UTC 7 Jan 1983.

c.

CASE 6 KUO, TAU 24-1200 UTC 7 JAN 1983 300MB

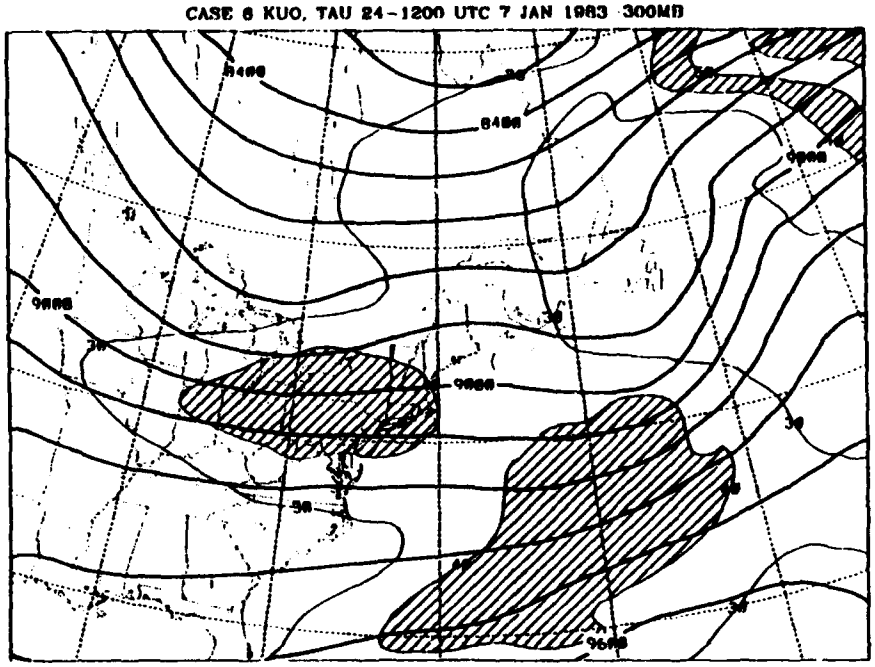

CASE 6 DRY, TAU 24-1200 UTC 7 JAN 1983-300MB

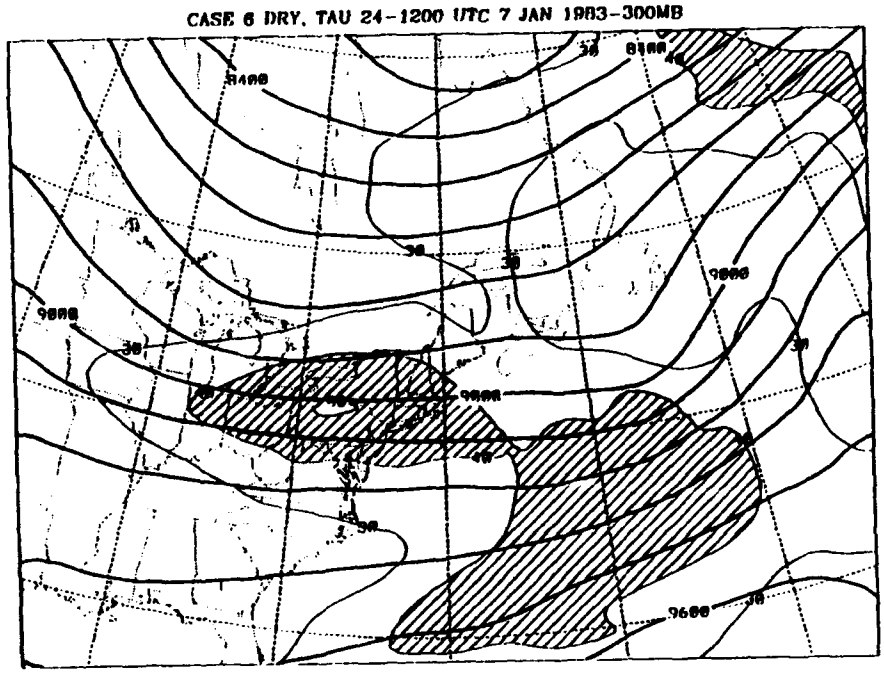

d.

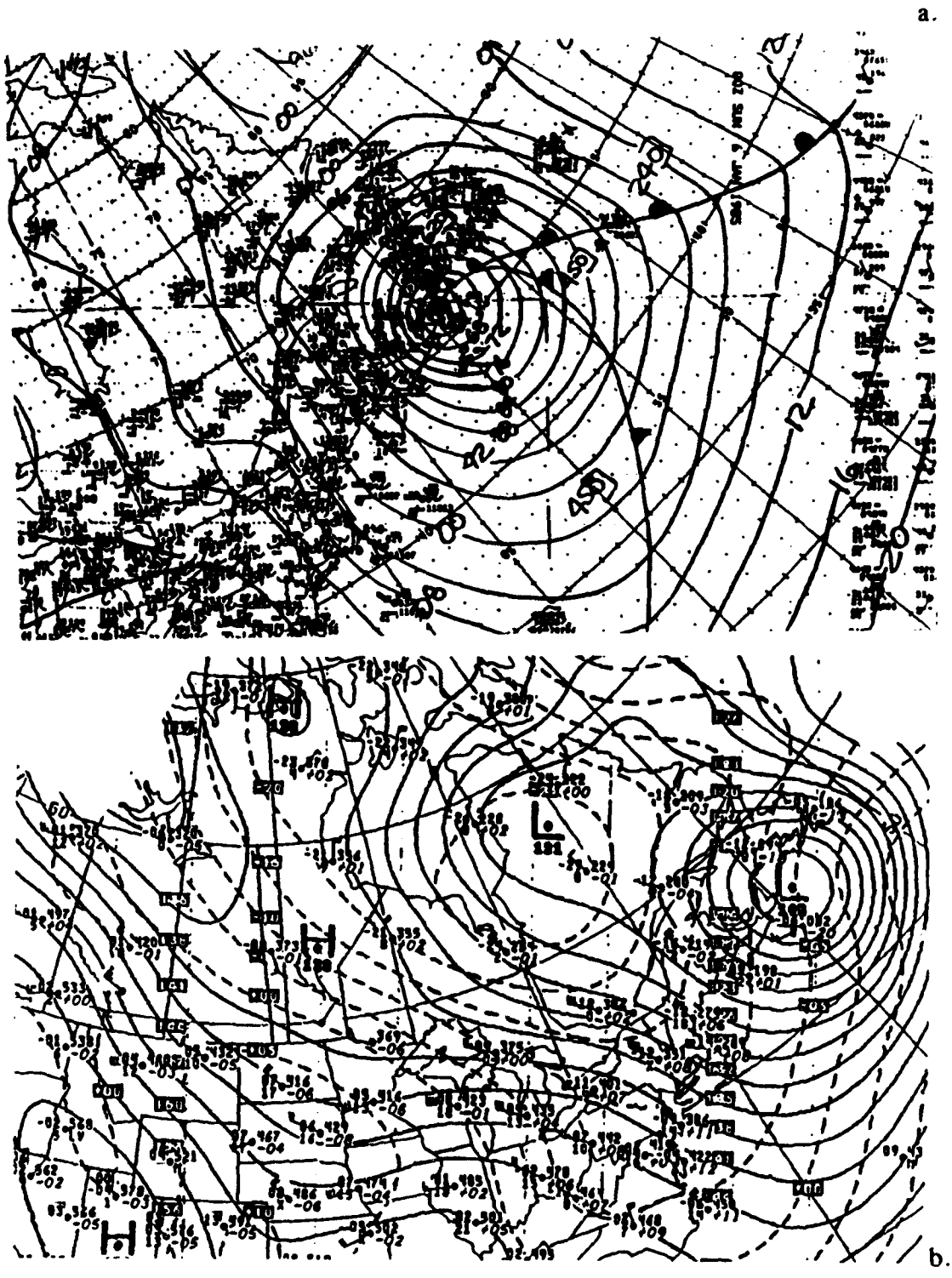

FIG. 4.63. Same as Fig. 4.8 except for case 7, 0000 UTC 6 Jan 1985.

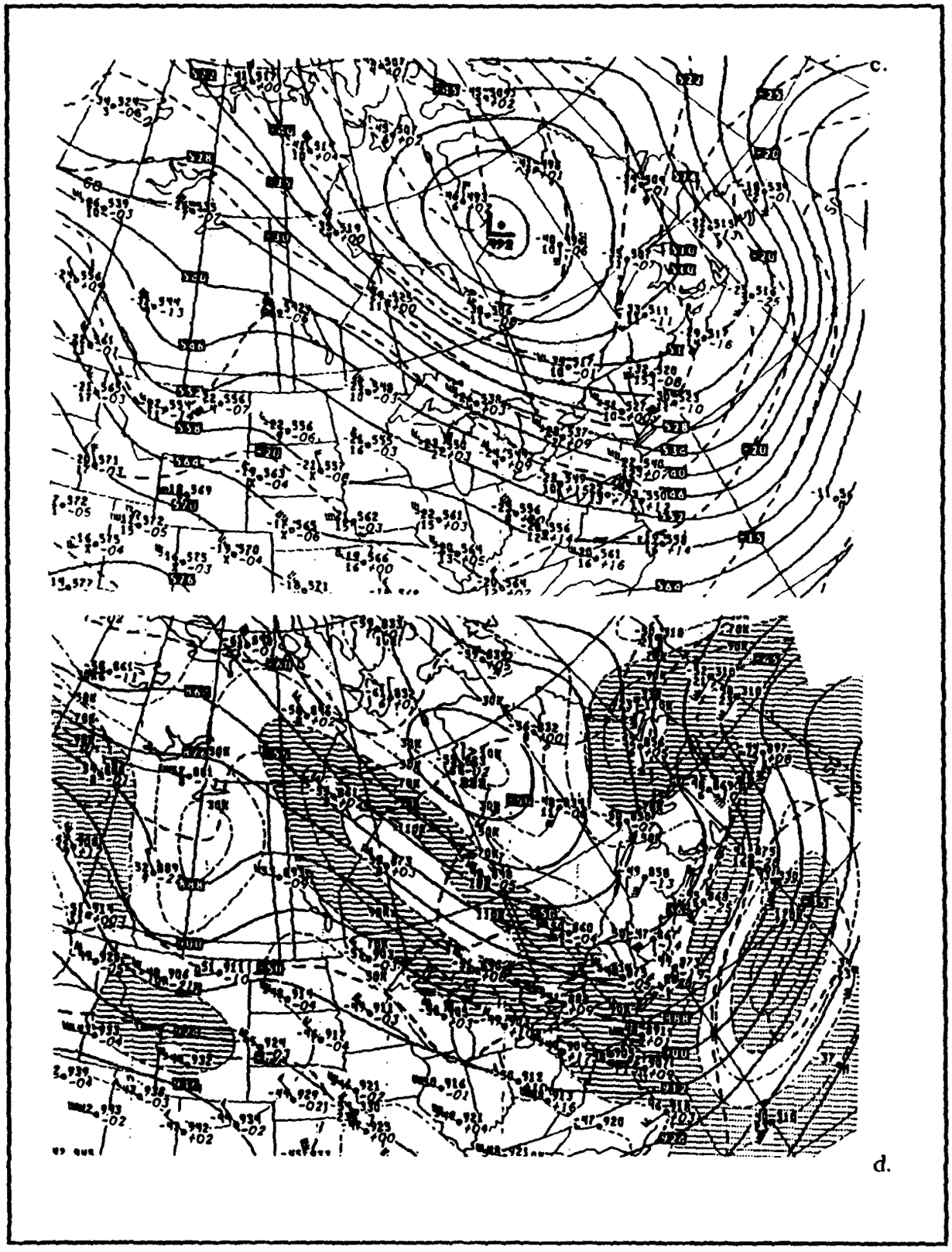
c.
d.

a.

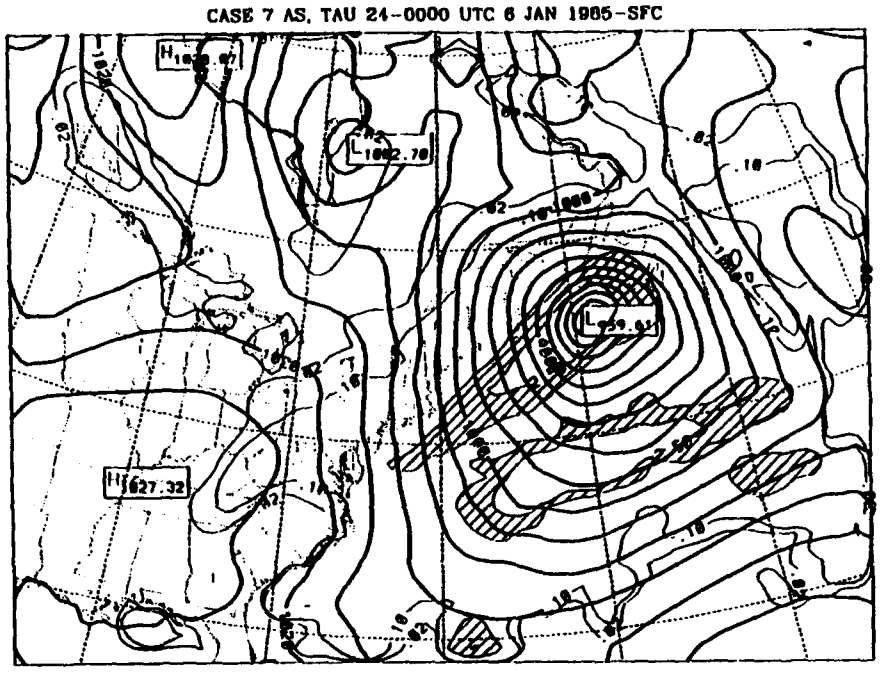

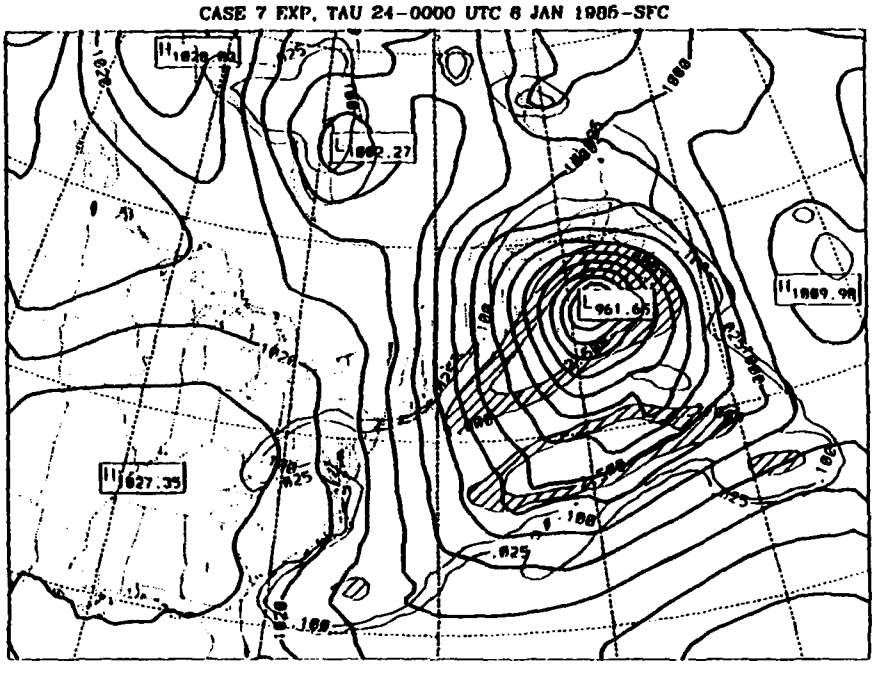

b.

FIG. 4.64. Same as Fig. 4.13 except for case 7, 0000 UTC 6 Jan 1985.

c.

CASE 7 KUO, TAU 24-0000 UTC 6 JAN 1985-SFC

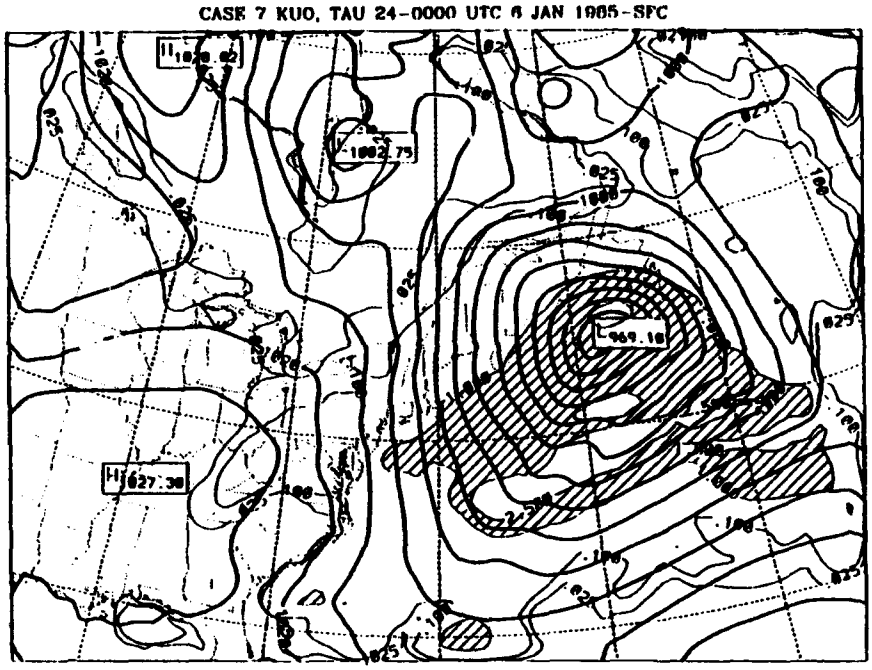

CASE 7 DRY, TAU 24-0000 UTC 6 JAN 1985-SFC

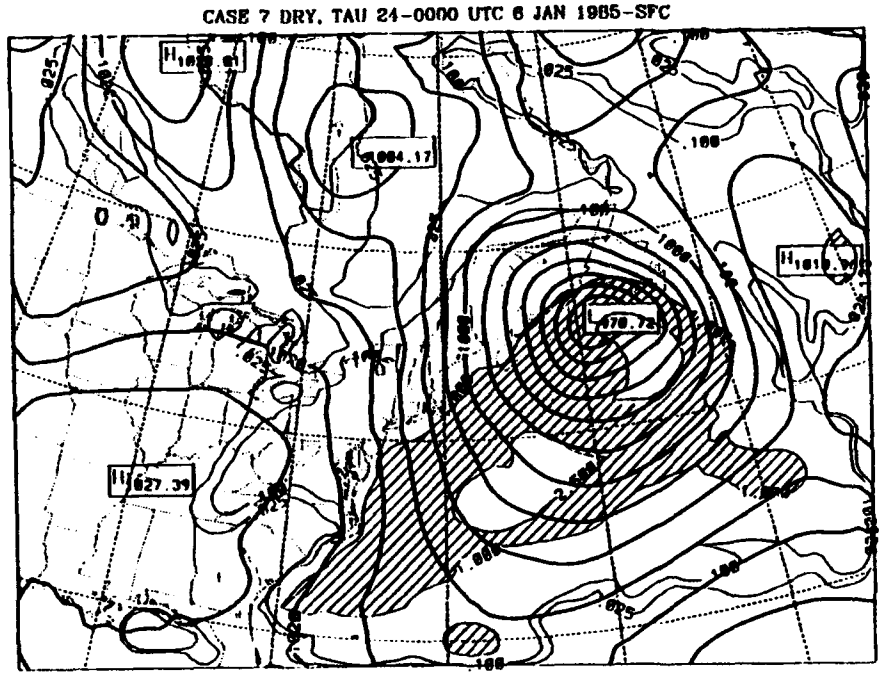

d.

a.

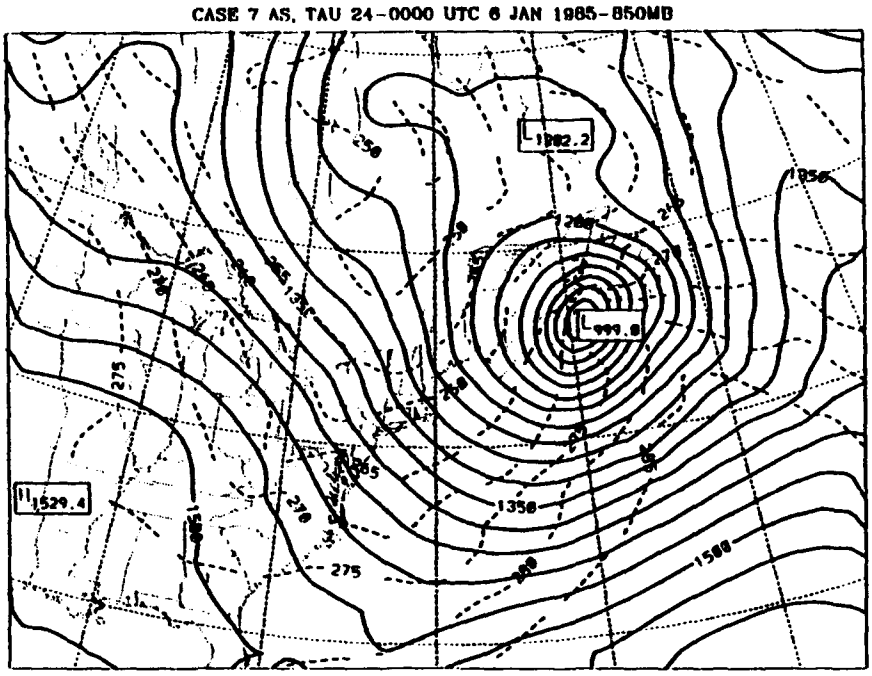

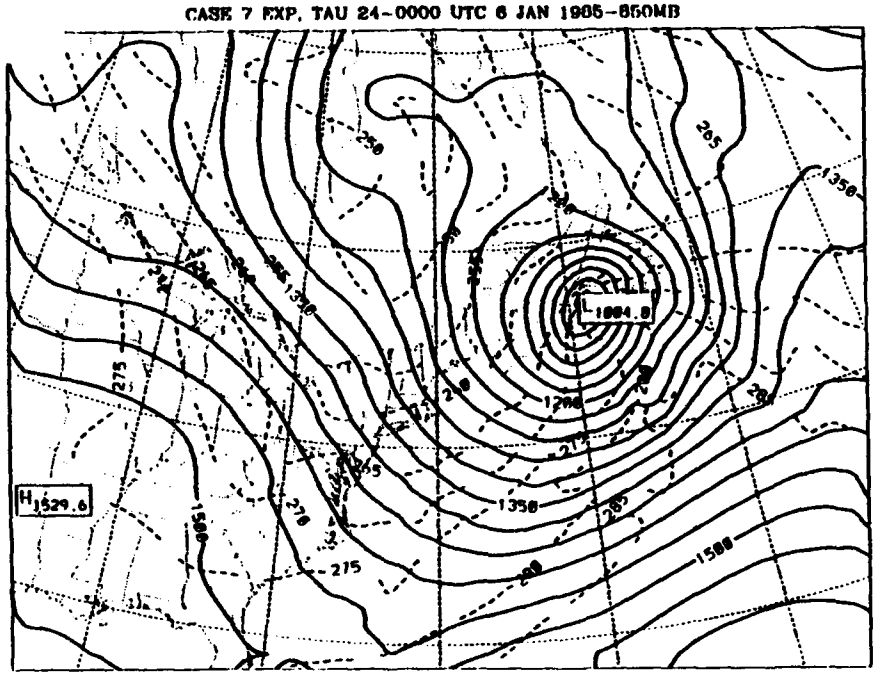

b.

FIG. 4.65. Same as Fig. 4.18 except for case 7, 0000 UTC 6 Jan 1985.

c.

CASE 7 KUO, TAU 24-0000 UTC 6 JAN 1985-850MB

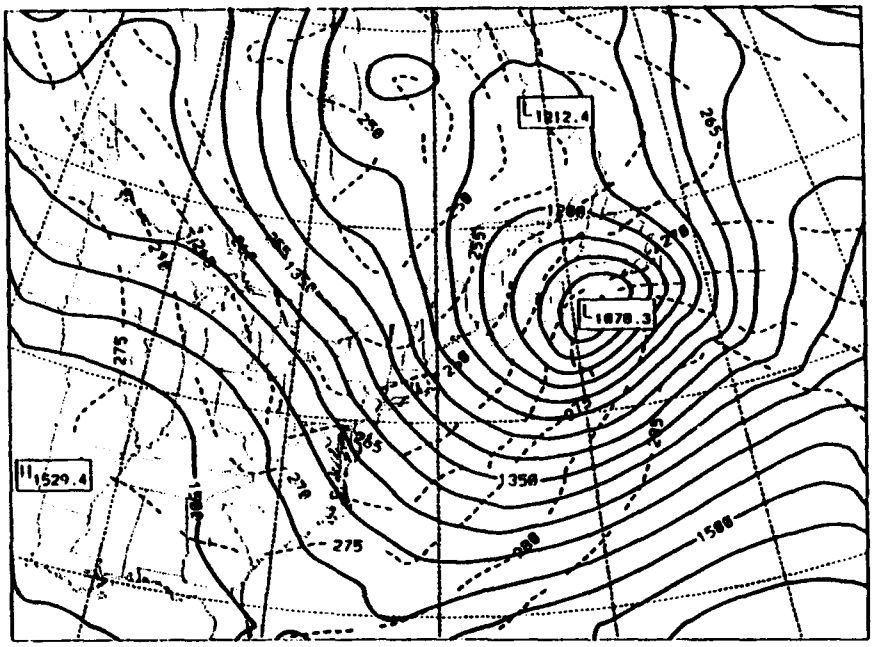

CASE 7 DRY, TAU 24-0000 UTC 6 JAN 1985-850MB

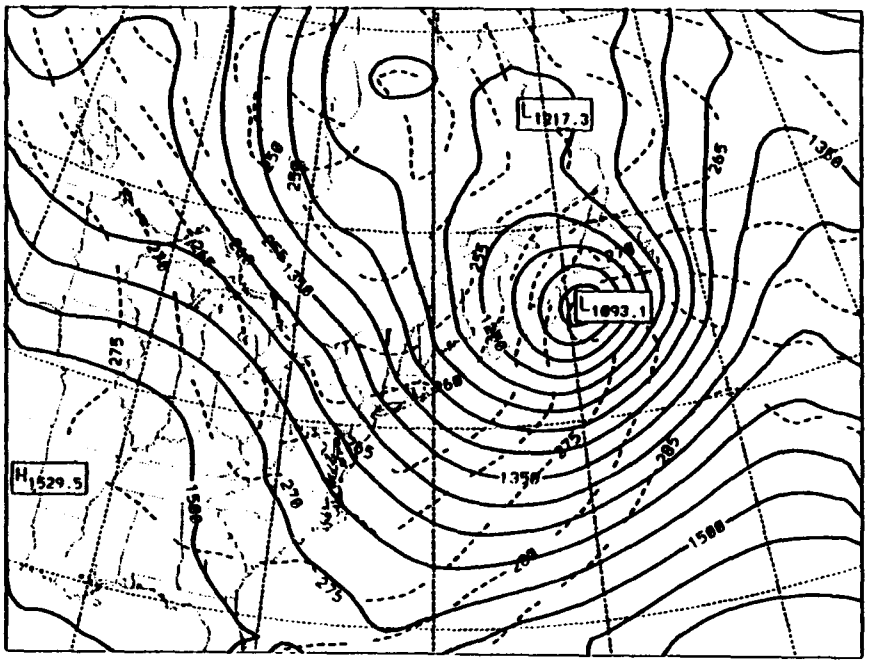

d.

a.

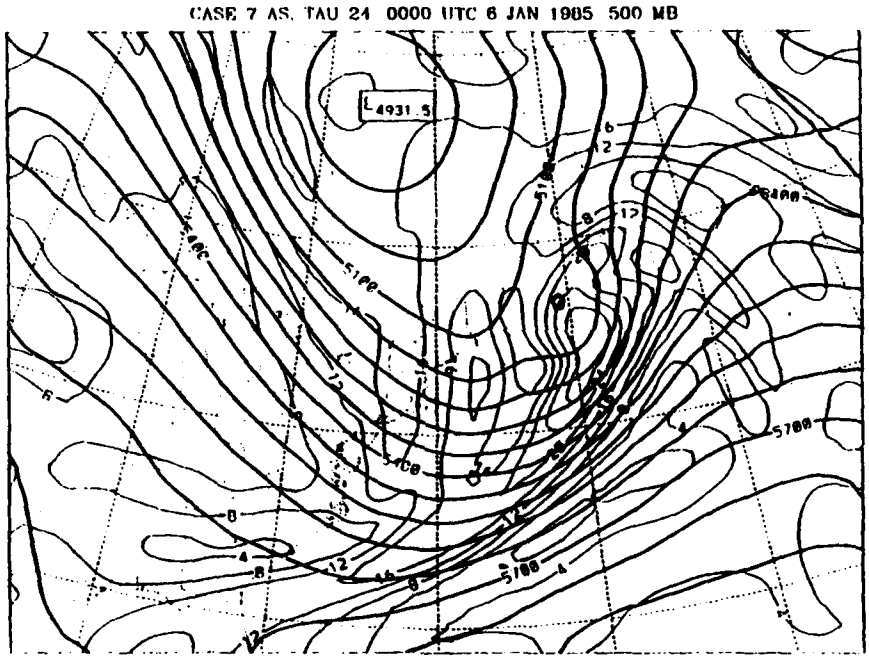

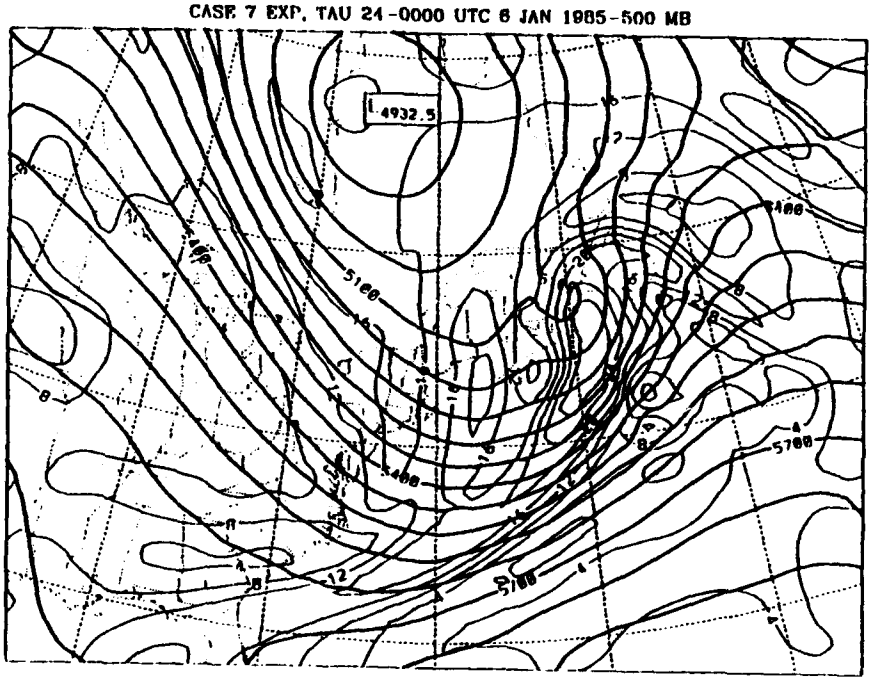

b.

FIG. 4.66. Same as Fig. 4.19 except for case 7, 0000 UTC 6 Jan 1985.

c.

CASE 7 KUO, TAU 24--0000 UTC 6 JAN 1985--500 MB

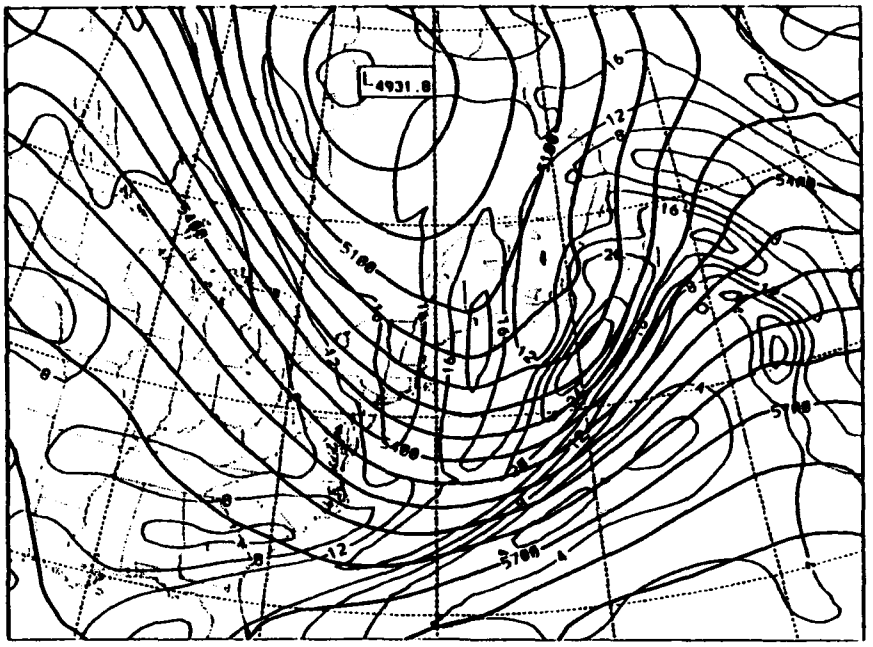

CASE 7 DRY, TAU 24--0000 UTC 6 JAN 1985--500 MB

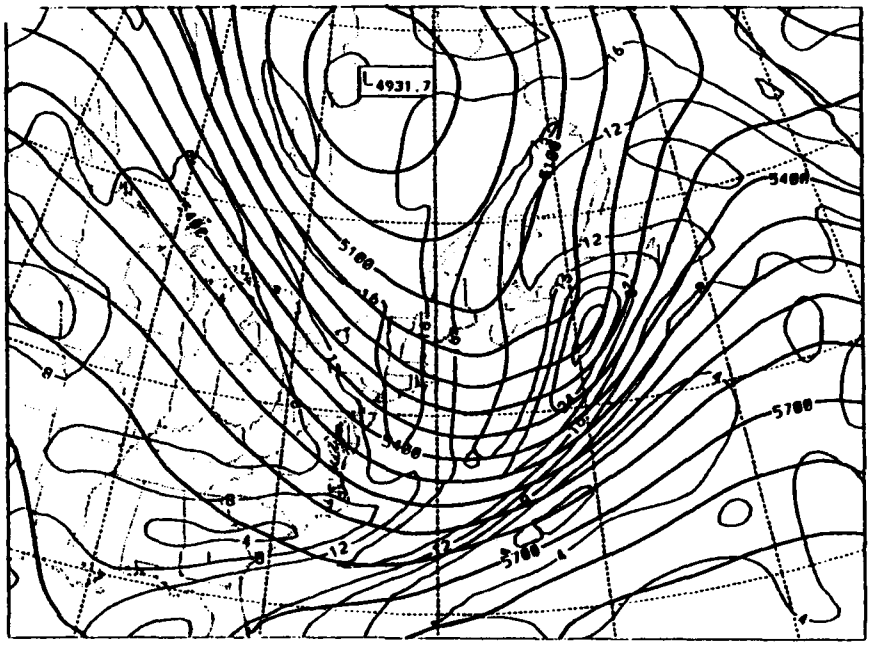

d.

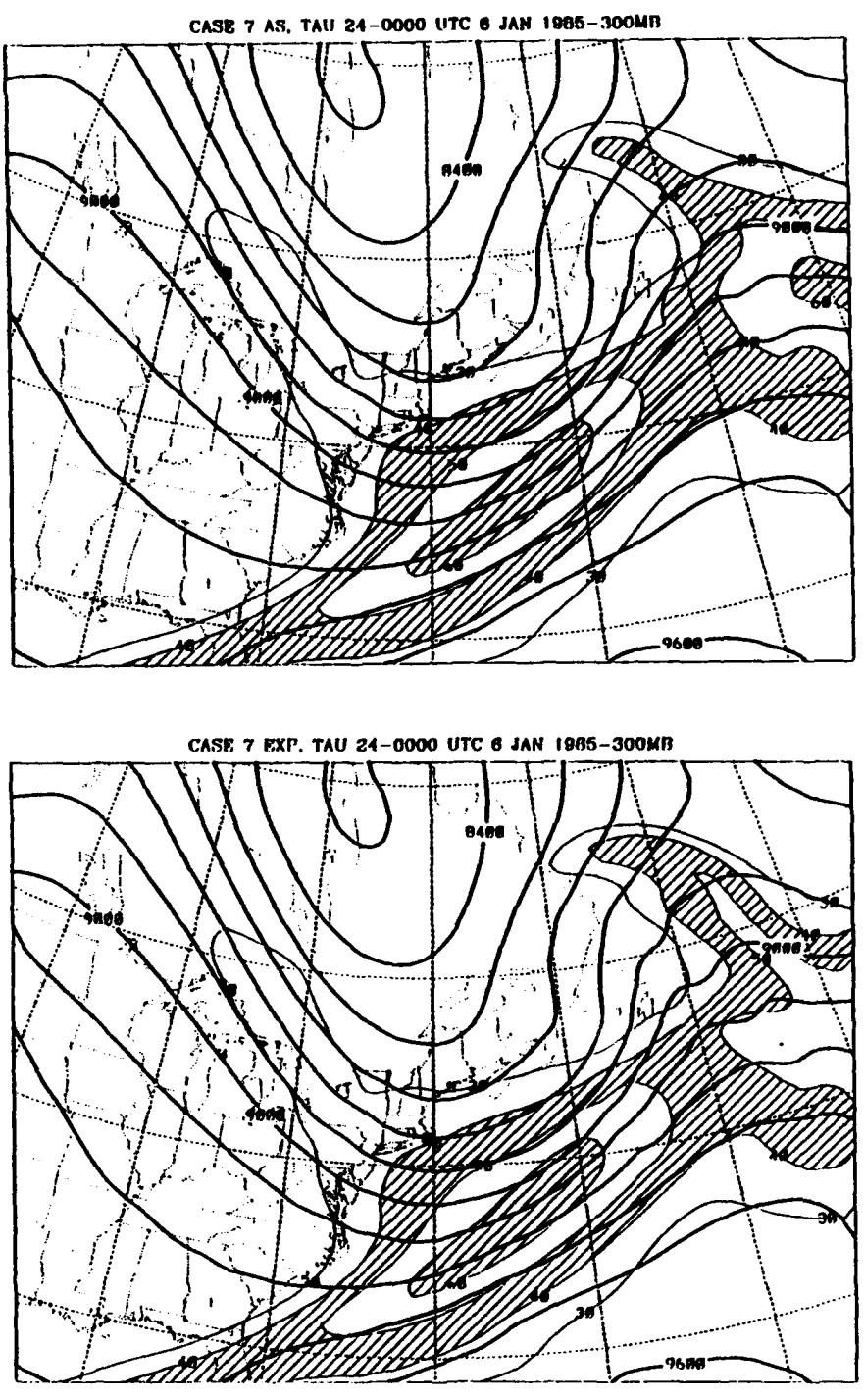

FIG. 4.67. Same as Fig. 4.20 except for case 7, 0000 UTC 6 Jan 1985.

c.

CASE 7 KUO, TAU 24-0000 UTC 6 JAN 1985-300MB

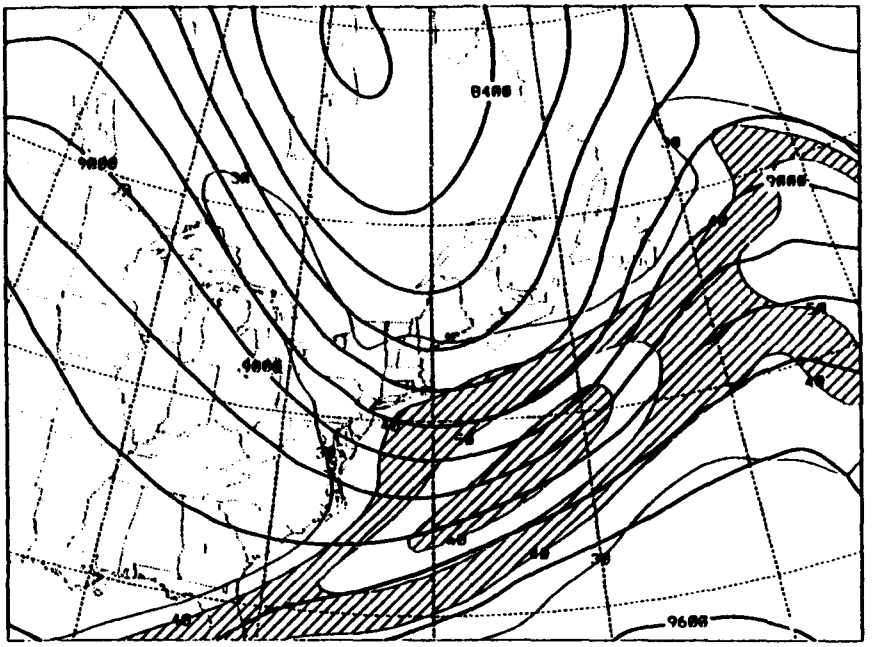

CASE 7 DRY, TAU 24-0000 UTC 6 JAN 1985-300MB

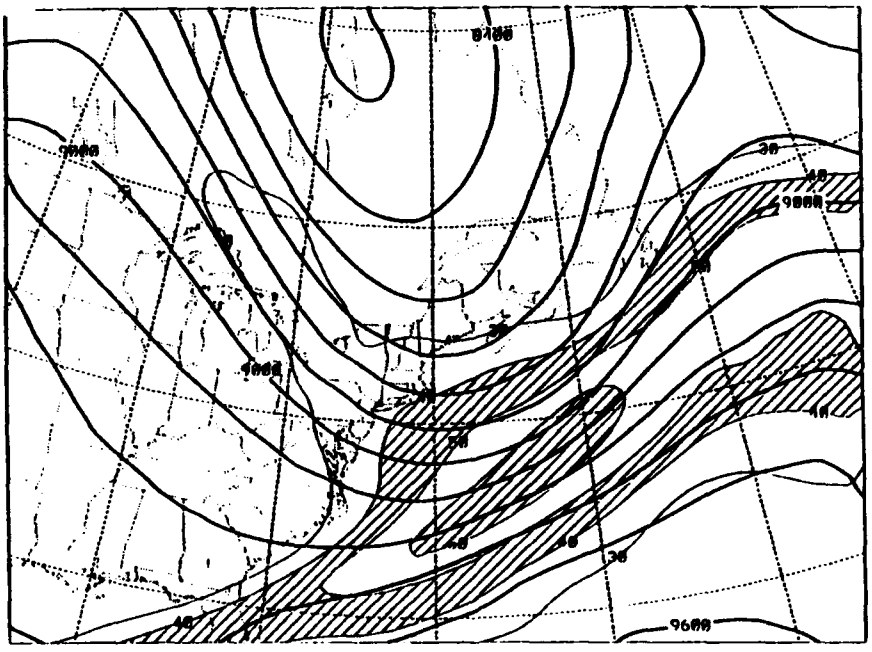

d.

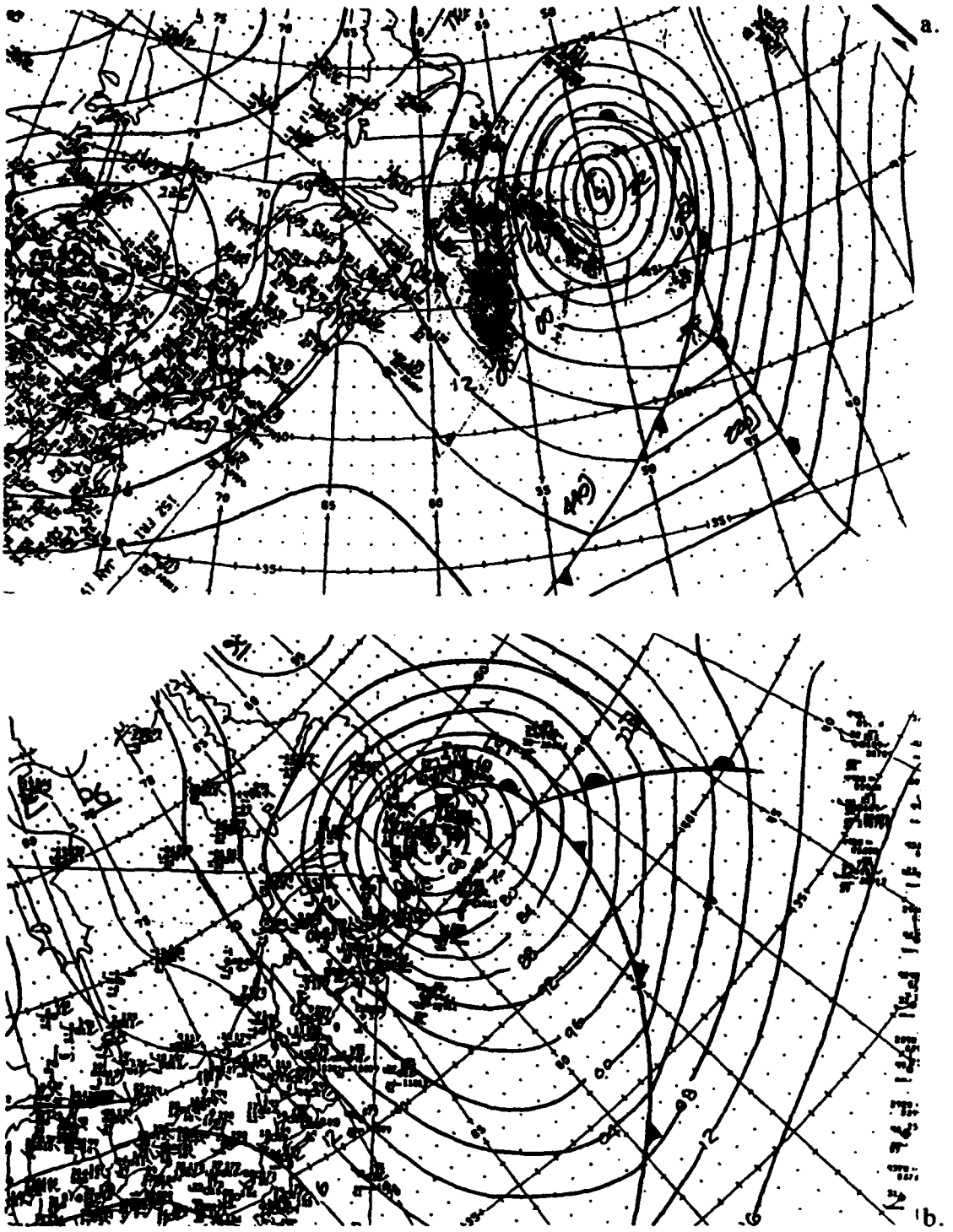

FIG. 4.68. Same as Fig. 4.6 except for (a) 1500 UTC 7 Jan 1983 and (b) 0300 UTC 6 Jan 1985.

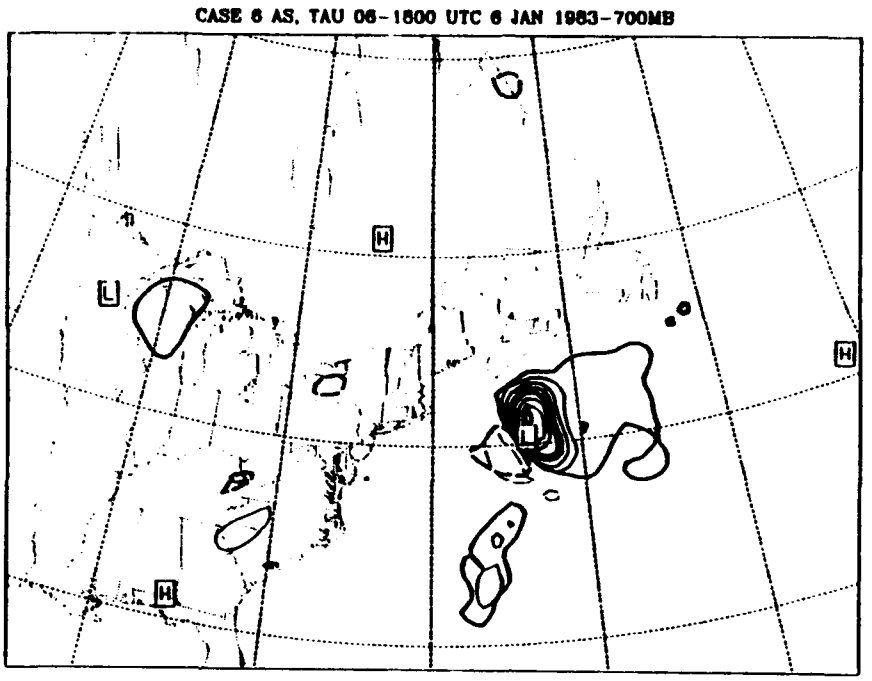

a.

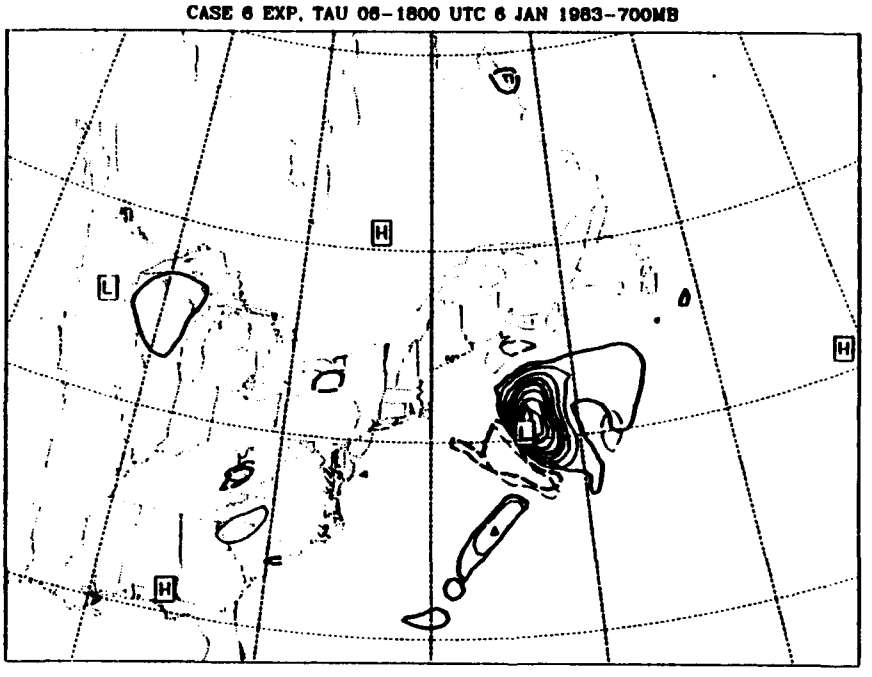

b.

FIG. 5.1. 1800 UTC 6 Jan 1983 case 6 model forecast fields of forecast surface low /high positions and 700 mb model total omega (heavy lines at -5 (dashed), 5, 25, and 50 microbar/sec) and calculated diabatic omega (thin lines at 5 micorbar/sec increment from -5 (dashed) to 50 microbar/sec not including zero) for (a) AS experiment, (b) EXP experiment, (c) KUO experiment, and (d) DRY experiment.

c.

CASE 6 KUO, TAU 06-1800 UTC 6 JAN 1983-700MB

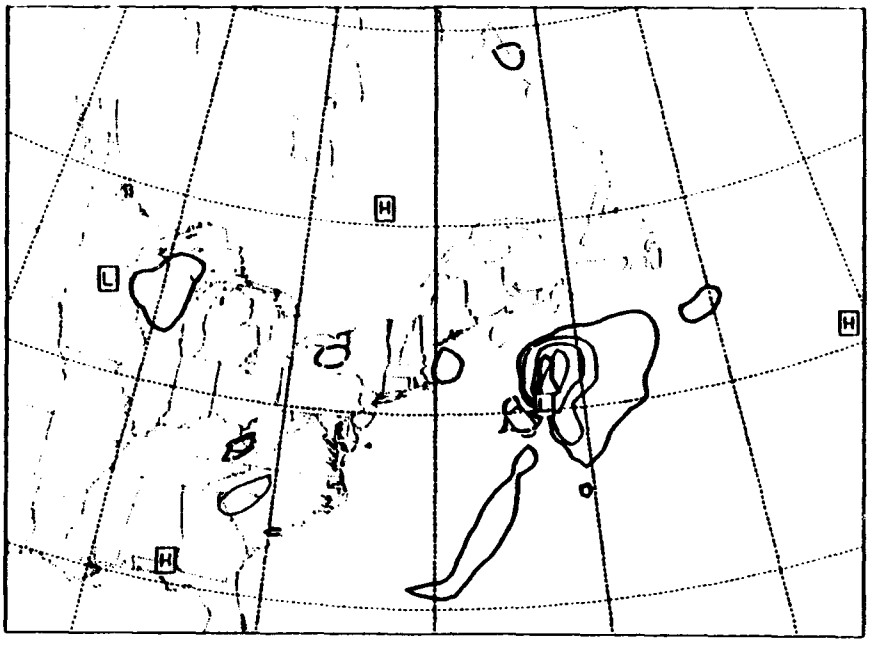

CASE 6 DRY, TAU 06-1800 UTC 6 JAN 1983-700MB

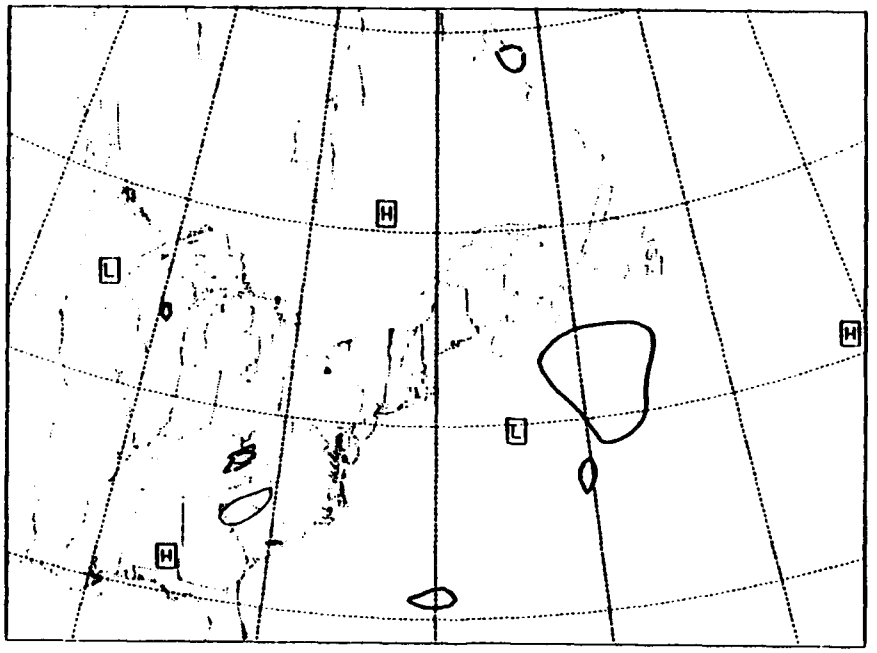

d.

a.

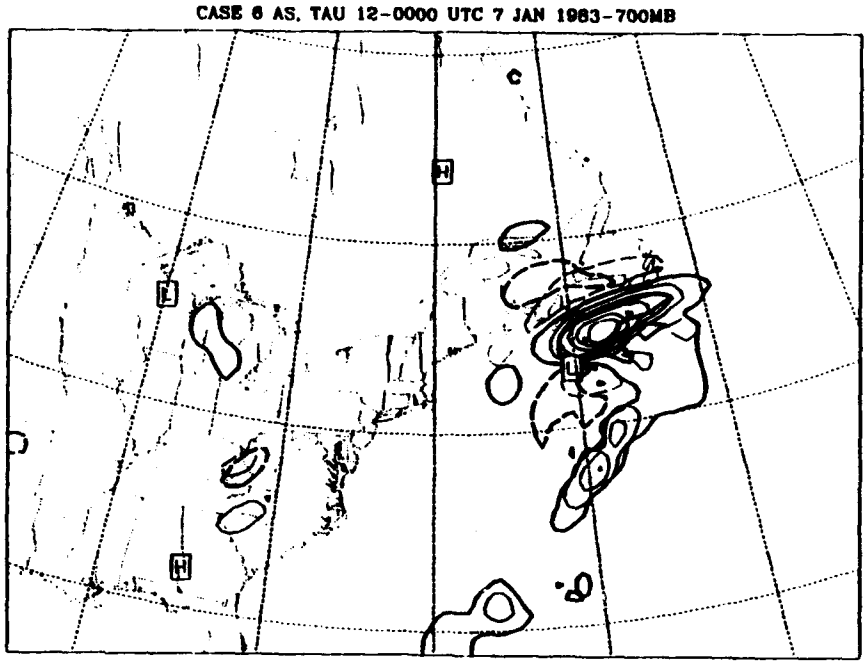

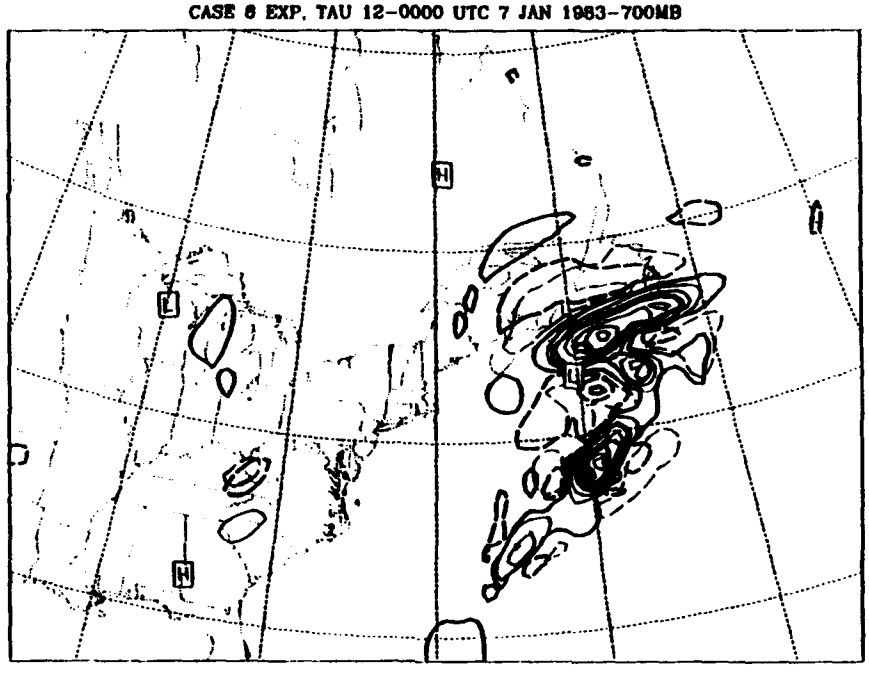

b.

FIG. 5.2. Same as Fig. 5.1 except for 0000 UTC 7 Jan 1983.

c.

CASE 6 KUO, TAU 12-0000 UTC 7 JAN 1963-700MB

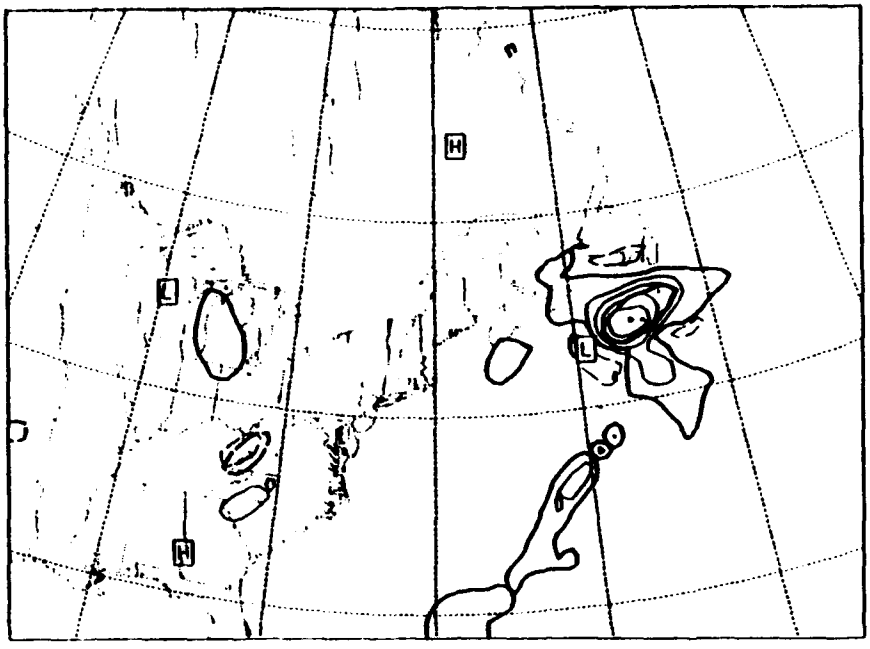

CASE 6 DRY, TAU 12-0000 UTC 7 JAN 1963-700MB

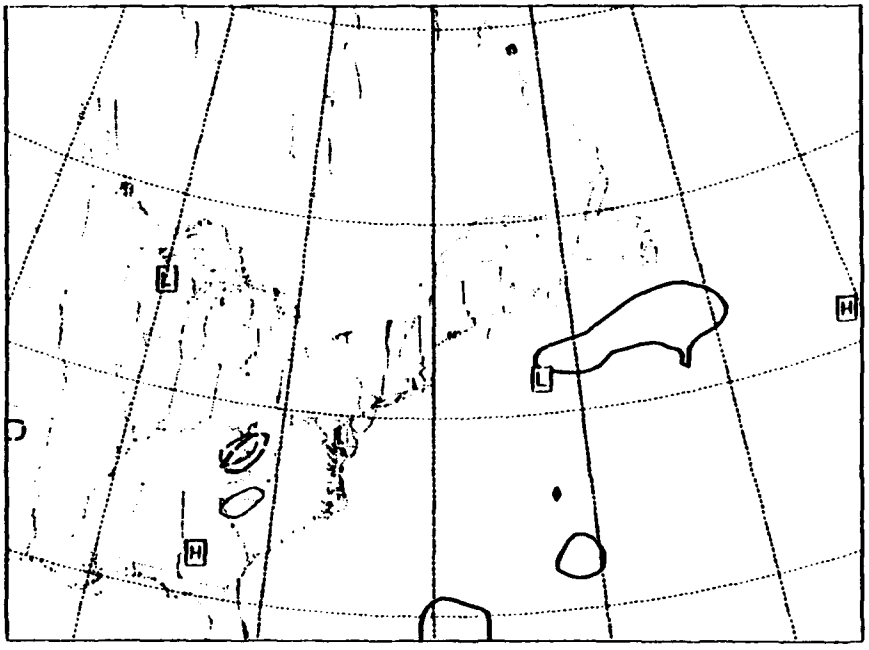

d.

a.

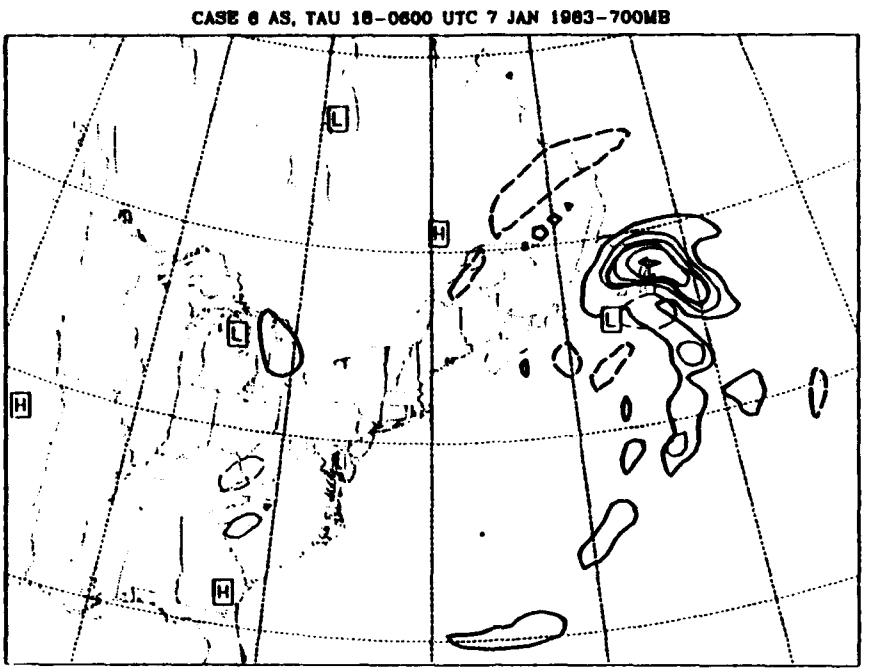

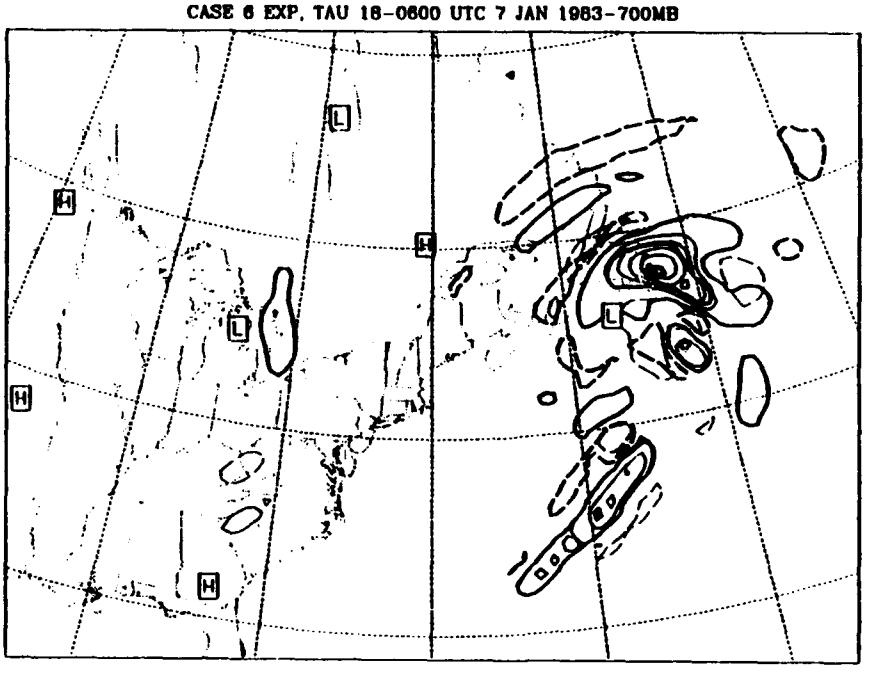

b.

FIG. 5.3. Same as Fig. 5.1 except for 0600 UTC 7 Jan 1983.

c.

CASE 6 KUO, TAU 18-0600 UTC 7 JAN 1983-700MB

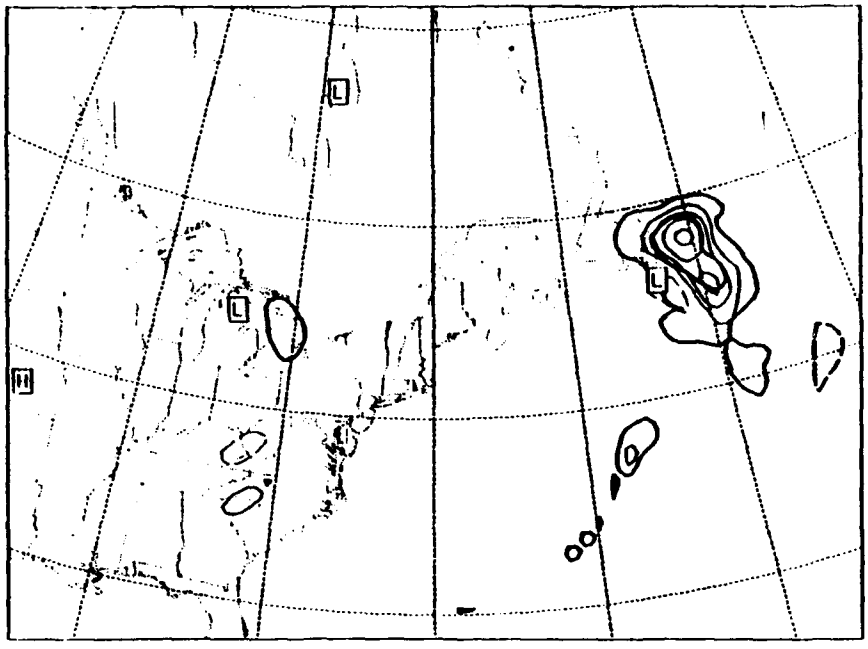

CASE 6 DRY, TAU 18-0600 UTC 7 JAN 1983-700MB

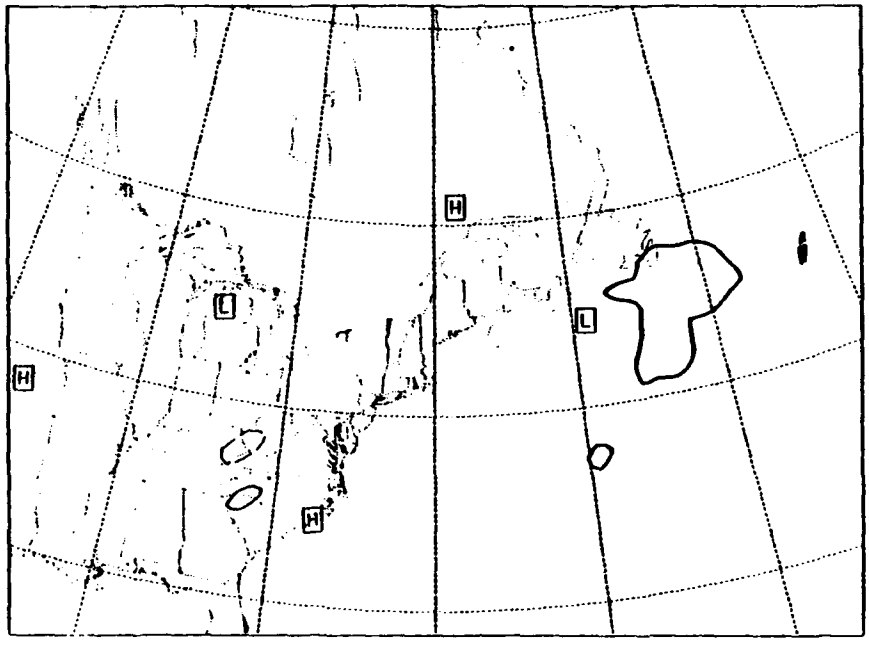

d.

a.

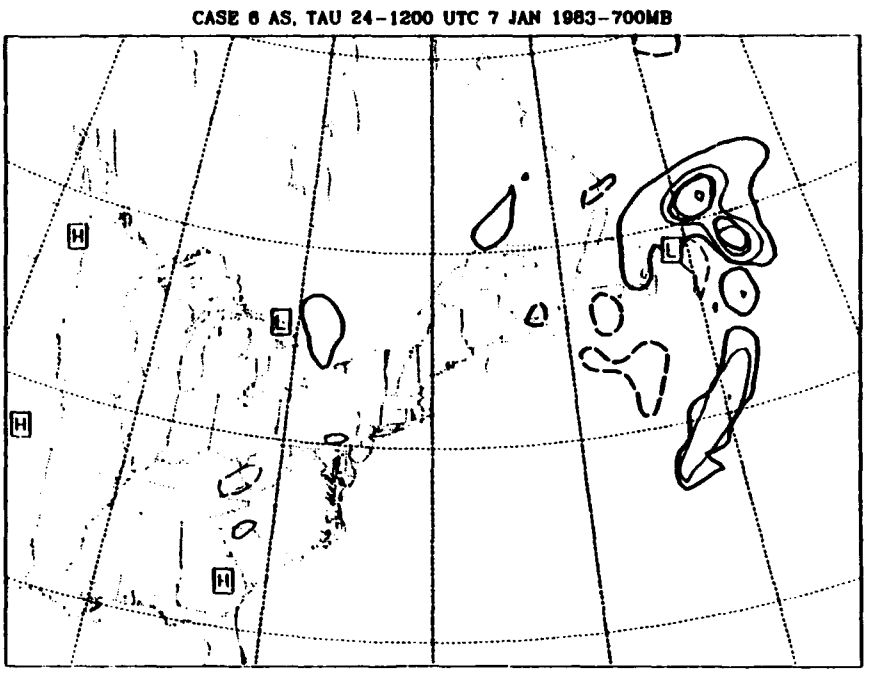

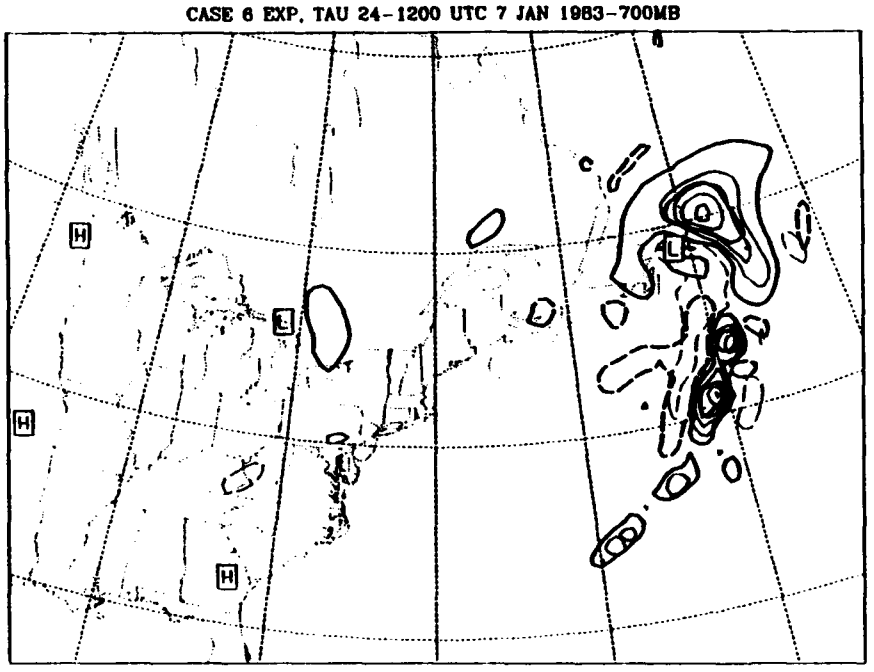

b.

FIG. 5.4. Same as Fig. 5.1 except for 1200 UTC 7 Jan 1983.

c.

CASE 6 KUO, TAU 24-1200 UTC 7 JAN 1983-700MB

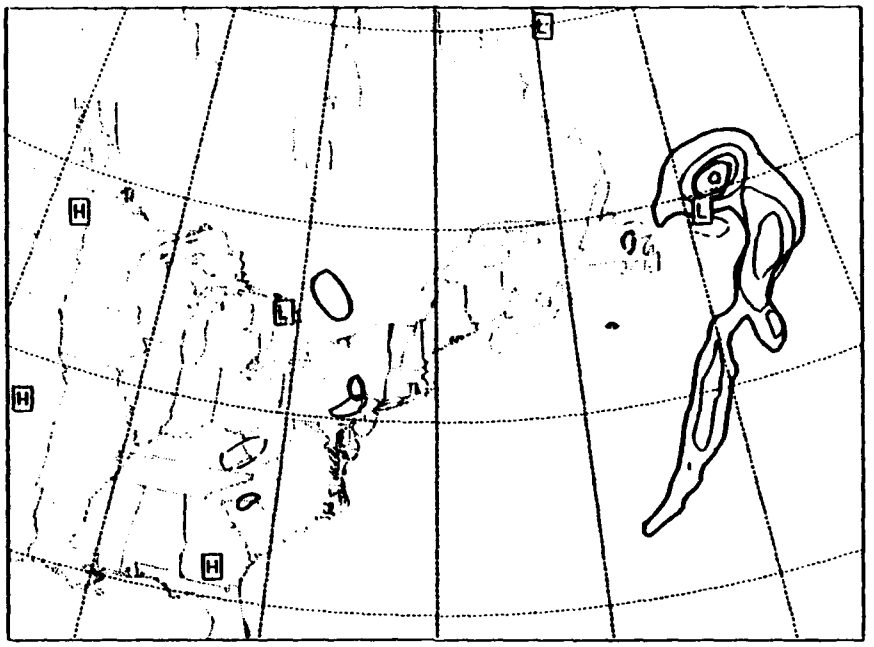

CASE 6 DRY, TAU 24-1200 UTC 7 JAN 1983-700MB

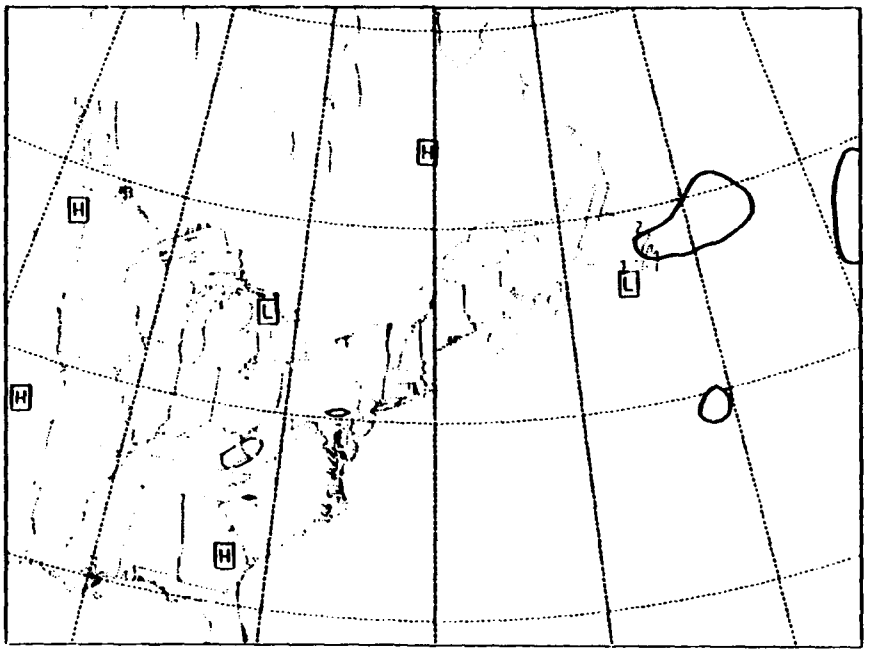

d.

a.

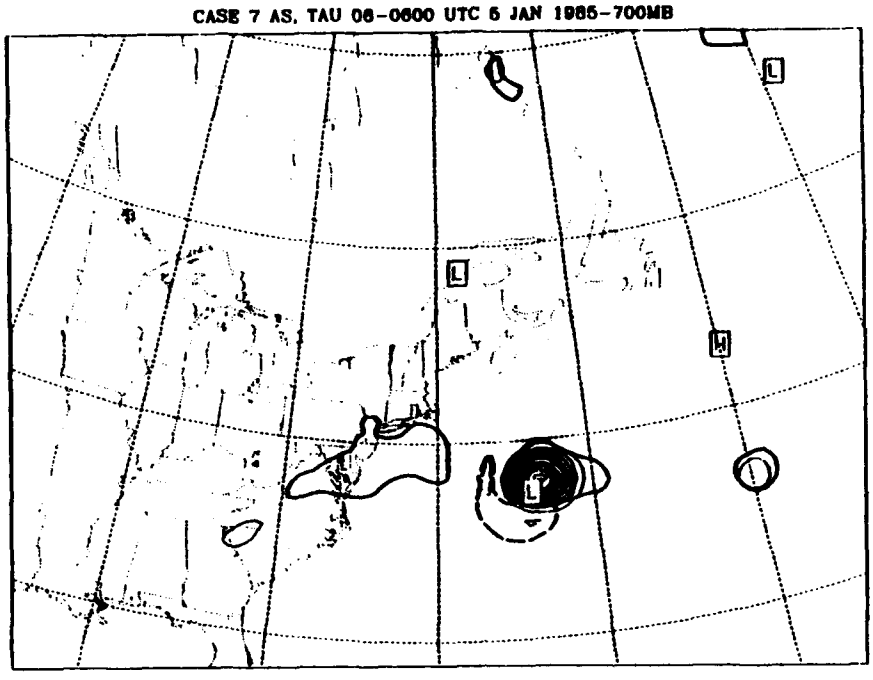

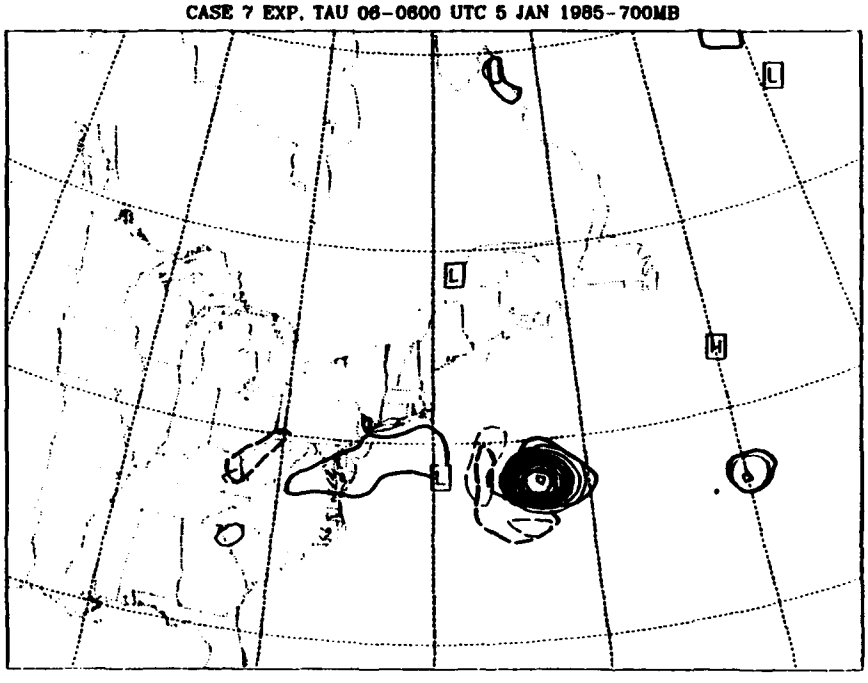

b.

FIG. 5.5. Same as Fig. 5.1 except for case 7, 0600 UTC 5 Jan 1985.

c.

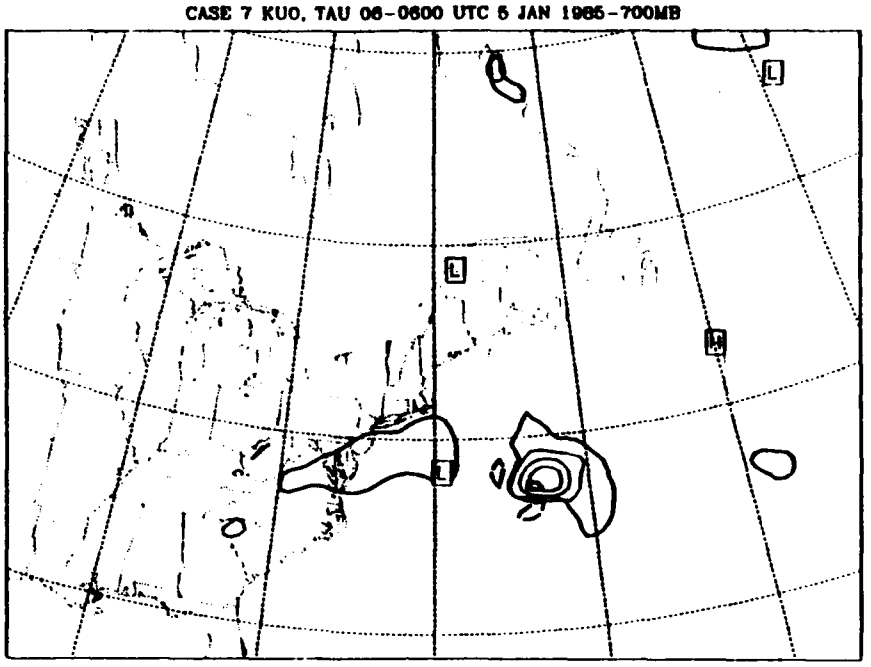
CASE 7 KUO, TAU 06-0600 UTC 5 JAN 1985-700MB
L
L
H
L

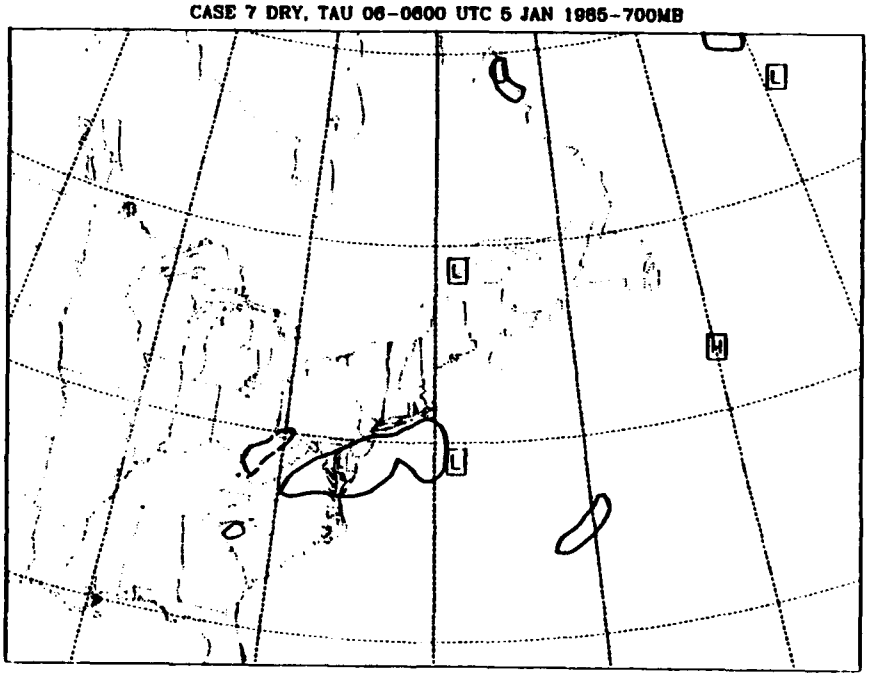
CASE 7 DRY, TAU 06-0600 UTC 5 JAN 1985-700MB
L
L
H
L

d.

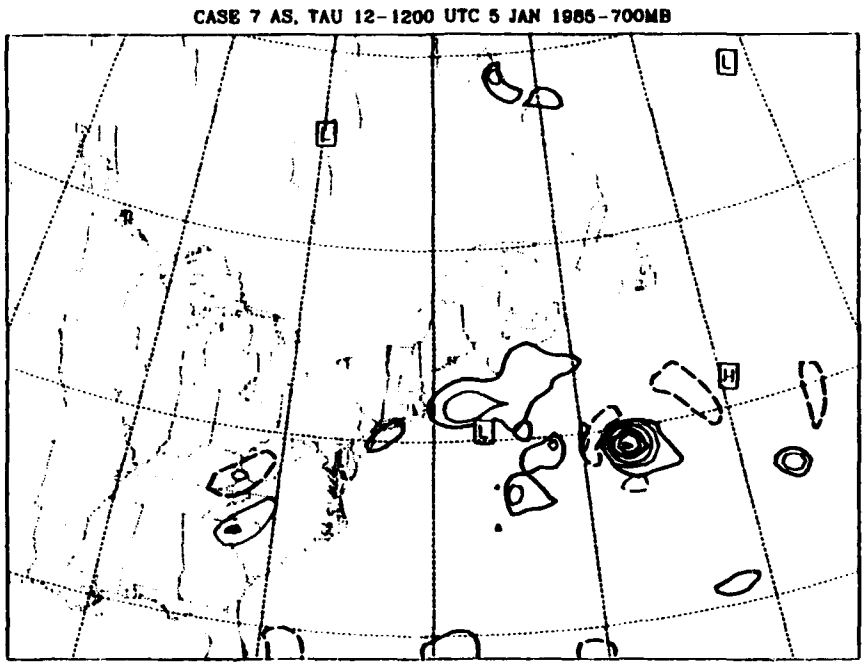

a.

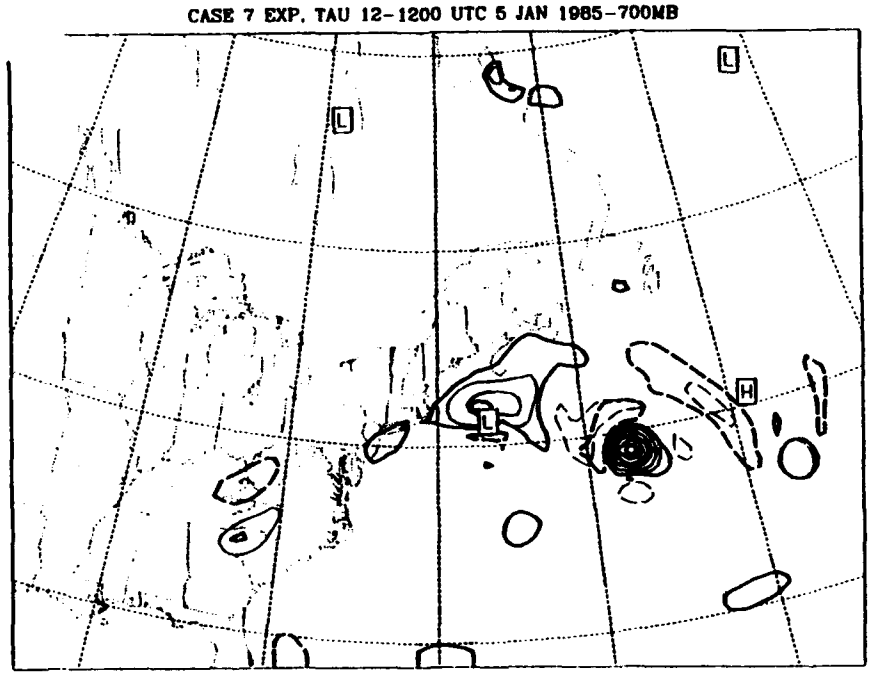

b.

FIG. 5.6. Same as Fig. 5.1 except for case 7, 1200 UTC 5 Jan 1985.

c.

CASE 7 KUO, TAU 12-1200 UTC 5 JAN 1985-700MB

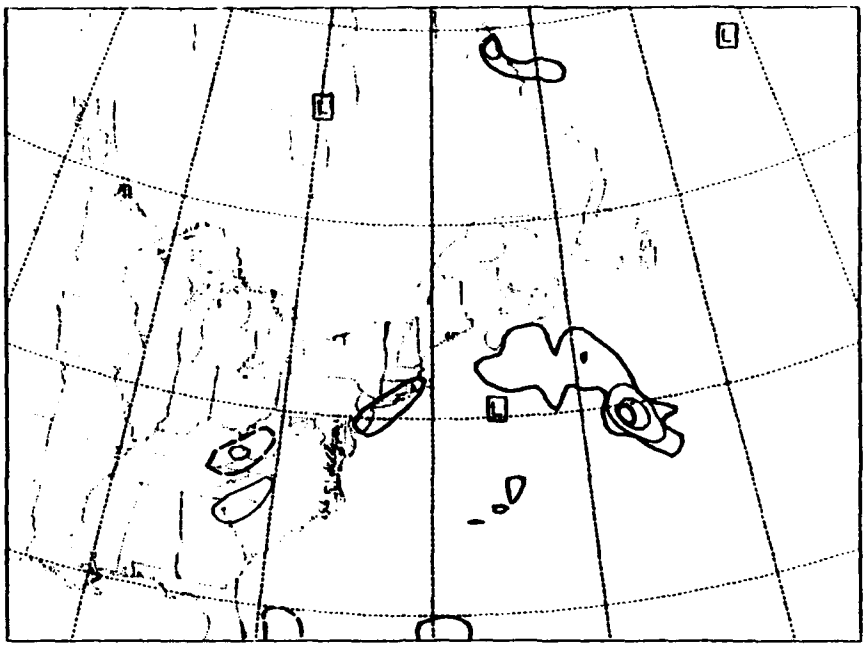

CASE 7 DRY, TAU 12-1200 UTC 5 JAN 1985-700MB

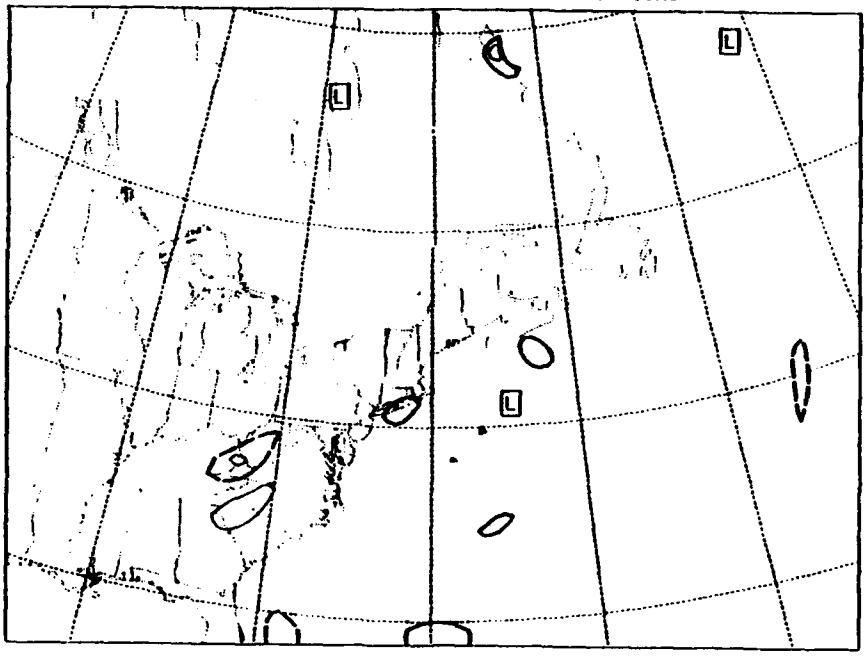

d.

a.

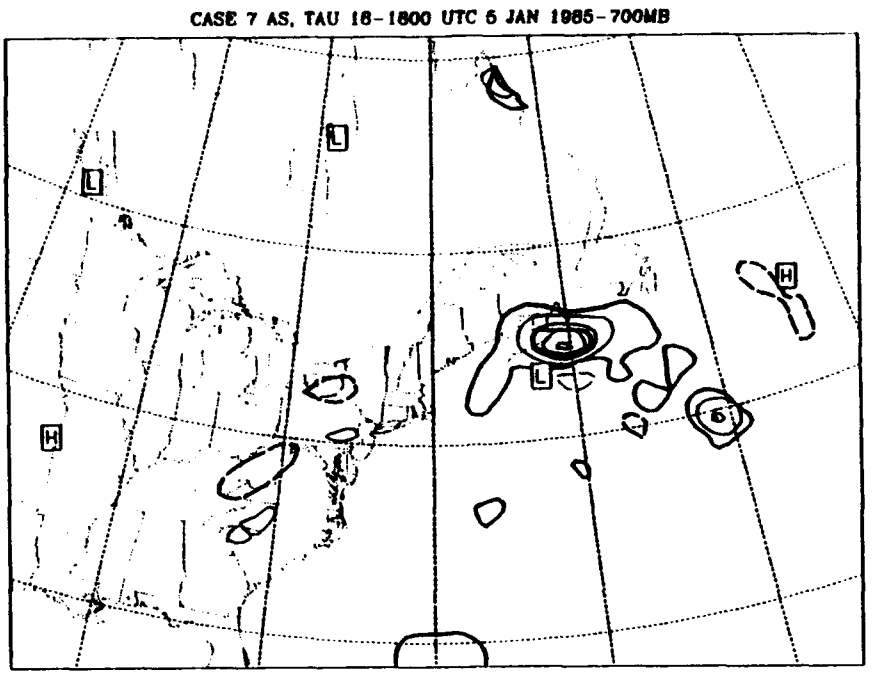

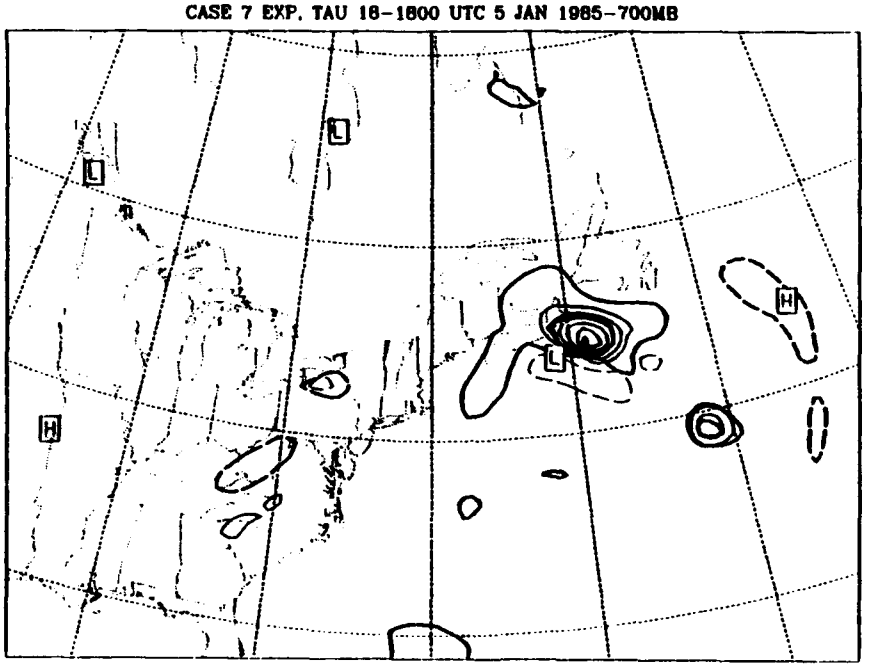

b.

FIG. 5.7. Same as Fig. 5.1 except for case 7, 1800 UTC 5 Jan 1985.

c.

CASE 7 KUO, TAU 18-1800 UTC 5 JAN 1985-700MB

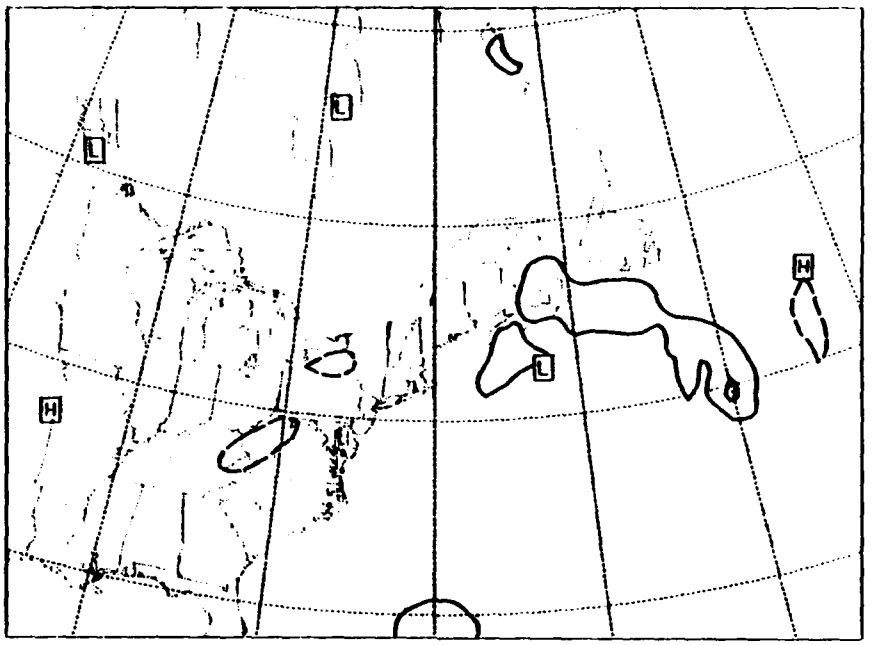

CASE 7 DRY, TAU 18-1800 UTC 5 JAN 1985-700MB

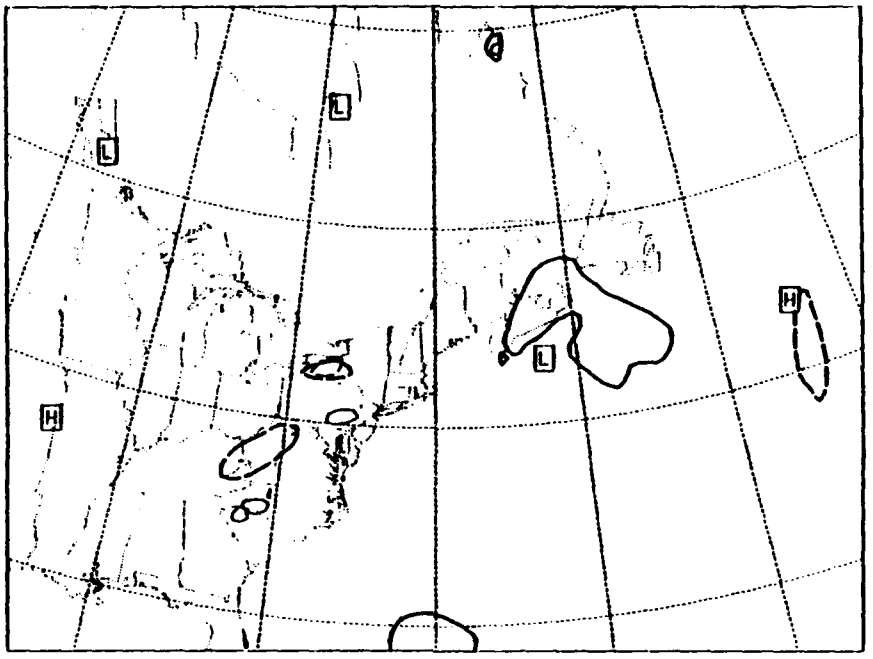

d.

a.

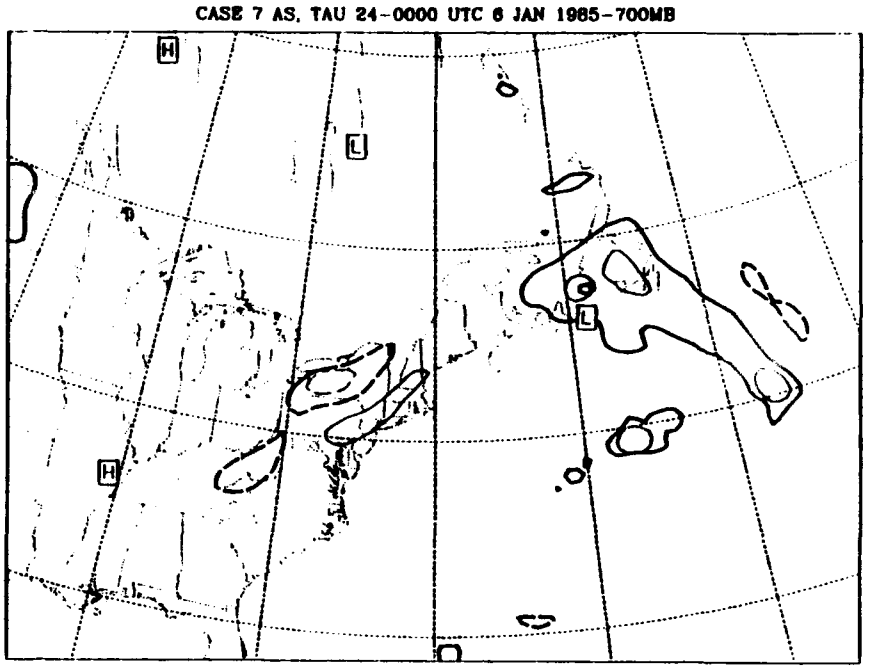

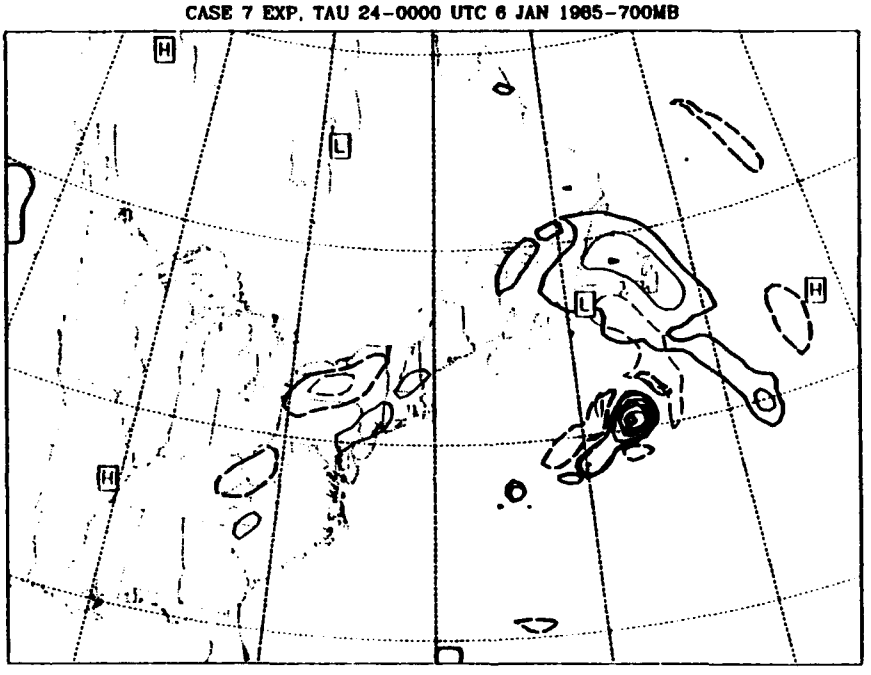

b.

FIG. 5.8. Same as Fig. 5.1 except for case 7, 0000 UTC 6 Jan 1985.

c.

CASE 7 KUO, TAU 24-0000 UTC 6 JAN 1985-700MB

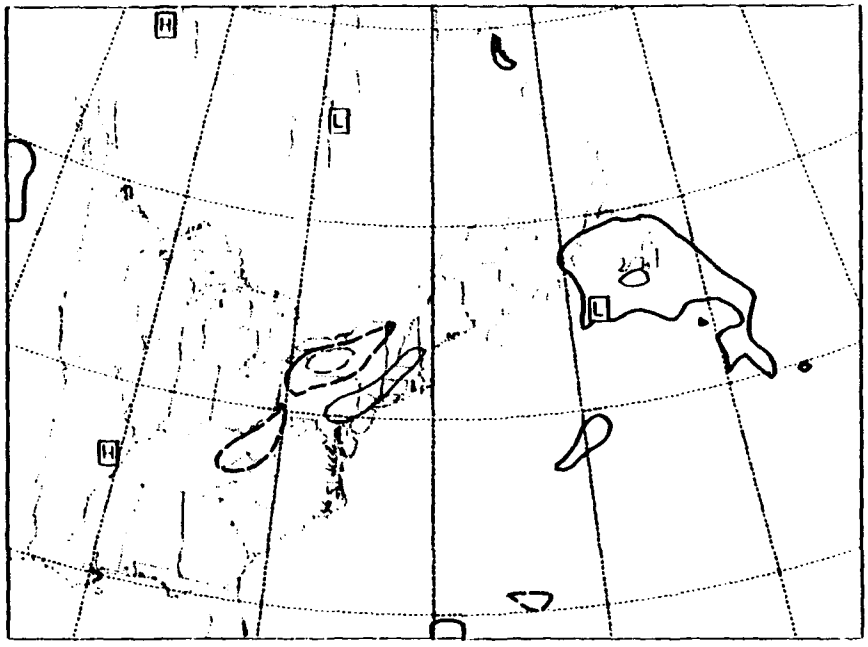

CASE 7 DRY, TAU 24-0000 UTC 6 JAN 1985-700MB

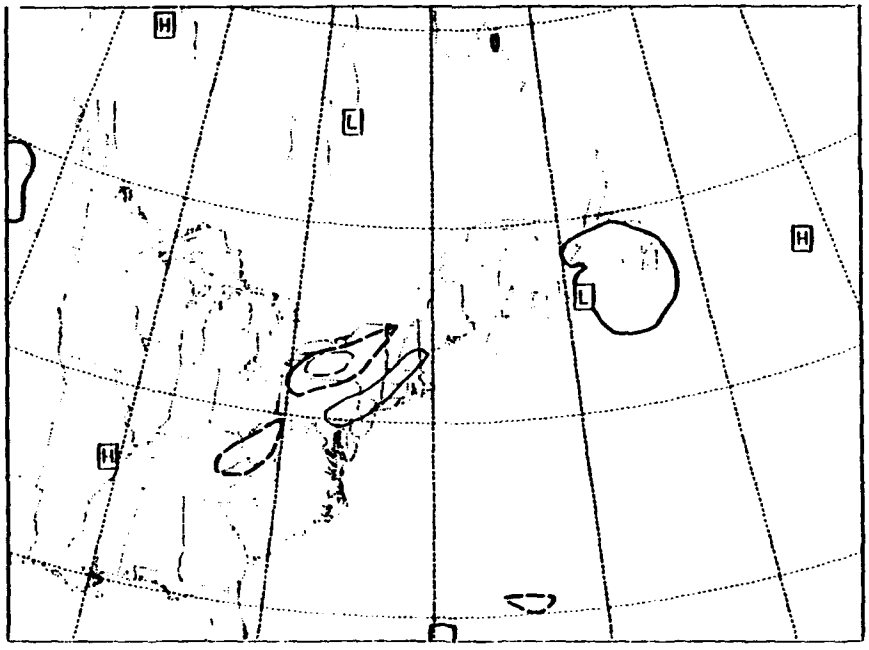

d.

LIST OF REFERENCES

Anthes, R. A., 1977: A cumulus parameterization scheme utilizing a one-dimensional cloud model. *Mon Wea. Rev.*, **105,** 270-286.

___, and E.-Y. Hsie and Y.-H. Kuo, 1987: Description of the Penn State/NCAR Mesoscale Model Version 4 (MM4). NCAR Tech. Note, NCAR/TN-282+STR, 66pp.

___, and Y. H. Kou, S. G. Benjamin and Y. F. Li, 1982: The evolution of the mesoscale environment of severe local storms: Preliminary modeling results. *Mon. Wea. Rev.*, **110,** 1187-1213.

Arakawa, A., and W. H. Schubert, 1974: interaction of a cumulus cloud ensemble with the large scale environment, Part I. *J. Atmos. Sci.*, **31,** 674-701.

Aubert, E. J., 1957: On the release of latent heat as a factor in large scale atmospheric motions. *J. Meteor.*, **14,** 527-542.

Baker, F. W., 1991: The effect of latent heat release on the ERICA IOP-5 cyclone. M. S. Thesis, Naval Postgraduate School.

Blackadar, A. K., 1979: High resolution models of the planetary boundary layer. *Advances in Environmental Science and Engineering*, 1, No. 1. Pfafflin and Zeigler, Eds., Gordon and Breach Sci. Publ., 50-85.

Chang, C. B., D. J. Perkey and C. W. Kreitzberg, 1982: A numerical case study of the effects of latent heating on a developing wave cyclone. *J. Atmos. Sci.*, **39,** 1555-1570.

___, ___, ___, 1984: Latent heat induced transformations during cyclogenesis *Mon. Wea. Rev.*, **112,** 357-367.

Chen, T. C., C. B. Chang, and D. J. Perkey, 1983: Numerical study of an AMTEX '75 oceanic cyclone. *Mon. Wea. Rev.*, **111,** 1818-1829.

Danard, M. B. 1964: On the influence of released latent heat on cyclone development. *J. Appl. Meteor.*, **3,** 27-37.

___, 1966: On the contribution of released latent heat to changes in available potential energy. *J. Appl. Meteor.*, **5,** 81-84.

Dimego, G. J., and L. F. Bosart, 1982: The transformation of tropical storm Agnes into an extratropical cyclone. Part I: The observed fields and vertical motion computations. *Mon Wea Rev.*, **110,** 385-411.

Grell, G., Y.-H. Kuo and R. Pasch, 1988: Semi-prognostic tests of three cumulus parameterization schemes for mid-latitude convective systems. *Preceeding, Eight Conference on Numerical Weather Prediction.* Baltimore, Amer. Meteor Soc., 363-370.

Haltiner, G. J., and R. T. Williams, 1980: *Numerical Prediction and Dynamic Meteorology*, 2nd ed., John Wiley & Sons, 477 pp.

Hsie, E.-Y., R. A. Anthes and D. Keyser, 1984: Numerical Simulation of frontogenesis in a moist atmosphere. *J. Atmos. Sci.*, **41,** 2581-2594.

Kenney, S. E., and P. J. Smith, 1983: On the release of eddy available potential energy in an extratropical cyclone system. *Mon. Wea. Rev.*, **111,** 745-755.

Krishnamurti, T. N., 1968: A study of a developing wave cyclone. *Mon Wea. Rev.*, **96,** 208-217.

Kuo, H. L., 1974: Further studies of the parameterization of the influence of cumulus convection on large scale flow. *J. Atmos Sci.*, **31,** 1232-1240.

Kuo, Y.-H., and S. Low-Nam, 1990: Prediction of nine explosive cyclones over the western Atlantic Ocean with a regional model. *Mon. Wea. Rev.*, **118,** 3-25.

___, and R. A. Anthes, 1984: Mesoscale budgets of heat and moisture in a convective system over the central United States. *Mon. Wea. Rev..*, **112,** 1482-1497.

Pagnotti, V., and L. F. Bosart, 1984: Comparitive diagnostic case study of east coast secondary cyclogenesis under weak versus strong synoptic scale forcing. *Mon. Wea. Rev.*, **112,** 5- 30.

Pauley, P. M., and S. J. Nieman., 1992: A comparison of quasigeostrophic and nonquasigeostrophic vertical motions for a model-simulated rapidly intensifying extratropical cyclone. *Mon. Wea. Rev.*, **120,** 1108-1134.

___, and P. J, Smith., 1988: Direct and indirect effects of latent heat release on a synoptic-scale wave sytem. *Mon. Wea. Rev.*, **116,** 1209-1235.

Robertson, F. R., and P. J. Smith, 1983: The impact of model moist processes on the energetics of extratropical cyclones. *Mon Wea. Rev.*, **111,** 723-744.

Shapiro R., 1975: Linear filtering, *Math. Comp.*, **29,** 1094-1097

Smith, P. J., P. M. Dare and S. J. Lin, 1984: The impact of latent heat release on synoptic scale vertical motions and the development of an extratropical cyclone system. *Mon. Wea. Rev.*, **112,** 2421-2430.

___, and, ___, 1986: The kinetic and available potential energy budget of a winter extratropical cyclone system. *Tellus*, **38A,** 49-59.

Tracton, M. S., 1973: The role of cumulus convection inthe development of extratropical cyclones. *Mon. Wea. Rev*, **101,** 573-593.

INITIAL DISTRIBUTION LIST

		No. Copies
1.	Defense Technical Information Center Cameron Station Alexandria, VA 22304-6145	2
2.	Librarian Code 52 Naval Postgraduate School Monterey, CA 93943-5002	2
3.	Chairman (Code OC/Co) Department of Oceanography Naval Postgraduate School Monetery, CA 93943-5122	1
4.	Chairman (Code MR/Hy) Department of Meteorology Naval Postgraduate School Monterey, CA 93943-5002	2
5.	Professor Patricia M. Pauley (Code MR/Pa) Department of Meteorology Naval Postgraduate School Monterey CA 93943-5002	2
6.	Professor Carlyle H. Wash (Code MR/Wx) Department of Meteorology Naval Postgraduate School Monterey CA 93943-5002	1
7.	LCDR James W. Allen Oceanographer USS CONSTELLATION (CV-64) FPO San Francisco Ca.	2
8.	Commander Naval Oceanography Command Stennis Space Center MS 39529-5000	1
9.	Commanding Officer FLENUMOCEANCEN 7 Grace Hopper Ave. Stop 4 Monetery, CA. 93943-0001-0120	1

10. Commanding Officer
Naval Oceanographic and Atmospheric 1
Research Laboratory
Stennis Space Center
MS 39529-5004